Environmental mobility of potentially toxic trace elements of Andean volcanic ashes

Flavia Ruggieri

**Departament de Geoquímica,
Petrologia i Prospecció Geològica**

Environmental mobility of potentially toxic trace elements of Andean volcanic ashes

Flavia Ruggieri

2011

Directors: Dr. José Luis Fernández Turiel, Dr. Domingo Gimeno Torrente

Programa de Doctorat Ciències de la Terra

List of Contents

PART 1. INTRODUCTION

Chapter 1. Volcanic eruptions and ash deposition

PART 4. RESULTS AND DISCUSSION

Chapter 5. Sample selection and characterisation

Chapter 6. Design of a single batch leaching test (SBLT) with deionised water

Chapter 7. Single Batch Leaching Tests (SBLTs)

Chapter 8. Column leaching tests

Chapter 9. Sequential Extraction Scheme (SES)

List of Figures

Chapter 1. Volcanic eruptions and ash deposition

Chapter 2. Andean Cordillera as paradigm of explosive volcanism setting

Chapter 3. Sampling

Chapter 4. Methodology and analytical techniques

Chapter 5. Sample selection and characterisation

Chapter 6. Design of a single batch leaching test with deionised water

Chapter 7. SBLT applied to the volcanic ash under study

Chapter 8. Column leaching tests

Chapter 9. Sequential Extraction Scheme (SES)

Appendix 2

Appendix 3

List of Tables

Chapter 1. Volcanic eruptions and ash deposition

Chapter 3. Sampling

Chapter 4. Methodology and analytical techniques

Chapter 5. Sample selection and characterisation

Chapter 6. Design of a single batch leaching test with deionised water

Chapter 7. SBLT applied to the volcanic ash under study

Chapter 8. Column leaching tests

(unsieved) ashes and 719 size fractions.

Chapter 9. Sequential Extraction Scheme (SES)

Appendix 4

Appendix 6

Acknowledgements

Objetivos y estructura de le Tesis

Objetivos

El principal objeto de esta Tesis es la caracterización geoquímica de diferentes cenizas volcánicas colectadas a lo largo de la Cordillera Sur de los Andes desde un punto de vista medioambiental. En concreto los principales objetivos de esta investigación son:

(1) desarrollar una metodología de análisis específica para la caracterización físico-química de cenizas volcánicas;

(2) proponer una nueva metodología de lixiviación de cenizas que sea útil tanto para las cenizas volcánicas recientes como antiguas.

(3) averiguar el impacto geoquímico que ocurre después de la deposición de cenizas volcánicas en el medio ambiente a través de diferentes experimentos de lixiviación.

Estructura de la Tesis

Con el fin de desarrollar correctamente los objetivos sobre citados, esta tesis se ha dividido en cincos partes.

La primera incluye un capítulo de introducción en donde se exponen los fundamentos teóricos sobre las erupciones volcánicas, los mecanismos de producción de cenizas volcánicas y la manera con la cual las partículas de ceniza se depositan en la superficie terrestre. En este capítulo se incluyen también los principales efectos de las cenizas volcánicas sobre el medio ambiente ya sea a nivel global (por ej. sobre el clima) como a nivel regional (por ej. sobre la calidad de la aguas).

La segunda parte de la tesis está formada por un capitulo. Una breve explicación de las principales características geológica de las Cordilleras de los Andes desde un punto de vista de paradigmático caso de erupciones explosivas, la descripción de las diferentes zonas de estudio y de cada volcán es el objeto del segundo capítulo. En este, además, se incluye una descripción del clima variable que se encuentra a lo largo de la Cordillera, ya que es un factor determinante en el impacto ambiental de dichas cenizas.

La tercera parte incluye dos capítulos. El primero (Capítulo 3) resume el trabajo de campo y recogida de muestras. El segundo (Capítulo 4) recapitula la

metodología utilizada en este estudio. Dado que este trabajo está enfocado en un marco multi-analítico y que parte de la investigación se ha llevado a cabo en diferentes laboratorios, se ha considerado conveniente dedicar un capítulo completo.

Los resultados y su discusión están expuestos en la cuarta parte, la cual incluye 5 capítulos. En el capítulo 5 se definen los criterios utilizados para distinguir entre productos volcánicos y no volcánicos recolectados durante la campaña de campo. Una vez identificadas las cenizas volcánicas puras, los resultados de la caracterización física, mineralogía, química, y el estudio de espectroscopia FTIR sobre roca total son extensamente descritos. El capitulo 6 describe el diseño experimental llevado a cabo para delinear una especifica metodología de lixiviación con agua desionizada para identificar de manera confiable y rápida la contribución de elementos trazas potencialmente tóxicos (ETPTs) de una ceniza volcánica (tanto fresca como ya depositada en el suelo) al equilibrio geoquímico local. Los resultados de la precedente metodología aplicada a todas las cenizas volcánicas investigadas es el objeto del séptimo capítulo. Además, en este capítulo se introducen los resultados obtenidos a partir del ensayo de lixiviación con acido nítrico. El capitulo 8 incluye los resultados obtenidos mediante ensayo de lixiviación en columna, favoreciendo información sobre la movilidad de los ETPTs en el tiempo. La determinación de los perfiles de asociación, es decir, del reparto de los ETPTs entre las distintas fracciones de un sólido mediante el uso de la metodología de extracciones químicas secuenciales es la esencia del capítulo 9.

La ultima parte, la quinta, incluye las principales conclusiones y nuevas ideas para continuar el estudio de movilidad de los ETPTs que ocurre mediante la interacción agua-ceniza.

Finalmente se presenta la bibliografía citada en esta tesis así como siete anexos. En el primero se presentan todos los protocolos utilizados en la preparación de las muestras para las diferentes técnicas analíticas. En el segundo se reportan fotos SEM adicionalmente a las incorporadas en el capítulo 5. El tercer anexo contiene los espectros del análisis mineralógico llevado a cabo para todas las cenizas volcánicas estudiadas en esta tesis. El cuarto anexo recoge el tratamiento estadístico llevado a cabo para el diseño del ensayo de lixiviación con agua desionizada. El quinto anexo incluye los

protocolos metodológicos de todos los ensayos de lixiviación. El sexto releva los resultados obtenidos a partir del ensayo de lixiviación con agua desionizada e con nítrico, adicionalmente a los incluidos en el capítulo 7. Finalmente, el último anexo (séptimo) incluye las publicaciones producidas a lo largo de estos años, así como la asistencia a congresos.

Resumen extendido

1. Introducción

Las erupciones volcánicas son una de las expresiones más notables y de mayor alcance de la fuerza de la naturaleza. Los volcanes muestran una amplia gama de estilos de erupción. En general, las erupciones volcánicas varían desde la efusión de lava (típica de magma basáltico con bajo contenido de sílice) a eventos muy explosivos (típicos de magmas riolíticos y dacíticos con alto contenido de sílice). A pesar de que en la mayoría de las erupciones se produce ceniza volcánica, son las erupciones explosivas las que inyectan mayores cantidades de ceniza a la atmosfera, pudiendo afectar a la estratosfera. Las erupciones explosivas son la manifestación más poderosa y destructiva de la actividad volcánica. Durante una erupción explosiva hay dos tipos básicos de mecanismos que producen cenizas volcánicas: (1) magmático por exolución y expansión de los gases en el magma, y (2) freatomagmático por enfriamiento del magma en ascenso debido al contacto con aguas subterráneas o superficiales. La formación de cenizas volcánicas en general se presenta como una combinación de ambos mecanismos.

1.1 Componentes y morfología de las partículas cenizas

La ceniza volcánica se compone de tres componentes principales: (1) fragmentos de vidrio, (2) fragmentos de minerales y (3) fragmentos líticos accidentales. Las propiedades de la ceniza dependen sobre todo de las proporciones relativas de estos componentes. La morfología de las partículas de ceniza puede ayudar a identificar la naturaleza de la erupción. Distintos procesos de fragmentación producen diferentes características texturales. La forma de las partículas vítreas de la erupción magmática depende principalmente de la evolución cinética de los gases (Verhoogen, 1951), que determinan el número y la densidad de las burbujas. La morfología de las partículas de cenizas de erupciones freatomagmáticos está controlada por las tensiones en el magma que se producen debido a la presencia de agua y que generan partículas de vidrio poco vesiculadas.

1.2 Impacto ambiental de las cenizas volcánicas

Las erupciones volcánicas explosivas son capaces de causar importantes repercusiones medioambientales afectando, al mismo tiempo, muchos compartimentos en el sistema terrestre (Jones y Gislason, 2008). Los aerosoles volcánicos son un componente activo del sistema climático y desempeñan múltiples funciones en los intercambios físicos y biogeoquímicos entre la superficie terrestre, la atmósfera y las aguas oceánicas (Niemeier et al., 2009). Cuando la ceniza volcánica está suspendida en una columna eruptiva, una cierta proporción de los componentes solubles se condensa en las superficies de las partículas de dicha ceniza. Por lo tanto, el impacto ambiental producido por la caída de ceniza volcánica incluye:

(1) la liberación a corto plazo de los compuestos solubles presentes en la superficie de las partículas (lixiviación a corto plazo);

(2) la liberación a largo plazo de los elementos presentes en el vidrio volcánico y en las fases cristalinas (lixiviación a largo plazo).

1.2.1 Lixiviación a corto plazo

Las reacciones que ocurren entre los gases/aerosoles y las partículas de ceniza en una columna eruptiva siguen siendo poco conocidas. Entre los gases liberados los principalmente involucrados son HCl, HF y SO_2. Los ácidos clorhídrico y fluorhídrico se disuelven en el agua y caen como lluvia ácida, mientras que la mayoría de SO_2 se convierte lentamente en aerosoles de ácido sulfúrico (H_2SO_4). Las partículas de ceniza pueden adsorber estas gotas de aerosol en sus superficies y caer en el suelo a medida que la temperatura y la presión disminuyen (Allard et al., 2000). Por otra parte, la formación de sales solubles en las superficies de las partículas de cenizas parece también ser debida a la disolución parcial de las partículas a través de las reacciones con los gases ácidos (es decir, HCl, HF) y aerosoles (es decir, H_2SO_4) de la pluma eruptiva, seguida por la precipitación en la interfase líquido-partícula. Este proceso se ha postulado principalmente para los elementos con una baja volatilidad en el magma (es decir, los elementos litófilos) (Delmelle et al., 2007). Tras la deposición, el material adsorbido se puede dispersar en el medio ambiente. La interacción de tefra recientemente eruptada con las aguas superficiales determina la disolución de los componentes solubles resultando

en cambios químicos y, por tanto, en la calidad del agua (Jones y Gislason, 2008; Stewart et al., 2006; Witham et al.,2005).

1.2.2 Lixiviación a largo plazo

El vidrio volcánico se puede ver como un líquido meta-estable enfriado (White, 1984). El vidrio volcánico representa ~12% de la media de la corteza continental superficial, siendo superado en abundancia sólo por plagioclasa (~35%) y cuarzo (~20%) (Nesbitt y Young, 1984). Estudios pioneros sobre la disolución de vidrio riolítico han comparado la composición de la fase vítrea recientemente eruptada con la composición residual de su homólogo alterado demostrando una importante movilidad de las especies químicas durante su meteorización (Lipman et al., 1969; Noble, 1967). Debido a su abundancia y a su rápida meteorización, el vidrio juega un papel importante en el ciclo global y local de numerosas especies químicas en la superficie de la Tierra (de Wolff-Boenisch et al., 2004b). Además, la disolución y precipitación de fases secundarias durante la meteorización es capaz de alterar la composición química de las aguas de ríos y lagos (Stefansson et al., 2001; Blanco y Claassen, 1980).

1.3 Estudios previos sobre la lixiviación de ceniza

La existencia de materiales fácilmente solubles en las superficies de las partículas de cenizas se documentó por primera vez a principios del siglo XX (Lacroix, 1907). A partir de esta observación, muchos estudios de lixiviados se han diseñado con el fin de cuantificar los volátiles adsorbidos en una ceniza volcánica. Una revisión de 55 estudios (que presenta los datos de lixiviados de cenizas de 27 volcanes) concluye que la comparación de los datos se ve obstaculizada debido a la amplia gama de metodologías de lixiviación utilizadas (Witham et al., 2005). En este sentido, uno de los principales objetivos de esta investigación es proponer una nueva metodología de lixiviación de cenizas que contribuya a la armonización de estos métodos.

En bibliografía no existen muchos trabajos que estudien la lixiviación de cenizas volcánicas desde un punto de vista medioambiental. Algunos de estos trabajos revisan la tasa de disolución del vidrio volcánico mediante ensayos de tipo dinámico (ensayos de lixiviación en columna en los que la ceniza está

sometida a un flujo constante de solución lixiviante) (Gislason y Oelkers, 2003; Wolff-Boenisch et al., 2004a, 2004b, 2006). Los experimentos en columna permiten evaluar el comportamiento temporal de los elementos en los depósitos de ceniza, como por ejemplo los del Rift de Etiopía (Rango et al., 2011). Otro tipo de ensayos es el que considera el flujo total de elementos lixiviados a partir de cenizas volcánicas (ensayos *batch*) y que se han aplicado a erupciones erupciones históricas como por ejemplo Hekla, 2000, y monte St. Helens, 1980 (Jones y Gislason, 2008). Por último, hay una gran cantidad de estudios que suponen la disolución del vidrio volcánico como fuente geogénica de elementos traza potencialmente tóxicos (por ejemplo, F, As, Mo) en aguas superficiales y subterráneas en diferentes partes de Argentina (Bhattacharya et al., 2006; Bundschuh et al., 2004; Francisca y Pérez, 2009; Nicolli et al., 1989, 2001, 2011).

2. Marco geográfico y geológico

La Cordillera de los Andes forma una cadena montañosa continua de >7.500 km a lo largo del margen occidental de América del Sur. A lo largo de la Cordillera de los Andes se diferencian cuatro zonas de vulcanismo activo: Zona Volcánica Norte (ZVN), Central (ZVC), Sur (ZVS) y Austral (ZVA). Este estudio se refiere a la caracterización de cenizas volcánicas en la parte sur de la ZVC y la parte norte de la ZVS. La ZVC (16-28° S) de los Andes Centrales es una de las mayores regiones volcánicamente activas del mundo. El área de estudio (sur de la Puna y zonas limítrofes) se caracteriza por un magmatismo ácido (principalmente magma andesítico). La ZVS (33-46° S) incluye, al menos, 60 edificios volcánicos históricos, así como tres sistemas de calderas gigantes. Las cenizas producidas durante las erupciones históricas de Copahue (2000), Lonquimay (1988), Llaima (2008), Chaitén (2008), y Hudson (1991) son estudiadas.

3. Muestreo

Los trabajos de campo se llevaron a cabo en diferentes campañas durante el período 2006-2008. Se han tomado muestras de veintiún supuestos depósitos de cenizas volcánicas en el sur de la Puna y zonas limítrofes (provincias de

Catamarca y Salta, Argentina) y ocho supuestos depósitos de cenizas volcánicas en Uruguay. Muchos de estos depósitos de cenizas están muy bien preservados en la Puna debido a las condiciones extremadamente áridas de dicha región desde hace millones de años (García-Vallés et al., 2008; Stern, 2004). En Uruguay, el área de estudio se encuentra entre 33 y 34º S y entre 56 y 58º W. Las cenizas muestreadas se depositaron durante el Pleistoceno, con alternancia de condiciones semiáridas y templadas (Aguilar, 2006; Calarge et al., 2006; Ubilla et al., 2004). Las muestras de cenizas de los volcanes Copahue, Lonquimay, Llaima y Hudson fueron generosamente proporcionadas por la institución chilena SERNAGEOMIN (Dr. J. Naranjo). Tres cenizas del volcán Chaitén se tomaron en el campo por un miembro del grupo de investigación PEGEFA (Dr. E. Polanco) y una muestra fue proporcionada por el Dr. A. Caselli (Universidad de Buenos Aires, Argentina). Tres cenizas del Chaitén se recogieron durante la fase explosiva inicial mientras que una se recogió más tarde.

4.   Caracterización de las cenizas volcánicas recolectadas

La parte metodológica se puede considerar el cuerpo principal de este trabajo. La Figura 1.1 resume las técnicas utilizadas. Después de la caracterización (física, mineralógica y química) de la roca total, la contribución de la ceniza volcánica al balance geoquímico local se evaluó mediante diferentes ensayos de lixiviación. Estos ensayos han permitido estudiar:

(1)   El comportamiento a corto plazo de la lixiviación de cenizas volcánicas mediante ensayos de tipo *batch* (*Single Batch Leaching Tests, SBLTs*). En el presente estudio, se llevaron a cabo dos ensayos de tipo *batch*, uno con agua desionizada y otro con ácido nítrico. El primer lixiviante permite la rápida detección de los elementos potencialmente peligrosos que pueden ser liberados de las cenizas. La extracción con ácido nítrico es útil para la evaluación de las cantidades máximas de elementos traza potencialmente tóxicos (ETPTs) ambientalmente disponibles (Papastergios et al., 2009, 2010; Sastre et al., 2002). Además, reproduce circunstancias ambientales como las condiciones muy acidas de algunas aguas superficiales (p. ej., rio Agro en el área volcánica del Copahue, Argentina).

(2)   El comportamiento temporal de los elementos potencialmente peligrosos se evaluaron mediante ensayos de lixiviación en columna.

(3)   La asociación de los ETPTs a las distintas fracciones químicas de las cenizas se estudiaron mediante ensayos de extracción química secuencial (*Sequential Extraction Scheme, SES*).
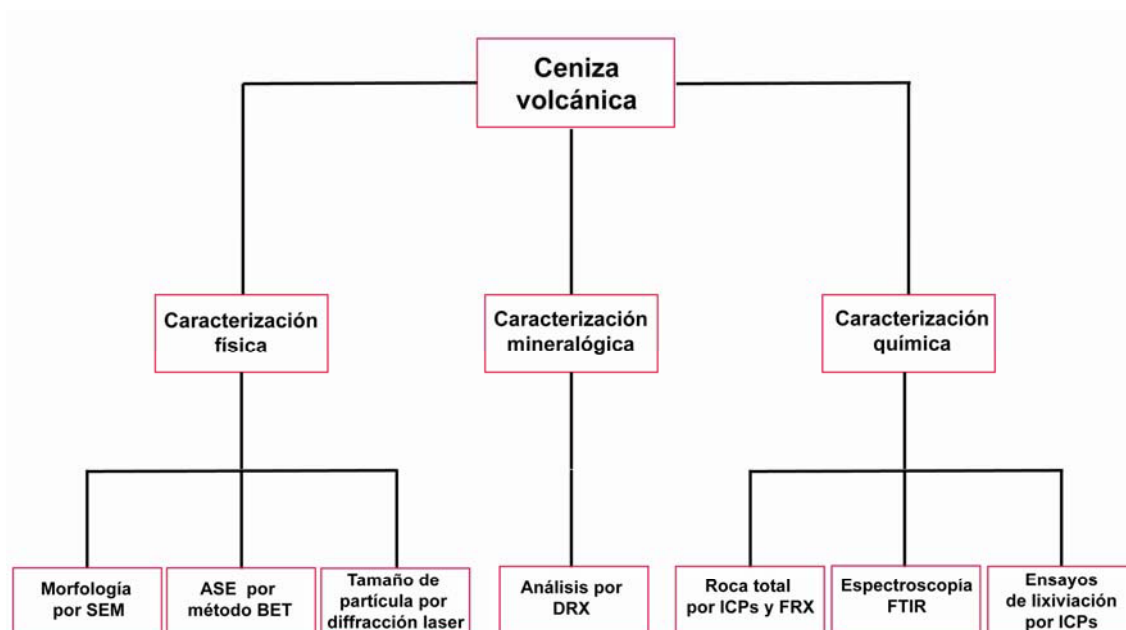
Figure 1.1 Técnicas analíticas utilizadas en este estudio. SEM, microscopio electrónico de barrido; ASE, área superficial específica; DRX, difracción de rayos X; ICPs, espectrometrías de emisión de masas con fuente de plasma acoplado por inducción; FRX, fluorescencia de rayos X; FTIR Espectroscopía infrarroja por transformada de Fourier.

4.1 Técnicas analíticas

La mayoría de los análisis se han llevado a cabo en los Servicios Cinetífico-Técnicos de la Universidad de Barcelona. Partes de los demás análisis se han realizado en el Instituto de Ciencias de la Tierra J. Almera del CSIC, Barcelona, y en la Agencia Nacional Italiana para las Nuevas Tecnologías, Energía y Desarrollo Económico Sostenible (ENEA), Roma.

La caracterización física de las cenizas volcánicas se ha dividido en el estudio de las propiedades morfológicas de las partículas mediante microscopía

electrónica de barrido con analizador de energía dispersiva de rayos X (*Scanning Electron Microscopy with Energy Dispersive Analyser, SEM-EDX*) con un instrumento FEI Quanta 200; el análisis del Área Superficial Específica (ASE) (*Specific Surface Area, SSA*) mediante el método Brunauer-Emmett-Teller (BET) y el análisis de tamaño de grano (*Grain size analysis, GSA*) por difracción de láser con un equipo Malvern Masterziser 2000 HydroMU.

La caracterización mineralógica se realizó por difracción de rayos X (DRX) utilizando un difractómetro Bruker D-5005. Solo para la muestra No. 719 se calculó la composición mineralógica cuantitativa con el método RockJock del Dr. D.D. Eberl (Andrews et al., 2006; Eber, 2003). El análisis mineralógico cuantitativo se utilizó con el fin de definir las mejores condiciones operativas para el análisis de tamaño de grano.

La metodología desarrollada para el análisis químico de roca total es útil para todos los tipos de rocas volcánicas y permite la determinación de los elementos mayores y trazas (véase el protocolo para la determinación de elementos mayores y trazas en las rocas por medios de ataque total en el Apéndice 1). Las soluciones obtenidas por el ataque conjunto de diferentes ácidos se analizaron con Espectrometría de Emisión Óptica con Plasma Acoplado por Inducción (ICP-OES) y Espectrometría de Masas con Plasma Acoplado por Inducción (ICP-MS y HR-ICP-MS, equipos con cuadrupolo y sector magnético, respectivamente). Los elementos se han analizado de la siguiente manera:

• los elementos mayoritarios (Al, Ca, Fe, K, Mg, Mn, Na, P, Ti y Si) y algunos elementos trazas (Ba, Sr y Zr) mediante ICP-OES o HR-ICP-MS;

• los elementos trazas (incluyendo Tierras Raras) mediante ICP-MS o HR-ICP-MS; y

• el contenido de SiO_2 (%, m/m) se ha determinado indirectamente teniendo en cuenta el contenido de los óxidos principales y los valores de calcinación;

• los contenidos de Zr y Nb se determinaron por medio de fluorescencia de rayos X (FRX).

Las soluciones lixiviadas obtenidas en los ensayos de lixiviación de cenizas se analizaron mediante ICPs de la siguiente manera:

• Los elementos mayoritarios (K, Na, Ca, Mg, Sr, Fe, S, P, B, y Si) a través de ICP-OES y ICP-MS; y

• los elementos trazas (incluyendo los elementos de la Tierra Rara) mediante ICP-MS o HR-ICP-MS;

Por otra parte, la determinación de fluoruro en los lixiviados de cenizas con agua desionizada se realizó con el método de electrodos de iones selectivos (*Ion Selective Electrode, ISE*).

La espectroscopía infrarroja de transformada de Fourier (FTIR) es una técnica potente para el estudio de las estructuras moleculares. Esta técnica se utilizó para proporcionar información acerca de los enlaces químicos estructurales del agua presente en las cenizas (es decir, la cantidad total de H_2O (H_2O_t), H_2O molecular (H_2O_m) y OH). Las muestras fueron analizadas con un Perkin-Elmer 2000 16PC.

5. Selección de las muestras y caracterización

5.1 Caracterización física

5.1.1 Morfología y textura por SEM-EDX

La microscopía electrónica de barrido (SEM) y los espectros por energía dispersiva de rayos X (EDX) de partículas individuales permitieron identificar inequívocamente los depósitos de cenizas volcánicas. De los 29 supuestos depósitos de ceniza volcánica muestreados en el sur de la Puna y de Uruguay sólo 11 resultaron ser ceniza volcánica pura. Estas muestras se caracterizaron por estar constituidas por vidrio y pequeñas cantidades de fases cristalinas. En los sedimentos mixtos las partículas de cenizas volcánicas coexisten con partículas no volcánicas (por ejemplo, sílice biogénica, principalmente diatomeas).

Después de la observación por SEM, las 11 muestras han sido clasificadas en:

(1) muestras (UR-1, UR-6, UR-7 y 808) con una composición exclusiva de fase vítrea y gran abundancia de partículas de tamaño fino (<5 µm).

(2) muestras (719, 721, 733, 809, AS-28, CHA-1F, CHA-2R, CHA-G, la CHA-E) con una gran cantidad de fase vítrea y una moderada cantidad de fases cristalinas.

(3) muestras (AS-29 y AS-33) compuestas de partículas de vidrio en forma de bloques poco vesiculados (5-200 µm), con alto contenido de fases cristalinas y muy pocas partículas de tamaño fino; y

(4) muestras (COP, LON, LLA, y HUD) constituidas por fragmentos vítreos en bloques (5-200 μm), con exigua cantidad de partículas de tamaño fino y contenido bajo de fases cristalinas.

Estos grupos reflejan los diferentes estilos volcánicos que generaron las cenizas. Para los grupos 1 y 2 se puede inferir un origen eruptivo magmático. El alto contenido de vidrio, prácticamente sin cristales en el grupo 1, indica un ascenso muy rápido del magma hacia la superficie, mientras que el alto contenido de partículas de tamaño fino en el grupo 2 podría indicar una erupción altamente explosiva. La morfología de las partículas de la ceniza del grupo 3 (los bordes angulares) indica una fragmentación por fractura térmica, lo que implica procesos eruptivos de tipo freatomagmático. La morfología observada en las cenizas de los volcanes Hudson, Copahue, Llaima y Lonquimay indicaría una erupción de tipo freatomagmático. Otros autores corroboran los datos obtenidos (Kratzmann et al., 2009, 2010; Naranjo y Moreno, 1991; Naranjo y Polanco, 2004; Naranjo et al.,1992; Naranjo y Stern, 1998).

5.1.1 Área Superficial Específica (ASE)

El Área Superficial Específica (ASE) se determinó para las cenizas volcánicas puras de la Puna y para sedimentos mixtos que contienen una parte de ceniza. Para las cenizas puras los valores de ASE variaron entre 0,55 y 7,74 $m^2 \, g^{-1}$, con el valor más bajo para la muestra 719 y el más alto para la muestra 808. En una ceniza volcánica pura, las diferencias entre los valores de ASE están relacionados con el tamaño de las partículas de ceniza y con la morfología de las vesículas (Papelis et al., 2003). Los resultados obtenidos fueron consistentes con la morfología de las partículas observadas en las imágenes SEM. Los sedimentos mixtos presentaron valores mucho más altos, debido a la presencia de minerales de la arcilla y/o sílice biogénica, que suelen desarrollar ASE más elevados (Fowler et al., 2004; Fubini, 1997).

5.1.2 Análisis del tamaño de grano

El análisis del tamaño de grano con difracción láser demostró que en algunas muestras hay una tendencia hacia una distribución granulométrica unimodal. Las muestras AS-29, AS-33, COP, LON, LLA y HUD presentan un elevado

contenido de partículas con tamaño entre 500-1000 µm, mientras que en las muestras 808, UR-1, UR-6, UR-7 y CHA-E hay una preponderancia de partículas con tamaño entre 10 y 100 µm. Otras muestras (721, 809, CHA-2R y CHA-G) presentaron una distribución bimodal con picos en 10-50 µm y 50-100 µm. Por último, las muestras 719, 733, AS-28 y la CHA-1F presentaron una distribución de tipo multimodal.

La cantidad de partículas finas es importante porque refleja varias características, incluyendo: (1) el estilo y la dinámica de la erupción; (2) la localización geográfica, es decir, la distancia desde el volcán hasta el sitio de muestreo, y (3) la repercusión en la evaluación del riesgo ambiental, porque cenizas con alto contenido de partículas pequeñas son potencialmente más peligrosas que las compuestas por partículas más grandes.

En general, las erupciones basálticas producen una cantidad relativamente pequeña de partículas finas en comparación con las erupciones más silícicas. Esta característica es visible en las cenizas estudiadas. Las muestras riolíticas (incluyendo la mayoría de las cenizas de la Puna, Uruguay y del volcán Chaitén) presentaron un contenido más alto de partículas finas que las cenizas menos silícicas (muestras COP, LON, LLA y HUD). La distribución de tamaño de grano en las muestras del Chaitén sugiere una posible evolución durante la erupción del 2008. La muestra recogida en la fase inicial (CHA-G) evidencia una distribución bimodal mientras que las muestras CHA-1F y CHA-E, tomadas sólo unos pocos días más tarde, presentan una distribución multimodal. Por otra parte, la muestra CHA-2R recogida en agosto 2008 (después del colapso del domo) presenta la misma distribución de la muestra recogida durante la primera fase.

La fracción de materiales muy finos (<5 µm) en las cenizas estudiadas varía desde 1,2 hasta 40,9 % en volumen. El alto contenido de finos implica un mayor riesgo medioambiental en general y para la salud en particular porque las partículas con diámetro aerodinámico inferior a 4 µm se consideran "fracción respirable" (Horwell, 2007). Teniendo en cuenta el contenido de partículas <10 µm, el peligro medioambiental que suponen las cenizas estudiadas es en el siguiente orden: UR-1>721>808>809>CHA-1F>733>CHA-G>AS-28>UR-6>719>CHA-2R>CHA-E>UR-7>AS-29>COP>LLA>AS-33> HUD> LON.

5.2 Caracterización mineralógica

La composición mineralógica permitió definir cuatro grupos: (1) cenizas volcánicas antiguas de la Puna en las que el vidrio volcánico está acompañado por pequeñas cantidades de cuarzo, albita, sanidina y biotita; las muestras 721 y AS-28 presentaron cristobalita mientras que la 808 presentó sólo vidrio volcánico;

(2) cenizas volcánicas antiguas de Uruguay constituidas sólo por vidrio volcánico;

(3) cenizas volcánicas recientes de la ZVS (muestras COP, LON, LLA y HUD) en las cuales se detectó notable cantidad de anortita; y

(4) cenizas de la erupción del Chaitén, en las cuales el vidrio está acompañado por cuarzo, andesita y una notable cantidad de cristobalita.

5.3 Análisis de roca total

Las cenizas volcánicas se han clasificados en el diagrama TAS (contenido de total de álcalis *vs*. sílice) en:

- (1) ceniza de tipo basáltico: LLA;
- (2) ceniza de tipo traqui-basáltico: HUD;
- (3) cenizas de tipo traqui-basáltico-andesítico: LON y COP; y
- (4) cenizas de tipo riolítico: 719, 721, 733, 808, 809, AS 28, AS 29, AS-33, UR-1, 6-UR, UR-7, CHA-1F, CHA-2R, CHA-G y CHA-E.

5.4 Espectroscopía FTIR

La espectroscopía FTIR se utilizó para proporcionar información sobre el agua presente en las cenizas volcánicas. Los espectros de infrarrojos permiten estimar el contenido H_2O_t mediante la integración del área bajo del pico entre 3612 y 3411 cm^{-1}. El hecho de que un magma de tipo riolítico contenga mayor cantidad de agua que un magma basáltico es una característica bien conocida. Este hecho explica el bajo contenido de agua obtenido en todas las cenizas volcánicas de la ZVS excepto en las cenizas del Chaitén (de tipo riolítico). Por otra parte, las muestras riolíticas antiguas presentan un mayor contenido de agua que las cenizas del volcán Chaitén. Dado que durante la meteorización, el agua migra en un vidrio predominantemente como H_2O_m (Yokoyama et al.,

2008), las observaciones realizadas indican que las muestras antiguas (cenizas de la Puna y Uruguay) están afectadas por diferentes grados de alteración.

5.4.1 Reactividad de las cenizas

La disolución de agua en un magma altera su estructura produciendo cambios en sus propiedades físicas y químicas. La idea dominante clásica consiste en que el agua se disuelve en los fundidos silicatados y reacciona con el fundido (altamente polimerizado) rompiendo las cadenas of los enlaces tetraédricos (Si, Al)O_4 con el oxígeno, resultando dos terminaciones OH de dos cadenas más cortas por despolimerización (Dingwell, 1998). Este fenómeno causa un aumento de la fragilidad a medida que aumenta el grado de despolimerización del vidrio volcánico, implicando, desde un punto de vista medioambiental, una mayor reactividad de la ceniza (Giordano et al., 2009; Ruggieri et al., 2010).

Diferentes estudios muestran que la distribución de los grupos OH y del agua en el vidrio volcánico refleja la distribución del agua en el magma que generó dicho vidrio, salvo a temperaturas muy altas (Ihinger et al., 1999; Stolper, 1982, 1989). A raíz de esos trabajos, esta investigación demuestra que las cenizas estudiadas tienen abundantes cantidades de grupos hidroxilo, lo que indica una alteración de la cadena tetraédrica que a su vez afecta a la estabilidad química del vidrio. La alta reactividad de una ceniza no depende sólo del contenido de vidrio, pero en las antiguas esta característica juega un papel mayor en la liberación de elementos mayores y traza que en las actuales. Teniendo en cuenta el contenido de grupos hidroxilo, las cenizas pueden ser ordenadas según su reactividad en: 809>719~721~733~AS-28>AS-29~AS-33>CHA-G~CHA-2R~CHA-1F~CHA-E>COP>LON>LLA~HUD. Esta clasificación debe tomarse con cautela debido al gran número de factores que controlan la reactividad de una ceniza en el medioambiente (tamaño de grano de las partículas, características geológicas de los depósitos de cenizas, etc.).

6. Diseño experimental de un ensayo de lixiviación tipo *batch* con agua desionizada

Diferentes ensayos de lixiviación se han diseñado para simular la liberación de los elementos traza potencialmente tóxicos (ETPTs) de una ceniza volcánica con el fin de evaluar el impacto ambiental causado por su deposición en el medioambiente. Estos ensayos consisten en la lixiviación en un solo paso de una cantidad fija de ceniza con una cantidad fija de solución lixiviante. Una revisión de 55 estudios (que recoge los datos de lixiviados de 27 volcanes) llegó a la conclusión que el uso de una amplia gama de metodologías (por ej., en la composición de lixiviante, tiempo de contacto y relación líquido/sólido) hace muy difícil la comparación entre diferentes estudios. La conclusión es que hay una necesidad imperiosa de armonizar las metodologías de lixiviación de ceniza volcánica (Witham et al., 2005).

Uno de los objetivos principales de esta investigación es la puesta a punto de una metodología de lixiviación con agua desionizada que sea capaz de definir de manera rápida y fiable los ETPTs que se pueden lixiviar a partir de una ceniza volcánica (independientemente de su edad) y simulando, al mismo tiempo, condiciones parecidas a las naturales. Este estudio se llevó a cabo investigando las condiciones experimentales (es decir, los factores) que influyen sobre el ensayo *batch.* Dichos factores se dividen en los intrínsecamente vinculados a las propiedades de la ceniza (factores primarios como la porosidad, granulometría, etc.) y los que se pueden variar con el fin de buscar las condiciones experimentales más adecuadas (por ej., pH, tipo lixiviante y relación líquido/sólido). Para reducir el gran número de posibles condiciones experimentales se fijaron algunas de ellas:

(1) utilizar ceniza volcánica original, sin separar granulométricamente, ni moler;

(2) usar agua desionizada como solución lixiviante; y

(3) realizar los ensayos a temperatura ambiente.

Dos muestras de cenizas volcánicas riolíticas se seleccionaron para cubrir un amplio rango de edad de las cenizas (CHA-1F, de la erupción del 2008 del volcán Chaitén, y 719, una ceniza antigua de la Puna). Los ensayos se realizaron con diferentes relaciones de líquido/sólido (L/S), variando la cantidad

de ceniza (0,1 y 1 g) y el volumen de lixiviante (1, 2.5, 10, 25 y 50 ml de agua desionizada). Además se consideraron distintos tiempos de contacto (1,5, 4 y 16 h). Se llevaron a cabo cuatro replicas para asegurar la reproducibilidad de los datos experimentales, resultando 18 ensayos por cada muestra y un total de 72 ensayos en el conjunto del diseño experimental. Los elementos analizados cubren un amplio rango de comportamiento geoquímico durante la lixiviación. Incluyen:

(1) los elementos menos móviles durante los procesos de lixiviación (es decir Si, Al, Mn y Fe) (Chang, 1999; Gayer et al., 1958; Wollast y Chou, 1992);

(2) los componentes altamente solubles (es decir, SO_4^{2-} y Cl^-) y con enriquecimiento preferencial en las superficies de las partículas de ceniza (Delmelle et al., 2000, 2007);

(3) los elementos que se combinan con los halógenos, los sulfatos y que reaccionan con los aerosoles en la pluma volcánica (Ca, Na, Mg, Ba y Sr) y los elementos asociados a la disolución del vidrio volcánico durante su meteorización (por ej., As, Ni, V, Mo y Sb) (Hinkley, 1991, 1994, 1999; Nicolli et al., 2001, 2011; Francisca and Perez, 2009; Symonds et al., 1987, 1992, 1994). El tratamiento estadístico de los datos se llevó a cabo con el programa STATA 10.0. En términos estadísticos se investigaron las condiciones experimentales que producen una menor dispersión de las concentraciones elementales y, por tanto, proporcionan una alta reproducibilidad de los experimentos.

6.1 Cantidad de ceniza volcánica utilizada y relación L/S

En general, las concentraciones más altas se obtuvieron con 0,1 g de muestra de ceniza. Aunque parezca contradictorio, utilizar una baja cantidad de muestra permite extraer de forma más activa las especies presentes en las cenizas volcánicas. Esta cantidad podría ser una buena opción metodológica, ya que detecta mejor los analitos de interés. Sin embargo, los resultados muestran que independientemente del volumen de lixiviante, el uso de 0,1 g de ceniza tiene una reproducibilidad inferior a la de los experimentos efectuados con 1 g de ceniza. Este aspecto es claramente detectable en los compuestos muy solubles (como SO_4^{2-} y Cl^-), los elementos alcalinos (como Na, Ba, Sr y K) y los elementos trazas (como As, Ni, V, Mo y Sb) normalmente combinados con los halógenos y los sulfatos en las superficies de las partículas de cenizas. Su

fracción lixiviable debería estar limitada sólo por la cantidad elemental disponible en dicha ceniza. Estos resultados indican que una cantidad baja de la muestra no siempre es representativa de la ceniza, porque en esas condiciones es más difícil alcanzar el equilibrio químico. En general, el volumen de lixiviante tiene una baja influencia sobre la lixiviación cuando se utiliza 1 g de muestra. Una baja reproducibilidad se ha obtenido para valores elevados de L/S (principalmente con alto tiempo de contacto). Por otra parte, L/S es una variable interesante en el diseño de un ensayo de lixiviación por razones analíticas. La elección de una alta relación L/S significa una dilución mayor, lo que podría dar lugar a concentraciones cercanas o inferiores a los límites de detección para algunos elementos.

6.2 Lixiviación en función del tiempo de contacto

El tiempo de contacto es un factor importante, ya que está directamente asociado con las reacciones químicas heterogéneas que ocurren cuando la ceniza volcánica interactúa con el agua. El tratamiento estadístico de los datos muestra que el tiempo de contacto afecta a la fracción lixiviable de muchos elementos, especialmente cuando los tiempos de contacto bajos (1,5 y 4 h) se comparan con 16 h. Sin embargo, componentes muy solubles (como SO_4^{2-} y Cl^-) se movilizan inmediatamente después del contacto con el agua. Es decir, la fracción lixiviable es independiente de este factor. Sin embrago, la lixiviación de otros elementos (como Ca, Sr, Cu y As) se ve afectada por otros procesos, algunos de los cuales si dependen del tiempo de contacto. Este hecho es debido a que a varias reacciones ocurren en la interacción. Dichas reacciones pueden ser rápidas (por ej., la disolución de compuestos alcalinos, ácido-base y reacciones de complejación) (Oelkers et al., 2009; Toscano et al., 2008) mientras que otras son más lentas (por ejemplo, absorción superficial, procesos de precipitación y disolución y reacciones redox) (Stumm y Furrer, 1987). Este aspecto es aún más complicado en la lixiviación de cenizas debido a que la fase sólida es multicomponente, con fases de diferentes solubilidades (principalmente vidrio, pero también algunos minerales cristalinos). La reproducibilidad más baja se ha obtenido para el tiempo de contacto más bajo (1,5 h) y el más alto (16 h) y especialmente para la lixiviación de la ceniza

prístina (CHA-1F). Por lo tanto, los ensayos de lixiviación a 4 h produjeron los mejores resultados en términos de reproducibilidad.

6.3 Procedimiento propuesto para el ensayo de lixiviación de cenizas volcánicas con agua desionizada

Teniendo en cuenta los resultados experimentales obtenidos en este estudio, el procedimiento propuesto es el siguiente:

(1) Utilizar ceniza volcánica sin tratar, ni separada granulométricamante ni molida.

(2) utilizar agua desionizada como lixiviante que permite una rápida y reproducible detección de los componentes solubles. Además, debido a su disponibilidad general permite comparar fácilmente los resultados de diferentes laboratorios.

(3) Utilizar una relación L/S de 10 (alcanzada mezclando 1 g de ceniza con 10 ml de agua desionizada).

(4) Determinar el pH del lixiviado inmediatamente después del contacto ceniza-agua y al final del ensayo.

(5) Agitar la mezcla durante 4 h en reactores de polipropileno o polietileno.

(6) Filtrar la mezcla usando filtros de membrana de 0,45 μm. Centrifugar las muestras antes de filtrarlas permite acelerar la filtración y facilita la recuperación de la muestra de ceniza.

Los resultados de lixiviación deben ser expresados como concentración de lixiviados (mg l^{-1}) o como contenido lixiviado (mg kg^{-1} de ceniza). Su elección depende del tipo de datos que se desea comparar. Los resultados expresados en concentraciones de lixiviados permiten la comparación de los componentes en las condiciones de lixiviación especificadas. Los contenidos lixiviados permiten la determinación de la fracción disponible para la lixiviación.

7. Aplicación del ensayo *batch* a las muestras estudiadas

En la presente investigación, se realizaron dos ensayos de lixiviación de tipo *batch*. El primero con agua desionizada (siguiendo la metodología propuesta anteriormente) y el otro con ácido nítrico. La extracción con ácido nítrico permite la evaluación de la carga máxima de ETPTs ambientalmente disponible

(Papastergios et al., 2009, 2010; Sastre et al., 2002.). Además, la lixiviación ácida es una herramienta muy útil para reproducir las circunstancias medioambientales en un sistema ácido (por ejemplo, el río Agrio en la zona volcánica del Copahue, Argentina).

7.1 Batch con agua desionizada

La aplicación del método desarrollado en el capítulo precedente ha permitido definir el impacto geoquímico potencial que la ceniza volcánica puede causar sobre el medioambiente.

Los datos geoquímicos de los lixiviados se trataron con el programa R (R Development Core Team, 2010). El pH y la conductividad específica (CE) se han controlado por duplicado al principio del ensayo (pH_0 y CE_0), inmediatamente después del contacto agua-ceniza, y al final del experimento (pH_f y CE_f), antes de filtrar.

7.1.1 pH y conductividad específica

El pH obtenido inmediatamente después del contacto con agua desionizada (con un pH ligeramente ácido) incrementó a débilmente alcalino (pH_0) para las cenizas antiguas, excepto las de Uruguay. Para las cenizas recientes el pH subió meno, excepto en una de las muestras del Chaiten. El aumento de pH se debe a la rápida disolución de los compuestos alcalinos presentes en la superficie de las partículas de ceniza. Al final del ensayo (es decir, después de 4 h) los valores pH_f aumentaron.

La conductividad específica (CE) da una idea de los constituyentes iónicos en la solución. En las cenizas antiguas los valores finales de CE (CE_f) han sido dos o más veces más altos que los CE_0 mientras que para las cenizas recientes este incremento no ha sido tan evidente. Esto podría sugerir una menor cantidad de materiales fácilmente solubles en las cenizas recientes que en las antiguas.

7.1.2 Comparación entre los lixiviados de las cenizas antiguas *vs.* recientes

Las cenizas volcánicas antiguas se depositaron hace decenas a cientos de miles de años y durante ese tiempo se han visto afectadas por diferentes

procesos hidrológicos, cuyo efecto principal ha consistido en eliminar los componentes solubles asociados a la superficie de las partículas de ceniza. El tratamiento estadístico de los datos de los lixiviados mostró que las medianas de Ca, Mg, Cl⁻, SO_4^{2-}, F, Mn, Ni, Cu, As, Sr, Mo, Ba y Pb fueron más altas en los lixiviados de las cenizas recientes, mientras que Na, Si, Al, P, Ti, V, Fe, Zr, y U mostraron mayores concentraciones en los lixiviados de las antiguas. Los elementos enriquecidos en los lixiviados de cenizas recientes incluyen los implicados en las reacciones químicas que se producen en la pluma volcánica. Independientemente del contenido de sílice del magma, sulfatos y cloruros son los principales compuestos observados en los lixiviados de Chaitén, Hudson y Copahue. El lixiviado de la ceniza del Hudson presenta los valores más altos de F⁻. Algunos de los elementos trazas enriquecidos en los lixiviados de las cenizas recientes como Ni, Cu, As, Sr, Ba y Pb corresponden a elementos que se combinan con halógenos y sulfatos y que interactúan con los aerosoles ácidos precipitando en forma de sales solubles sobre la superficie de las partículas de ceniza (Delmelle et al., 2007). Los elementos enriquecidos en los lixiviados de las cenizas antiguas (Na, Si, Al, P, Ti, V, Fe y Zr) deben proceder de orígenes distintos a la interacción gases-ceniza. Algunos de estos (Si, Al, Ti, Fe) suelen definirse como los elementos menos móviles durante los procesos de meteorización ya que son los elementos formadores de los minerales.

El análisis de Componentes Principales (ACP) permitió separar los lixiviados en función de la edad geológica de las cenizas. Los dos grupos de lixiviados de cenizas (antiguas y recientes) se separaron principalmente por las variables incluidas en el eje PC2. Corroborando las observaciones indicadas anteriormente, las variables del PC2 con más altas concentraciones en los lixiviados de las cenizas recientes son Mn, Zn, Mg, SO_4^{2-} y F, mientras que en las cenizas antiguas los elementos con concentraciones más elevadas son B, Si, Fe, V, y Ti. Además, con el fin de evaluar la separación estadística de los dos tipos de lixiviados de cenizas según el análisis de ACP se utilizó la distancia de Jeffries-Matusita (JM). Los valores JM demostraron una elevada separación (JM = 1.99) (Richards, 1986), lo que implica una gran diferencia en términos de composición de los lixiviados.

7.1.3 Contribución al equilibrio geoquímico regional

La masa relativa lixiviada (*relative mass leached* o *RML*,%), definida como la fracción lixiviada de un componente de la ceniza, ha permitido predecir las cantidades elementales que pueden ser fácilmente transferibles al medioambiente a través del agua para cada ceniza investigada. Calcio, Mg, Na, Si, K, y Al mostraron una gran capacidad de movilización tanto en las cenizas antiguas como en las recientes. Por su parte, las cenizas antiguas de la Puna y Uruguay son capaces de lixiviar los mismos elementos trazas en el medioambiente (P, Ti, Fe, Mn, Zn y Sr). Algunos de estos elementos forman minerales esenciales, sugiriendo que la ceniza volcánica, una vez depositada, está sometida a irreversibles reacciones geoquímicas de meteorización que provocan una lenta desestabilización de la cadena tetraédrica de los silicatos con la consiguiente lixiviación de los elementos asociados. En las cenizas recientes se observó una mayor variabilidad. Las cenizas del Chaitén muestran gran cantidad de As, Pb, Fe, Zn medioambientalmente disponible, mientras que las otras muestras recientes (COP, LON, LLA y HUD) lixivian principalmente P, Ti, Mn, Zn y Pb.

A partir de estos datos, se han modelado las cantidades de cada elemento que cada erupción estudiada puede transferir al medioambiente mediante la interacción agua-ceniza. Este modelado ha requerido del conocimiento del volumen de la erupción (expresado en roca densa equivalente, V_{DRE}) y la densidad de la ceniza. Los valores de V_{DRE} se han tomado de la literatura o han sido modelados. Los resultados finales mostraron que tanto las cenizas antiguas como las recientes pueden transferir al medioambiente principalmente elementos como Ca y Na. Algunos de los elementos ambientalmente disponibles son macro y micronutrientes (por ej., Mn, Fe y P), evidenciando el potencial fertilizante de las cenizas. Muchos otros son ETPTs que pueden causar serios problemas incluso con concentraciones muy bajas. Las cantidades de ETPTs medioambientalmente disponibles han mostrado considerable variabilidad de unas cenizas a otras. Por ejemplo algunos de los depósitos de cenizas de la Puna (719, 721, 808, 809 y AS-28) mostraron una alta movilidad de Pb, As y Cu, mientras que Pb, Cu y Ni mostraron una elevada movilidad en la 733 y en los depósitos de Uruguay. Los depósitos de AS-29 y AS-33 mostraron el más alto contenido de Zn potencialmente disponible para el

medioambiente. Los depósitos de Chaitén, Llaima y Lonquimay podrían liberar principalmente Pb. La ceniza del Chaitén puede ser también considerada como un almacén de As. Por último, las cenizas de Hudson y Copahue pueden liberar principalmente Ni y Cu. Estas observaciones son fundamentales para la evaluación de riesgos geoquímicos de los depósitos de tales cenizas.

Algunos de estos los últimos elementos (As, Cu, F, Mo, Ni, Pb y Zn), debido a su potencial toxicidad, están incluidos en las normas de agua potable (ANMAT, 2007; INN, 2006; OMS, 2008). En consecuencia, se aconseja su control en la evaluación ambiental de estos depósitos de cenizas. Este aspecto es muy importante si tenemos en cuenta las condiciones ambientales en las que la ceniza se deposita. El drenaje de estos depósitos en cuencas hidrográficas pequeñas y cerradas como las de la Puna puede afectar a los flujos geoquímicos de los ríos y lagos, en especial inmediatamente después de las escasas lluvias, porque el proceso es muy rápido (Ruggieri et al., 2010). Por el contrario, la alta tasa de precipitación en el flanco occidental de la Cordillera de los Andes en la ZVS implica una interacción prácticamente constante con el agua y por tanto una activa meteorización de los depósitos de cenizas.

7.2 SBLTs con ácido nítrico

El ensayo de lixiviación con acido nítrico ha permitido evaluar la máxima cantidad extraíble de los ETPTs a partir de las cenizas volcánicas estudiadas (Ruggieri et al., 2010, 2011; Smith et al., 1982, 1983). Al igual que en el caso de las lixiviaciones con agua desionizada, la primera observación se relaciona con la mayor movilidad de los elementos en las cenizas antiguas. Esta circunstancia sugiere que el tiempo transcurrido desde el depósito de la ceniza volcánica tiene repercusión sobre el resultado de los ensayos de lixiviación confirmando la meteorización de la ceniza a lo largo del tiempo. Teniendo en cuenta los valores de masa relativa lixiviada obtenidos con ácido nítrico (*RML*, %), la movilidad de los elementos analizados en las cenizas volcánicas antiguas ha sido:

(1) elementos móviles (RML> 5%): Ca, Mg, Fe, Mn, P, As, Ba, Co, Cu, Mo, Ni, Sb, Sr, V, S, Zn, y REE;

(2) elementos moderadamente móviles (RML entre 0,5 y 5%): Na, K, Al, Ti, Be, Bi, Cr, Cs, Ga, Hf, Li, Nb, Pb, Rb, Sn, Ta, Th, Tl , U, y Zr; y

(3) elementos con baja movilidad (RML <0,5%): Si.

Para las cenizas volcánicas más recientes los elementos se agrupan de la siguiente manera:

(1) elementos móviles (RML> 5%): Ca, Mg, Fe, P, Co, Ni, Cu, Zn, As, Mo, V, Cd y Pb;

(2) elementos moderadamente móviles (RML entre 0,5 y 5%): Na, K, Mn, Li, Be, Al, Ti, V, Cr, Fe, Ga, Rb, Sr, Y, Sn, Ba, Hf, Tl, Bi, U y REE; y

(3) elementos con baja movilidad (RML <0,5%): Si, Mn, Zr, Nb, Sb, C, Ta y Th.

8. Ensayos en columna

Los ensayos de lixiviación en columna se han diseñado para evaluar la liberación de elementos en función del tiempo, obteniendo información sobre su potencial movilidad. Concretamente, se realizaron tres ensayos de lixiviación para: (1) evaluar las diferencias de movilidad de los ETPTs entre las cenizas antiguas (muestras 719 y 808) y una reciente (muestra CHA-1F); y (2) ver si estas diferencias de movilidad se ven afectadas por la granulometría de la muestra, considerando las fracciones <100 μm y 100-200 μm de la ceniza 719.

8.1 Ensayo en columna de las muestras 808, 719 y CHA-1F

<u>8.1.1 pH e hidrólisis</u>

Los valores de pH subieron rápidamente en todos los ensayos en columna llevados a cabo (característica precedentemente observada en los ensayos de tipo *batch*). Según varios estudios sobre la disolución de aluminosilicatos, el proceso se desarrolla en tres etapas: (1) el intercambio casi instantáneo de los iones alcalinos (Na^+, K^+, Mg^{2+}, Ca^{2+}) por H^+ (o como H_3O^+), es decir, con un aumento inicial de pH; (2) la generación y el crecimiento rápido de una capa residual pobre en esos álcalis y rica en silicio, y (3) la interacción de sólido-solución a través de la capa residual y el comienzo de una disolución incongruente (proceso necesariamente lento, con un pH menor que en los pasos anteriores) (Oelkers y Gislason, 2001; Oelkers et al., 2009; Schott y Oelkers, 1995; Wollast y Chou, 1992). La tercera etapa, la más lenta, controla el proceso de disolución acuosa. Estos son los procesos (junto con la disolución rápida de la fracción soluble) que explican la variación de pH. Entre

las cenizas volcánicas ensayadas, el mayor incremento de pH se observó en la muestra 808, que está prácticamente compuesta sólo por vidrio volcánico.

8.1.2 Disolución de sílice y aluminio

La tasa de disolución del vidrio volcánico puede ser razonablemente descrita en términos de variación de pH y concentración de aluminio (Duggen et al., 2010; Flaathen et al., 2010; Wolff-Boenisch et al., 2004.).

Una ceniza volcánica podría ser definida como compuesta por sílice amorfa y cristalina (incluyendo vidrio volcánico y cuarzo) y en menor cantidad aluminosilicatos (principalmente feldespatos alcalinos en este caso). Los dos tipos de sílice (amorfa y cristalina) están constituidos por cadenas altamente polimerizadas de SiO_4 en las que el grupo Si-O-Si es el grupo reactivo. Este grupo puede romperse por efecto del agua en dos pasos: (1) la absorción de agua cerca de un grupo Si-O-Si, y (2) la formación de un nuevo enlace Si-O por el oxígeno del agua adsorbida y la ruptura del grupo Si-O-Si (Schott y Oelkers, 1995). La disolución está asociada al último paso, que a 25 ºC implica un equilibrio entre la fase sólida y una forma monomérica de sílice (Si $(OH)_4$) en la solución (Alexander et al., 1954). El incremento de la sílice disuelta total (el componente mayoritario más abundante en las cenizas) a pH básico está bien establecida (Alexander, 1957) y se ha observado en los ensayos realizados

La estructura de los aluminosilicatos (por ej., feldespato alcalino) contiene cationes intercambiables (por ejemplo Na^+, Ca^{2+}) en dos sitios hidrolizables del polímero: grupos de silicatos (Si-O-Si) y aluminatos (Al-O-Si). Estudios experimentales evidencian que en la cadena tetraédrica los grupos aluminatos son más débiles que los enlaces Si-O-Si (Casey et al., 1989, Hellmann et al., 1990, Wollast y Chou, 1992). Estos estudios concluyen que el paso final durante la disolución de los aluminosilicatos es, como en los silicatos, la hidrólisis de los enlaces Si-O-Si. La disolución de Al en la muestras 719 y CHA-1F es debida también a la notable presencia de feldespatos alcalinos (constatada por difracción de rayos X). Por el contrario, la ausencia de aluminosilicatos en la muestra 808 explicaría el diferente comportamiento del Al de esta muestra respecto al de las muestras 719 y CHA-1F.

8.1.3 Comportamiento de los elementos mayores y trazas

La composición geoquímica de los lixiviados en los experimentos en columna fue controlada principalmente por la disolución incongruente del vidrio y de los minerales cristalinos (si existen) y la disolución de los revestimientos de las superficies de las partículas de ceniza. Por lo tanto, deberíamos distinguir entre los elementos rápidamente liberados a partir de la superficie de las partículas de ceniza y los relacionados con reacciones más complejas como los procesos de disolución. Los componentes con alta solubilidad en las primeras fases de los ensayos en columna han sido Ca, Na, Si, Cl⁻, SO_4^{2-}, Li, B, V, Mn, Rb, Sr, Mo, Ba y U. El tiempo necesario para que 200 ml de agua desionizada pasen a lo largo de la columna (es decir, ~26 horas) se considera suficiente para que empiece una rápida e incongruente disolución del vidrio volcánico (que es la fase más reactiva) mediante procesos de intercambio catiónico, que podrían ser también la fuente de los elementos antes mencionados (Rango et al., 2010). Elementos que intervienen en otros procesos, como la hidrólisis, han sido P, Fe y As. Estos elementos no muestran una marcada disminución durante el tiempo de lixiviación. Esta característica sugiere la relación con el proceso de disolución del vidrio y de las fases cristalinas. Si tenemos en cuenta el comportamiento de la lixiviación de la ceniza reciente CHA-1F, también B y V se pueden relacionar con procesos de disolución en estas condiciones experimentales. Es bien conocido que los últimos elementos (incluyendo As) están normalmente enriquecidos en las cenizas riolíticas debido a su incompatibilidad magmática.

8.2 Ensayo en columna de las fracciones granulométricas de la muestra 719

8.2.1 pH, y disolución de sílice y aluminio

Al igual que en los experimentos en columnas sobre ceniza total, el pH aumenta rápidamente cuando se produce la interacción ceniza-agua. Sin embargo, el muy rápido aumento de pH detectado en la fracción más fina (<100 µm) y que, a su vez, es la fracción con mayor cantidad de vidrio volcánico, indicaría una rápida disolución incongruente del vidrio volcánico y sería confirmada por la concentración más alta de Si lixiviado en esa fracción.

El comportamiento del Al resultó ser inverso respecto al de Si, presentando mayor concentración en la fracción gruesa (100-200 μm).

8.2.2 Comportamiento de los elementos mayores y trazas

Los componentes con alta solubilidad en las primeras fases de los ensayos en columna han sido Ca, Na, Mg, SO_4^{2-}, Rb, Sr y Ba. Este comportamiento fue similar en los tres experimentos indicando una débil asociación con las superficies de las partículas de ceniza independientemente de la fracción considerada. La combinación de dos procesos (es decir, la disolución incongruente de vidrio volcánico y la disolución del recubrimiento de las partículas) se considera la fuente de estos componentes. Los elementos trazas enriquecidos en la fracción de granulometría más pequeña han sido Li, B, P, V, Fe, Mo y U. Diferentes estudios asocian las elevadas concentraciones de algunos de los elementos antes mencionados (As, Mo, V, B, y U) en aguas subterráneas de la Pampa en Argentina con la presencia de altos contenidos de ceniza volcánica en los loess de los sedimentos de los acuíferos. Los resultados de la presente investigación confirman, a través de ensayos de laboratorio, la asociación de la disolución de las partículas de cenizas con los mencionados elementos trazas.

9. Extracción química secuencial

El diseño de una metodología de extracción química secuencial (EQS) aplicable a cenizas volcánicas ha sido otro objetivo de esta investigación. El enfoque metodológico ha sido, en primer lugar, definir las fracciones químicas de interés en una ceniza volcánica, proponer diferentes reactivos químicos para liberar los elementos a ellas asociados y, por último, establecer los reactivos químicos más adecuados a través de experimentos de lixiviación.

9.1 Definición de las fracciones químicas de interés en ceniza volcánica

Cuatro fracciones químicas básicas pueden ser consideradas:

(1) F1: los elementos no específicamente adsorbidos en las superficies de las partículas de ceniza y fácilmente liberables por procesos de intercambio iónico;

(2) F2: elementos asociados con los óxidos amorfos;

(3) F3: elementos asociados con los óxidos cristalinos; y

(4) F4: fase residual.

9.2 Posibles candidatos como reactivos químicos

Varios reactivos se han utilizado para la lixiviación de las fracciones químicas consideradas. Los reactivos químicos se eligieron después de una meticulosa revisión bibliográfica. La Tabla 1.1 muestra los reactivos químicos estudiados antes de la aplicación de la EQS.

Tabla 1.1 Reactivos químicos estudiados mediante ensayos de lixiviación antes de la aplicación de la EQS.

Fracción química	Reactivo químico	
F1	E1a	Agua desionizada
	E1b	NH_4NO_3-$(NH_4)_2SO_4$ 10^{-4}M a pH 7 con NaOH
F2	E2a1	NH_4Ac 0.25M a pH 4.5 con HNO_3
	E2a2	NH_4Ox 0.25M a pH 4.5 con HNO_3
	E2a3	NH_4Cit 0.25M a pH 4.5 con HNO_3
F3	E3	NH_4Ox 0.25M a pH 4.5 con HNO_3+ acido ascórbico 0.1M

Muchos procedimientos de extracción secuencial utilizan el agua desionizada como reactivo para la cuantificación de la fracción más móvil (es decir, elementos débilmente adsorbidos y que pueden ser fácilmente liberados por procesos de intercambio iónico). En este estudio los datos obtenidos a través de los ensayos *batch* con agua desionizada se compararon con los resultados obtenidos con NH_4NO_3 - $(NH_4)_2SO_4$ 10^{-4} M (E1b).

La lixiviación selectiva de la fracción extraíble a partir de los óxidos amorfos (F2) se ha propuesto mediante la extracción de ácidos amónicos orgánicos. A raíz de la propuesta de Chao y Zhou (1983), los resultados de tres ácidos amónicos orgánicos ($E2a_1$, $E2a_2$ y $E2a_3$) a una concentración 0,25 M y pH 4.5

(ajustado añadiendo HNO$_3$) sobre una ceniza se compararon a través de ensayos de lixiviación.

Varios autores propusieron el oxalato de amonio con la adición de ácido ascórbico (0.1 M) en la oscuridad a 70 ºC (30 min agitando) para la extracción de los elementos asociados con los óxidos cristalinos (Krishnamurti et al., 1995; Wenzel et al., 2001). A raíz de estas observaciones, esta solución se utilizó en este estudio.

9.3 Ajuste de las condiciones experimentales

La fracción F1 y F2 se estudiaron con el fin de:

(1) elegir el mejor reactivo en términos de eficacia de la extracción.

(2) definir el tiempo necesario para alcanzar la condición de pseudo-equilibrio.

La misma metodología se aplicó para cada uno de los reactivos químicos (E1b, E2a$_1$, E2a$_2$ y E2a$_3$). Los ensayos de lixiviación se realizaron a través de una batería de lixiviaciones de tipo *batch* a fin de obtener información sobre el comportamiento temporal de los elementos analizados. Estos incluyen:

(1) los elementos menos móviles durante los procesos de lixiviación (Al, Mn y Fe) (Chang, 1999; Gayer et al., 1958; Wollast y Chou, 1992);

(2) elementos traza (Zn, As, V, y Pb) que se combinan con los halógenos y los sulfatos y/o que reaccionan con los aerosoles en la pluma volcánica (Delmelle et al., 2007; Hinkley, 1991, 1994; Symonds et al., 1987, 1992, 1994) y están asociados con la disolución del vidrio volcánico en la Pampa de Argentina (es decir, As y V) (Francisca y Pérez, 2009; Nicolli et al., 2001, 2011).

9.3.1 Lixiviación de la fracción fácilmente intercambiable (F1)

Utilizando el reactivo E1b se observaron concentraciones apreciables sólo para As, V y Zn. Comparando estos resultados con los obtenidos mediante el ensayo *batch* con agua desionizada, este último reactivo resulta ser más apropiado. La hipótesis es que algunos elementos (es decir, Mn, Fe y Al) precipitan durante el tratamiento con E1b. En otras palabras, el reactivo E1b no es adecuado en el caso de ceniza volcánica y a partir de los resultados del *batch* la fracción fácilmente intercambiable se extrajo agitando la muestra con agua desionizada durante 4 horas a temperatura ambiente.

9.3.2 Lixiviación de la fracción de óxidos amorfos (F2)

La eficiencia de extracción del reactivo $E2a_1$ resultó escasa. Las curvas de lixiviación obtenidas con los reactivos $E2a_2$ y $E2a_3$ tuvieron tendencias temporales similares llegando al pseudo-equilibrio entre 2 y 4 horas. Sin embrago, concentraciones más altas se observaron con $E2a_2$. Teniendo en cuenta que una adecuada EQS tiene que ser rápida y fiable en condiciones de laboratorio y de acuerdo con la propuesta por Chao y Zhou (1983), la extracción de óxidos amorfos se realizó con una solución de $E2a_2$ 0.25 M a pH 4.5 (2 h de agitación) .

9.4 Aplicación de la EQS

Dos cenizas volcánicas riolíticas se utilizaron en este estudio: la ceniza del Chaitén (CHA-2R) y las cenizas antiguas (808) del sur de la Puna.

La suma de los porcentajes parciales extraídos de cada elemento en los primeros tres pasos de la EQS, es decir, exceptuando la fracción residual, se puede considerar la fracción potencialmente móvil y susceptible de introducir cambios medioambientales, afectando a parámetros como el potencial redox o el pH (Filgueiras et al., 2002; Hernández-Moreno et al., 2007). Los resultados muestran una baja movilización geoquímica para las dos cenizas. Sin embargo, la ceniza antigua presentó una mayor movilidad que la ceniza reciente. Este estudio demuestra que después de la liberación rápida de los compuestos solubles presentes en la superficie de partículas de las cenizas, la meteorización del vidrio y componentes cristalinos provoca una liberación muy lenta de los elementos en el medioambiente. Por lo tanto, el tiempo de residencia de la ceniza volcánica en el medio geológico tendría un importante papel sobre la lixiviación de los elementos. Desde el punto de vista metodológico, el método de EQS es una herramienta útil para evaluar la movilidad de los elementos tanto para cenizas volcánicas antiguas como para las recientes. La EQS propuesta proporciona información fiable sobre los elementos lixiviados en las fracciones químicas de interés. La F1 se puede utilizar para predecir los elementos más móviles y, por lo tanto, susceptibles de pasar con una mayor rapidez al medioambiente. Las fracciones F2 y F3 proporcionan información sobre la potencial lixiviabilidad de las fases sólidas como resultado de la meteorización. Dentro de las limitaciones inherentes al

fraccionamiento químico, los reactivos utilizados son bastante adecuados. Este estudio debe considerarse como un buen comienzo para el desarrollo y aplicación de esta metodología a la ceniza volcánica.

10. Conclusiones

Los resultados de los ensayos *batch* con agua desionizada se pueden resumir de la siguiente manera:

1) Los elementos enriquecidos en los lixiviados de las cenizas recientes corresponden a los principalmente involucrados en la interacción de gases volcánicos con las partículas de ceniza en la pluma volcánica.

2) Los elementos enriquecidos en los lixiviados de las cenizas antiguas son principalmente los que forman los minerales esenciales, sugiriendo que una vez depositada, la ceniza volcánica está sometida a irreversibles reacciones de meteorización que provocan una lenta desestabilización de la cadena tetraédrica de los silicatos y la lixiviación de los elementos asociados. La desestabilzación de la red de los silicatos de cenizas antiguas se ha deducido también por observaciones con espectroscopía FTIR, lo que permitió concluir la notable importancia de la estabilidad química del vidrio en la reactividad de la ceniza antigua.

(3) Experimentos dinámicos de lixiviación permitieron definir los elementos involucrados en la disolución del vidrio y de las fases minerales cristalinas. A partir de los datos actualmente disponibles, se demostró la asociación entre la disolución de cenizas procedentes de la zona sur de los Andes y algunos elementos traza (As, Mo, V, B, y U).

La información física y química de las cenizas (sobre todo las características morfológicas, distribución de tamaño de grano y la cuantificación del contenido total de ETPTs) debería ser conocida antes de la aplicación de ensayos de tipo *batch*.

En términos de movilidad de los elementos y, por tanto, de la contribución al balance geoquímico regional, esta investigación ha permitido modelar la fracción medioambientalmente disponible. Los datos demuestran que las cenizas antiguas y recientes podrían liberar considerable cantidad de elementos a través del agua. Los elementos mayoritarios más móviles son Ca,

Mg, Na, Si, K, y Al. A nivel de elementos trazas las cenizas de la Puna y Uruguay pueden liberar en el ambiente P, Ti, Fe, Mn y Zn. Se trata de macro y micronutrientes que acreditan el potencial fertilizante de las cenizas. Las cenizas del Chaitén mostraron altas concentraciones de As, Pb, Fe y Zn, mientras que las cenizas de Copahue, Lonquimay, LLaima y Hudson podrían liberar principalmente P, Ti, Mn, Ni, Zn y Pb. Muchos de estos ETPTs son potencialmente tóxicos incluso en concentraciones muy bajas. Algunos están incluidos en las normas de agua destinada al consumo humano y, por tanto es prioritario su control en la evaluación medioambiental de estos depósitos. Este aspecto es muy importante si tenemos en cuenta las condiciones ambientales en las que la ceniza se deposita. El drenaje de depósitos de cenizas en cuencas hidrográficas pequeñas y cerradas como las de la Puna puede afectar a los flujos geoquímicos de ríos y lagos, en especial inmediatamente después de las escasas lluvias, porque el proceso es muy rápido (Ruggieri et al., 2010). Por el contrario, la alta tasa de precipitación en el flanco occidental de la Cordillera de los Andes en la ZVS implica una interacción prácticamente constante con el agua y por lo tanto la meteorización rápida de los depósitos de cenizas.

Este estudio representa un gran avance en términos de enfoque metodológico en el conocimiento del riesgo geoquímico medioambiental de las cenizas volcánicas, en general, y de los Andes, en particular. El método de lixiviación *batch* con agua desionizada es una contribución muy importante de esta investigación a la armonización de ensayos de lixiviación aplicable a las cenizas volcánicas. Además, los experimentos de lixiviación en columna y el esquema de extracción secuencial complementan la información obtenida por los ensayos de *batch* facilitando la toma de decisiones sobre la gestión del riesgo geoquímico asociado a la caída de ceniza volcánica.

Extended abstract

1. Introduction

Volcanic eruptions are one of the most remarkable and powerful expressions of nature's force. Volcanoes display a wide range of eruption styles. In general, volcanic eruptions range from effusion of lava fountains and flows (typical of basaltic magma with low silica content) to extremely explosive events (typical of rhyolitic and dacitic magma with high silica content). Though volcanic ash is produced at least in some degree in most eruptions, the explosive eruptions are those that can inject large quantities of ash high into the stratosphere. Explosive eruptions are the most powerful and destructive type of volcanic activity. There are two basic types of mechanisms during an explosive eruption that produce volcanic ash: (1) magmatic by exsolution and expansion of gases in the magma, and (2) phreatomagmatic by chilling of the rising magma when contact with ground or surface water. Volcanic ash formation broadly occurs as a combination of both mechanisms.

1.1 Ash particle components and morphology

Volcanic ash consists of three main components: (1) glass shards and pumice grains, (2) fragments of minerals and (3) accidental lithic fragments. The properties of the ash depend mostly on the relative proportions of these constituents. The morphology of ash particles can help identify the nature of the eruption. Distinct fragmentation processes produce different textural features. The shape of glassy particles from magmatic eruption depends mainly on the kinetic evolution of gas (Verhoogen, 1951), which determine the number and density of bubbles. The morphology of ash particles from phreatomagmatic eruptions is controlled by stresses within the chilled magma which result in fragmentation of the glass to form small blocky or pyramidal glass ash particles.

1.2 Environmental impact of volcanic ash

Explosive volcanic eruptions are capable of causing significant environmental repercussions affecting, simultaneously, many cycles in the Earth system

(Jones and Gislason, 2008). Volcanic aerosols are an active component of the climate system and play multiple roles in physical and biogeochemical exchanges between the atmosphere, land surface and ocean (Niemeier et al., 2009). When volcanic ash is suspended in an eruptive column, a certain proportion of soluble component is condensed onto ash particles surfaces. Therefore, the environmental impact produced by volcanic ash fall includes:

(1) Short term release of soluble compounds present on particle surface (short term leaching);

(2) Long term release of elements from weathering of volcanic glass and crystalline mineral phases (long term leaching).

1.2.1 Short term leaching

The reactions occurring between gases/aerosols and silicate ash particles in volcanic eruption plumes remain poorly understood. Among the gases released those mainly involved are HCl, HF and SO_2. Hydrochloric and hydrofluoric acids will dissolve in water and fall as acid rain whereas most SO_2 is slowly converted to sulphuric acid (H_2SO_4) aerosols. Ash particles may absorb these aerosol droplets onto their surfaces, and subsequent fallout, as temperature and pressure decrease (Allard et al., 2000). Moreover, the formation of coating soluble salts on ash particle surfaces seem also likely due to partial dissolution of the ash through the reactions with acidic gases (i.e., mainly HCl, HF) and aereosols (i.e., H_2SO_4) of the plume, followed by precipitation at the ash liquid interface. This process has been postulated principally for the elements with a low volatility in magma (i.e., lithophilic elements) (Delmelle et al., 2007).

Upon deposition, the adsorbed materials can be dispersed into the environment. Interaction of pristine tephra with water dissolves soluble accumulations on particle surfaces resulting in changes of local water chemistry and, hence, quality (Jones and Gislason, 2008; Stewart et al., 2006; Witham et al., 2005).

1.2.2 Long term leaching

Volcanic glass may be viewed as metastable supercooled liquid (White, 1984). According to Nesbit and Young (1984) volcanic glass makes up ~12% of the

average exposed continental crust surface, being exceeded in abundance only by plagioclase (~35%) and quartz (~20%) (Nesbitt and Young, 1984). Pioneering studies on the aqueous dissolution of rhyolitic and other commonly occurring silicic glasses have been investigated by comparing the composition of the pristine glass phase with the residual composition of its weathered counterpart demonstrating substantial mobility of chemical species during the weathering (Lipman et al., 1969; Noble, 1967). Owing to its abundance and rapid mechanical and chemical weathering, glass plays an important role in the global and local cycling of numerous elements and chemical species at the Earth surface (Wolff-Boenisch et al., 2004b). Dissolution and secondary phase precipitation during weathering alter the chemistry of solutions in contact with glass and affect the chemical composition of surface water (e.g., rivers and lakes) (Stefansson et al., 2001; White and Claassen, 1980).

1.3 State of art of the ash leaching studies

For the short term leaching the existence of readily soluble materials on freshly erupted volcanic ash was documented for the first time at the beginning of the XX century (Lacroix, 1907). Since this observation, many leachate studies have been designed in order to quantify the volatile budget adsorbed onto ash in volcanic plumes. A review of 55 studies (which report the ash leachate data for 27 volcanoes) concluded that the comparison of leaching data is hindered due to the broad range of leaching methodologies used (Witham et al., 2005). As already explained, one of the main purposes of this Thesis is to propose a new ash leaching methodology in order to improve the need of harmonization previously commented by other authors (Witham et al., 2005).

Few works study the long term leaching of volcanic ash in terms of element release from an environmental point of view. Some of these works revise the dissolution rate of natural glasses by flow-through leaching tests (dynamic leaching test in which the leachant solution is continuously renewed) (Gislason and Oelkers, 2003; Wolff-Boenisch et al., 2004a, 2004b, 2006). Only few works focused on the element mobility from volcanic ash. Column laboratory experiments were employed to assess the leaching behaviour in terms of element release of pyroclastic glassy ash deposits collected in the central Main

Ethiopian Rift (Rango et al., 2011). Total fluxes of element release from volcanic ash of different historical eruptions (e.g., Hekla, 2000, Mt. St. Helens, 1980) were the aim of the study of Jones and Gislason (2008). This study was principally focused on the nutrient elements released in the sea water rather than the potentiallly toxic trace elements (PTTEs). Finally, there are a lot of studies which suppose the volcanic glass dissolution as geogenic source of some PTTEs (e.g., F, As, and Mo) in surface and groundwater in different parts of Argentina, (Bhattacharya et al., 2006; Bundschuh et al., 2004; Francisca and Perez, 2009; Nicolli et al., 1989, 2001, 2011).

2. Geographical and geological setting

The Andean Cordillera forms a >7,500 km morphologically continuous mountain chain along the western margin of South America. Four linear zones of active volcanism are present along the Andean Cordillera: Northern (NVZ), Central (CVZ), Southern (SVZ) and Austral (AVZ) Volcanic Zones. This study is concerned with the volcanic ash characterisation in the southern part of the CVZ and the northern part of the SVZ, hence, only these portions are described in this Thesis. The CVZ (16–28° S) of the Central Andes is one of the largest volcanically active regions of the world. Our study area (southern Puna region and neighbouring areas) is characterised by intermediate to acid volcanism magmatism (principally andesitic magma). The SVZ (33–46° S) includes, at least, 60 historically and potentially active volcanic edifices, as well as three giant silicic caldera systems. Ashfalls produced by historical eruptions of Copahue (2000), Lonquimay (1988), Llaima (2008), Chaiten (2008), and Hudson (1991) were investigated.

3. Sampling

Field works were carried out in different campaigns during the period 2006-2008. Twenty one supposed volcanic ash deposits in the southern Puna and neighbouring areas (Catamarca and Salta provinces, Argentina) and eight supposed volcanic ash deposits in Uruguay were sampled. Many of the ash deposits are extremely well preserved due to the hyper-arid conditions which are prevailing in the region for millions of years (Garcia-Vallés et al., 2008;

Stern, 2004). In Uruguay the study area is located between 33 and 34º S and between 56 and 58º W. The samples collected were deposited during the Pleistocene with alternance of semiarid and temperate conditions (Aguilar, 2006; Calarge et al., 2006; Ubilla et al., 2004). Samples from Copahue, Lonquimay, Llaima, and Hudson volcanoes were generously provided by the Chilean institution SERNAGEOMIN (Dr. J. Naranjo). Three Chaiten ashes were sampled in the field by a member of PEGEFA research group (Dr. E. Polanco) and one sample was supplied by Dr. A. Caselli (Universidad de Buenos Aires, Argentina). Three Chaiten ashes were collected during the initial explosive phase and one was collected later.

4. Ash characterisation

The methodological part can be considered the main body of this work. Figure 1.1 summarises the techniques used to characterise several volcanic ashes from the central and southern Andean volcanic zones.
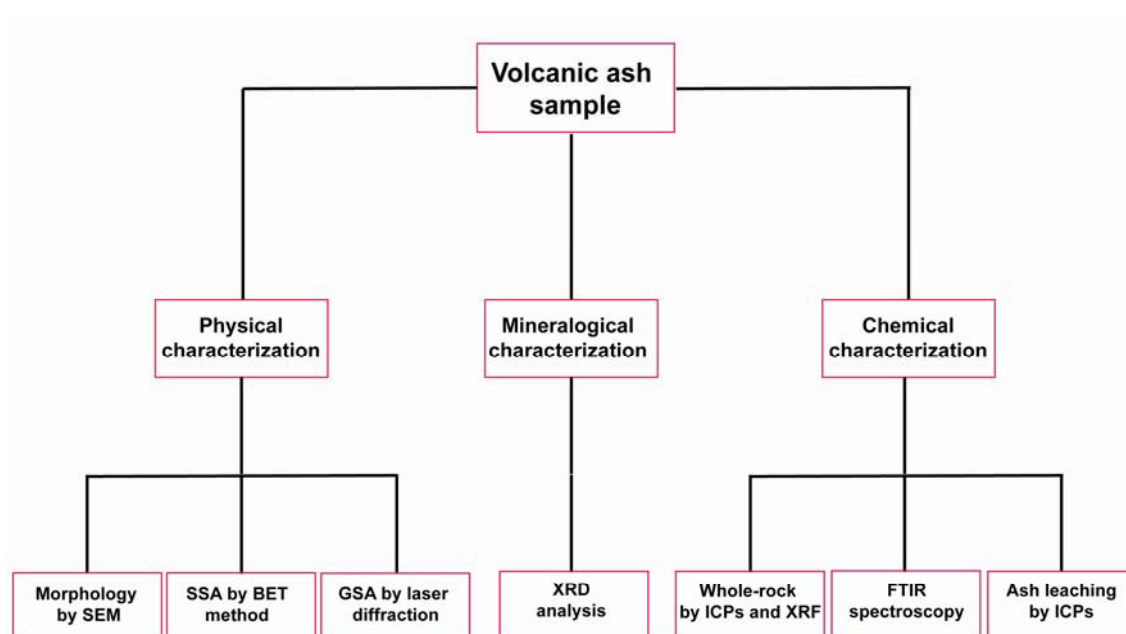
Figure 1.1 Summary of the analytical techniques used in this research. SEM, Scanning Electron Microscopy; SSA, Specific Surface Area; BET, Brunauer-Emmett-Teller; XRD, X-Ray Diffraction; ICP, Inductively Coupled Plasma; XRF, X-Ray Fluorescence; FTIR, Fourier transform infrared.

After the bulk characterisation (physical, mineralogical and chemical) the contribution of the volcanic ash to the local geochemical balance was carried out by different types of leaching tests. They include:

(1) Short term leaching behaviour of volcanic ash by single batch leaching tests (SBLTs). In the present study, two SBLTs were performed using deionised water and nitric acid as leachant. The former leachant allows a rapid screening of the potentially hazardous elements that can be leached from the ashes. Nitric acid extraction is useful for the assessment of the maximum load of PTTEs environmentally available (Papastergios et al., 2009, 2010; Sastre et al., 2002). In addition, it reproduces environmental circumstances in which very acidic conditions occur (e.g., Agro river in the Copahue volcanic area). (2) Temporal leaching behaviour of potentially hazardous elements by column leaching test. (3) Sequential extraction scheme (SES) to obtain information on element phase associations and their potential mobility.

4.1 Analytical techniques

Most of the analyses have been carried out at the Serveis Cientifico-Tècnics, Universitat de Barcelona, the Institute of Earth Sciences, J. Almera, CSIC, Barcelona, and at the Italian National Agency for New Technologies, Energy and Sustainable Economic Development (ENEA), Rome.

The physical characterisation of volcanic ashes has been divided in the study of the morphological properties of particles using Scanning Electron Microscopy with an Energy-Dispersive Analyser (SEM-EDX) using a FEI Quanta 200 instrument, the analysis of the Specific Surface Area (SSA) by the application of the gravimetric nitrogen Brunauer-Emmett-Teller (BET) surface analysis technique, and the grain size analysis (GSA) by laser diffraction using a Malvern Masterziser 2000 HydroMU.

The mineralogical characterisation of all volcanic ashes was made by X-ray diffraction (XRD) analysis using a Bruker D-5005 instrument. In this research a quantitative XRD method was applied only to one volcanic ash (sample No. 719) in order to define the best operating conditions for the GSA analysis. The quantitative mineralogical composition was done with the RockJock method of Dr D.D. Eberl (Andrews et al., 2006; Eberl, 2003).

The analytical methodology presented for the whole-rock chemical analysis has been developed for the determination of major and trace (including REE) elements that can be applied to all kind of volcanic rocks (see Protocol for the determination of major and trace elements in rocks by means of total attack in Appendix 1). The solutions obtained by the acid attack of the whole-rock were analysed using Inductively Coupled Plasma–Optical Emission Spectrometry (ICP-OES), Inductively Coupled Plasma–Mass Spectrometry (ICP-MS), and single collector High Resolution–Inductively Coupled Plasma–Mass Spectrometry (HR-ICP-MS) as follows:

- Major elements (Al, Ca, Fe, K, Mg, Mn, Na, P, Ti, and Si) and trace elements (Ba, Sr and Zr) through ICP-OES or HR-ICP-MS;
- Trace elements (including REE) by ICP-MS or HR-ICP-MS;
- SiO_2 (%, m/m) content was indirectly determined taking into account the rest of the major oxides and LOI values.

The leachant solutions obtained by the ash leaching tests were analyzed using ICPs as follows:

- Major elements (K, Na, Ca, Mg, Sr, Fe, S, P, B, and Si) through ICP-OES or HR-ICP-MS;
- Trace elements (including REE) by ICP-MS or HR-ICP-MS.

Concentration of Zr and Nb were determined by X-Ray Fluorescence Spectrometry (XRF).

Furthermore, the fluorine determination in water ash leachates was done by the Ion Selective Electrode (ISE) technique.

Fourier transform infrared (FTIR) spectroscopy is a powerful technique for studying molecular structures. FTIR was used to provide information about structural chemical bonds of the water present in the ashes (i.e., total amount of H_2O (H_2O_t), H_2O molecular (H_2O_m) and OH). The samples were examined with a Perkin-Elmer Spectrum 2000 instrument Optical FTIR 16PC.

5. Sample selection and characterisation

5.1 Physical characterisation

5.1.1 Morphology and texture by SEM-EDX

Scanning electron microscopy (SEM) and the Energy Dispersive X-Ray (EDX) spectra of single particles allow unequivocally identify ash deposits. Thus, from 29 potential volcanic ash deposits sampled in the southern Puna and Uruguay, the SEM-EDX analyses confirmed that only 11 corresponded to volcanic ash deposits. These samples were constituted by glass and minor amounts of crystalline phases. The other samples were mixed sediments in which volcanic ash particles coexist with non volcanic particles (e.g., biogenic silica, mainly as diatoms) or samples with a total absence of volcanic ash particles.

After SEM observation, the samples were classified as follows:

(1) Samples UR-1, UR-6, UR-7, and 808 were almost fully glassy with abundant Y-shaped, plate like, curved, and angular shards and abundant fine size particles (<5 µm).

(2) Samples 719, 721, 733, 809, AS-28, CHA-1F, CHA-2R, CHA-G, CHA-E were glassy with a certain amount of crystalline phases; the amount of particle size <5 µm was abundant.

(3) Samples AS-29 and AS-33 consist of poorly vesicular equant blocky fragments (5-200 µm) of glass, high content of crystalline phases and rare fine grain-size particles.

(4) Samples COP, LON, LLA, and HUD were poorly vesicular with equant blocky fragments (5-200 µm) of glass, scarce fine grain-size particles and relatively low crystal content.

These groups likely fingerprint different explosive volcanic styles. Magmatic eruption was inferred for groups 1 and 2. The high content of glass with practically no crystals in the 1 group indicates a very fast ascent of magma to the surface, whereas the high content of fine grains in group 2 could indicate highly explosive eruptions. The shape of the group 3 indicates fragmentation by thermal fracturing (i.e., angular edges) associated with phreatomagmatic eruptions. The same shape features were observed for Hudson, Copahue, Llaima, and Lonquimay ashes confirming results of previous works (Kratzmann

et al., 2009, 2010; Naranjo and Moreno, 1991; Naranjo and Polanco, 2004; Naranjo et al., 1992; Naranjo and Stern, 1998).

5.1.1 Specific Surface Area (SSA)

The Specific Surface Area (SSA) analysis was performed on the mixed and pure ashes from Puna and neighbouring area. SSA results of pure volcanic ashes were between 0.55 and 7.74 m^2 g^{-1} with the lower value for 719 ash and the higher for the 808 sample. In pure volcanic ash, the differences between the SSA values are related to the sizes of ash particles and morphology (e.g., vesicle content) (Papelis et al., 2003). These results were consistent with particle morphology observed by SEM images. The higher SSA values found in impure ashes were due to the occurrence of clay minerals and/or biogenic silica, which typically develop large SSA (Fowler et al., 2004; Fubini, 1997).

5.1.2 Grain-size analysis

The grain-size analysis (GSA) by laser diffraction shows that some samples tended toward an unimodal distribution. High content of large particles (500-1000 µm) were reported in samples AS-29, AS-33, COP, LON, LLA, and HUD, in contrast to samples 808, UR-1, UR-6, UR-7, CHA-E which presented fine size (10-100 µm) contents. Other samples (721, 809, CHA-2R, and CHA-G) presented a bimodal distribution with peaks at 10-50 µm and 50-100 µm. Finally, samples 719, 733, AS-28, and CHA-1F indicated a multimodal distribution.

The amount of fine particles is important because reflect several features including: (1) Style and dynamics of eruption; (2) geographical location, i.e., the distance from the volcano to the sampling site; (3) higher environmental hazard, i.e., high contents of small particles are potentially more dangerous than samples composed by large particles.

In general, basaltic volcanoes produce relatively small amount of fine particles when compared with more silicic eruptions. This feature was visible in the ashes under study being the rhyolitic samples (including most of the ashes from Puna, Uruguay, and Chaiten volcano) much more fine-grained than the less silicic ashes (samples COP, LON, LLA, and HUD). The Chaiten ashes are the only

samples collected in this study from the same volcano in which we can observe a possible increase of fine grain-size with the distance. However, the Chaiten ashes present similar fine grained content (<10 µm) in the closest ash to the vent (sample CHA-1F) than in the furthest samples (CHA-G and CHA-E), being 20-24 volume (%). The grain size distribution in the Chaiten ash samples suggests a possible evolution during the 2008 eruption passing from a bimodal distribution in the initial phase (sample CHA-G) to a more homogeneous distribution afterwards (samples CHA-1F and CHA-E, collected only a few days later). Moreover, the sample CHA-2R collected on August 2008 (after dome collapse) presents the same distribution of the sample collected during the first fallout.

The amount of very fine materials (<5 µm) in the ashes under study varies from 1.16-40.9 volume (%). High fine content implies a greater environmental and health hazard because particles with aerodynamic diameter lower than 4 µm are considered "respirable" (Horwell, 2007). Taking into account the fine materials lower than 10 µm, the environmental hazard posed by the ash under study could be as follows: UR-1>721>808>809>CHA-1F> 733>CHA-G>AS-28>UR-6>719>CHA-2R> CHA-E> UR-7> AS-29> COP >LLA> AS-33> HUD> LON.

5.2 Mineralogical characterisation

Mineralogical composition allowed to organize the samples into four groups:

(1) Ancient volcanic ashes from Puna and neighbouring areas. The glass was accompanied by minor amounts of quartz, albite, sanidine, and biotite. Samples 721 and AS-28 present cristobalite and sample 808 was made up only of volcanic glass.

(2) Ancient volcanic ashes from Uruguay composed only by volcanic glass.

(3) Recent volcanic ashes from the SVZ (samples COP, LON, LLA, and HUD), in which conspicuous amount of anorthite was detected.

(4) Pristine volcanic ashes from Chaiten eruption, in which quartz, andesite, and remarkable amount of cristobalite were identified.

5.3 Bulk chemical analysis

The studied volcanic ashes have been geochemically classified using the Total Alkali *vs.* Silica (TAS) diagram as follows:

(1) Basaltic sample: LLA;

(2) Trachy-basaltic sample: HUD;

(3) Basaltic trachy-andesitic samples: LON and COP;

(4) Rhyolitic samples: 719, 721, 733, 808, 809, AS-28, AS-29, AS-33, UR-1, UR-6, UR-7, CHA-1F, CHA-2R, CHA-G, and CHA-E.

5.4 FTIR spectroscopy

FTIR was used to provide information on the water chemical bonds present in the volcanic ashes under study. The IR spectra allow estimating the H_2O_t content by integration of the area under the peak at 3612-3411 cm^{-1} wave number. It is well known that rhyolitic magma may have a great amount of water if compared with less silicic magma. This feature explains the lower integrated area of water peaks in the IR spectral of the low silica ashes from the SVZ respect to the rhyolitic samples of Chaiten volcano. Moreover, the ancient samples (Puna and Uruguay) present high water content than the more recent ashes (i.e., Chaiten volcano). During weathering the water migrates into glass predominantly as H_2O_m (Yokoyama et al., 2008). Following this remark, spectra of Puna and Uruguay rhyolitic ashes indicate that they are affected in some degree by weathering.

5.4.1 Ash reactivity

The structure of a silicate melt is altered with the dissolution of water (changing their physical and chemical properties). The dominant classical idea consist of water dissolves in silicate melts and reacts with the melts (highly polymerized) breaking the chains of the tetrahedral bonds (Si, Al)O_4 with oxygen, resulting two OH ends of two shorter chains by depolymerisation (Dingwell, 1998). This means that the fragility increases as the degree of depolymerisation increases (Giordano et al., 2009). From an environmental point of view, a high degree of depolymerisation of volcanic glass implies more ash reactivity (Ruggieri et al., 2010).

Pioneering studies show that the distribution of OH and water in the glass formed by melt quenching reflects their distribution on melt, except at very high temperatures (Ihinger et al., 1999; Stolper, 1982, 1989). Following these works, this research proves that conspicuous amount of hydroxil groups are present in these samples, indicating a relative disruption of the silicate network, which in turn affects the chemical stability of the glasses. High ash reactivity depends not only on glass content but this feature is particularly remarkable in ancient ashes. As result, the role of glass in the release of major, minor and trace elements is potentially greater in ancient ashes than in current ones. Taking in to account the amount of hydroxyl groups present in glass as a proxy of ash reactivity the studied ashes can be ordered: 809>719~721~733~AS-28>AS-29~AS-33>CHA-G~CHA-2R~CHA-1F~CHA-E>COP>LON>LLA~HUD.

However, this classification must be taken with caution because many factors control the reactivity of a given ash in the environment (i.e., grain size particles, geological setting of the ash deposits, etc.).

6. Design of a single batch leaching test (SBLT) with deionised water

Leaching tests are often designed to simulate the release of potentially toxic trace elements (PTTEs) under laboratory conditions in order to assess the environmental impact of ash deposition. Such tests consist of leaching in one step a fixed amount of ash with a fixed amount of leachant. A review of 55 studies reporting ash leachate data for 27 volcanoes concluded that the use of a wide range of methodological variable values (in leachant composition, contact time and liquid to solid or L/S ratio) makes the comparison between the different studies difficult. This review concludes that a great need of harmonization is advisable (Witham et al., 2005). In this research a proved methodology for a single batch leaching test (SBLT) with deionised water is proposed. The appropriate experimental conditions were chosen studying the factors that influence the rate at which the constituents are dissolved from the matrix. These factors can be divided in once intrinsically linked to the properties of the ash (primary factors as porosity, particle size, etc.), and those depending on the leaching conditions that can be varied to design more suitable

procedures (control factors as pH, leachant type, L/S ratio). The main purpose of the SBLT proposed in this Thesis is a rapid and reproducible screening of soluble constituents simulating ordinary natural conditions. Therefore, it was previously decided to perform the SBLT under some fixed conditions: (1) using no ground and no sieved volcanic ash; (2) using non-aggressive leachant as deionised water; (3) at room temperature.

Two rhyolitic volcanic ash samples have been selected to cover a wide range of ash age (2008 Chaiten eruption- CHA-1F- and ancient 719 ashes). The SBLTs were conducted at different conditions of L/S ratios, varying the amount of ash (0.1 and 1 g), leachant volume (1, 2.5, 10, 25, and 50 ml of deionized water) and contact time (1.5, 4 and 16 h). Four replicates were run to ensure the reproducibility of the experimental data conditions, resulting 18 tests by ash sample and a total of 72 leachate samples. Element selection covers the geochemical behaviour range of the main groups of elements implied during leaching and takes into account:

(1)   the less mobile elements during the leaching processes (e.g., Si, Al, Mn, and Fe) (Chang, 1999; Gayer et al., 1958; Wollast and Chou, 1992);

(2)   highly soluble components (i.e., SO_4^{2-}, and Cl^-) with preferential enrichment on tephra surfaces (Delmelle et al., 2000, 2007);

(3)   elements dominantly combined with halogens and sulphate forming salts (e.g., Ca, Na, Mg, Ba, and Sr) and acid droplets on particle surfaces in pristine ashes or associated with the volcanic glass dissolution during dry weathering environment (e.g., As, Ni, V, Mo, and Sb) (Hinkley, 1991, 1994, 1999; Nicolli et al., 2001, 2011; Francisca and Perez, 2009; Symonds et al., 1987, 1992, 1994). Data set was statistical treated with the STATA 10.0 software. Hence, in terms of statistical observation, the experimental conditions that produced low dispersion of values (and therefore high reproducibility of the leaching tests) were investigated.

6.1   Amount of volcanic ash and L/S ratio

In general, higher concentrations were reported by the lowest amount of sample (0.1 g). Although it seems contradictory, a low amount of sample allows extracting more actively the species present in volcanic ash. This amount is a

good option because it detects better the analytes under study. However, the results show that ash amounts of 0.1 g have a lower reproducibility of the leaching tests than 1 g of ash for all the leachant volumes tested. This aspect is clearly detectable for highly soluble compounds (as SO_4^{2-} and Cl^-), the alkali elements (as Na, Ba, Sr, and K) and trace elements (as As, Ni, V, Mo, and Sb) dominantly combined with halogens and sulphate on tephra surfaces, whose concentrations should be only limited by their available amount in the ash. These results indicate that a low amount of sample is not always representative of the ash under study, because it is more difficult to reach the chemical equilibrium in these experimental conditions.

In general, the leachant volume has a low influence on the element release when 1 g of sample is employed in the leaching tests. Lower reproducibility was obtained at high L/S ratio (mainly at high contact time). Furthermore, the L/S ratio is an interesting variable designing a leaching test due to analytical reasons. The choice of a high L/S ratio means a larger dilution, which could lead to the inconvenience of concentrations close or lower to the detection limits.

6.2 Leachability as a function of contact time

Contact time is an important factor because it is directly associated with the heterogeneous chemical reactions occurring when the volcanic ash interacts with water. Statistical treatment of the data set shows that contact time affects the released fraction of many elements, especially when the low contact times (1.5 and 4 h) are compared with 16 h. However, highly soluble elements (as SO_4^{2-} and Cl^-) become mobile immediately after contact with water and reach the same leached fraction independently of this factor. Leachability of other elements (as Ca, Sr, Cu, and As) may be controlled by many other processes, some of them dependent of the contact time. This feature may be due to several reactions occurring in solution. They vary from fast reactions (e.g., dissolution of alkaline compounds, acid-base or complexation reactions) (Oelkers et al., 2009; Toscano et al., 2008) to slower reactions (e.g., surface sorption, precipitation, dissolution, and redox reactions) (Stumm and Furrer, 1987). This aspect is complex in the ash leaching system because the solid

phase is multicomponent, containing many discrete phases of different solubilities (mainly glass but also some crystalline minerals). The worst reproducibility was obtained at low (1.5 h) and high (16 h) contact times, especially for the pristine ash (CHA-1F) leaching. Therefore, leaching tests performed at 4 h produced the best results.

6.3 Proposed leaching test for volcanic ash

Considering the experimental results obtained in this study, the proposed procedure is as follows:

(1)   Unground and unsieved volcanic ash must be used.

(2)   Use deionised water as leachant because is the best leachant if the purpose is the accurate, reproducible and rapid screening of soluble constituents. Moreover, it is a worldwide available and allows comparing the results among different laboratories.

(3)   Use an L/S ratio of 10 (reached by the mixture of 1 g of ash and 10 ml of deionised water).

(4)   Determine the leachate pH immediately after the contact between the ash and water and at the end of the experiment.

(5)   Shake the mixture for 4 h in polypropylene or polyethylene reactors.

(6)   Filter the mixture using 0.45 μm surfactant-free cellulose acetate membrane filters. Centrifuging samples prior to filtration will prevent clogging of the membranes facilitating ash sample recovery.

Leaching test results must be expressed either as leachate concentration (mg l^{-1}) or as release of constituent (mg kg^{-1} of dry material). The basis selected for expressing depends on the type of data which is desired to be compared. Results expressed as leachate concentrations allow a comparison of constituents/compounds solubility in the specific leaching conditions (e.g., contact time, L/S ratio, etc.). The mass leached data allow determining the fraction available for leaching and, making the comparison between samples easier.

7. Single Batch Leaching Tests (SBLTs)

In the present study, two batch leaching tests were performed using deionised water (following the methodology proposed above) and nitric acid as leachants. Nitric acid extraction is useful for the assessment of the maximum load of PTTEs environmentally available (Papastergios et al., 2009, 2010; Sastre et al., 2002). In addition, the acid leaching is a very useful tool because it reproduces environmental circumstance in which very acidic condition occurs (e.g., Agro river in the Copahue volcanic area).

7.1 SBLTs with deionised water

The application of the SBLT (with deionised water) method developed in the latter chapter have allowed to define the potential geochemical impact of the volcanic ashes investigated on the environment.

Geochemical data of major elements (mg kg^{-1}) and trace elements (µg kg^{-1}) in water ash leachates of ashes were statistical observed with the R software package (R Development Core Team, 2010). The pH and the specific conductivity (SC) was monitored in duplicate batches at the beginning (pH$_0$ and SC$_0$), immediately after ash–water mixing, and at the end of the experiment (pH$_f$ and SC$_f$), without filtering.

7.1.1 pH and Specific Conductivity

The geochemical pH data of ash leachates suggests that immediately after adding deionised water (with a pH slightly acid) to the ash, the pH increased to weakly alkaline (pH$_0$) for ancient ashes, except samples from Uruguay. Instead, the pH$_0$ of recent ashes was acid, except for one of the Chaiten samples. After 4 h of shaking, the leachates increase the pH. Exceptions are samples 808 and 809 suggesting that the slow geochemical processes (e.g., hydrolysis) which decrease pH have started. The increase of pH is due to both a fast and large dissolution of alkaline compounds present on the particle ash surface.

Specific conductivity (SC) gives an idea of the ionic constituents in solution. The final SC$_f$ values were usually twice or much higher than the initial SC$_0$ in the ancient ashes. Lower increments were observed in the recent ash leachates than in the ancient ash leachates. These features suggest a low amount of

readily soluble materials in the recent ashes than in the ancient ashes, as well as in the rhyolitic ashes than in the basaltic ones.

7.1.2 Comparison of ancient *vs.* recent water leachates

There are interesting differences between recently erupted volcanic ashes and ancient ashes. Ancient volcanic ashes were deposited tens to hundreds of thousands of years ago and during this time they were affected by hydrological and oils processes, which effectively removed any soluble salts attached to the surface of ash particles. Statistical treatment of the data set showed that in terms of median values some compounds (i.e., Ca, Mg, Cl^-, SO_4^{2-}, F^-, Mn, Ni, Cu, As, Sr, Mo, Ba, and Pb) presented higher values in the pristine ash leachates, whereas some others (i.e., Na, Si, Al, P, Ti, V, Fe, Zr, and U) showed higher concentrations in the ancient ash leachates. The elements enriched in pristine ash leachates were usually implicated in the chemical reactions occurred in the volcanic plume. Independently of the magma silica content, sulphates and chlorides are the major compounds observed in Chaiten, Hudson and Copahue ash water leaching tests. The F^- release from the Hudson ash is far greater than for any other sample. The trace elements (e.g., Ni, Cu, As, Sr, Ba, and Pb) enriched in the pristine water leachates correspond to the elements dominantly combined with halogens and sulphate forming salts and/or acid droplets coating the ash-grain surfaces (Delmelle et al., 2007). The elements with preferential enrichment (i.e., Na, Si, Al, P, Ti, V, Fe, and Zr) in the ancient ash leachates should come from different origin than ash-acidic gases interaction in the volcanic plume. Some of these are termed as rock forming mineral elements (e.g., Si, Al, Ti, Fe) which are usually defined as the less mobile elements during the weathering processes.

Principal Component analysis (PCA) performed on the water ash leachate data allows to split the samples by geological age. Differences between ancient and recent ash leachates were separated better by the PC2 axis. This was mainly produced by positive weights of Mn, Zn, Mg, SO_4^{2-}, F, Ca (more abundant in recent ash leachates) and negative contribution of B, Si, Fe, V, and Ti (more abundant in the ancient ash leachates), corroborating the observations reported above. In order to assess the statistical separability of the two types of ash

leachates, PCs were used to calculate the Jeffries-Matusita (JM) distance. The JM values proved high separability (JM = 1.99), implying great difference in terms of leachate composition (Richards, 1986).

7.1.3 Contribution to regional geochemical balance

The relative mass leached factors (RMLs, %), defined as the fraction of leached element (element/solid by weight), obtained from the batch leaching tests have allowed to predict the amount of the elements easily transferable to the environment through the water pathway. The values obtained from the ashes investigated showed that major elements (i.e., Ca, Mg, Na, Si, K, and Al) potentially releasable in the environment for both ancient and recent ashes. Puna and Uruguay ash could release in the environment the same trace elements (P, Ti, Fe, Mn, Zn, and Sr) but at different concentrations. Some of these are rock forming mineral elements supporting the idea that once deposited, the volcanic ash undergoes irreversible geochemical weathering reactions (e.g., oxidation followed by slow dissolution), causing destabilization of the silicate framework and release of the elements associated with it. More variability was observed in recent ashes. Chaiten ashes show high amount of As, Pb, Fe, and Zn environmentally available, whilst the other samples (i.e., COP, LON, LLA, and HUD) can release principally P, Ti, Mn, Zn, and Pb.

From this data the estimation of element amounts that each eruption (i.e., entire ash deposits) under study could potentially transfer to the environment by water pathway has been inferred. Additional knowledge (i.e., the volume of the pyroclastic materials ejected during each eruption expressed as dense rock equivalent, V_{DRE}, and the density of the samples) was necessary for this calculation. The V_{DRE} has been taken from the literature or has been modelled. Final results showed that both ancient and recent ashes could transfer to the environment high amounts of major elements, mainly Ca and Na. Some of the elements available from these ash deposits are macro- and micronutrients (e.g., Mn, Fe, and P), evidencing the fertilizing potential of the ashes. Many others are potentially toxic trace elements (PTTEs). The environmentally amounts of the PTTEs (i.e., As, Cu, Mo, Ni, Pb, Zn, and U) available have shown a substantial variability. Puna ash deposits of samples 719, 721, 808, 809 and AS-28 showed

high environmental available content of Pb, As, and Cu. Lead, Cu, and Ni were enriched in 733 and Uruguay ash deposits. High content of available Zn was displayed for AS-29 and AS-33 ash deposits. Chaiten, Llaima, and Lonquimay tephra deposits might release mainly Pb. The Chaiten deposit could considered also a reservoir of As. Finally, Hudson and Copahue might release mainly Ni and Cu in the environment. These observations are coherent with the results of the statistical treatment of the data set and are the basis for the environmental monitoring of these ash deposits.

Some of the latter elements (As, Cu, F, Mo, Ni, Pb, and Zn) are included in the drinking water guidelines (ANMAT, 2007; INN, 2006; WHO, 2008) due to their potential toxicity even at very low concentrations and must be especially monitored in the environmental assessment of these ashfall deposits. This aspect is very important if we take into account the environmental conditions in which the ash is deposited. The drainage in small and closed hydrographic basins such as the ones in the Puna can greatly affect the geochemical fluxes of streams and lakes, especially immediately after the scarce rainfalls, because the process is very fast (Ruggieri et al., 2010). On the contrary, the high rainfall on the western flanks of the Andean Cordillera in the SVZ implies a practically constant interaction with water (and therefore weathering) of the ash deposits.

7.2 SBLTs with nitric acid

Acid leach tests remove larger amount of material from ash than water (Ruggieri et al., 2010, 2011; Smith et al., 1982, 1983). As in the case of the water ash leaching tests, the first general observation is related to the higher capability of element mobility in ancient ashes respect to recent ashes. This feature suggests that the residence time of the volcanic ash in the environment seem to have a critical reflection on the element leachability. Once deposited, the volcanic ash undergoes irreversible geochemical weathering reactions (e.g., oxidation followed by slow dissolution), causing destabilization of the silicate framework and release of the elements associated with it.

The calculated Relative Mass Leached (RML %) values indicate that for ancient volcanic ashes the element mobility was as follows:

(1) High mobile elements (RML > 5%): Ca, Mg, Fe, Mn, P, As, Ba, Co, Cu, Mo, Ni, Sb, Sr, V, Y, Zn, and REE.

(2) Moderate mobile elements (RML between 0.5 and 5%): Na, K, Al, Ti, Be, Bi, Cr, Cs, Ga, Hf, Li, Nb, Pb, Rb, Sn, Ta, Th, Tl, U, and Zr.

(3) Low mobile elements (RML < 0.5%): Si.

For more recent volcanic ashes the mobility was:

(1) High mobile elements (RML > 5 %): Ca, Mg, Fe, P, Co, Ni, Cu, Zn, As, Mo, V, Cd, and Pb.

(2) Moderate mobile elements (RML between 0.5 and 5 %): Na, K, Mn, Li, Be, Al, Ti, V, Cr, Fe, Ga, Rb, Sr, Y, Sn, Ba, Hf, Tl, Bi, U, and REE.

(3) Low mobile elements (RML < 0.5 %): Si, Mn, Zr, Nb, Sb, Cs, Ta, and Th.

8. Column leaching tests

A dynamic test as a column leaching test can be designed to evaluate the release of species as a function of time, giving information on the breakthrough of the leached compounds and their potential mobility.

Three column leaching tests were carried out being the main objectives:

(1) to understand the differences in mobility of PTTEs between pristine (sample CHA-1F) and ancient volcanic ashes (samples 719 and 808).

(2) to know the mobility difference of PTTEs in grain size-fractions (<100 μm; 100-200 μm) of 719 ash.

8.1 Column leaching tests on raw ashes

<u>8.1.1 pH and hydrolysis</u>

The pH value rises quickly upon leachant contacts with ash in all the experiments (as previously shown for water ash batch leachates). According to several studies on aluminosilicate dissolution, the process develops in three stages: (1) virtually instantaneous exchange of the alkaline ion (Na$^+$, K$^+$, Mg^{2+}, Ca^{2+}) by H$^+$ (or as H$_3$O$^+$), i.e., with initial increase of pH; (2) generation and fast growth of a residual layer poor in that alkalis and rich in Si; and (3) interaction of solid-solution through the residual layer and beginning of an incongruent dissolution (process necessarily slower, at pH lower than in previous steps) (Oelkers and Gislason, 2001; Oelkers et al., 2009; Schott and Oelkers, 1995;

Wollast and Chou, 1992). The third stage, the slow one, controls the process of aqueous dissolution. These are the processes (together with dissolution of soluble fraction) taking place on the column leaching tests studied here explaining the variation of pH. Among the volcanic ashes the sharpest pH was shown for sample 808, which is practically made up only of volcanic glass.

8.1.2 Silica and aluminium dissolution

The rate of silicate glass dissolution in the aqueous phase can be reasonably described in terms of pH and aluminium dependencies (Duggen et al., 2010; Flaathen et al., 2010; Wolff-Boenisch et al., 2004).

Volcanic ash could be defined as formed by amorphous-crystalline silicates (including volcanic glass and quartz) and minor amount of aluminosilcates (i.e., principally alkali feldspars in our samples). Both silicates (i.e., amorphous-crystalline) have highly polymerized chains of SiO_4 in which the silicate group (Si—O—Si) is the reactive group. This group could be broken by water in two steps: (1) the absorption of water near a Si—O—Si group; and (2) the formation of a new Si—O bond by the oxygen of the adsorbed water and the cleavage of the Si—O—Si group (Schott and Oelkers, 1995). Dissolution is associated with the latter step, which at 25 °C involves an equilibrium between the solid phase and a monomeric form of silica ($Si(OH)_4$) in solution (Alexander et al., 1954). The increase in total dissolved silica (the most abundant major component in ashes) at basic pH is well established (Alexander, 1957). According to pH variation, it was observed a higher solubility of Si at more basic pH conditions.

The structure of aluminosilicates (e.g., alkali feldspar) contains exchangeable cations (e.g., Na^+, Ca^{2+}) along two hydrolysable sites in the polymer: silicate groups (Si—O—Si) and aluminate groups (Al—O—Si). Experimental studies on aluminosilicate dissolution show that within the tetrahedral framework, Al—O—Si bonds are weaker than Si—O—Si bonds (Casey et al., 1989, Hellmann et al., 1990, Wollast and Chou, 1992). These studies conclude that the final and rate limiting step of these compound dissolutions are, as for silicate, the hydrolysis of Si—O—Si bonds. Aluminum dissolution depicted in the 719 and CHA-1F ashes were due to the noticeably presence of alkali feldspars determined by XRD. On the contrary the practically absence of aluminosilicate minerals in the

sample 808 explains the difference of the Al behaviour of this sample respect to the other ashes.

8.1.3 Major and trace element behaviour

The geochemical composition of leachates in the column experiments was predominantly controlled by incongruent dissolution of glass and mineral phases (if present) and dissolution of coatings on the ash particle surfaces. Therefore, we should discriminate between the elements rapidly released from the ash surface and those related to more complex reactions as dissolution processes. Elements with high solubility during the first of the experiment were Ca, Na, Si, Cl$^-$, SO$_4^{2-}$, Li, B, V, Mn, Rb, Sr, Mo, Ba, and U. The time required for passing 200 ml along the column (i.e., ~26 hours) was considered enough for begin the chemical weathering and a rapid incongruent dissolution of volcanic glass (that is the reactive phase) by cation-exchange processes that could be also the source of the aforementioned elements. Elements involved in other processes (e.g., hydrolysis) were P, Fe, and As. These elements do not show a very sharp decrease during the leaching time. This feature enhances the undoubtedly relation with glass dissolution process. If we take into account the leaching behavior of the CHA-1F pristine ash, also B, and V are certainly associated with the glass dissolution in these experimental conditions. It is very well known that the latter elements (including As) are normally enriched in rhyolitic melts due to their incompatibility.

8.2 Column leaching tests on size fractions

8.2.1 pH, silica and aluminium dissolution

As in the bulk sample, the pH increases quickly when ash-water interaction occurs. Very rapid increase was detected in the finest fraction (<100 µm), which, in turn, is the fraction with the highest amount of volcanic glass. Therefore, a very rapid incongruent dissolution of volcanic glass by cation-exchange processes was suggested. This feature was confirmed by the higher Si leaching concentration observed in that fraction. Aluminum concentration was reversed, with the higher concentration in the coarse fraction.

8.2.2 Major and trace element behaviour

The components rapidly released within the first stage of leaching were Ca, Na, Mg, SO_4^{2-}, Rb, Sr, and Ba. This behaviour was similar in the three experiments indicating a weak association to the ash particle surfaces, independently of the size fraction. Combination of two processes (i.e., incongruent dissolution of volcanic glass and coating dissolution on ash particles) are the sources of these components. The trace elements enriched in the lower fraction were Li, B, P, V, Fe, As, Mo, and U. Several studies on the very high concentrations of some of the above mentioned elements (As, Mo, V, B, and U) in shallow and ground water of northwestern Argentine are associated with the presence of high contents of volcanic ash in the loess of the aquifer sediments. Therefore, this study confirms through laboratory experiments, the association with ash dissolution of the aforementioned trace elements.

9. Sequential extraction scheme (SES)

Design of a suitable sequential extraction scheme (SES) for volcanic ash has been other objective of this Thesis. The methodological approach for a suitable SES has been, firstly, to define the fractions of interest in volcanic ash, to propose different chemical reagents and, finally, to set the best chemical reagents throughout leaching experiments.

9.1 Definition of chemical fractions of interest in volcanic ash

For volcanic ashes, four basic chemical fractions may be considered:

(1) F1: elements non-specifically adsorbed on the ash particle surfaces and easily releasable by ion-exchange processes.

(2) F2: elements associated with the amorphous oxides;

(3) F3: elements associated with the crystalline oxides;

(4) F4: Residual phase.

9.2 Possible candidates as chemical reagents

Several chemical reagents have been used for releasing the chemical fractions reported above. The chemical extractants were chosen after a meticulous

literature research and based on theoretical and practical consideration. Table 1 shows the chemical reagents studied before the SES application.

Table 1 Chemical reagents studied by leaching experiments before the SES application.

Chemical fraction		Chemical reagent
F1 Easily exchangeable	E1a	deionised water
	E1b	NH_4NO_3-$(NH_4)_2SO_4$ 10^{-4}M adjusted to pH 7 with NaOH
F2 Amorphous Al, Fe, Mn oxides	E2a1	NH_4Ac 0.25M adjusted to pH 4.5 with HNO_3
	E2a2	NH_4Ox 0.25M adjusted to pH 4.5 with HNO_3
	E2a3	NH_4Cit 0.25M adjusted to pH 4.5 with HNO_3
F3 Crystalline Al, Fe, Mn oxides	E3	NH_4Ox 0.25M adjusted to pH 4.5 with HNO_3 + ascorbic acid 0.1M

Many sequential extraction procedures use deionised water as first extractant for quantifying the most mobile and potentially most available elements, including the weakly adsorbed elements retained on the ash particle surfaces (i.e., elements that can be easily released by ion-exchange processes). In this study the data obtained throughout the Single Batch Leaching Test (SBLT) with deionised water reported in the chapter 6 were compared with the results obtained using the NH_4NO_3 - $(NH_4)_2SO_4$ 10^{-4} M (E1b).

A selective leaching of amorphous Al, Fe and Mn oxides fraction (F2) from soils has been proposed with acid ammonium organic extraction. Following the suggestion proposed by Chao and Zhou (1983), the effects of three acid organic solutions (E2a$_1$, E2a$_2$, E2a$_3$) at 0.25 M concentration and pH 4.5 (adjusted adding HNO_3) were compared through leaching experiments.

Several authors proposed the acid ammonium oxalate extraction adding ascorbic acid (0.1 M) in darkness at 70 ºC (30 min shaking) to release the elements associated with the well crystallized Al and Fe hydrous oxides (Krishnamurti et al., 1995; Wenzel et al., 2001). Following these observations, this solution was used in this study.

9.3 Setting the operating conditions

The easily exchangeable and the amorphous oxides fraction were studied by leaching experiments in order to:

(1) choose the best reagent in terms of extraction efficiency.

(2) define the time necessary to achieve the pseudo-equilibrium condition.

The same methodology was applied for each one of the chemical reagents (E1b, E2a$_1$, E2a$_2$, and E2a$_3$) under study. The dynamic leaching experiments were performed through a battery of batch leaching test in order to give information on the breakthrough of the leached compounds. Element selection in this study covers:

(1) the less mobile major elements during the leaching processes (Al, Mn, and Fe) (Chang, 1999; Gayer et al., 1958; Wollast and Chou, 1992);

(2) trace elements (Zn, As, V, and Pb) dominantly combined with halogens and sulphate forming salts and/or acid droplets coating the ash-grain surfaces (Delmelle et al., 2007; Hinkley, 1991, 1994; Symonds et al., 1987, 1992, 1994) and associated with volcanic glass dissolution in a dry weathering environment of Argentina (i.e., As and V) (Francisca and Perez, 2009; Nicolli et al., 2001, 2011).

9.3.1 Leaching data for the easily exchangeable fraction (F1)

Appreciable content was verified only for As, V, and Zn, which present similar temporal profiles using E1b as extractant. Comparing these results with those obtained by the SBLT with deionised water higher concentrations were obtained with the latter reagent. The hypothesis drawn is that some of these elements (i.e., Mn, Fe, and Al) precipitated during the treatment with E1b. In order words, the E1b reagent is not suitable in the case of volcanic ash and following the results of the SBLT, the easily exchangeable fraction was extracted shaking the sample with deionised water for 4 hours at room temperature.

9.3.2 Leaching data for the amorphous oxides fraction (F2)

Extraction efficiency for the E2a$_1$ acid solution is very poor. Leaching curves obtained of some elements extracted with E2a$_2$ and E2a$_3$ follow similar temporal trend reaching the pseudo-equilibrium between 2 and 4 hours, but relatively

higher element concentrations were observed with $E2a_2$ extraction. Taking into account that a suitable SES has to be fast and reliable in laboratory conditions and in agreement with the suggestion proposed by Chao and Zhou (1983), the amorphous oxides extraction was performed with $E2a_2$ 0.25 M solution at pH 4.5 (2 h shaking).

9.4 Application of the proposed SES

Two rhyolitic volcanic ashes were used in this study: the Chaiten volcanic ash (CHA-2R) and the ancient volcanic ash (808) of the southern Puna.

The sum of the amounts (expressed as percent of the total) of an element extracted in the first three steps (excluding the residual fraction) can be considered a potentially mobile fraction susceptible of environmental changes such as redox potential or pH (Filgueiras et al., 2002; Hernandez-Moreno et al., 2007). The results show a general low element mobilization for both ashes. However, ancient ash showed higher element mobility than pristine ash. This study demonstrates that after the fast release of the soluble compounds present on the particle surfaces of pristine ash, the weathering of glass and crystalline components causes a very slow release of the elements in the environment. Therefore, the residence time of the volcanic ash in the environment seems to have a reflection on the element leachability. Once deposited, the volcanic ash undergoes irreversible geochemical weathering reactions (e.g., oxidation followed by slow dissolution), causing destabilization of the silicate framework and release of the elements associated with it.

From a methodological point of view, the sequential leaching approach is a powerful tool to evaluate the element mobility from both ancient and pristine volcanic ashes. The proposed SES provides reliable information on the elements released in the different chemical fractions of volcanic ashes. These operationally defined fractions represent non-specifically bound, specifically bound as amorphous hydrous oxide-bound, crystalline hydrous oxide-bound and, finally, the residual. Fraction 1 can be used for predicting the most mobile and potentially most environmentally available elements, including the weakly adsorbed elements that can be easily released by ion-exchange processes. Such information is useful to assess the readily bio-available fraction. Fractions

2-3 may provide information on potential lability from the different solid phases as a result of weathering and change of environmental factors (i.e., redox, pH). Within the inherent limitations of the chemical fractionation, the reagents used are fairly powerful for the determination of the chemical form in which the element occurs and this study should be considered a good beginning for a further development of this methodology applied to volcanic ash.

10. Conclusions

From water leaching tests the main remarks can be summarised as follows:

1)   The elements enriched on recent ashes correspond to those mainly involved in the volcanic gas-ash interaction in volcanic plume. These include trace elements (e.g., Ni, Cu, As, Sr, Ba, and Pb) dominantly combined with halogens and sulphate forming salts and/or acid droplets coating the ash-grain surfaces.

2)   The elements enriched on ancient ash leachates are rock forming mineral elements supporting the idea that once deposited, the volcanic ash undergoes irreversible geochemical weathering reactions (e.g., oxidation followed by slow dissolution), causing destabilization of the silicate framework and release of the elements associated with it. Relatively disruption of the silicate network of ancient ashes has been inferred also by FTIR observations, which allowed concluding the remarkable importance of chemical stability of ancient glass on the ash reactivity.

(3)   Dynamic leaching tests conducted on raw ashes and grain-size fractions allowed to define the element implied during glass and mineral dissolution. From the data nowadays available on the temporal leaching of Andean rhyolitic ashes (from CVZ to SVZ), the association between ash dissolution and some trace elements (As, Mo, V, B, and U) through laboratory experiments was demonstrated.

In terms of element mobility and, hence, contribution to regional geochemical balance both type of ashes, ancient and recent, could release substantially amount of elements through water. This study shows that major elements with high mobility are Ca, Mg, Na, Si, K, and Al. Puna and Uruguay ashes could

release in the environment the same trace elements (i.e., P, Ti, Fe, Mn, Zn), however, in different concentrations. These are macro- and micronutrients evidencing the fertilizing potential of the ashes. Chaiten ashes showed high concentrations for As, Pb, Fe, and Zn, whilst the other samples (i.e., COP, LON, LLA, and HUD) could release principally P, Ti, Mn, Ni, Zn, and Pb. Many others are potentially toxic trace elements (PTTE) even at very low concentrations. Some of the latter elements are included in the drinking water guidelines due to their potential toxicity and must be especially monitored in the environmental assessment of these ashfall deposits. This aspect is very important if we take into account the environmental conditions in which the ash deposits occurred. The drainage in small and closed hydrographic basins such as the ones in the Puna and surrounding regions can greatly affect the geochemical fluxes of streams and lakes, especially immediately after the scarce rainfalls, because the process is very fast. On the contrary, the high rainfall on the western flanks of the Andean Cordillera in the SVZ implies a practically constant contact with water (and therefore weathering) of the ash deposits.

This study represents a great advance on the knowledge of the geochemical environmental hazard posed by volcanic ashes, in general, and from the Andes, in particular in terms of methodological approach. The developed method of Single Batch Leaching Test (SBLT) is a very important contribution of this research because there is a need to harmonize the batch leaching tests applied to volcanic ash. The physico-chemical information of ashes (mainly the morphological features, grain-size distribution and PTTE identification and quantification) should be known prior the application of a SBLT. In addition, column leaching test and sequential extraction scheme complement the information obtained by SBLT and facilitate decision making on management of geochemical hazard associated with the volcanic ash fall.

Objectives and Thesis structure

Objectives

The main purpose of this work is to investigate the geochemical environmental hazard posed by different types of volcanic ashes in general, and from the Andes, in particular. The specifics aims of this research are:

(1) to develop an analytical methodology for the physico-chemical characterisation of volcanic ash;

(3) to propose a new ash leaching methodology that can be useful both for recent and ancient volcanic ashes;

(4) to recognize the geochemical impact occurring after the deposition of volcanic ash on the environment through leaching experiments.

Chronological development of this research

This research was carried out in the framework of the PEGEFA Working Group (Catalonian Government "Grup de Recerca Consolidat" SGR-2005-00795 and 2009-SGR 972), and was partly funded by the Project ASH of the Spanish Ministry of Science and Technology (CGL2008-00099) and by the FPU Grant of the Spanish Ministry of Education (F. Ruggieri, Ref. AP2006-04592). It is substantially carried out step by step over the years of my FPU Grant (Table I). The purpose of the first two years of the PhD was to define which criteria may be useful to recognize if the samples collected in the field are really volcanic ashes and to design a specific methodology for the bulk geochemistry characterization. In this part of research, ash deposits from an Andean region in NW Argentina (Catamarca and Salta provinces) and Uruguay have been studied. In the two last years, the main goal was to study the contribution of different types of volcanic ashes from the Andes to the local geochemical balance by several types of leaching tests. A new ash leaching methodology was also performed and proposed.

Table I. Chronological development of this Thesis.

	Year 1º	Year 2º	Year 3º	Year 4º
Sample collection	**21 samples from Andes CVZ of Argentina** **8 samples from Uruguay**			
	Geochemistry bulk ash characterization			
Sample collection			**8 samples from Andes SVZ of Chile**	
			Geochemical environmental hazard **by different ash leaching tests**	
			Propose new methodology	
Interpretation and diffusion of results			**Publication of Papers and PhD preparation**	

CVZ: Central Volcanic Zone of Andes
SVZ: Southern Volcanic Zone of Andes

Methodology

The methodological part can be considered the main body of this research. Due to their importance, an entire part summarizes the sample collection and the analytical techniques used in this research. The whole-ash characterisation has been divided in physical, mineralogical and chemical characterisation. In each category one or more analytical techniques have been used. Training on different techniques has been an important part of this research. It is mention to note that nowadays these protocols are used by other researchers that form part or collaborate with our Consolidated Research Group (PEGEFA).

The physical characterisation of volcanic ashes has been divided in the study of the morphological properties of the ash particles by SEM-EDX, the Specific Surface Area (SSA) by the BET method and the grain-size analysis (GSA) by laser diffraction. Mineralogical composition was also inferred by XRD. The chemical characterisation has been divided in whole-rock chemical analysis and leaching experiments by ICP-OES, ICP-MS, HR-ICP-MS, and FTIR spectroscopy. The developed protocols for the different chemical analysis are reported in Appendix 1.

Most of the analysis (SEM, BET, ICP-OES, ICP-MS) have been carried out at the Serveis CientíficoTècnis, Universitat de Barcelona. Parts of the other analyses (XRD, GSA, HR-ICP-MS) have been undertaken at the Institute of Earth Sciences J. Almera, CSIC, Barcelona and at the Italian National Agency for New Technologies, Energy and Sustainable Economic Development (ENEA), Rome. Finally, FTIR analysis was performed at the Departamento de Cristalografía, Mineralogía y Depósitos Minerales, Universitat de Barcelona.

Thesis structure

The research presented in this work is organized as follows:

Part 1. Introduction

- Chapter 1. Presents, briefly, theoretical information about volcanic eruptions, which mechanisms produce the volcanic ashes, and how the ash particles can be deposited on the land. This chapter also includes the environmental impact of erupted volcanic ash on the Earth system and the main related features.

Part 2. Geographical and geological setting

- Chapter 2. Describes the general characteristics of the sampling areas in the Andes, with a concise description of each one of the volcanoes under study.

Part 3. Methodology

- Chapter 3. Summarises the field work and sample collection.
- Chapter 4. Includes the analytical techniques used in this research. It has been considered appropriate to dedicate an entire chapter on introducing the analytical techniques used, underlining the respective methodological protocols.

Part 4. Results and discussion

The performed results are presented separately for the bulk ash characterisation and the ash leaching tests with a summary and conclusions section at the end of each chapter. The proper methodology carried out for each one of the ash leaching tests is reported within the respective chapter. The structure of this part is as follows:

- Chapter 5. Reports the useful criteria to distinguish between volcanic and non-volcanic products collected during the field campaign and, once identified pure volcanic ashes, the results of their physical, mineralogical and chemical characterisation are listed.

- Chapter 6. Delineates the specific methodology used for designing a single batch leaching test with deionised water. An entire chapter is devoted to this new methodology because it is a proven proposal for harmonization of batch leaching tests for volcanic ashes.

- Chapter 7. Shows the results of the proposed batch leaching test applied to the samples under study. Moreover, it includes the results obtained by the nitric acid leaching tests.

- Chapter 8. Includes the results of a column leaching tests performed to both ancient and recent volcanic ashes. In addition, leaching of different grain-size fractions of an ancient sample was also studied.

- Chapter 9. Embraces the application of a sequential extraction procedure to ancient and recent volcanic ashes.

Part 5. Conclusions

- The main conclusions are summarised in terms of element mobility and in the methodology applied for the characterisation of the geochemical environmental hazard posed by both ancient and recent volcanic ashes. Furthermore, new ideas for future works are also suggested.

Finally, the references cited in this work, as well as 7 appendixes are reported. The first one includes the procedure of sample preparation for whole-rock chemical analysis. The second reports additional SEM images of the samples under study. The third includes the XRD patterns of the ash samples. The fourth reports the average element concentrations and relative standard deviation of the single bath leaching test (SBLT) data set used for defining a suitable methodology. In the fifth appendix the protocols of the totality of the ash leaching tests carried out in this research are presented. The sixth appendix includes the results obtained in the SBLTs (both with deionised water and nitric acid). In the last appendix, the publications derived from this study and the contributions to conferences, congresses and workshops are listed.

PART 1. INTRODUCTION

Chapter 1. Volcanic eruptions and ash deposition

This chapter introduces the ash deposition in relation to explosive volcanic eruptions. It has been divided in two parts:

(1)   Part 1 contains a description of the mechanisms that produce volcanic ash and how the ash particles can be deposited on the land surface.

(2)   Part 2 includes the environmental impact of erupted volcanic ash on the Earth system and the main related features.

1.1 Volcanic eruption style

Volcanic eruptions are one of the most remarkable and powerful expressions of nature's force. Every year about 50 volcanoes throughout the world are active above sea level, threatening the lives and property of millions of people (Sigurdsson, 2000). A bewildering variety of volcanic processes occur at the surface during an eruption, and the list of the volcanic rocks and types of volcanic deposits is apparently endless. Fortunately, volcanology has progressed in the latter half of the 20th century from a descriptive endeavor to a truly interdisciplinary science, and the major factors controlling eruption processes and the diversity of the products have been discovered.

Volcanoes display a wide range of eruption styles. The style of an eruption is controlled by characteristics of the erupting magma (molten rock), including chemistry, crystal content, temperature, dissolved gases, and also by water interaction, especially groundwater. These features determine the category of products ejected during the eruption process. In general, volcanic eruptions range from effusion of lava fountains and flows (typical of basaltic magma with low silica content) to extremely explosive events (typical of rhyolitic and dacitic magma with high silica content). Though volcanic ash is produced at least in some degree in most eruptions, the explosive eruptions are those that can inject large quantities of ash high into the stratosphere. Explosive eruptions are the most powerful and destructive type of volcanic activity. The large quantities of fragmental pyroclastic materials (including volcanic ash) produced are carried

upward in convecting columns and, subsequently, dispersed in the surrounding environment. The percentage of fragmentation of pyroclastic materials can be used as measure of explosiveness allowing to classify volcanic eruptions (Walker, 1973) (Figure 1.1).
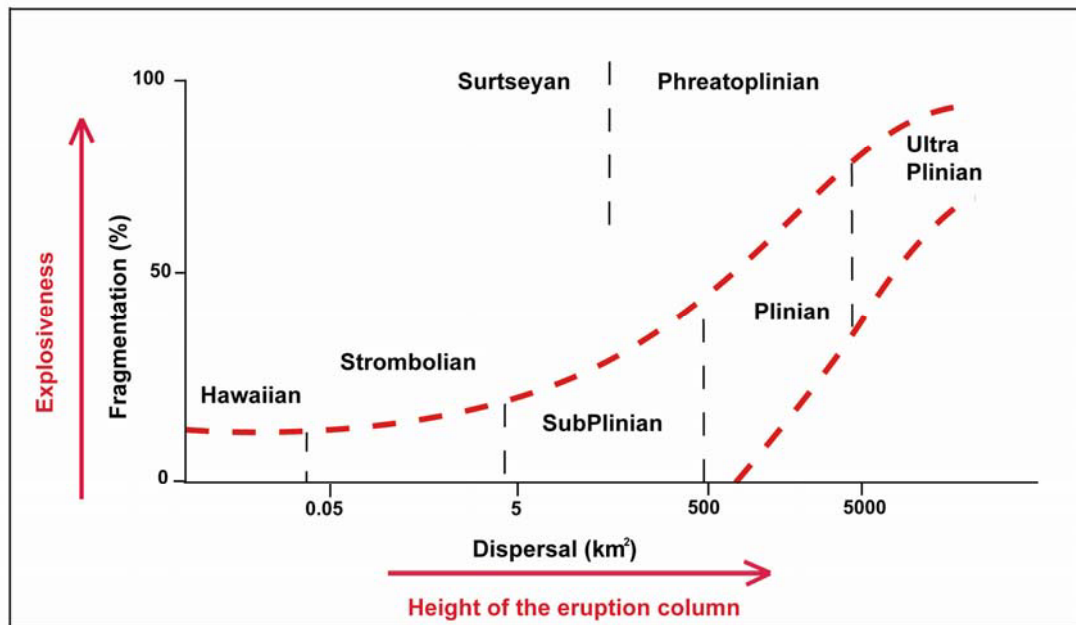
Figure 1.1 Diagram showing the amount of magma fragmentation and resulting dispersal of tephra (ash and larger-sized particles) that typically accompanies different styles of eruption (e.g., Hawaiian and Plinian) (modified after Walker, 1973).

This scheme shows the amount of magma fragmentation and resulting dispersal of tephra (ash and larger-sized particles) that typically accompanies different styles of eruption (e.g., Hawaiian and Plinian). High fragmentation breaks or shatters the erupting magma into particles, including volcanic ash. Hawaiian-style eruptions generally do not fragment lava into ash-sized particles which are typical of large Plinian-style eruptions (explosive eruptions).

1.2 What mechanisms produce ash in a volcanic eruption?

In general, volcanoes from a subduction volcanic zone are more likely to generate large amount of ash than volcanoes from a hot spot (Duggen et al., 2010). However, independently of the geotectonic setting of the volcano there are two basic types of mechanisms during an explosive eruption that produce volcanic ash: (1) magmatic by exsolution and expansion of gases in the magma, and (2) phreatomagmatic by chilling of the rising magma when contact with ground or surface water. Volcanic ash formation broadly occurs as a combination of both mechanisms.
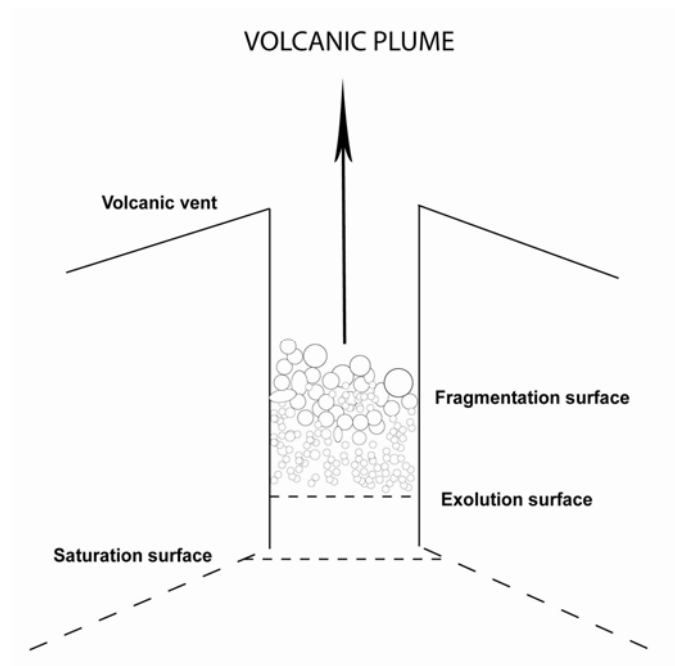
Figure 1.2 Schematic illustration of processes that occur in volcanic conduits during a explosive magmatic eruption (modified after Sparks, 1978).

The explosive force of magmatic eruptions is generated during fragmentation, where the potential energy of an expanding magma (melt and bubbles) is converted to the kinetic energy of individual fragments and, then, thermally expanded in volcanic plumes (Cashman et al., 2000; Sparks, 1978) (Figure 1.2). This mechanism can take place when magma ascends rapidly after rapid decompression caused by collapse of volcanic edifices or lava domes (Sparks et al., 1997). This fragmentation process occurs with viscous and volatile rich magma, in which the discharged material out of the vent forms the volcanic plume.

A phreatomagmatic eruption is driven primarily by the volumetric expansion of external water after it has been rapidly heated by contact with magma (Figure 1.3). Exsolving magmatic volatiles may also contribute to expansion and fragmentation during a phreatomagmatic event. When water comes into contact with magma, it will either transform to steam (vapor) or a two-phase (liquid and vapor) fluid, depending on the relative masses of water and magma interacting (Morrissey et al., 2000; Wohletz, 1986).
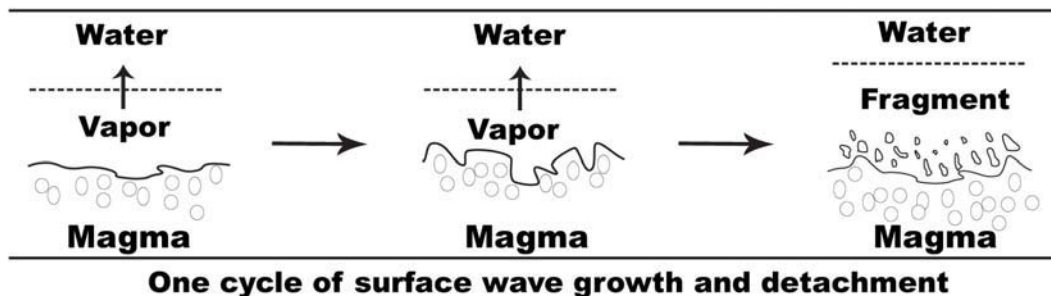
Figure 1.3 Schematic illustration of a complete cycle of instability growth. Oscillation of the film thickness transmits sufficient momentum to the magma so that its surface distorts into waves that can grow until they detach to form small fragments (modified after Wohletz, 1986).

Not all magma-water interactions are explosive. The model in which generation of explosive activity takes place is due to the development of a thin vapour film at the boundary between magma and water. Heat transfer causes the film to

expand rapidly outwards, causing disruption of magma interface and resulting in fragmentation (Morrissey et al., 2000; Wohletz, 1986).

1.3 Pyroclastic materials produced during explosive volcanic eruptions

Tephra is a general term used for all particles ejected during volcanic eruptions by mechanical fragmentation of magma and/or country rock that fall to the ground from an eruption column. The term tephra, originally coined by Aristotle, is the most convenient term for loose deposits made of volcanic particles because it is independent of composition. Classification schemes of volcanic tephra are based upon grain size, composition of pyroclast and magma, genesis of the pyroclast and mechanism of deposition. However, the most commonly used is based on the classification of tephra according to the fragment size. Fragments less than 2 mm in diameter are termed ash, those between 2 and 64 mm are called lapilli, and fragments larger than 64 mm are called blocks.

In general, volcanic ashes are clastic rocks composed of grains or fragments of rocks and minerals that have been ejected and, afterwards, deposited in a simple layer. Identification of volcanic ash requires the observation of grain size, grain shape, the degree of sorting of the grain and the chemical composition that are linked of the environment in which they were formed. In terms of the grain size ash could be further subdivided in coarse ash (particles diameter lower than 2 mm), and fine ash (particles diameter lower than 1/16 mm) (Schmid, 1981).

The grain shape refers to the degree of rounding of the grains. The degree of sorting refers to whether the particles are relatively uniform in size or there are many sizes. Volcanic ash can vary from well-sorted sediment consisting of grains of uniform size to poorly-sorted sediment, containing particles of many sizes (Heiken and Wohletz, 1985).

1.4 Volcanic plume, transport and deposition of ash

This paragraph gives rapidly a framework for the main points by which the materials ejected in explosive eruptions are transported and deposited to form pyroclastic deposits in the sub-aerial environment. Explosive volcanism involves the transfer of fragmented magma from some depth onto the Earth surface. The clast larger than 10 cm describes ballistic ejecta and fall from low height of the plume. The atmospheric dispersal of airborne volcanic ash is governed by the type and magnitude of the volcanic eruption, wind direction and size and density of the ash particles (Figure 1.4). Sedimentation of airborne ash particles from the volcanic eruption plume depends on settling velocity, which in turn, depends on density and particle diameter. In general, particle size decreases with distance from the volcanic source (aeolian fractionation) (Walker et al., 1971). The fallout of smallest particles (<200 µm) from an eruption plume is influenced by additional factors. First, atmospheric turbulent diffusion can have major influence on their dispersal than for larger particles. Second, fine particles can aggregate by a variety of processes (e.g., through electrostatic forces and under the effect of moisture) and fall much faster and nearer that individual particles (Wilson, 1999). Individual volcanic fine ash with a particle size smaller than 15 µm can have a lifetime of days to weeks in the stratosphere and deposition can occur at large distance from the volcano (Niemeier et al., 2009). This feature has been reported for many explosive historical eruptions as those of Mount St Helens in 1980 and Hudson in 1991 (Carey and Sigurdsson, 1982; Kratzmann et al., 2010b) or in the more recent eruption of Chaiten volcano, 2008 (Martin et al., 2009). Moreover, there are two principal ways by which the ash reaches the ground: (1) dry deposition: the particles fall down due to gravity (gravitational sedimentation); (2) wet deposition: it involves the interaction with fog or cloud water prior to deposition into the land or surface ocean.

1.5 Ash particle components

Volcanic ash consists of three main components: (1) glass shards and pumice grains, (2) fragments of minerals and (3) accidental lithic fragments. The properties of the ash depend mostly on the relative proportions of these constituents.

1.5.1 Glass shards and pumice grains

Volcanic glass shards and pumice grains are fragments of the molten part of magma that cooled and solidified during eruption (quenched magma). Since an explosive eruption is violent, the magma is broken into small pieces of bubbly pumice and even smaller glass shards. Glass shards are typically remnants of tiny gas bubbles that developed and grew in size during the final ascent toward the surface. The density and percentage of bubbles in the pumice can be measured to estimate indirectly the amount of gas originally present (i.e., bubble-rich, low-density pumice implies high gas contents).

1.5.2 Crystalline mineral phases

Mineral fragments are crystals which originally precipitated from the magmatic liquid before the eruption. These minerals crystallize in the magma during the ascent to the surface due to the cooling of the magma. The type of minerals within an ash deposit depends upon the chemistry of the magma from which it was erupted. Common crystals in the products of explosive volcanism are quartz, aluminosilicates (e.g., feldspar), ferromagnesian silicates (e.g., orthopyroxene, clinopyroxene and hornblende), and oxides (titanomagnetite and ilmenite). Their size varies from few tens of micrometers to a few millimeters. Minerals are more abundant in the grain size range of 63 μm to 2 mm and are generally absent below 10 μm, whereas glass shards can be micrometric in size. Mineral grains could also contain small inclusions of

trapped magma, typically 0.05–0.2 mm in diameter, which have solidified to glass (Sparks et al., 1997). In Table 1.1 minerals typically present in different magma compositions are reported.

Table 1.1 Typical minerals occurring in volcanic ashes (grouped by magma composition).

Magma composition	Minerals typically present
Rhyolite	Quartz, feldspar, +/- mica, +/-orthopyroxene, +/- amphibole
Dacite	Quartz, feldspar, +/- mica, +/-orthopyrocene, +/- clinopyroxene,+/-amphibole
Andesite	Feldspar, clinopyroxene, +/- quartz, +/- orthopyroxene,+/- amphibole
Basalt	Feldspar, clinopyroxene, +/- olivine, +/-orthopyroxene,+/- amphibole

1.5.3 Accidental lithic fragments

Rising magma will incorporate pieces of different types of rocks through which it moves, including rocks located deep beneath a volcano and within the volcano itself. Essentially, lithic fragments are accidental or secondary-produced materials. The rapid ascent of magma during explosive eruption will often rip fragments from the walls of the magma conduit, which are ejected and fragmented further by the explosive expansion of volcanic gases. These non-magmatic rock fragments are found in varying abundances within ash deposits and often have a different shape and texture than glass shards (Heiken and Wohletz, 1985).

1.6 Ash particle morphology

The morphology of ash particles can help identify the nature of the eruption. Distinct fragmentation processes produce different textural features. The excellent collection of scanning electron microscope (SEM) images assembled by Heiken and Wohletz (1985) illustrates the tremendous diversity of volcanic ash morphologies. The ashes are best placed into two broad genetic

categories: magmatic and phreatomagmatic. Within these two genetic categories, ashes from different magma types can be characterised.

1.6.1 Morphologies from magmatic eruptions

The shape of glassy ash particles is mostly dependent on the kinetic evolution of gas. This determine the number and density of bubbles (vesicles) which, in turn, are function of the initial water content in magma, degree of oversaturation developed, viscosity, surface tension, temperature, depth and amount of suspended crystals (Verhoogen, 1951). Thus, ash particle shapes from different magmas present peculiar features. Explosive eruptions of magmas with *low viscosity*, caused by expanding, coalescing gas bubbles at the surface are mostly droplets. Droplet shapes are controlled mainly by the effect of surface tension and deformation of the droplet by acceleration and air resistance. Shapes range from perfect spheres to a variety of twisted, elongate droplets with smooth, fluidal surfaces. Ash from magma with slightly higher viscosities, such as basaltic magmas with abundant phenocrysts or some andesitic magmas, are composed of vesicular juvenile clasts (scoria) with few fluidal shapes (there is a small droplet component). The morphology of ash particles from magmatic eruptions of high viscosity magmas (rhyolitic, dacitic and some andesitic magmas) are entirely dependent on the shape of the vesicles in the rising magma before disintegration. The explosive expansion of vesicles disintegrates the rising magma column resulting in ash falls and ash flows (Ross and Smith, 1961). The concavities, troughs and tubes of grain surfaces are broken vesicle walls. Elongate grain shapes are controlled by elongate vesicles (pipe) and equant grain shape by undeformed vesicles. Flat or slightly curved platy shards are from broken vesicles walls.

1.6.2 Morphologies from phreatomagmatic eruptions

The morphology of ash particles from phreatomagmatic eruptions is controlled by stresses within the chilled magma which result in fragmentation of the glass

to form small blocky or pyramidal glass ash particles. Vesicle density and shape play only a minor role in determining the morphology of these ash particles. In many instances, it appears that the chilling occurs before much of the gas is released from the magma, explaining the general low vesicularity characteristics of ash formed by the chilling-fractures process (Heiken, 1972). The principal effects of water interaction are to promote quenching and inhibit vesiculation. Their shapes may indicate fragmentation by thermal fracturing (i.e., angular edges) and not by abrasion (i.e., rounded edges). In terms of grain size, phreatomagmatic tephra generally are finer grained than magmatic tephra particularly for high water/magma ratios (Wohletz, 1986). Under optical and electron microscopes, the juvenile (glass) component of phreatomagmatic tephra contains distinct grain shapes. Shards formed by phreatomagmatic eruptions often have a particular angular shape resulting from the violent explosive interaction between magma and water. These shapes include blocky, fusiform, mosslike, platey, and spherical or droplike types. Also, the glass constituents may be more hydrothermally altered than magmatic tephras of equivalent age, especially in samples from wet tephra deposits in which hot water was captured (Heiken and Wohletz, 1985).

1.7 Environmental impact of volcanic ash

Explosive volcanic eruptions are capable of causing significant environmental repercussions affecting, simultaneously, many cycles in the Earth system (Jones and Gislason, 2008). The environmental impact ranges from the truly global scale to more regional scale. The impact of volcanic eruptive products on climate (global scale) is a consequence of injection of sulphur aerosols into the stratosphere (Manville et al., 2009). Volcanic aerosols are an active component of the climate system and play multiple roles in physical and biogeochemical exchanges between the atmosphere, land surface and ocean (Niemeier et al., 2009). Little attention has been paid to the impact of fine ash on biogeochemical processes. Agriculture and biosphere are greatly affected over the ash-covered areas (Cronin and Sharp, 2002; Inbar et al., 1995; Stewart et al., 2006).

Actually, more subtle chemical impacts may be undergone over much larger areas, because fine volcanic ash, usually, is dispersed widely by the prevailing atmospheric motions, as in the case of the last eruption of Chaiten volcano in 2008 (Gangale et al., 2010; Martin et al., 2009) or the more recent eruption of Eyjafjallajokull (April-May 2010).

A layer of one centimetre thick volcanic ash disrupts agriculture for more than a growing season, and lesser amounts (a few millimetres) can destroy many kinds of crops (Self, 2006). Furthermore, changes in soil composition can be expected (Ping, 2000).

Deposition of volcanic ash may provide an external nutrient source for primary production in ocean surface waters, in particular through iron fertilisation (Duggen et al., 2010). This effect has been studied in high-nutrient but low productivity (low-iron) areas in the Pacific and the Southern Ocean. In these areas the fallout of ash have also a high potential to induce globally significant, transient net CO_2 removal from the upper ocean and hence from the atmosphere (Duggen et al., 2010).

Furthermore, once deposited, the ash fall deposits can remain in the local environment for years to decades, and in the case of hyper-arid conditions (as the Puna, Argentina) may be preserved during millions of years (Ruggieri et al., 2010b). Frequent strong wind storms may re-suspend the ash, causing environmental effects similar to those of the original eruption (Horwell and Baxter, 2006; Inbar et al., 1995).

There is also a human health aspect to consider because the exposure to respirable fraction (<15 μm aerodynamic diameter) can lead to silicosis, a disease resulting in scarring of the lungs and impairment of their function. This feature may be enhanced by the presence of highly crystalline silica nanofibers of cristobalite as in the case of Chaiten ash (Horwell and Baxter, 2006; Horwell et al., 2003a; Horwell et al., 2010; Horwell et al., 2003b; Ruggieri et al., 2010a).

1.7.1 Environmental impact at regional scale

During an eruption, magma and gases are expelled from the volcanic vent into the atmosphere. When volcanic ash is suspended in an eruptive column, a

certain proportion of soluble component is condensed onto ash particles surfaces. Thus, volcanic ash is composed of fine grained rock and mineral fragments, with acid droplets coating the ash-grain surfaces. These compounds are rapidly released when ash-water interaction occurs. Furthermore, after the initial washing, prolonged exposure of the ash particles to weathering may cause slow release of elements from the components of volcanic ash, the glass and the crystalline phases (Smith et al., 1982; Smith et al., 1983). Therefore, the environmental impact at regional scale produced by volcanic ash fall includes:

(1) Short term release of soluble compounds present on particle surface (short term leaching);

(2) Long term release of elements from weathering of volcanic glass and crystalline mineral phases (long term leaching).

These two aspects are discussed in more details in the sections below.

1.7.1.1 Short term leaching: soluble compounds on volcanic ash

Volcanic plumes in the atmosphere are heterogeneous environments in which gases, aerosols and silicate ash particles coexist and interact in various ways. The principal gases released during volcanic activity are water vapour (H_2O), carbon dioxide (CO_2), sulphur dioxide (SO_2), hydrogen (H_2), hydrochloric acid (HCl), hydrofluoric acid (HF), hydrogen sulphide (H_2S), and carbon monoxide (CO). Many volatile metal elements are also released (Allard et al., 2000; Symonds et al., 1994).

The sulphur and halogen gases and metals are subsequently removed from the atmosphere by process of chemical reaction, dry and wet deposition, and adsorption of volatiles onto the ash surfaces (Witham et al., 2005). Several previous studies have discovered that ash particles have a significant potential for scavenging sulphur and halogen gases from the plume. Up to 40 % of sulphur species and 10 - 20 % of HCl can be scavenged by tephra in eruption columns (Oskarsson, 1980; Rose, 1977; Varekamp et al., 1984). Figure 1.4 shows the diagram for the formation of soluble components on ash particles and their dispersion in the surrounding environment. The reactions occurring
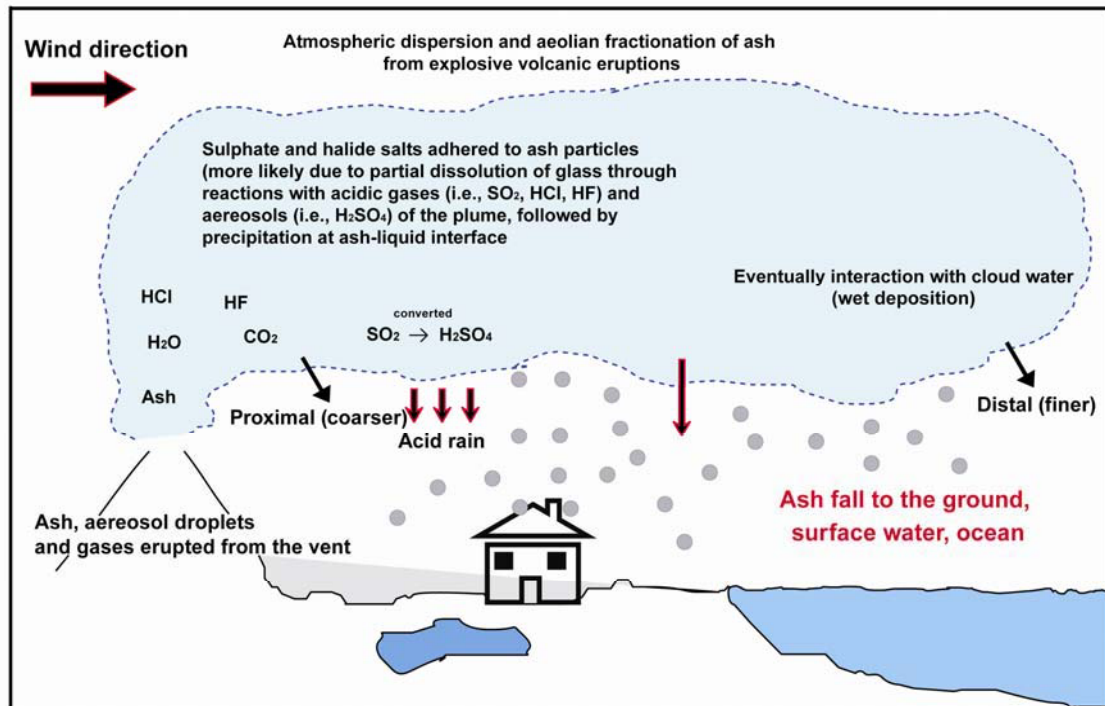
Figure 1.4 Sketch displaying the possible effects of an explosive volcanic eruption on the surrounding environment.

between gases/aerosols and silicate ash particles in volcanic eruption plumes remain poorly understood. Among the gases released those mainly involved are HCl, HF and SO_2. Hydrochloric and hydrofluoric acids will dissolve in water and fall as acid rain whereas most SO_2 is slowly converted to sulphuric acid (H_2SO_4) aerosols. Ash particles may absorb these aerosol droplets onto their surfaces, and subsequent fallout, as temperature and pressure decrease (Allard et al., 2000). Moreover, the formation of coating soluble salts on ash particle surfaces seem also likely due to partial dissolution of the ash through the reactions with acidic gases (i.e., mainly HCl, HF) and aereosols (i.e., H_2SO_4) of the plume, followed by precipitation at the ash liquid interface. This process has been postulated principally for the elements with a low volatility in magma (i.e., lithophilic elements). Extremely thin sulphate and halide deposits (<10 nm) on the ash surface are formed by this process (Delmelle et al., 2007).

Several factors control the adsorption of soluble compounds onto tephra. Firstly, magma type influences the composition of the volcanic gas phase, involving

variability in gas solubilities and degrees of magma degassing (Obenholzner et al., 2003). Furthermore, it leads to different adsorption and deposition characteristics and, thus, the magma source is probably one of the main control factors on metal contents released from volcanic ash (Armienta et al., 2002). Other key parameters that determine the capacity of a solid to react with a gas are their textural properties, namely the specific surface area (Delmelle et al., 2005; Horwell et al., 2003a). Adsorption is much greater for smaller particles (Oskarsson, 1980; Rose, 1977). In addition, the different fragmentation processes produce ash particles with different end-members in relation to morphological characteristic and surface features (Heiken and Wohletz, 1985). Finally, the environmental condition could also affect the amount of compounds adsorbed on ash surface. Increased humidity promotes the role of water in adsorption and coating of particles with an aqueous layer may facilitate the adsorption of volatile species. Humidity is thought to have a strong influence on the distribution of adsorbed sulphur on ash. The increase in sulphur adsorption in higher humidity conditions was explained by enhanced growth of sulphuric acid droplets, which increases the probability of contact with ash particles (Armienta et al., 2002).

Upon deposition, the adsorbed materials can be dispersed into the environment. The rate of their dispersal depends on the affinity of the materials to the ash, the nature of the surface of the ash, the substrate on which the ash is deposited (e.g., deposition straight onto a plant leaf will have a much faster impact than deposition onto a previous layer of ash), the presence of water, either as standing water, surface run-off or rainfall and the environmental conditions (Witham et al., 2005). Interaction of pristine tephra with water dissolves soluble accumulations on particle surfaces resulting in changes to local water chemistry and, hence, quality (Jones and Gislason, 2008; Stewart et al., 2006; Witham et al., 2005). Thus, initial release of soluble ash compounds into the environment may cause short term, but potentially significant, changes on the regional geochemical background.

1.7.1.2 Long term leaching: weathering of volcanic ash constituents

Volcanic glass may be viewed as a metastable supercooled liquid, which exists because of a reduction of nucleation and crystallization rate during rapid magma cooling (White, 1984). The metastable nature of the vitric phase explains the near-absence of glass from volcanic rocks older than Miocene (Marshall, 1961). According to Nesbit and Young (1984) volcanic glass makes up ~12% of the average exposed continental crust surface, being exceeded in abundance only by plagioclase (~35%) and quartz (~20%) (Nesbitt and Young, 1984). Dispersal of volcanic glass particles, which follows explosive volcanic eruptions, primarily of high silicic composition, is an important part of the sedimentary processes (Haflidason et al., 2000; Lacasse and van den Bogaard, 2002; Larsen et al., 1999). Glass shards (>100 µm) fall on land and on the seafloor within a few hours or days after an explosive eruption. However, if highly vesicular pumice is produced, it can float for days or even years and consequently influence the chemistry of the ocean surface (Duggen et al., 2010; Flaathen and Gislason, 2007; Jones and Gislason, 2008) governing also the long term atmospheric CO_2 content and, therefore, climate (Wolff-Boenisch et al., 2006).

Pioneering studies on the aqueous dissolution of rhyolitic and other commonly occurring silicic glasses have been investigated by comparing the composition of the pristine glass phase with the residual composition of its weathered counterpart demonstrating substantial mobility of chemical species during the weathering (Lipman et al., 1969; Noble, 1967; Noble et al., 1967). Furthermore, glass of various compositions is one of the most important constituents of andisols, the main soil type present in volcanic terrains (Shoji et al., 1993). Owing to its abundance and rapid mechanical and chemical weathering, glass plays an important role in the global and local cycling of numerous elements and chemical species at the Earth surface (Wolff-Boenisch et al., 2004b). Dissolution and secondary phase precipitation during weathering alter the chemistry of solutions in contact with glass and affect the chemical composition of surface water (e.g., rivers and lakes) (Stefansson et al., 2001; White and Claassen, 1980).

1.8 State of art of the ash leachate studies

For the short term leaching the existence of readily soluble materials on freshly erupted volcanic ash was documented for the first time at the beginning of the XX century (Lacroix, 1907). However, the plume gas condensation on particle surfaces as source of the leachable elements was suggested much more recently (Taylor and Stoiber, 1973). From this observation, many leachate studies have been designed in order to quantify the volatile budget adsorbed onto ash in volcanic plumes. These experiments were performed mixing a specific amount of ash with a specific volume of solution (normally deionised water) in a determined period of time and, then, analysed for the elements of interest. A review of 55 studies, which reports the ash leachate data for 27 volcanoes, explains that over time a wide variety of the ash leaching experiments were carried out. This study concluded that the comparison of leaching data is hindered due to the broad range of leaching methodologies used (Witham et al., 2005). As already explained, one of the main purposes of this research is to propose a new ash leaching methodology in order to improve the need of harmonization previously commented by other authors (Witham et al., 2005).

Not many works study the long term leaching of volcanic ash in terms of element release from an environmental point of view. Some of these works revise the dissolution rate of natural glasses by flow-through leaching tests (dynamic leaching test in which the leachant solution is continuously renewed) (Gislason and Oelkers, 2003; Wolff-Boenisch et al., 2004a, 2006; Wolff-Boenisch et al., 2004b). Characteristic of these works is the far from equilibration condition of the experimental methodology which allows study the influence of several factors (i.e., glass composition, pH, temperature, etc.) on the glass dissolution rate. Other studies propose dynamic weathering models of crystalline and amorphous silicate in order to explain the time-dependent difference in field and laboratory rates (Velbel, 1993; White and Brantley, 2003). Only few works focused on the element mobility from volcanic ash. Column laboratory experiments were employed to assess the leaching behaviour in terms of element release of pyroclastic glassy ash deposits collected in the

central Main Ethiopian Rift (Rango et al., 2011). Total fluxes of element release from volcanic ash of different historical eruptions (e.g., Hekla, 2000, Mt. St. Helens, 1980) were the aim of the study of Jones and Gislason (2008). This study was principally focused on the nutrient elements released in the sea water rather than the potentially toxic trace elements (PTTEs). In this instance, a very good review was more recently proposed to improve the understanding of the role of volcanic ash for the marine primary productivity (Duggen et al., 2010). Finally, there are a lot of studies which suppose the volcanic glass dissolution as geogenic source of some potentially toxic trace element (e.g., F, As, Mo) concentrations in surface and groundwater in different parts of Argentina, (Bhattacharya et al., 2006; Bundschuh et al., 2004; Francisca and Perez, 2009; Nicolli et al., 1989, 2001, 2011).

PART 2. GEOGRAPHICAL AND GEOLOGICAL SETTING

Chapter 2. Geographical and geological setting

2.1 Climate system along the Andean Cordillera

The Andean Cordillera forms a >7500 km, morphologically continuous mountain chain, along the western margin of South America, from the Caribbean Coast in the north to Cape Horn in the south (Figure 2.1). It is segmented into geological regions with distinct pre-Andean basement ages, Mesozoic and Cenozoic evolution, crustal thickness, structural trends, active tectonics, and volcanism. In general, subduction of the oceanic Nazca and Antarctica plates beneath the continental South American plate are responsible for the formation of magmas and volcanic processes along the western edge of South America.

Two important along-strike variables in the Andes are precipitation and temperature (Clapperton, 1993). These features control, for example, snow lines on volcanoes. From an environmental point of view rainfall and the amount of water available to leach compounds from ash deposits are among the most important features determining glass and mineral weathering and, therefore, the chemical property of the surrounding environment (e.g., soil, water surface, etc.). Volcanic ash is the main component of andisols, which formation (i.e., pedogenesis) is strictly regulated by climate (Teutsch et al., 1999). Water is added to ash deposits by precipitation where it is held against gravitational leaching by adhesive forces. Vectors of water loss are variable within the Andean system. In general, in arid areas the soluble weathering products such as cations (e.g., Na^+, K^+, Ca^{2+}, Mg^{2+}) and Si are leached to shallow depths only, and less soluble components such as Al do not move at all. In humid areas, nearly all major elements could be easily leached and Si is nearly depleted relative to parent material whereas Al has decreased by as much as 60 %. The rate of chemical weathering increases by 2-3 times when the temperature increases by 10 degrees Celsius (Chadwick et al., 2003).

Figure 2.2 illustrates very well the differences along the Andean Cordillera. With a north-south length of approximately 7500 km, peak elevations in excess of 6
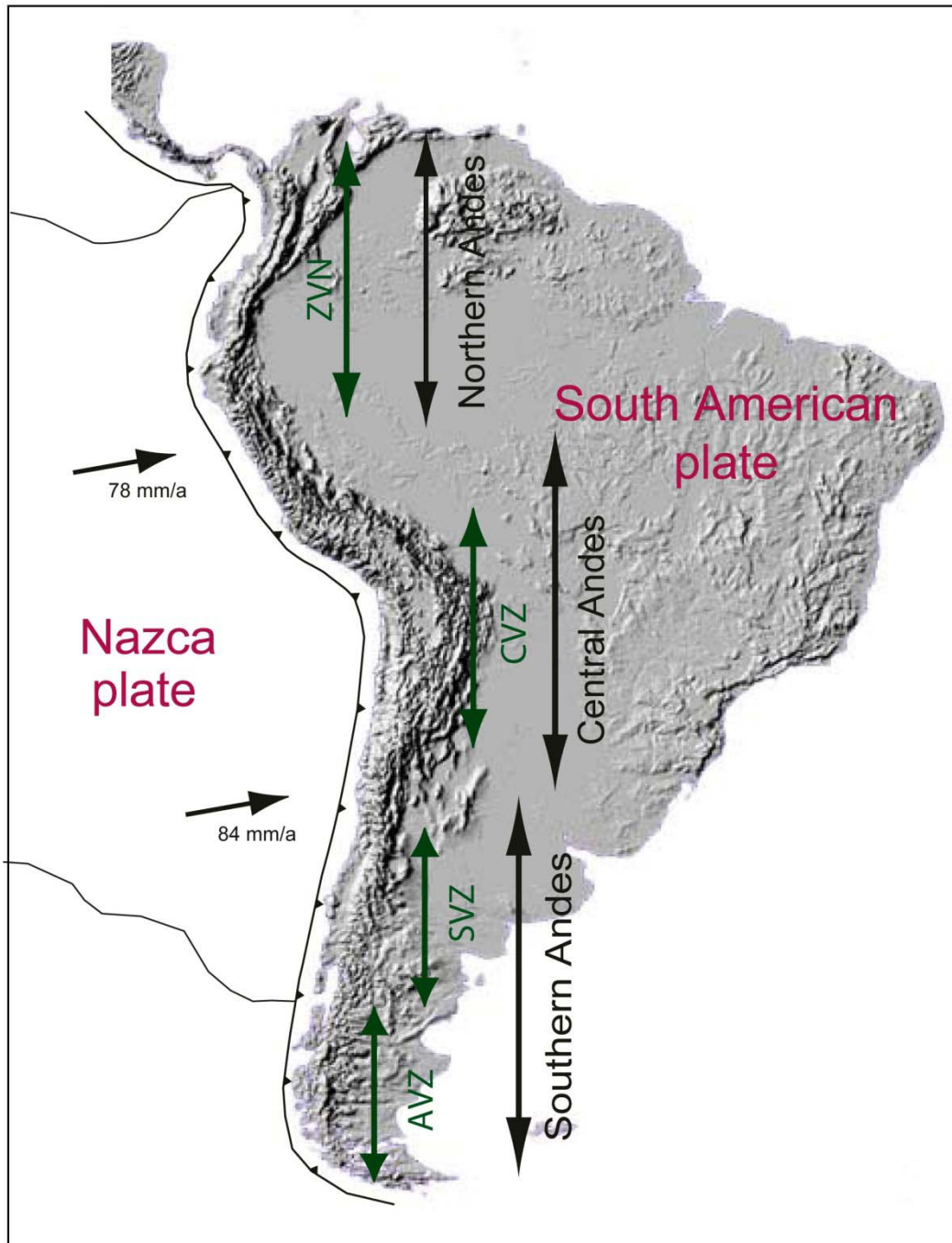
Figure 2.1 Schematic map of South America and the Pacific Ocean plate (Nazca plate) showing the four volcanically active segments in the Andes. Modified after Polanco, 2010.
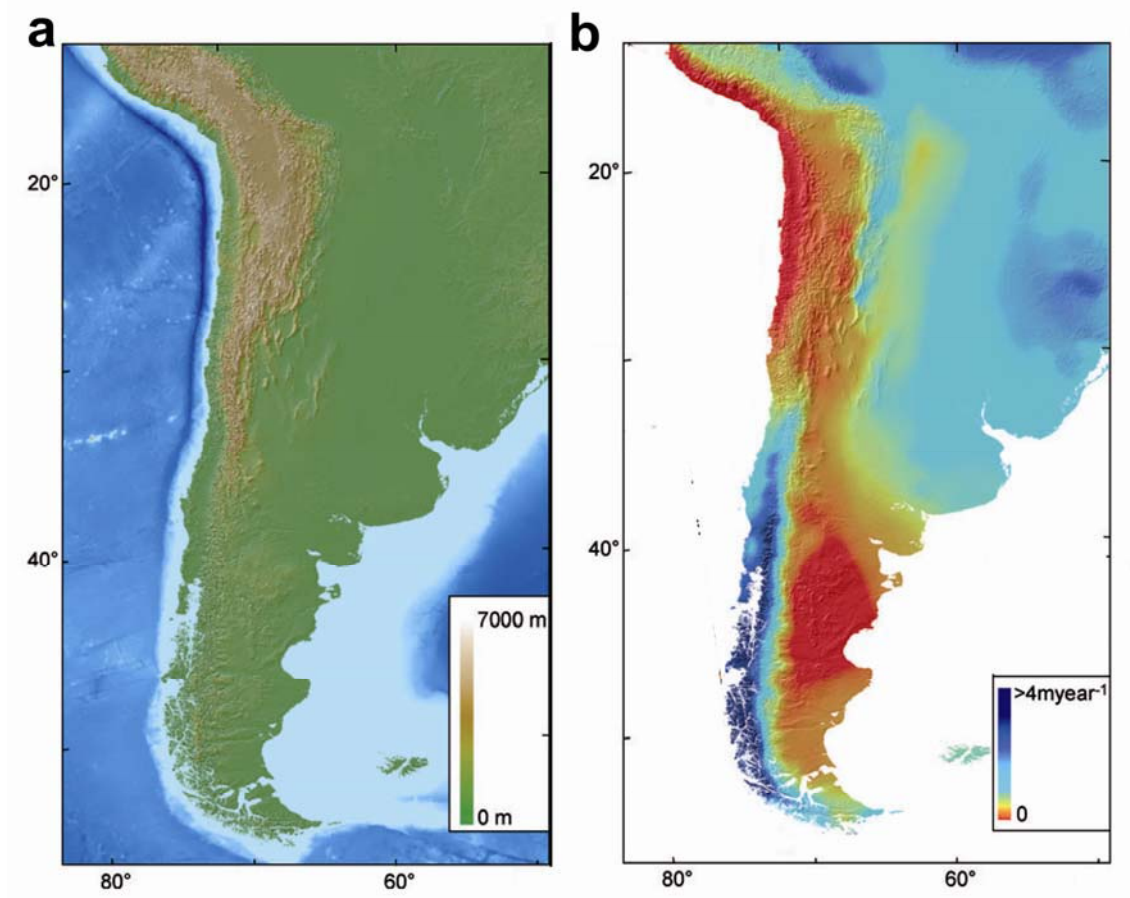
Figure 2.2 (a) Shaded relief of the central and southern Andes and (b) Shaded relief map and precipitation in the central and southern Andes and adjacent areas. Modified after Strecker et al., 2007.

km, the Andes have marked tectonic activity, and strikingly different climatic regimes across and along the strike of the mountain chain. The morphotectonic provinces of the Andes are perpendicular to moisture-bearing winds that impinge on the eastern and western flanks of the orogen, resulting in pronounced gradients (Figure 2.2) (Strecker et al., 2007). For example, in the southern central Andes, including Bolivia and NW Argentina, the Subandean, and Eastern Cordillera ranges block moisture-bearing winds originated in the Amazon basin and the Atlantic Ocean, leading to humid eastern flanks and aridity within the Puna-Altiplano Plateau and the Western Cordillera (Figure 2.2).

The southern central Andes are extremely arid between about 15 and 27º S, comparable to the desert of Australia at the same latitude (Houston and Hartley, 2003). With hyperaridity on the western flank, and less than 200 mm/year rainfall on the Puna-Altiplano plateau and in the intermontane basins east of the Puna, the southern central Andes comprise the most arid sector of the orogen (Grau, 2001). About 80 % of the annual precipitation falls in summer from November to February (Garreaud et al., 2003). The opposite situation exists farther south at approximately 27º S, where the Southern Hemisphere westerlies cause high rainfall on the western flanks of the Principal

Cordillera and the Patagonian Andes and semiarid conditions in the lee of the ranges. Rainfall in the humid western foreland is >3000 mm/yr, contrasting with only ~300 mm/yr to the east of the mountains (Blisniuk et al., 2005).

2.2 Andean Cordillera as paradigm of explosive volcanism setting

Four linear zones of active volcanism are present along the Andean Cordillera: Northern (NVZ), Central (CVZ), Southern (SVZ) and Austral (AVZ) Volcanic Zones (Figure 2.1). The NVZ (5° N–2° S) is located in Colombia and Ecuador, the CVZ (16–28° S) primarily in south Peru and north Chile, but extending easterly into southwestern Bolivia and northwestern Argentina, the SVZ (33–46° S) and the AVZ (49-55° S) in southern Chile and southern Argentina. These zones are divided into a number of smaller volcanic arc segments. The larger zones and smaller segments have magmatic differences reflecting the geologic and tectonic segmentation of the Andean Cordillera (Stern, 2004).

The Andean cycle began in the earliest Jurassic in association with the opening of the Southern Atlantic Ocean. Subduction-related magmatic activity had begun along the west coast of the Northern and Central Andes by at least 185 Ma and the Andes evolved as a result of variations in the subduction process (James, 1971). Andean Cordillera lists 60 historically active and another 118 recently (Holocene) active volcanoes, for a total of 178 volcanoes among 1,511 volcanoes worldwide (Stern, 2004). This study is concerned with the volcanic

ash characterisation in the southern part of the CVZ and the northern part of the SVZ, hence, only these portions are briefly described below.

2.2.1 Central Volcanic Zone

The Central Volcanic Zone (CVZ) of the Central Andes is one of the largest volcanically active regions of the world. The principal magma source for the volcanoes of the CVZ is believed to be derived from the partial melting of an asthenospheric wedge between the overriding continental South American plate and the descending oceanic Nazca plate (De Silva and Francis, 1991; Thorpe and Francis, 1979). The age of the oceanic Nazca Plate being subducted below the South American plate is <60 million years (Stern et al., 2007). The CVZ includes 44 active volcanic edifices, as well as 18 active minor centers and at least 6 potentially active Quaternary large silicic ignimbrite centers and/or caldera systems. Most of the recent (Holocene) volcanic centers in the CVZ occur along the western boundary of the morphotectonic region of the Central Andes referred as Altiplano-Puna (15–23° S and 23–28° S), respectively. The Altiplano-Puna is a high central plateau, at an elevation of 3700 to 4200 m above sea level, bounded by eastern and western Cordilleras with numerous peaks reaching >6000 m of elevation. It is an area in which, from the upper Miocene to Pleistocene, hosted several large-volume explosive eruptions which resulted in the deposition of extensive ignimbrites and volcanic ashes (Soler et al., 2007). The general agreement among authors is that these eruptions began during the late Miocene and continued through the Pliocene into the Quaternary (Baker and Francis, 1978; Tosdal et al., 1981). Furthermore, a number of large stratovolcanoes that initially developed during the Pleistocene accommodated Holocene volcanism within the CVZ (Tosdal et al., 1981). A singular example in the southern Puna is the Cerro Galán caldera, which was active since the latest Miocene but whose culminating eruption, with >1000 km^3 of erupted material, was at about 2 Ma (Schnurr et al., 2007; Sparks et al., 1985).

Although most of the active volcanoes of this area are located in remote areas, with few people living nearby, future eruptions of some of them could affect inhabited areas located in southwestern Bolivia and/or northwestern Argentina,

as during the 1993 eruption of Láscar volcano. Also, although low-altitude prevailing winds in the area blow generally from west to east, high-altitude winds may blow from east to west in some seasons. Therefore, tephra falls from large eruptions could disperse to the west into Chile. The ash deposits could affect both the local population and wetlands, which are the main feeding area of altiplanic camelids (llamas and alpacas), and therefore damage the local economy and quality of the surface water (Stern et al., 2007).

Our study area is comprised between S 25º 26' and S 27º 29' and between W 65º 30' and W 67º 59', in the southern Puna region and neighboring areas in which magmatism is mostly represented by intermediate to acid volcanism (principally andesitic magma). It covers the same age interval as the CVZ activity and although most individual deposits are small in volume (<10 km^3) they occur over a wide area (Schnurr et al., 2007).

2.2.2 Southern Volcanic Zone

The Southern Volcanic Zone (SVZ) includes, at least, 60 historically and potentially active volcanic edifices, as well as three giant silicic caldera systems and numerous minor eruptive centers (Figure 2.3). Volcanoes of the Southern Volcanic Zone occur both in Chile and Argentina. In Chile alone, the SVZ includes >70 Pleistocene and Holocene composite stratovolcanoes and large volcanic fields, and at least nine caldera complexes as well as hundreds of minor eruptive centres (MEC) formed by scoria cones and lava flows. These form a continuous volcanic arc segment 1400 km long, extending from 33.3º S to 46º S. On the basis of the tectonic controls affecting the distribution of volcanic centres, as well as petrologic and geochemical considerations, the Pleistocene and Holocene volcanoes of the SVZ are divided into four main provinces or segments (Figure 2.3) (Stern, 2004). These are the Northern (NSVZ; 33.3–34.4° S), Transitional (TSVZ; 34.4–37° S), Central (CSVZ; 37–42° S) and Southern (SSVZ; 42–46° S) segments (Figure 2.3). Between 33.3º S and 34.4º S the SVZ arc is a narrow chain of volcanoes located along the Chile–Argentina border, but between 34.4º S and 39.5º S the arc widens to >200 km and occurs in both Chile and Argentina. South of 39.5º S the SVZ

again consists of a relatively narrow chain of volcanoes with the volcanic front in Chile, and south of 42° S all the volcanic arc is located in Chile.

Post-glacial eruptions of SVZ volcanoes include the full range of Hawaiian, Strombolian, Subplinian, Plinian, Vulcanian and phreatomagmatic types, with Volcanic Explosivity Index (VEI) ranging from 0 to 6 (Newhall and Self, 1982). The SVZ has more historic volcanic activity, with about one eruption per year on average, than either of the other two volcanic zones. Ashfall produced by explosive eruptions in the SVZ has the potential to significantly disrupt international air traffic across the southern part of South America (Stern et al., 2007). Villarrica and Llaima volcanoes in the CSVZ are two of the most active volcanoes in the entire Andean arc, with together more than 80 reported episodes of activity since 1558 (Stern et al., 2007). Ashfall produced by the 1991 eruption of Hudson adversely affected very large regions to the east in Argentina. In this study many of the volcanic ashes come from eruptions of the SVZ, hence, each volcano (including the volcanic hazards) are described separately below.
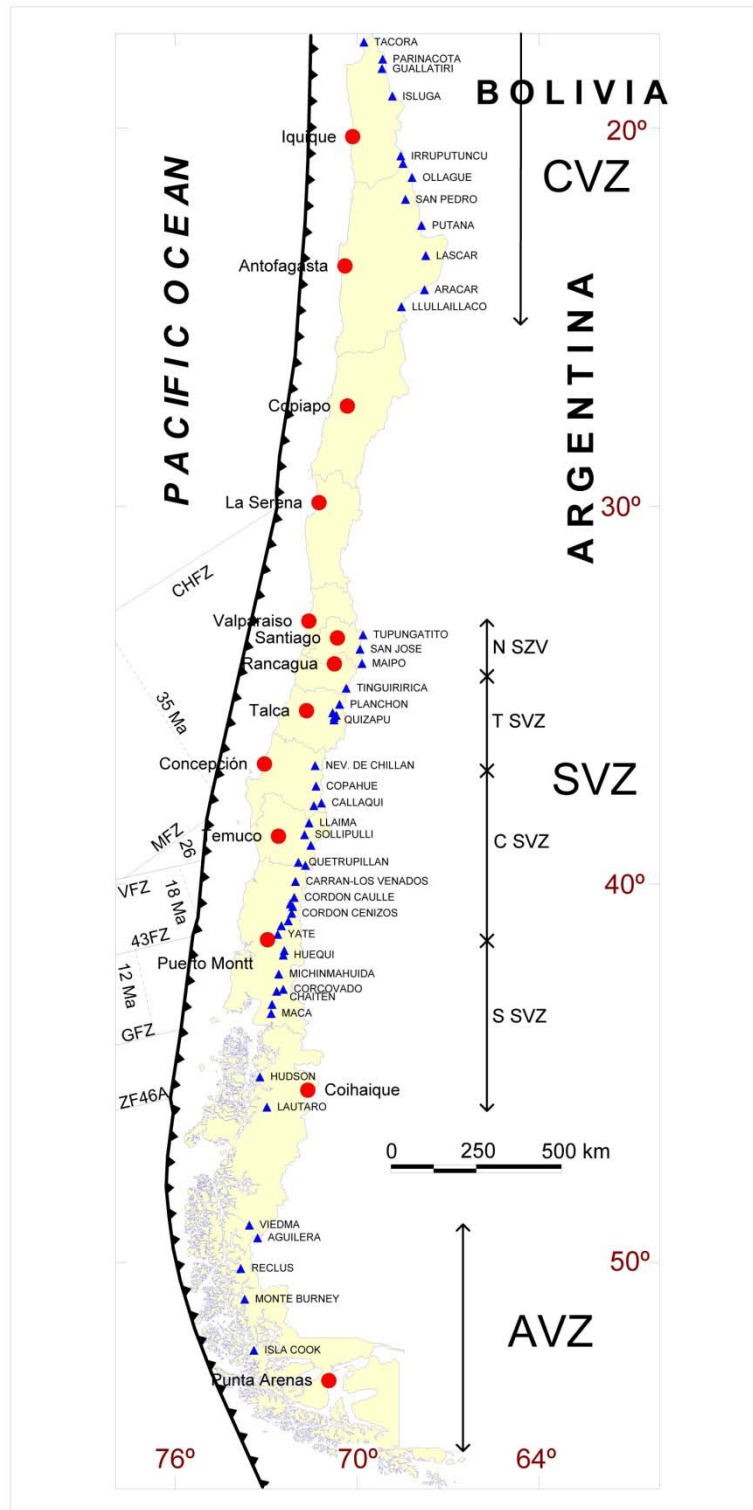
Figure 2.3 Schematic map of the location of some the volcanoes and the calderas system in the three volcanically active segments in the southern Andes: central (CVZ), southern (SVZ) and austral (AVZ). The sub-classification of the SVZ is northern or NSVZ (33-34.5**°** S), transitional or TSVZ (34.5-37**°** S), central or CSVZ (37-41.5**°** S) and southern or SSVZ (41.5-46**°** S). Modified after Polanco, 2010.

2.2.2.1 Copahue volcano

The northernmost studied volcano in the SVZ is the Copahue volcano (37.85º S 71.17º W, 2997 m a.s.l.), the major active stratovolcano in the central part of the

Figure 2.4 The 2000 eruption of Copahue volcano (Photo: J.A. Naranjo, after Polanco, 2010).

SVZ, located in the border between Chile and Argentina. Its eruptive episode from July to October 2000 is the largest eruption known from this volcano (Figure 2.4). Frequent explosions caused basaltic andesite ashfall around the village of Caviahue. Acid rain and small-volume mud-flows were other volcanic hazards observed at this time (Naranjo and Polanco, 2004). However, the presence of an acid lake within the active crater represents one of the most hazardous aspects that could threaten Caviahue, the closest village to the volcano (Varekamp et al., 2009).

2.2.2.2 Lonquimay volcano

The Lonquimay volcano in Chile (38.37º S 71.58º W, 2865 m a.s.l.) is located 50 km south of the Copahue volcano. This is a stratovolcano that has been active mainly in Holocene times (Moreno and Gardeweg, 1989; Naranjo et al., 1992; Polanco, 2010). Its eruptive activity has been divided into six lava units,

including the most recent eruptive products generated in the 1988–89 eruption. This eruption generated a flank pyroclastic cone (Navidad cone; Figure. 2.5) and an associated lava flow which resulted in the death of several thousands of animals (Naranjo et al., 1992; Stern, 2004). It was the first strombolian type eruption in the last 100 years, active during 13 months and characterized by the production of 0.12 km^3 of basaltic andesite tephra distributed over ~500 km^2 (Moreno and Gardeweg, 1989). The maximum eruptive column height was estimated in 9 km above the vent with an estimated VEI of 1–2, and the lava flow reached up to 10.2 km from the source. The high fluorine content produced widespread pollution of land, air and water which strongly affected both humans and grazing animals. According to the historical and post-glacial activity, the main hazards related to Lonquimay volcano are the formation of new flank vents, the emission of volcanic products with high fluorine content and the consequent contamination of water, grass and atmosphere, and tephra fallout (Moreno and Gardeweg, 1989; Naranjo et al., 1992; Polanco, 2010). Another important hazard, although less recurrent, is the production of small-volume of pyroclastic flows, which can reach populated areas (Stern et al., 2007).

Figure 2.5 The 1988-1989 eruption of the Navidad cone flanking the Lonquimay volcano. (Photo: H. Moreno , after Polanco, 2010).

2.2.2.3 Llaima volcano

The Llaima volcano (38.69º S 71.73º W, 3125 m a.s.l.) is one of the most active volcanoes in the Andes, with more than 49 reported episodes of activity since 1640. It began a new strombolian eruption episode on January 2008 (Venzke et al., 2009). Activity started with strong Strombolian eruption that dropped lava fragments on the high flank glaciers, generating lahars that flowed ~15 km to reach Captrén River to the north and Calbuco River to the west. The eruptive column rose to an altitude of ~11 km and ash was accumulated to a depth of 11 cm at a distance of ~7 km from the crater (Venzke et al., 2009). The main hazard related to Llaima volcano corresponds to the generation of lahars due to ice/snow melting of its ice-cap during an eruption from either the central or a flank vent (Stern et al., 2007). Emission of lava flows (up to 30 km long) and tephra fallout (mainly distributed towards the east) are also two important hazards that could damage villages located on the lower flanks of the volcano.

Figure 2.6 The 2008 eruption of Llaima volcano showing the volcanic plume towards the east (Photo: V. Sepúlveda, after Polanco, 2010).

2.2.2.4 Chaiten volcano

The most recent ash sample comes from the (2 May) 2008 Plinian eruption of

Figure 2.7 The 2008 eruption of Chaiten volcano. Photo taken in the Chaiten village at 8 km from the crater. (Photo: R. Flores, after Polanco, 2010).

the Chaiten volcano (42.83° S 72.64° W, 1122 m a.s.l.). It is a small elliptical (3x4 km in diameter) post-glacial caldera, located 10 km northeast of Chaiten town in the Gulf of Corcovado, in southern Chile (Naranjo and Stern, 2004). Chaiten volcano is one of the 120 actives volcanoes of the continental Chile, but its threat was not considered at a high priority level (Lara, 2009). The 2008 eruption was the largest explosive eruption globally since Hudson, Chile, in 1991, and was the first explosive rhyolitic eruption since Novarupta, Alaska, in 1912 (Martin et al., 2009; Watt et al., 2009).

Preventive evacuation of ca. 5,000 residents was ordered on May 4-5 (2008) and two security radius were defined at 30 and 50 km. Impacts of the eruption were extensive in Chile and Argentina. Floods and lahars inundated the already evacuated Chaitén town on May 12. Ash clouds shut down regional airports and

forced the cancellation of hundreds of domestic flights and several international flights in Argentina and Chile. Floods also disrupted the backbone road of continental Chile and the active aquiculture industry was severely affected (Lara, 2009).

2.2.2.5 Hudson volcano

Finally, the southernmost eruption studied in the SVZ is from the Hudson volcano or Cerro Hudson (45.90º S, 72.47º W, 1905 m a.s.l.). The August 1991 eruption of Hudson volcano was developed in two phases. Phase 1 (P1, August 8) produced both lava flows and a phreatomagmatic tephra fall (0.2 km^3, bulk volume). The paroxysmal phase P2 was Plinian and lasted four days (August 12-15). The tephra was basaltic in phase P1 and trachyandesitic in phase P2. The second phase produced a much great damage than the first in agriculture and cattle sheep. The large 1991 Plinian eruption of Hudson was one of the largest explosive eruptions of the 20th century involving 4.3 km^3 (bulk volume) of tephra fall deposits covering more than 150,000 km^2 in Chile and Argentina (Naranjo and Stern, 1998, 2004; Stern, 2004). Some 8,000,000 ha of agricultural land in Patagonia, Argentina, was covered by volcanic ash (Inbar et al. 1995). Ash thickness ranged from 2 m in the Andean area to <1 mm at the Atlantic coast zone, with traces of ash deposited as far away as the Falkland Islands (Inbar et al., 1995). Significant livestock deaths from ash covering and burying pastures and horticultural crops were impacted by wind-remobilised, not fluorosis hazards as first thought (Inbar et al., 1995; Rubin et al., 1994).

PART 3. METHODOLOGY

Chapter 3. Sampling

3.1 Field work and sample collection

Field works were carried out in different campaigns during the period 2006-2008 (Table 4.1). Most of the field work was done by members of the PEGEFA research group. In addition, some samples were obtained through the collaborative work with other researchers and Institutions.

Table 3.1 Chronological field works during this research.

Periods	Sample collection	Area under study
2006-2007	21 supposed volcanic ash deposits	Argentina, Central Volcanic Zone (CVZ)
	8 supposed volcanic ash deposits	Uruguay
2008-2009	8 volcanic ash samples	Chile, Southern Volcanic Zone (SVZ)

Descriptions of the field work, the sampling method, as well as, the location of sampling sites are reported below.

3.1.1 Field work in the Central Volcanic Zone (CVZ) and Uruguay

Twenty one supposed volcanic ash deposits in the southern Puna and neighbouring areas (Catamarca and Salta provinces, Argentina) and eight supposed volcanic ash deposits in Uruguay were sampled throughout the period 2006–2007.

In Argentina the study area is located between 25.5 and 26º S and between 65 and 67º W (Figure 3.1). The Puna area has been one of the regions most affected by explosive volcanism worldwide over the past several million years. It has some of the largest and most explosive supervolcanoes in the world (e.g., Cerro Galán, Cerro Blanco). Many of the ash deposits are extremely well preserved due to the hyper-arid conditions which are prevailing in the region for

millions of years (Figure 3.2) (Garcia-Vallés et al., 2008; Stern, 2004). By taking into account their stratigraphic position, the age of these deposits was constrained to hundreds of thousands to several million years (Risse et al., 2008).

In Uruguay the study area is located between 33 and 34º S and between 56 and 58º W (Figure 3.3). The Uruguayan Quaternary record has been studied by several authors in the last four decades (Aguilar, 2006; Calarge et al., 2006; Ubilla et al., 2004). The Quaternary glacial and interglacial record consist of a few tens meters of thickness of sediments and shows several non-depositional surfaces. The samples collected were deposited during the Pleistocene with alternance of semiarid and temperate conditions. The source magmas were silica-rich, the eruptions were highly explosive (Axerold, 1981).

The same methodological sampling process was applied in the two field surveys. Sampling sites were located by GPS and the coordinates are shown in Table 3.2. Also a brief description of the ash specimens is given in this table. Ash layers were identified in the field upon visual examination by considering the local geological setting, the morphology of the layered deposit, the grain size of the sediment (fine sand to silt) and the colour (gray, cream and white). After SEM observation, only 11 samples were confirmed as pure ashes while the rest
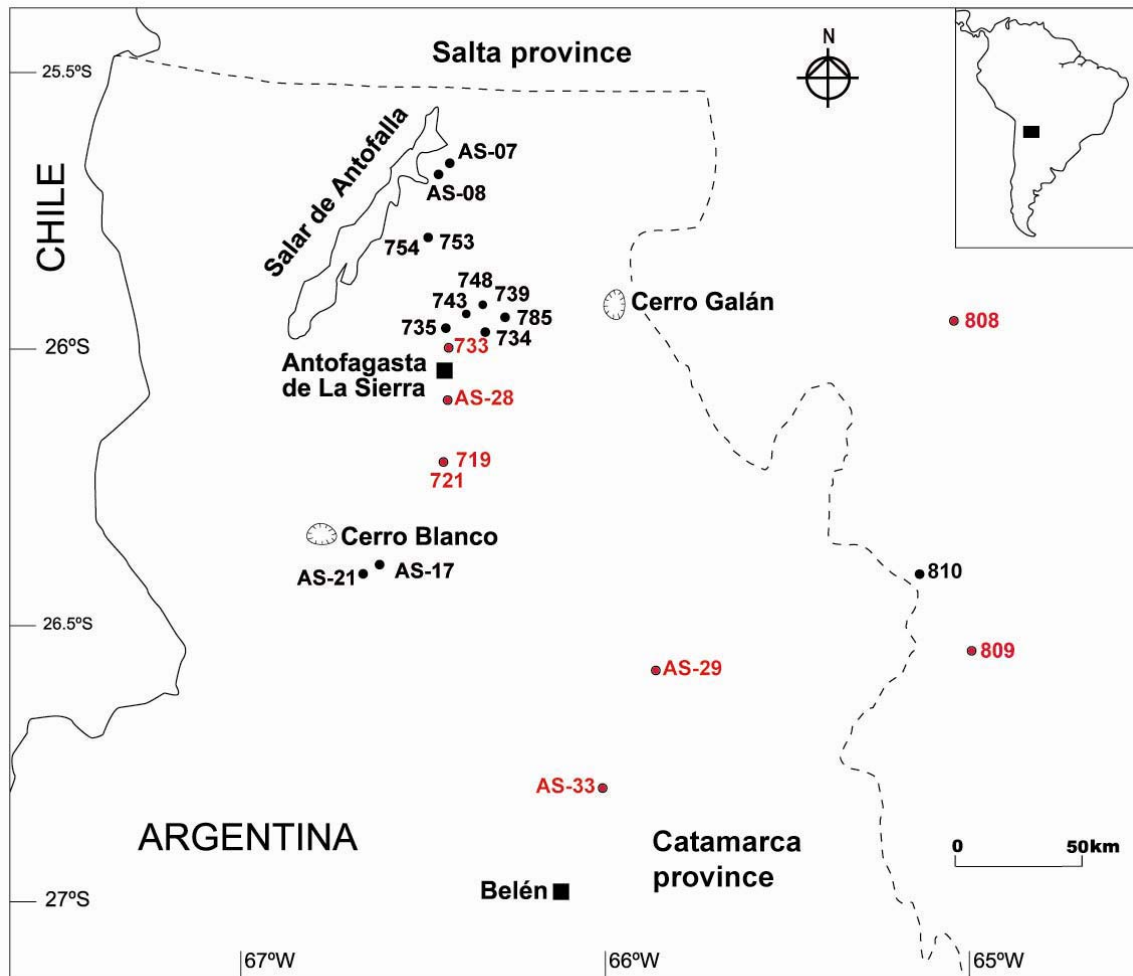
Figure 3.1 Location of the sampling sites of the supposed 21 volcanic ash deposits in the Puna and neighbouring area. Black circles refer to mixed volcanic ashes and red circles to pure volcanic ashes.
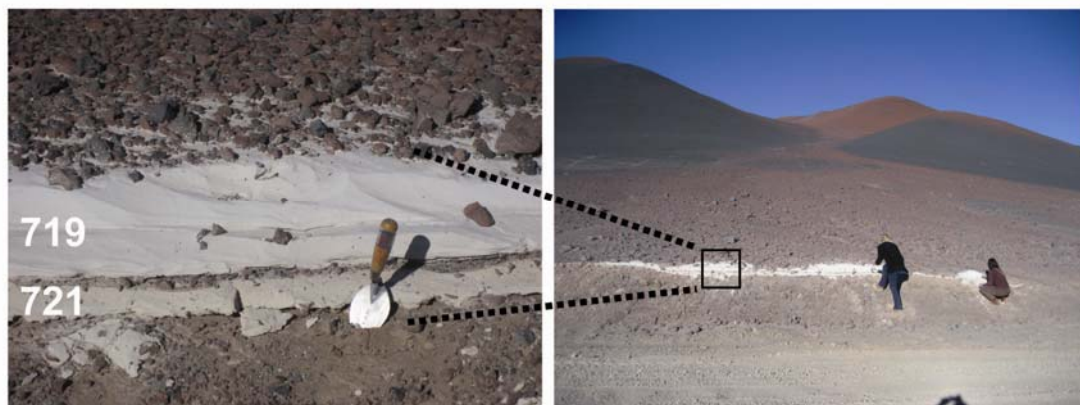
Figure 3.2 Photographies of the 719 and 721 ash deposits of the Puna region.

corresponds to ash mixed in different degrees whit other materials. Locations of sampling sites and photographies of an example of ash deposits are reported in Figures 3.1-3.3. Samples were collected with a stainless steel shovel excluding the most surficial (2 cm depth) ash in order to avoid the most weathered materials. About 2 kg of sample were placed in polyethylene bags and carried to the laboratory. Samples were dried at 40 ºC in an oven and stored in polyethylene vessels until preparation for analysis.

Table 3.2 Coordinates of the sampling sites (geodetic reference WGS 84), colour and grain size of the sediments.

Sample	Latitude	Longitude	Height (m)	Colour	Grain size
719	W 67° 23' 47''	S 26° 18' 52''	3144	white	silt
721	W 67° 23' 47''	S 26° 18' 52''	3144	cream	silt
733	W 67° 25' 39''	S 26° 02' 39''	3371	white	silt
734	W 67° 24' 32''	S 26° 29' 21''	3371	cream	silt
735	W 67° 24' 51''	S 26° 29' 25''	3371	pale-gray	silt
739	W 67° 25' 42''	S 26° 9' 19''	3457	pale-gray	silt
743	W 66° 44' 20''	S 26° 58' 40''	3457	white	silt
748	W 66° 55' 5''	S 26° 8' 56''	3457	cream	silt
753	W 67° 23' 47''	S 26° 18' 52''	3875	pale-gray	silt
754	W 67° 46' 24''	S 26° 18' 20''	3875	pale-gray	silt
785	W 67° 25' 40''	S 26° 2' 39''	3500	cream	silt
808	W 65° 44' 31''	S 25° 57' 00''	1473	cream	silt
809	W 65° 40' 34''	S 26° 55' 56''	1883	cream	silt
810	W 65° 52' 47''	S 25° 59' 53''	3125	cream	silt
AS-07	W 67° 23' 22''	S 25° 59' 53''	3966	cream	silt
AS-08	W 67° 23' 20''	S 25° 59' 53''	3014	cream	silt
AS-17	W 67° 29' 6''	S 26° 49' 32''	3003	tan	silt
AS-21	W 67° 29' 9''	S 26° 49' 32''	3328	cream	silt
AS-28	W 67° 25' 41''	S 26° 2' 45''	3328	cream	silt
AS-29	W 66° 44' 19''	S 26° 55' 56''	2471	tan-cream	sand
AS-33	W 66° 53' 47''	S 26° 18' 52''	3328	cream	sand
UR-1	W 57° 59' 14''	S 33° 12' 49''	95	white	silt
UR-2	W 56° 59' 9''	S 34° 34' 6.3''	45	cream	silt
UR-3	W 56° 59' 9''	S 34° 34' 6.3''	45	cream	silt
UR-4	W 57° 59' 14''	S 33° 12' 49''	50	cream	silt
UR-5	W 56° 59' 9''	S 34° 43' 6.3''	45	cream	silt
UR-6	W 56° 59' 9''	S 34° 34' 6.3''	45	white	silt
UR-7	W 56° 59' 9''	S 33° 12' 49''	45	pale gray	silt
UR-8	W 57° 59' 14''	S 33° 12' 49''	40	cream	silt
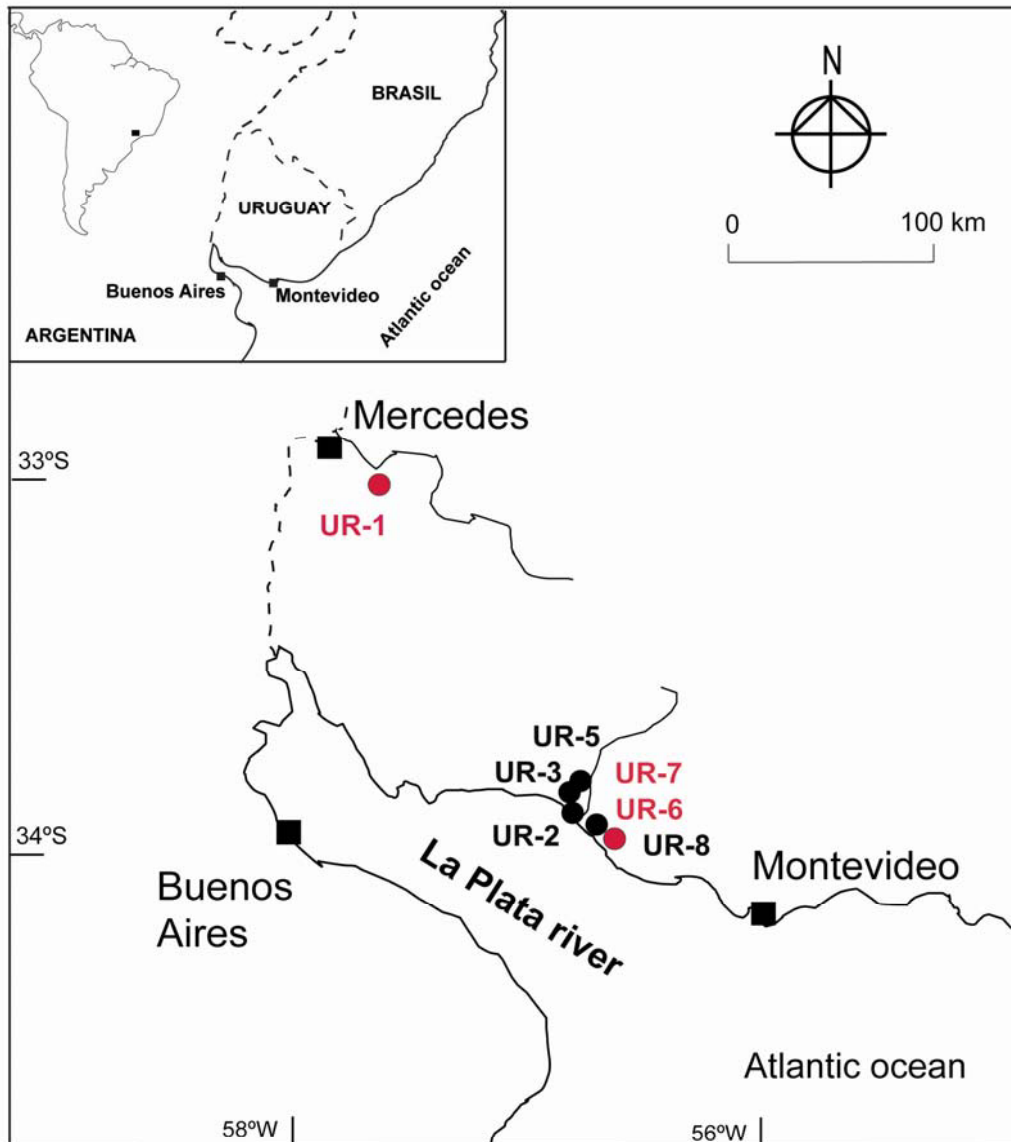
Figure 3.3 Location map of the sampling sites of the supposed 8 volcanic ash deposits found in Uruguay. Black circles refer to mixed volcanic ashes and red circles to pure volcanic ashes. Photograph of the UR-6 ash deposit.

3.1.2 Sample collection from the Southern Volcanic Zone (SVZ)

The 8 samples coming from volcanoes of the Southern Volcanic Zone (SVZ) of the Andes are from historical eruptions, which have been documented by the Smithsonian's Global Volcanism Network (http://www.volcano.si.edu/). Namely these volcanoes are: Copahue. Lonquimay, Llaima, Chaiten, and Hudson. Figure 3.4 shows their location. Samples from Copahue. Lonquimay, Llaima, and Hudson volcanoes were generously provided by the Chilean institution SERNAGEOMIN (Dr. J. Naranjo). Table 3.3 shows sampling location, distance from volcano, eruption date, collection date and pristinity of studied ashes. Eruptions are ordered according to their N-S position along the SVZ.

The Chaiten ash samples have been sampled in the field during or soon after the volcanic eruption. Three of these were sampled by a member of PEGEFA research group (Dr. E. Polanco) and one sample was supplied by Dr. A. Caselli from the Facultad de Ciencias Exactas y Naturales, Universidad de Buenos Aires, Argentina. Table 3.4 and Figure 3.5 shows the location and general information of Chaiten ash samples. Field work was conducted during the first month of the Chaiten eruption in the case of CHA-G, CHA-1F, and CHA-E samples. This means that these samples are ashes erupted during the initial explosive phase (2–5 May 2008). CHA-1F ash was collected on a building surface in the town of Chaiten at 10 km southeast of the Chaiten crater and the last two samples (CHA-G and CHA-E) were collected in the Esquel village at 106 km of the Chaiten crater. The very pristine CHA-G ash was sampled on a plastic surface during the first fallout of volcanic ash. CHA-E was sampled on the ground with a stainless steel shovel. Finally, the sample CHA-2R is a volcanic ash affected by the rainwater action and it was collected at August 2008 being generated after dome growth began (from 21 May 2008). Samples were dried at 40 ºC until the preparation for analysis.

Table 3.3 Coordinates of sampling sites and general information of the ashes from the Southern Volcanic Zone of the Andes. Chaiten ashes are in Table 3.4.

	COPAHUE	LONQUIMAY	LLAIMA	HUDSON
Longitude	71°09'51.23"W	71°33'12.69"W	71°37'30.69"W	72°41'2.19"W
Latitude	37°51'16.93"S	38°22'18.75"S	38°41'57.39"S	45°24'11.70"S
Eruption date	01-Sep-00	25-Dec-88	Jan -08	08-Apr-91
Collection date	01-Sep-00	21-Jan-09	03- Jan-08	08-Apr-91
Distance from volcano	0.73 km	0.20 km	9 km	60 km
Pyroclastic materials	ash	ash	lapilli	ash
Pristine	yes	no	yes	yes

Table 3.4 Coordinates of sampling sites and general information of the ashes from Chaiten volcano.

	CHA-1F	CHA-2R	CHA-G	CHA-E
Collection date	10-may-08	15-ago-08	03-may-08	08-may-08
Location	Chaiten	-	Esquel	Esquel
Longitude	W 72°42'18.68"	W 72°38'45.09"	W 71°20'45.56"	W 71°20'45.56"
Latitude	S 42°55'9.04"	S 42°57'16.01"	S 42°54'29.94"	S 42°54'29.94"
Distance from volcano	10.5 km	60 km	106 km	106 km
Pristine	yes	no	yes	yes
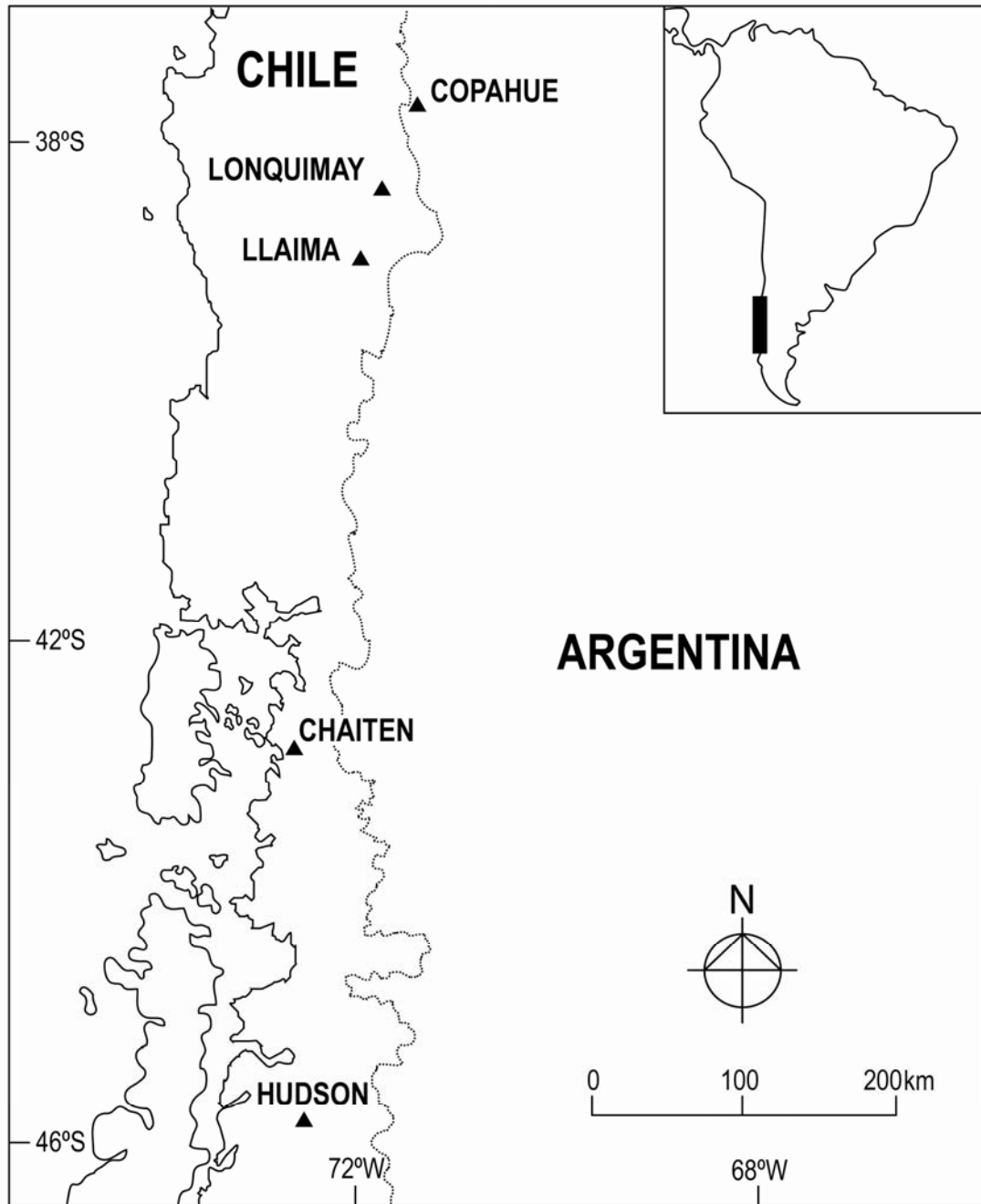
Figure 3.4 Location of the volcanoes under study in the SVZ.

Figure 3.5 Location of the sampling sites of the Chaiten ashes. Red circles refer to pristine volcanic ashes.

Chapter 4. Methodology and analytical techniques

4.1 Introduction

The methodological part can be considered the main body of this research. The characterisation carried out has been divided in physical, mineralogical and chemical (Figure 4.1). One or more analytical techniques have been used in each category. The physical characterisation of volcanic ashes consists of the study of the morphological properties of the ash particles, the Specific Surface Area (SSA) and the grain-size distribution (GSA). Whilst, the chemical characterisation has been divided in whole rock chemical analysis, leaching experiments, and FTIR spectroscopy study. The ash leaching tests are one of the main objectives of the methodological work because they allow recognizing the local geochemical impact occurring after the deposition of volcanic ashes on the environment. Several types of leaching tests were carried out. Hence, it has been considered appropriate a brief introducing on them, before to describe the analytical techniques used in this research (Figure 4.2). The developed protocols for the different chemical analysis are reported in Appendix 1.

Most of the analyses have been carried out at the Serveis Científico-Tècnics, Universitat de Barcelona. Parts of the other analyses have been undertaken at the Institute of Earth Sciences J. Almera, CSIC, Barcelona, and at the Italian National Agency for New Technologies, Energy and Sustainable Economic Development (ENEA), Rome.

In the further paragraphs each one of the analytical techniques are carefully described. Training on different techniques has been an important part of this research. It is mention to note that these protocols are nowadays used by other researchers that form part or collaborate with our Consolidated Research Group PEGEFA.

4.1.1 Relevance of the ash leaching tests

Leaching tests are typically used to provide information about the constituent concentration and release from a specific sample under conditions simulating actual scenarios. In general, a leaching test involves contacting a solid material with a leachant to determine which components in the solid will dissolve in the leachant creating a leaching solution or leachate. A number of different types of leaching tests exist. In this research, the contribution of the volcanic ash to the local geochemical balance was performed by (Figure 4.2):

(1)   Short term leaching behaviour of volcanic ash by single batch leaching tests (SBLTs). In the present study, two SBLTs were performed using deionised
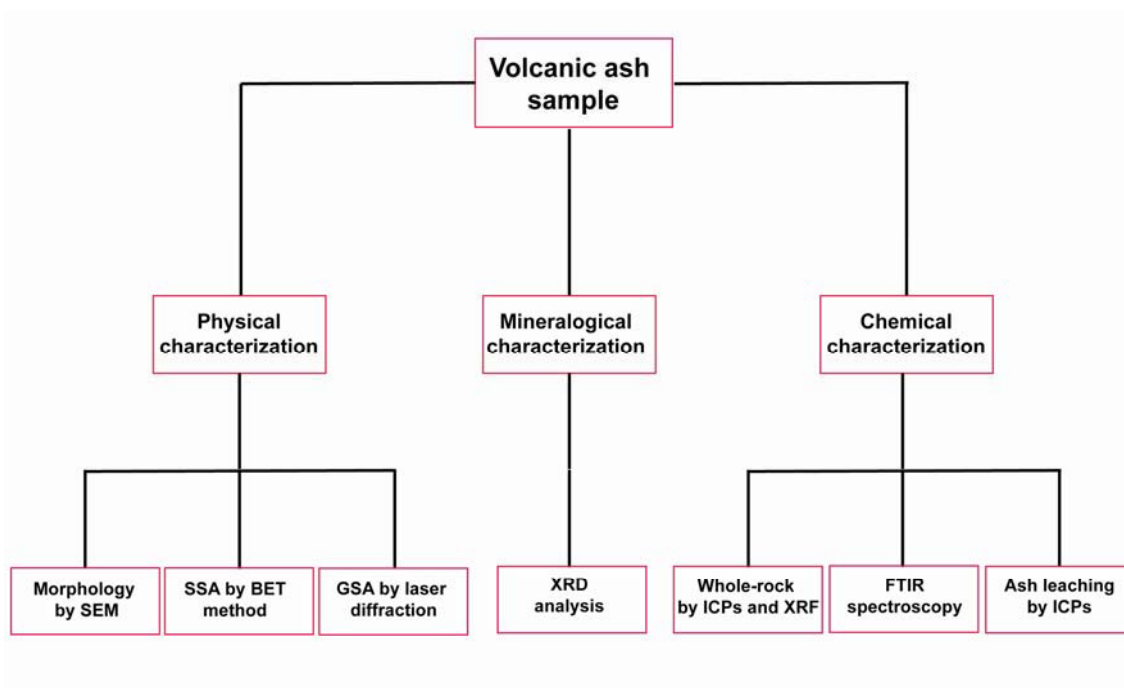
Figure 4.1 Summary of the analytical techniques used in this research. SEM, Scanning Electron Microscopy; SSA, Specific Surface Area; BET, Brunauer-Emmett-Teller; XRD, X-Ray Diffraction; ICP, Inductively Coupled Plasma; XRF, X-Ray Fluorescence; FTIR, Fourier transform infrared.

water and nitric acid as leachants. The former leachant is less aggressive and its slightly acid pH allows a rapid screening of the potentially hazardous elements that can be leached from the ashes. Nitric acid extraction is useful for the assessment of the maximum load of PTTEs environmentally available

(Papastergios et al., 2009, 2010; Sastre et al., 2002). Moreover, a new methodology of SBLT with deionised water from both recently erupted and ancient volcanic ashes is proposed.

(2)   Temporal leaching behaviour of potentially hazardous elements by column leaching tests. The eluted solutions were periodically collected and analysed.

(3)   Sequential extraction scheme (SES) using different types of reagents as extractants to obtain information on element phase associations and their potential mobility. The basic concept of this kind of test is that the mobility of elements in the environment depends not only on their total concentrations but also on the chemical form in the solid phase to which they are bound.
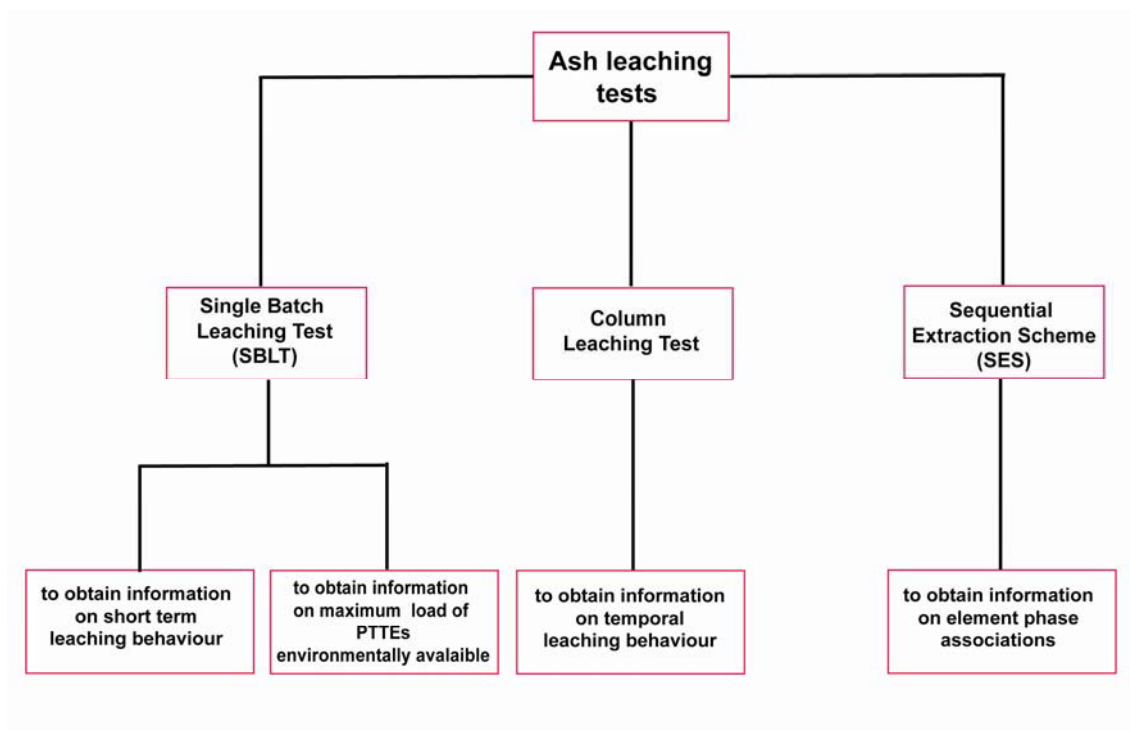
Figure 4.2 Summary of the ash leaching tests performed on the volcanic ashes.

A brief explanation of the theory of the leaching tests used in this research is reported here. The proper methodology of these tests is reported within the respective chapter. The developed protocols for the ash leaching tests are reported in Appendix 5.

These leaching tests could be divided on the basis of whether or not the leachant is renewed. The SBLT and the SES are extraction tests in which a specific quantity of leachant is contacted and with a specific amount of sample for a certain time. They are shacked, generally, in polyethylene reactors without leachant renewal. A sequential chemical extraction test is composed of a battery of extraction tests. It involves sequential elutions of aliquots of a sample with different leachants, which are increasingly more aggressive in terms of chemical attack towards the residue. For both, the leachate is separated from the solid and analysed at the end of the test. The underlying assumption in these tests is that an equilibrium condition is achieved at the end of the extraction test (i.e., the concentrations of solutes in the leachate become constant). The agitation increases the leaching rate and allows reaching steady-state conditions as quickly as possible.

The flow-through or column leaching tests are dynamic tests where the leachant is continuously renewed to maintain a driving force for leaching that is solution-controlled. Such tests provide information about the kinetics of solid phase dissolution and component flux. Information is generated as a function of time, and it is a priority to preserve the physical integrity of the residue. In a flow-through test, a small cylindrical container is packed with a porous solid and leachant is passed through. The system may be operated either in an up-flow or down-flow mode. Here, mini columns (8 cm height and a cross-sectional area of 2.5 cm^2) in down-flow mode were used to achieve a relatively rapid breakthrough of leached species. The effluent is periodically sampled and analysed for the parameters of interest.

4.2 Physical characterisation

The physical characterisation of volcanic ashes has been divided in the study of the morphological properties of particles using Scanning Electron Microscopy with Energy-Dispersive Analyser (SEM-EDX), the analysis of the Specific Surface Area (SSA) by the application of the gravimetric nitrogen Brunauer-Emmett-Teller (BET) surface analysis technique, and the grain size analysis (GSA) by laser diffraction.

4.2.1 SEM-EDX analysis

Scanning electron microscopy (SEM) is a fast and cost-effective analytical tool to identify volcanic ash. SEM examination facilitates the description of particle shape, vesicularity and external surface texture as well as the eventual occurrence of surface alteration or secondary minerals, and the particle size determination (Ersoy et al., 2006; Heiken and Wohletz, 1985). Moreover, the X-Ray Energy Dispersive analyzer (EDX) currently coupled with SEM helps to identify through a semi-quantitative chemical analysis the mineral phases associated with the glass shards (Severin, 2004). Elements occurring in concentrations of 1 %, m/m and even lower are readily detectable. There are, however, two requirements for the samples being studied by SEM-EDX: they must be dry and they must be conductive. In this case, particles from volcanic ash samples were dried in an oven at 40 ºC and after were mounted on carbon stubs and coated with carbon. SEM images and spot EDX analysis were performed using a FEI Quanta 200 instrument, equipped with the Genesi program and an EDX detector for determination of mineral chemistry (minimum spot size: 5.3 µm; working distance: 9.6 mm; accelerating voltage: 20 kV). Images of surface samples were recorded at various magnifications. Spot EDX elemental analyses were performed on different particles.

4.2.2 BET specific surface area analysis

Brunauer-Emmett-Teller (BET) analysis has ability to provide information about textural features as the Specific Surface Area (SSA) of a particular specimen. SSA estimation based on gas sorption experiments requires an estimate of the gas cross sectional area and the amount of gas necessary to form a monolayer. The more commonly used gas adsorbates are nitrogen (N_2) and krypton (Kr), and the BET model is typically used to estimate the amount of gas required for the formation of a monolayer (Papelis et al., 2003). In this research, the SSA analysis was conducted by the application of gravimetric nitrogen BET specific surface analysis technique using a Micromeritics ASAP 2010, automatic physisorption analyzer with multi-gas option. All analyses were performed with N_2 as gas adsorbate at liquid nitrogen temperature (≈77 ºK). To improve

analysis accuracy, the ASAP 2010 has a high vacuum molecular drag pump capable of producing a vacuum of 10^{-5} mm Hg or better, 1000 and 10 mm Hg pressure transducers, completely independent vacuum systems for sample outgassing and analysis, and patented isothermal jackets to maintain constant sample temperature throughout the experiment. The instrument was calibrated using both high (216 ± 6 m^2 g^{-1}) and low (0.61 ± 0.08 m^2 g^{-1}) silica-alumina surface area standards, although the measured SSA of the almost of samples was much close to the lower standard. Prior to the determination of the adsorption isotherm, the sample was evacuated while heating at 90 ºC for one hour and then at 350 ºC for at least four hours. This procedure assures complete outgassing of the finer pores that may contribute substantially to the total SSA of porous materials. BET estimates of surface areas were based on isotherms with at least 5 points in the linear range and correlation coefficients typically greater than 0.9999. The typical accuracy of SSA determinations based on the BET model is considered to be $\pm$ 10% (Gregg and Sing, 1982).

4.2.3 Grain-size analysis (GSA) by laser diffraction

The grain-size distribution of the volcanic ash is of critical importance to discuss the associated environmental hazard. Airborne particles with low grain-size (e.g., lower than 36 µm) could be re-mobilised and dispersed from ash deposits by human activity and wind causing damage in the surrounding environment. There are many grain-size analysis (GSA) techniques available, ranging from state-of-the-art laser diffraction to basic sieving. The most time-efficient and robust way to obtain a GSA is by laser diffraction (Horwell, 2007). GSAs were carried out using a Malvern Masterziser 2000 HydroMU laser diffractometer. This equipment measures particles within the range of 0.1-1000 µm using Mie theory which utilize the optical properties of the particles to calculate their grain-size. Prior to analysis the samples are dried in an oven at 40 ºC for 24h. The technique assumes a spherical particle shape and requires the refractive index (RI) of the particles under analysis as an input parameter (Horwell et al., 2010). Lists of the RI of minerals are available (e.g., Kerr, 1977). However, the RI of a mineral may vary with its precise composition, and volcanic ash may be

composed of different minerals where the proportions of the minerals in the sample are unknown (Horwell, 2007, 2010). Following the recommendations from Horwell, 2007 the experiments to determine the more appropriate operating conditions (as RIs) for rhyolitic ashes are described in the Chapter 6.

4.3 Mineralogical characterisation

The mineralogical characterisation of all volcanic ashes was made by X-ray diffraction (XRD) analysis. Samples were powdered in an agatha mortar and the diffractograms were obtained using a Bruker D-5005 instrument (Cu K-α1 radiation, λ = 1.5406 Å, at 40 kV and 40 mA.), collecting data between 4 to 6° of 2θ, with a scan step of 0.05^o and a step duration of 3 s. Diffractogram evaluation was carried out using the DIFFRAC software.

In this research a quantitative XRD method was applied only to one volcanic ash (sample No. 719) in order to define the best operating conditions for the GSA analysis. The quantitative mineralogical composition was done with the RockJock method of Dr. D.D. Eberl (Andrews et al., 2006; Eberl, 2003). One gram of sample was weighed and mixed with 0.111g of zincite (ZnO). XRD analysis of pressed powder samples was performed using an automatic PANalytical X'Pert equipment. Diffraction patterns in the 4-80º 2θ range were obtained with 0.017 º2θ step scan and 2 s counting time, operating conditions were 45 kV and 40 mA, using CuK$_α$ radiation (1.54598 Å) and a graphite monochromator. The resulting XRD patterns were transformed to the XRD standard pattern used by the RockJock5 software (5 to 65º 2θ in 0.02º steps). The XRD patterns were analysed quantitatively for phases present using the RockJock5 computer program (Eberl, 2003). RockJock5 offers a relatively simple and mostly automatic method for determining quantitatively the mineralogical composition of samples, including volcanic glass, to within a few weight percent from powder XRD data.

4.4 Chemical characterisation

The analytical methodology presented for the whole-rock chemical analysis has been developed for the determination of major and trace (including REE) elements that can be applied to all kind of volcanic rocks. The proper methodologies for the major and trace elements are stated below:

(1) The samples were dried in an oven at 40 ºC overnight and they were grounded in a widia or agatha mortar.

(2) Loss on ignition (LOI) was determined by means of a furnace at 1000 °C (see Protocol for the Determination of LOI in Appendix 1).

(3) The preparation of samples for the determination of major and trace elements (except Zr and Nb) is done by means of an acid attack (see Protocol for the determination of major and trace elements in rocks by means of total attack in Appendix 1). The solutions obtained by the acid attack of the whole-rock were analysed using Inductively Coupled Plasma – Optical Emission Spectrometry (ICP-OES), Inductively Coupled Plasma – Mass Spectrometry (ICP-MS), and single collector High Resolution – Inductively Coupled Plasma – Mass Spectrometry (HR-ICP-MS) as follows:

- Major elements (Al, Ca, Fe, K, Mg, Mn, Na, P, Ti, and Si) and trace elements (Ba, Sr and Zr) through ICP-OES or HR-ICP-MS;
- Trace elements (including REE) by ICP-MS or HR-ICP-MS;
- SiO_2 (%, m/m) content was indirectly determined taking into account the rest of the major oxide contents and LOI values.

The leachant solutions obtained by the ash leaching tests were analysed using ICPs as follows:

- Major elements (K, Na, Ca, Mg, Sr, Fe, S, P, B, and Si) through ICP-OES or HR-ICP-MS;
- Trace elements (including REE) by ICP-MS or HR-ICP-MS.

(4) Concentrations of Zr and Nb were determined by X-Ray Fluorescence Spectrometry (XRF) (see Protocol for the determination of major and trace elements in rocks by XRF, in Appendix 1) making pressed powder pellets with H_3BO_3 and Elvacite.

(5)   Furthermore, the fluoride determination in water ash leachates was done by the Ion Selective Electrode (ISE) technique (see Protocol for the fluoride determination by means of ion selective electrode, in Appendix 1).

4.4.1 Inductively Coupled Plasma – Optical Emission Spectrometry (ICP-OES)

Major elements and trace elements (Ba, Sr and Zr) were determined at the *Serveis Científico-Tècnics, Universitat de Barcelona,* and at the *Italian National Agency for New Technologies, Energy and Sustainable Economic Development (ENEA), Rome*, using a spectrometer Perkin Elmer Optima 3200 RL. In every session the instrument was calibrated using the concentrations shown in Table 4.1 for whole-rock analyses and Table 4.2 for ash water leachate analyses. Limits of detection (LoDs) and Limits of Quantificaton (LoQs) for both whole-rock and ash water leachate analyses are Tables 4.3 and 4.4. LoD values have been calculated as 3 times the standard deviation for ten replicates of the reagent blank, while the LoQ values has been estimated in the same way multiplying the standard deviation for 10 times. Precision and accuracy were settled repeating measures of reference materials of the Geological Survey of Japan (JB1b and JB-3) for whole rock analysis (Table 4.5) (Imai et al., 1999). The precision is determined by the reference standard deviation of 3 replicates and accuracy by comparing the mean of the reference determinations with its actual composition.

Table 4.1 Calibration ranges for ICP-OES in whole-rock analysis.

element	wavelength (nm)	calibration concentrations (mg l^{-1})				
		p0	p1	p2	p3	p4
Al	308.215	0	10	25	50	100
Ca	317.933	0	20	50	100	200
Fe	259.939	0	10	25	50	100
K	766.49	0	2	5	10	20
Mg	279.077	0	10	25	50	100
Mn	257.61	0	0.2	0.5	1	2
Na	330.237	0	2	5	10	20
P	213.617	0	1	2.5	5	10
Ti	334.94	0	2.5	5	10	25
Sr	421.5	0	0.5	1.25	2.5	5
Zn	213.8	0	0.2	0.5	1	2
Ba	455.403	0	0.5	1.25	2.5	5
Si	212 / 288	0	1	2	5	10

Table 4.2 Calibration ranges for ICP-OES in ash leachate analysis.

element	wavelength (nm)	calibration concentrations (mg l^{-1})				
		p0	p1	p2	p3	p4
K	766.49	0	10	25	50	100
Na	330.237	0	10	25	50	100
Ca	317.933	0	10	25	50	100
Mg	279.077	0	5	13	25	50
Sr	421.552	0	1	1	2.5	5
Fe	259.939	0	0.1	0.25	0.5	1
S	181.975	0	5	12.5	25	50
P	213.617	0	1	2.5	5	10
B	249.677	0	0.2	0.5	1	2
Si	288.158	0	1	2.5	5	10

Table 4.3 LoD and LoQ values for major elements (mg l^{-1}) in whole-rock analysis by ICP-OES.

element	LoD	LoQ
Al	0.5	1.67
Ca	0.1	0.33
Fe	0.01	0.03
K	0.5	1.67
Mg	0.1	0.33
Mn	0.005	0.02
Na	5	16.67
P	0.5	1.67
Ti	0.01	0.03
Sr	0.005	0.02
Zn	0.02	0.07
Ba	0.005	0.02

Table 4.4 LoD and LoQ values for major elements (mg l^{-1}) in ash leachate analysis by ICP-OES.

element	LoD	LoQ
K	0.45	1.50
Na	0.12	0.40
Ca	0.01	0.04
Mg	0.51	1.70
Sr	0.09	0.30
Fe	0.01	0.02
S	4.90	16.33
P	0.53	1.77
B	0.02	0.07
Si	0.23	0.77

Table 4.5 Chemical composition (%, m/m) of reference samples (JB1b and JB3), precision (1sd) and accuracy obtained in whole-rock analysis by ICP-OES (n= 3 replicates).

element	JB1b	1sd	accuracy	JB3	1sd	accuracy
SiO_2	51.11	2.59	101.08	50.96	2.02	103.8
Al_2O_3	14.38	0.08	96.76	17.2	0.37	97.89
CaO	9.6	0.09	98.82	9.79	0.21	99.18
Fe_2O_3	8.81	0.09	100.39	11.41	0.61	99.37
K_2O	1.32	0.01	97.07	0.78	0.03	99.41
Na_2O	2.63	0.07	104.04	2.73	0.16	98.35
MgO	8.14	0.07	99.59	5.19	0.20	97.78
MnO	0.147	0.01	96.40	0.18	0.01	99.97
P_2O_5	0.256	0.01	97.91	0.29	0.02	97.44
TiO_2	1.26	0.01	96.97	1.44	0.02	97.03

4.4.2 Inductively Coupled Plasma–Mass Spectrometry (ICP-MS and HR-ICP-MS)

Trace elements (including rare earth element group) were determined by using two spectrometers. In the analysis carried out at the *Serveis Científico-Tècnics, Universitat de Barcelona,* and at the *Italian National Agency for New Technologies, Energy and Sustainable Economic Development (ENEA), Rome,* a Perkin Elmer Elan 6000 ICP-MS spectrometer was used. In the analysis performed at the *Institute of Earth Sciences J. Almera, CSIC, Barcelona,* a High Resolution-Inductively Coupled Plasma – Mass Spectrometry (HR-ICP-MS), Element XR, Thermo Scientific, was employed. In every session the instrument was calibrated using the concentrations shown in Table 4.6 in whole-rock analysis and Table 4.7 in ash water leachate analysis. LoD and LoQ values are reported in Tables 4.8-4.9. Precision and accuracy for the whole-rock analysis were settled by repeating measures of JB1b and JB-3 for whole rock analysis by ICP-MS (Table 4.10) (Imai et al., 1999).

Table 4.6 Calibration concentrations for ICP-MS in whole-rock analysis.

element	atomic mass	calibration concentration (μg l^{-1})				
		p0	p1	p2	p3	p4
Li	7	0	1	2	5	10
Be	9	0	1	2	5	10
Sc	45	0	1	2	5	10
V	51	0	1	2	5	10
Cr	52	0	1	2	5	10
Co	59	0	1	2	5	10
Ni	60	0	2.5	5	10	25
Cu	65	0	1	2	5	10
Ga	71	0	1	2	5	10
Ge	74	0	1	2	5	10
As	75	0	1	2	5	10
Se	78	0	1	2	5	10
Rb	85	0	1	2	5	10
Y	89	0	1	2	5	10
Mo	98	0	1	2	5	10
Ag	107	0	1	2	5	10
Cd	111	0	1	2	5	10
Sn	120	0	1	2	5	10
Sb	121	0	1	2	5	10
Te	125	0	1	2	5	10
Cs	133	0	1	2	5	10
La	139	0	1	2	5	10
Ce	140	0	1	2	5	10
Pr	141	0	1	2	5	10
Nd	146	0	1	2	5	10
Sm	147	0	1	2	5	10
Eu	151	0	1	2	5	10
Gd	157	0	1	2	5	10
Tb	159	0	1	2	5	10
Dy	162	0	1	2	5	10
Ho	165	0	1	2	5	10
Er	166	0	1	2	5	10
Tm	169	0	1	2	5	10
Yb	174	0	1	2	5	10
Lu	175	0	1	2	5	10
Hf	178	0	1	2	5	10
Ta	181	0	1	2	5	10
W	182	0	1	2	5	10
Pt	195	0	1	2	5	10
Au	197	0	1	2	5	10
Tl	203	0	1	2	5	10
Pb	208	0	1	2	5	10
Bi	209	0	1	2	5	10
Th	232	0	1	2	5	10
U	238	0	1	2	5	10

Table 4.7 Calibration concentrations for ICP-MS in ash leachate analysis.

element	atomic mass	calibration concentration (µg l^{-1})				
		p0	p1	p2	p3	p4
Li	7	0	1	2	5	10
Be	9	0	1	2	5	10
B	11	0	10	20	50	100
Al	27	0	10	20	50	100
P	31	0	10	20	50	100
Cl	35	0	250	500		
Ti	49	0	1	2	5	10
V	51	0	1	2	5	10
Cr	52	0	1	2	5	10
Fe	54	0	10	20	50	100
Mn	55	0	10	20	50	100
Co	59	0	1	2	5	10
Ni	60	0	2.5	5	10	25
Cu	65	0	1	2	5	10
Zn	66	0	100	200	500	1000
Ga	71	0	1	2	5	10
Ge	74	0	1	2	5	10
As	75	0	1	2	5	10
Se	78	0	1	2	5	10
Br	81	0	250	500		
Rb	85	0	1	2	5	10
Y	89	0	1	2	5	10
Zr	90	0	1	2	5	10
Nb	93	0	1	2	5	10
Mo	98	0	1	2	5	10
Ag	107	0	1	2	5	10
Cd	111	0	1	2	5	10
Sn	120	0	1	2	5	10
Sb	121	0	1	2	5	10
Te	125	0	1	2	5	10
Cs	133	0	1	2	5	10
Ba	138	0	10	20	50	100
La	139	0	1	2	5	10
Ce	140	0	1	2	5	10
Pr	141	0	1	2	5	10
Nd	146	0	1	2	5	10
Sm	147	0	1	2	5	10
Eu	151	0	1	2	5	10
Gd	157	0	1	2	5	10
Tb	159	0	1	2	5	10
Dy	162	0	1	2	5	10
Ho	165	0	1	2	5	10
Er	166	0	1	2	5	10
Tm	169	0	1	2	5	10
Yb	174	0	1	2	5	10
Lu	175	0	1	2	5	10
Hf	178	0	1	2	5	10
Ta	181	0	1	2	5	10
W	182	0	1	2	5	10
Pt	195	0	1	2	5	10
Au	197	0	1	2	5	10
Hg	202	0	0.1	0.2	0.5	1
Tl	203	0	1	2	5	10
Pb	208	0	1	2	5	10
Bi	209	0	1	2	5	10
Th	232	0	1	2	5	10
U	238	0	1	2	5	10

Table 4.8 LoD and LoQ values for ICP-MS in whole-rock analysis (mg l^{-1}).

elements	LoD	LoQ
Li	0.03	0.08
Be	0.003	0.01
Sc	0.22	0.73
V	0.03	0.11
Cr	0.07	0.23
Co	0.00	0.01
Ni	0.17	0.57
Cu	0.09	0.30
Ga	0.01	0.02
Ge	0.04	0.15
As	0.08	0.26
Se	0.18	0.60
Rb	0.02	0.08
Y	0.02	0.07
Mo	0.02	0.06
Ag	0.05	0.17
Cd	0.01	0.02
Sn	0.01	0.02
Sb	0.01	0.02
Te	0.18	0.61
Cs	0.01	0.03
La	0.002	0.01
Ce	0.001	0.00
Pr	0.002	0.01
Nd	0.004	0.01
Sm	0.002	0.01
Eu	0.002	0.01
Gd	0.004	0.01
Tb	0.001	0.00
Dy	0.001	0.00
Ho	0.001	0.00
Er	0.005	0.02
Tm	0.002	0.01
Yb	0.002	0.01
Lu	0.004	0.01
Hf	0.01	0.03
Ta	0.01	0.04
W	0.02	0.08
Pt	0.02	0.08
Au	0.02	0.07
Tl	0.05	0.16
Pb	0.01	0.03
Bi	0.06	0.19
Th	0.002	0.01
U	0.003	0.01

Table 4.9 LoD and LoQ values for ICP-MS in ash leachate analysis ($\mu g \ l^{-1}$).

element	LoD	LoQ
Li	0.03	0.1
Be	0.005	0.02
B	0.99	3.3
Al	2.78	9.27
P	2.08	6.93
Cl	12.3	41
Ti	0.24	0.8
V	0.04	0.13
Cr	0.16	0.53
Fe	5.85	19.5
Mn	0.15	0.5
Co	0.01	0.03
Ni	0.2	0.67
Cu	0.14	0.47
Zn	1.75	5.83
Ga	0.01	0.03
Ge	0.01	0.03
As	0.11	0.37
Se	0.32	1.07
Br	2.23	7.43
Rb	0.02	0.07
Y	0.004	0.01
Zr	0.01	0.03
Nb	0.18	0.6
Mo	0.02	0.07
Ag	0.06	0.2
Cd	0.02	0.07
Sn	0.14	0.47
Sb	0.02	0.07
Te	0.2	0.67
Cs	0.01	0.03
Ba	0.07	0.23
La	0.004	0.01
Ce	0.003	0.01
Pr	0.002	0.01
Nd	0.006	0.02
Sm	0.011	0.04
Eu	0.004	0.01
Gd	0.012	0.04
Tb	0.002	0.01
Dy	0.006	0.02
Ho	0.002	0.01
Er	0.006	0.02
Tm	0.003	0.01

Table 4.9 continuation.

element	LoD	LoQ
Yb	0.007	0.02
Lu	0.002	0.01
Hf	0.02	0.07
Ta	0.03	0.1
W	0.05	0.17
Pt	0.03	0.1
Au	0.04	0.13
Hg	0.001	0.010
Tl	0.01	0.03
Pb	0.03	0.1
Bi	0.07	0.23
Th	0.005	0.02
U	0.007	0.02

Tables 4.11 and 4.12 show the calibration ranges for HR-ICP-MS in whole-rock and ash leachate analysis, respectively. LoD and LoQ values are reported in Tables 4.13-4.14. Finally, precision and accuracy for the whole-rock analysis were settled by repeating measures of JR for whole rock analysis by HR-ICP-MS (Table 4.15).

Table 4.10 Chemical composition (µg g^{-1}) of Reference samples (JB1b and JB3), precision (1sd) and accuracy obtained in whole-rock analysis by ICP-MS (n=3 replicates).

element	JB1b	1sd	accuracy	JB3	1sd	accuracy
Ba		1.96		245	2.35	95.66
Ce		2.61		21.5	0.77	99.79
Co	40.3	0.9	94.66	34.3	1.86	104.5
Cr	439	3.18	101.43	58.1	1.76	97.53
Cu	55.5	1.62	105.26	194	8.38	101.04
Dy		0.13		4.54	0.12	97.2
Er		0.06		2.49	0.1	105.35
Eu		0.06		1.32	0.03	98.67
Ga		0.5		19.8	0.39	101.82
Gd		0.21		4.67	0.17	92.2
Hf		0.65		2.67	0.17	101.75
Ho		0.02		0.8	0.03	114.08
La		1.42		8.81	0.32	96.71
Lu		0.01		0.39	0.01	95.36
Mo		0.03		1.09	0.14	112.05
Nd		1.08		15.6	0.53	98.79
Ni	148	6.42	104.7	36.2	4.82	101.52
Pb	6.8	0.15	91.57	5.58	0.33	101.45
Pr		0.26		3.11	0.14	100.72
Rb	39.1	0.99	88.77	15.1	0.64	95.48
Sc		2.32		33.8	4.07	103.55
Sm		0.21		4.27	0.13	95.73
Sn		0.16		0.94	3.71	330.76
Sr	439	0.91	99.11	403	1.31	100.52
Ta		0.18		0.15	0.39	10.72
Tb		0.03		0.73	0.02	101.32
Th		0.14		1.27	0.19	155.48
Tm		0.01		0.42	0.02	89.4
U		0.02		0.48	0.04	102
W		0.72		1.06	1.06	164.67
Y		0.48		26.9	0.62	87.47
Yb		0.06		2.55	0.06	96.51
Zn	80	0.27	130.94	100	0.79	114.78

Table 4.11 Calibration concentrations for HR-ICP-MS in whole-rock analysis.

element	atomic mass	Unit	calibration concentration						
			p0	p1	p2	p3	p4	p5	p6
Li	7	µg l^{-1}	0	1	2.0	5.0	10.0	100	
Be	9	µg l^{-1}	0	1	2.0	5.0	10.0		
Na	23	mg l^{-1}	0	1	10	25	50	100	
Mg	24	mg l^{-1}	0	1	10	25	50	100	
Al	27	mg l^{-1}	0	1	10	25	50	100	
P	31	mg l^{-1}	0	0.1	1.0	2.5	5.0	10.0	
K	39	mg l^{-1}	0	1	10	25	50	100	
Ca	43	mg l^{-1}	0	1	10	25	50	100	
Sc	45	µg l^{-1}	0	1	2.0	5.0	10.0		
Ti	48	mg l^{-1}	0	0.1	1.0	2.5	5.0	10.0	
V	51	µg l^{-1}	0	1	2.0	5.0	10.0	100	500
Cr	52	µg l^{-1}	0	1	2.0	5.0	10.0	100	500
Fe	54	mg l^{-1}	0	1	10	25	50	100	
Mn	55	mg l^{-1}	0	0.1	1.0	2.5	5.0	10.0	
Co	59	µg l^{-1}	0	1	2.0	5.0	10.0		
Ni	60	µg l^{-1}	0	1	2.0	5.0	10.0	100	
Cu	65	µg l^{-1}	0	1	2.0	5.0	10.0	100	
Zn	66	µg l^{-1}	0	10	20	50	100	500	
Ga	71	µg l^{-1}	0	1	2.0	5.0	10.0		
Ge	74	µg l^{-1}	0	1	2.0	5.0	10.0		
As	75	µg l^{-1}	0	1	2.0	5.0	10.0		
Se	78	µg l^{-1}	0	1	2.0	5.0	10.0		
Rb	85	µg l^{-1}	0	1	2.0	5.0	10.0	100	500
Sr	88	µg l^{-1}	0	10	20	50	100	500	
Y	89	µg l^{-1}	0	1	2.0	5.0	10.0	100	500
Zr	90	µg l^{-1}	0	1	2.0	5.0	10.0	100	500
Nb	93	µg l^{-1}	0	1	2.0	5.0	10.0	100	500
Mo	98	µg l^{-1}	0	1	2.0	5.0	10.0		
Ru	101	µg l^{-1}	0	0.1	0.25	0.5	1		
Rh	103	µg l^{-1}	0	0.1	0.25	0.5	1		
Pd	106	µg l^{-1}	0	0.1	0.25	0.5	1		
Ag	107	µg l^{-1}	0	0.1	0.25	0.5	1		
Cd	111	µg l^{-1}	0	0.1	0.25	0.5	1		
Sn	120	µg l^{-1}	0	1	2.0	5.0	10.0		
Sb	121	µg l^{-1}	0	1	2.0	5.0	10.0		
Te	125	µg l^{-1}	0	0.1	0.25	0.5	1		
Cs	133	µg l^{-1}	0	1	2.0	5.0	10.0		

Table 4.11 continuation.

element	atomic mass	unit	calibration concentration						
			p0	p1	p2	p3	p4	p5	p6
Ba	138	µg l^{-1}	0	10	20	50	100	500	
La	139	µg l^{-1}	0	1	2.0	5.0	10.0	100	500
Ce	140	µg l^{-1}	0	1	2.0	5.0	10.0	100	500
Pr	141	µg l^{-1}	0	1	2.0	5.0	10.0	100	
Nd	146	µg l^{-1}	0	1	2.0	5.0	10.0	100	
Sm	147	µg l^{-1}	0	1	2.0	5.0	10.0	100	
Eu	151	µg l^{-1}	0	1	2.0	5.0	10.0		
Gd	157	µg l^{-1}	0	1	2.0	5.0	10.0		
Tb	159	µg l^{-1}	0	1	2.0	5.0	10.0		
Dy	162	µg l^{-1}	0	1	2.0	5.0	10.0		
Ho	165	µg l^{-1}	0	1	2.0	5.0	10.0		
Er	166	µg l^{-1}	0	1	2.0	5.0	10.0		
Tm	169	µg l^{-1}	0	1	2.0	5.0	10.0		
Yb	174	µg l^{-1}	0	1	2.0	5.0	10.0		
Lu	175	µg l^{-1}	0	1	2.0	5.0	10.0		
Hf	178	µg l^{-1}	0	1	2.0	5.0	10.0	100	
Ta	181	µg l^{-1}	0	1	2.0	5.0	10.0		
W	182	µg l^{-1}	0	1	2.0	5.0	10.0		
Re	186	µg l^{-1}	0	1	2.0	5.0	10.0		
Ir	192	µg l^{-1}	0	0.1	0.25	0.5	1		
Pt	195	µg l^{-1}	0	0.1	0.25	0.5	1		
Au	197	µg l^{-1}	0	0.1	0.25	0.5	1		
Tl	203	µg l^{-1}	0	0.1	0.25	0.5	1		
Pb	208	µg l^{-1}	0	0.1	0.25	0.5	1	10	
Bi	209	µg l^{-1}	0	1	2.0	5.0	10.0		
Th	232	µg l^{-1}	0	1	2.0	5.0	10.0	100	
U	238	µg l^{-1}	0	1	2.0	5.0	10.0	100	

Table 4.12 Calibration concentrations for HR-ICP-MS in ash leachate analysis.

element	atomic mass	Unit	calibration concentrations					
			p0	p1	p2	p3	p4	p5
Li	7	µg l^{-1}	0	1	2.5	5.0	10.0	
Be	9	µg l^{-1}	0	1	2.5	5.0	10.0	
B	11	µg l^{-1}	0	10	25	50	100	500
Na	23	mg l^{-1}	0	1	10	25	50	100
Mg	24	mg l^{-1}	0	1	10	25	50	100
Al	27	µg l^{-1}	0	10	25	50	100	500
Si	28	mg l^{-1}	0	1	10	25	50	
P	31	µg l^{-1}	0	10	25	50	100	500
S	34	mg l^{-1}	0	10	50	100	250	
Cl	35	mg l^{-1}	0	10	50	100	250	
K	39	mg l^{-1}	0	1	10	25	50	100
Ca	43	mg l^{-1}	0	1	10	25	50	100
Sc	45	µg l^{-1}	0	1	2.5	5.0	10.0	
Ti	49	µg l^{-1}	0	1	2.5	5.0	10.0	
V	51	µg l^{-1}	0	1	2.5	5.0	10.0	
Cr	52	µg l^{-1}	0	1	2.5	5.0	10.0	
Fe	54	µg l^{-1}	0	10	25	50	100	500
Mn	55	µg l^{-1}	0	10	25	50	100	500
Co	59	µg l^{-1}	0	1	2.5	5.0	10.0	
Ni	60	µg l^{-1}	0	1	2.5	5.0	10.0	
Cu	65	µg l^{-1}	0	1	2.5	5.0	10.0	
Zn	66	µg l^{-1}	0	10	25	50	100	500
Ga	71	µg l^{-1}	0	1	2.5	5.0	10.0	
Ge	74	µg l^{-1}	0	1	2.5	5.0	10.0	
As	75	µg l^{-1}	0	1	2.5	5.0	10.0	
Se	78	µg l^{-1}	0	1	2.5	5.0	10.0	
Br	81	µg l^{-1}	0	100	250	500	1000	
Rb	85	µg l^{-1}	0	1	2.5	5.0	10.0	
Sr	88	µg l^{-1}	0	10	25	50	100	500
Y	89	µg l^{-1}	0	1	2.5	5.0	10.0	
Zr	90	µg l^{-1}	0	1	2.5	5.0	10.0	
Nb	93	µg l^{-1}	0	1	2.5	5.0	10.0	
Mo	98	µg l^{-1}	0	1	2.5	5.0	10.0	
Ru	101	µg l^{-1}	0	0.1	0.25	0.5	1	
Rh	103	µg l^{-1}	0	0.1	0.25	0.5	1	
Pd	106	µg l^{-1}	0	0.1	0.25	0.5	1	
Ag	107	µg l^{-1}	0	0.1	0.25	0.5	1	
Cd	111	µg l^{-1}	0	0.1	0.25	0.5	1	
Sn	120	µg l^{-1}	0	1	2.5	5.0	10.0	
Sb	121	µg l^{-1}	0	1	2.5	5.0	10.0	

Table 4.12 continuation.

element	atomic mass	unit	calibration concentrations					
			p0	p1	p2	p3	p4	p5
Te	125	µg l^{-1}	0	0.1	0.25	0.5	1	
I	127	µg l^{-1}	0	10	25	50	100	
Cs	133	µg l^{-1}	0	1	2.5	5.0	10.0	
Ba	138	µg l^{-1}	0	10	25	50	100	500
La	139	µg l^{-1}	0	1	2.5	5.0	10.0	
Ce	140	µg l^{-1}	0	1	2.5	5.0	10.0	
Pr	141	µg l^{-1}	0	1	2.5	5.0	10.0	
Nd	146	µg l^{-1}	0	1	2.5	5.0	10.0	
Sm	147	µg l^{-1}	0	1	2.5	5.0	10.0	
Eu	151	µg l^{-1}	0	1	2.5	5.0	10.0	
Gd	157	µg l^{-1}	0	1	2.5	5.0	10.0	
Tb	159	µg l^{-1}	0	1	2.5	5.0	10.0	
Dy	162	µg l^{-1}	0	1	2.5	5.0	10.0	
Ho	165	µg l^{-1}	0	1	2.5	5.0	10.0	
Er	166	µg l^{-1}	0	1	2.5	5.0	10.0	
Tm	169	µg l^{-1}	0	1	2.5	5.0	10.0	
Yb	174	µg l^{-1}	0	1	2.5	5.0	10.0	
Lu	175	µg l^{-1}	0	1	2.5	5.0	10.0	
Hf	178	µg l^{-1}	0	1	2.5	5.0	10.0	
Ta	181	µg l^{-1}	0	1	2.5	5.0	10.0	
W	182	µg l^{-1}	0	1	2.5	5.0	10.0	
Re	186	µg l^{-1}	0	1	2.5	5.0	10.0	
Ir	192	µg l^{-1}	0	0.1	0.25	0.5	1	
Pt	195	µg l^{-1}	0	0.1	0.25	0.5	1	
Au	197	µg l^{-1}	0	0.1	0.25	0.5	1	
Hg	202	µg l^{-1}	0	0.1	0.25	0.5	1	
Tl	203	µg l^{-1}	0	0.1	0.25	0.5	1	
Pb	208	µg l^{-1}	0	0.1	0.25	0.5	1	
Bi	209	µg l^{-1}	0	1	2.5	5.0	10.0	
Th	232	µg l^{-1}	0	1	2.5	5.0	10.0	
U	238	µg l^{-1}	0	1	2.5	5.0	10.0	

Table 4.13 LoD and LoQ values ($\mu g\ g^{-1}$) for HR-ICP-MS in whole-rock analysis.

element	LoD	LoQ
Li	0.103	0.342
Be	0.019	0.063
Na	0.0048	0.0160
Mg	0.0047	0.0155
Al	0.0034	0.0114
P	1.000	3.333
K	0.0065	0.0218
Ca	0.0198	0.0659
Sc	0.015	0.049
Ti	0.0013	0.0044
V	0.177	0.591
Cr	0.141	0.470
Fe	0.0058	0.0193
Mn	0.0002	0.0005
Co	0.019	0.063
Ni	0.097	0.324
Cu	0.040	0.133
Zn	0.019	0.064
Ga	0.009	0.031
Ge	0.094	0.314
As	0.016	0.054
Se	4.253	14.176
Rb	0.087	0.289
Sr	0.514	1.713
Y	0.023	0.076
Zr	0.197	0.657
Nb	0.023	0.076
Mo	0.065	0.217
Ag	0.008	0.027
Cd	0.004	0.014
Sn	0.050	0.167
Sb	0.003	0.010
Cs	0.025	0.084
Ba	0.352	1.174
La	0.046	0.153
Ce	0.088	0.293
Pr	0.010	0.033
Nd	0.039	0.130
Sm	0.008	0.026
Eu	0.004	0.014
Gd	0.013	0.043
Tb	0.001	0.004
Dy	0.006	0.020

Table 4.13 continuation.

element	LoD	LoQ
Ho	0.001	0.004
Er	0.002	0.007
Tm	0.001	0.003
Yb	0.002	0.005
Lu	0.001	0.003
Hf	0.012	0.040
Ta	0.012	0.040
W	0.102	0.340
Tl	0.003	0.010
Pb	0.004	0.014
Bi	0.014	0.045
Th	0.015	0.049
U	0.001	0.004

Table 4.14 LoD and LoQ ($\mu g\ g^{-1}$) values for HR-ICP-MS in ash leachate analysis.

element	LoD	LoQ
Li	3.98	3.69
Be	1.25	2.89
Na	4.39	4.03
Mg	6.14	5.47
Al	0.19	2.77
P	6.26	0.75
K	2.25	2.16
Ca	1.81	6.47
Sc	1.34	3.25
Ti	1.21	0.27
V	1.86	1.79
Cr	7.99	2.97
Fe	2.36	2.25
Mn	1.28	1.21
Co	2.76	4.94
Ni	0.34	4.67
Cu	0.59	0.58
Zn	1.12	1.10
Ga	0.77	0.78
Ge	9.50	11.73
As	2.06	1.98
Rb	9.32	9.60
Sr	1.47	0.98
Y	1.28	1.26
Zr	6.96	6.23
Nb	8.77	6.02
Mo	0.81	0.80
Ag	4.82	3.63
Cd	5.06	5.38
Sn	9.63	11.93
Sb	8.91	7.56
Cs	2.45	2.34
Ba	1.28	1.25
La	0.99	0.97
Ce	1.33	1.30
Pr	3.27	3.50
Nd	1.02	1.00
Sm	0.29	0.29
Eu	3.74	3.48
Gd	11.07	9.06
Tb	7.79	6.74
Dy	4.93	4.48

Table 4.14 continuation*.*

element	LoD	LoQ
Ho	1.22	1.19
Er	6.55	5.79
Tm	0.08	0.08
Yb	3.72	3.47
Lu	0.37	0.37
Hf	0.06	0.06
Ta	9.54	11.80
W	3.32	3.11
Tl	4.15	3.83
Pb	2.38	1.32
Bi	3.02	2.85
Th	1.36	1.40
U	2.01	1.94

Table 4.15 Chemical composition ($\mu g\ g^{-1}$) of reference material JR3, precision (1sd) and accuracy obtained in whole-rock analysis by HR-ICP-MS (n= 7 replicates).

element	JB1b	1sd	accuracy	JB3	1sd	accuracy
Ba		1.96		245	2.35	95.66
Ce		2.61		21.5	0.77	99.79
Co	40.3	0.9	94.66	34.3	1.86	104.5
Cr	439	3.18	101.43	58.1	1.76	97.53
Cu	55.5	1.62	105.26	194	8.38	101.04
Dy		0.13		4.54	0.12	97.2
Er		0.06		2.49	0.1	105.35
Eu		0.06		1.32	0.03	98.67
Ga		0.5		19.8	0.39	101.82
Gd		0.21		4.67	0.17	92.2
Hf		0.65		2.67	0.17	101.75
Ho		0.02		0.8	0.03	114.08
La		1.42		8.81	0.32	96.71
Lu		0.01		0.39	0.01	95.36
Mo		0.03		1.09	0.14	112.05
Nd		1.08		15.6	0.53	98.79
Ni	148	6.42	104.7	36.2	4.82	101.52
Pb	6.8	0.15	91.57	5.58	0.33	101.45
Pr		0.26		3.11	0.14	100.72
Rb	39.1	0.99	88.77	15.1	0.64	95.48
Sc		2.32		33.8	4.07	103.55
Sm		0.21		4.27	0.13	95.73
Sn		0.16		0.94	3.71	330.76
Sr	439	0.91	99.11	403	1.31	100.52
Ta		0.18		0.15	0.39	-10.72
Tb		0.03		0.73	0.02	101.32
Th		0.14		1.27	0.19	155.48
Tm		0.01		0.42	0.02	89.4
U		0.02		0.48	0.04	102
W		0.72		1.06	1.06	164.67
Y		0.48		26.9	0.62	87.47
Yb		0.06		2.55	0.06	96.51
Zn	80	0.27	130.94	100	0.79	114.78

4.4.3 X-Ray Fluorescence (XRF) analysis

Concentrations of Zr and Nb and were determined at the *Serveis Científico – Tècnics, Universitat de Barcelona*, using a PW2400 sequential X-Ray spectrometer. The analytical conditions are shown in Table 4.16. Precision of the results was determined using an internal standard (GSS-8). For Zr, precision was 3.37 µg g^{-1} (1σ, n = 11), while for Nb precision was 0.45 µg g^{-1} (1σ, n = 11).

Table 4.16 Analytical conditions for XRF in whole-rock analysis.

Element	U	R	s	T	L	C	D	X	kV	mA	A	F+	F-
Nb	µgg^{-1}	5 - 270	5	Rh	Ka	M	C	LIF 220	60	30	30.4	0.5	0.6
Zr	µgg^{-1}	20 - 780	16	Rh	Ka	M	C	LIF 220	60	50	32.1	0.9	1.2

U	Concentration in µg g^{-1}	X	dispersal crystal
R	calibration limits	O	optical order
s	sigma σ*	kV	kilovolts
D	detector		
T	X-Ray tube	A	goniometer angle
T	used spectral line	F+	relative position background +
C	collimator	F-	relative position background -

 * sigma (σ)

n	standards
k	regression coefficient
c.q.	chemical concentration
c.c.	calculated concentration

σ = √ [Σn (c.q. - c.c.)^2 / n - k]

4.4.4 FTIR spectroscopy

Fourier transform infrared (FTIR) spectroscopy is a powerful technique for studying molecular structures. FTIR was used to provide information about structural chemical bonds of the water present in the ashes. The samples were examined with a Perkin-Elmer Spectrum 2000 instrument Optical FTIR 16PC. It is a FTIR equipment with diffuse reflectance, infrared Fourier transform (DRIFT), and PC-controlled using Spectrum for Windows. Spectral range varies in the mid-infrared (mid-IR) between 7,800 and 375 cm^{-1} wave number. For each analysis, ~50 mg of powdered sample was used. The analyses were conducted in the same experimental conditions in order to compare qualitatively the IR spectra obtained. The observed absorption frequencies were compared with available data provided by other authors (Goryniuk et al., 2004; Ihinger et al., 1999; Mandeville et al., 2002; Stolper, 1982a, b; Yokoyama et al., 2008; Zhang et al., 1991). Many of these works quantify the total amount of H_2O (H_2O_t), H_2O molecular (H_2O_m) and OH in silicate glasses (natural and synthetic), and allow us to define the main peaks of water found in volcanic ashes. Following these works, the main peaks are in the range 6,000–1,600 cm^{-1} wave number. Figure 4.3 shows an example of the peaks under study and Table 4.17 reports the vibrational movement of the active molecule of water. Moreover, qualitatively total water content of volcanic ashes was estimated integrating the area under the peak at around 3,612-3,411 cm^{-1} wave number (corresponding to the H_2O_t, i.e., the sum of H_2O_m and OH). This peak corresponds to the overlap of OH-stretching vibrations under different chemical states including isolated or hydrogen bonded X—OH (X= H, Si, Al, etc). The background absorbance was removed prior to this calculation.
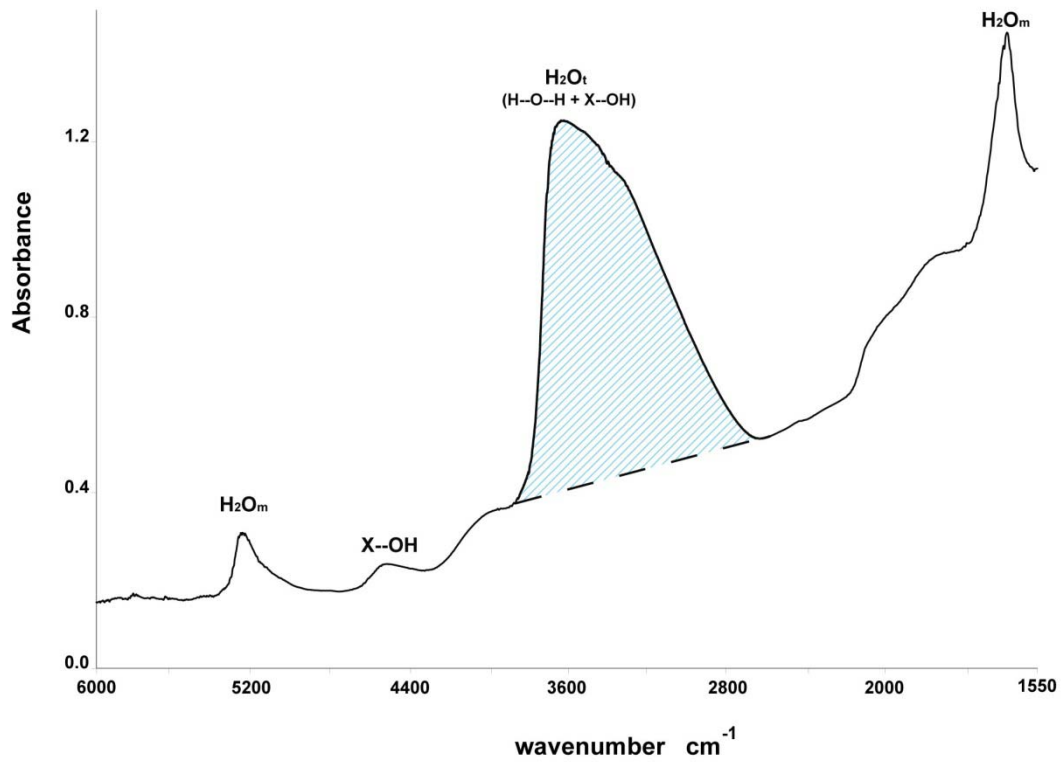
Figure 4.3 Typical IR spectra of volcanic glass (sample No. 808).

.

Table 4.17 IR absorption peaks of water in silicate glasses from Goryniuk et al., 2004, Stolper, 1982.

λ cm^{-1}	Vibrational movement	Interpretation
5245	H-O-H bending	H_2O_m
4500	-OH stretching	X-OH
3578	-OH stretching H-O-H bending	H_2O_t
1629	H-O-H bending	H_2O_m

PART 4. RESULTS AND DISCUSSION

Chapter 5. Sample selection and characterisation

This chapter discusses the results obtained from physical, mineralogical and chemical characterisation of ashes using different methods (detailed described in chapter 4 and appendixes).

Physical characterisation (mainly SEM-EDX, BET) has allowed at an early stage to distinguish between volcanic and non-volcanic products collected during the field campaigns of the period 2006–2007. Once identified pure volcanic ashes the physical properties (SEM, BET, and GSA) allowed describing the shape morphology, the amount of surface area available and the grain size distribution. The obtained results allowed infer the eruptive style and dynamics of the investigated eruptive products as well as the occurrence of magmatic and/or phreatomagmatic activity. The relative content of glass and crystalline phases on the samples was also determined by XRD analysis corroborating previous SEM analyses. Whole rock chemical characterisation and FTIR spectroscopy was also performed on the samples investigated.

5.1 Physical characterisation

5.1.1 Morphology and texture by SEM-EDX

Scanning electron microscopy (SEM) and the Energy Dispersive X-Ray (EDX) spectra of single particles allowed to classify 29 potential volcanic ash deposits from the southern Puna and Uruguay in:

- Sediment consisting of pure volcanic ash;
- Sediment with some content of volcanic ash particles (mixed ash);
- Sediment without volcanic ash particles.

Figure 5.1 shows a few examples of different cases. Additional SEM images are reported in Appendix 2. The results of these qualitative observations are reported in Table 5.1. Only 11 on 29 samples were found to be pure volcanic ashes. These samples were constituted by glass and minor amounts of

crystalline phases. Atlas of EDX mineral composition was used to recognise the mineral phases (Severin, 2004). A few examples of EDX spectra are reported in Figures 5.2a and b. The other samples were mixed sediments in which volcanic ash particles coexist with non volcanic particles (e.g., biogenic silica, mainly as diatoms) or samples with a total absence of volcanic ash particles. These were usually formed by high contents of calcite and/or minor amount of halite. Others contained only high levels of biogenic silica.
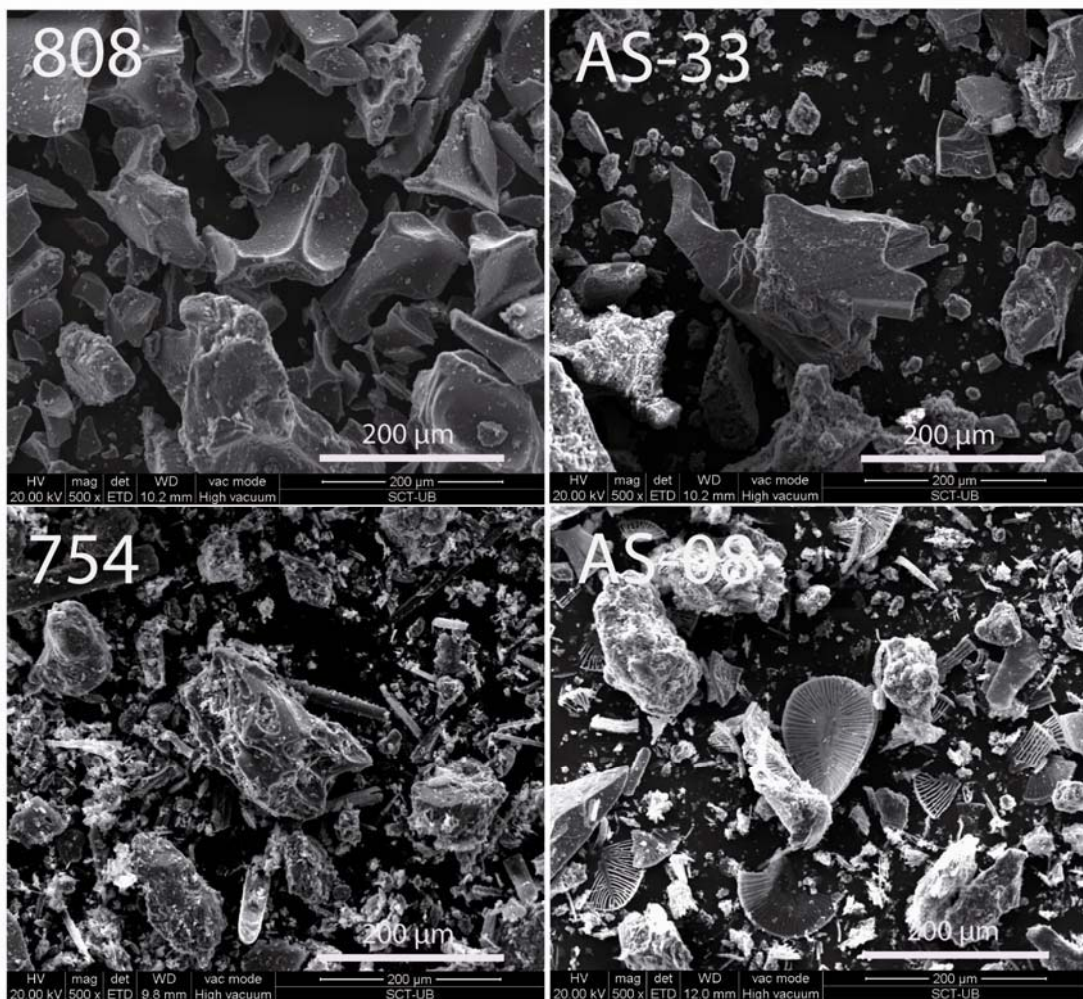
Figure 5.1 SEM images of sediment consisting of only volcanic ash (808 and AS-33), mixed volcanic ash (754) and without volcanic ash (AS-08).
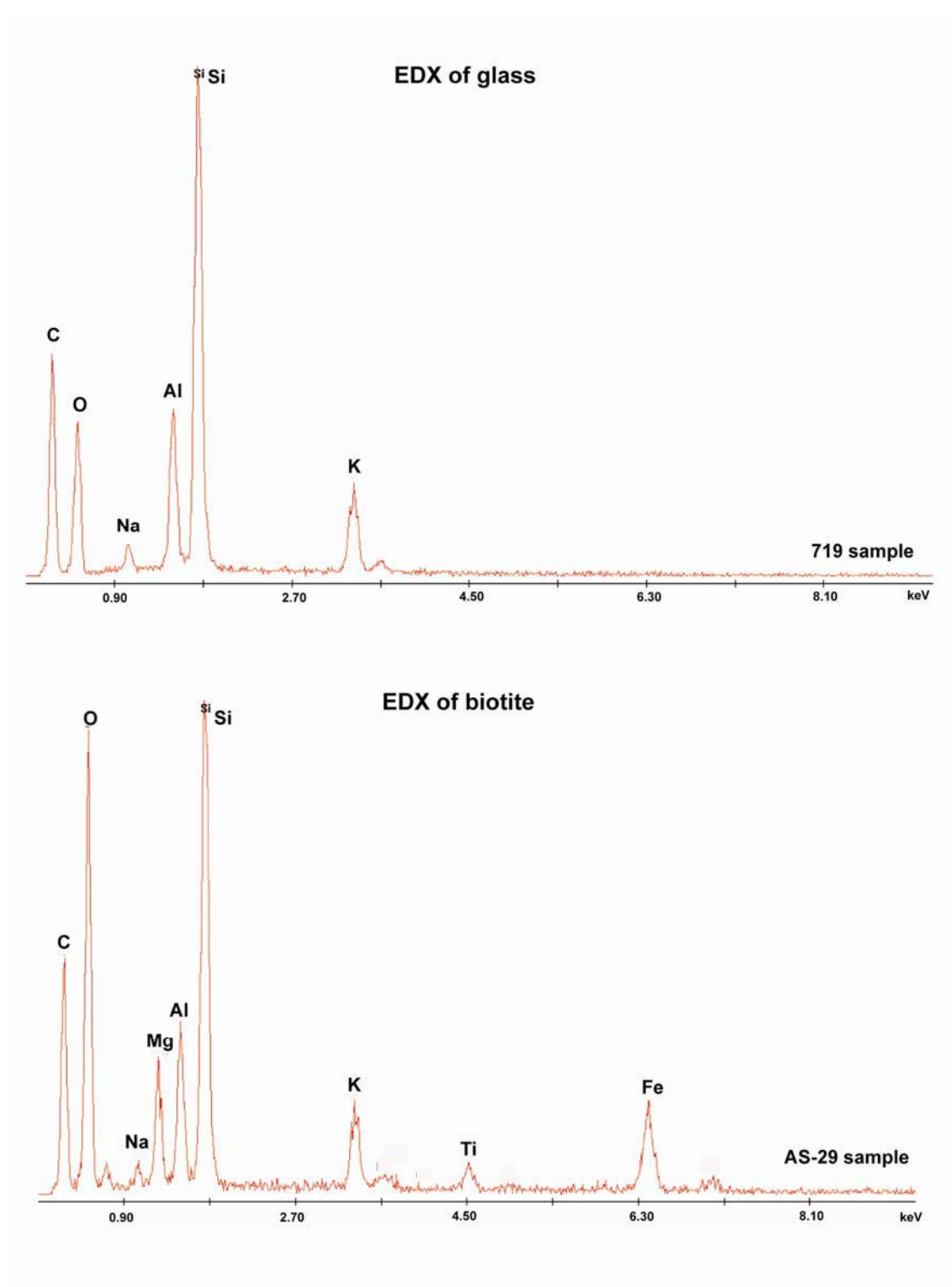
Figure 5.2a Typical EDX spectra for volcanic glass (sample 719) and biotite (sample AS-29) indentified in volcanic ash samples.
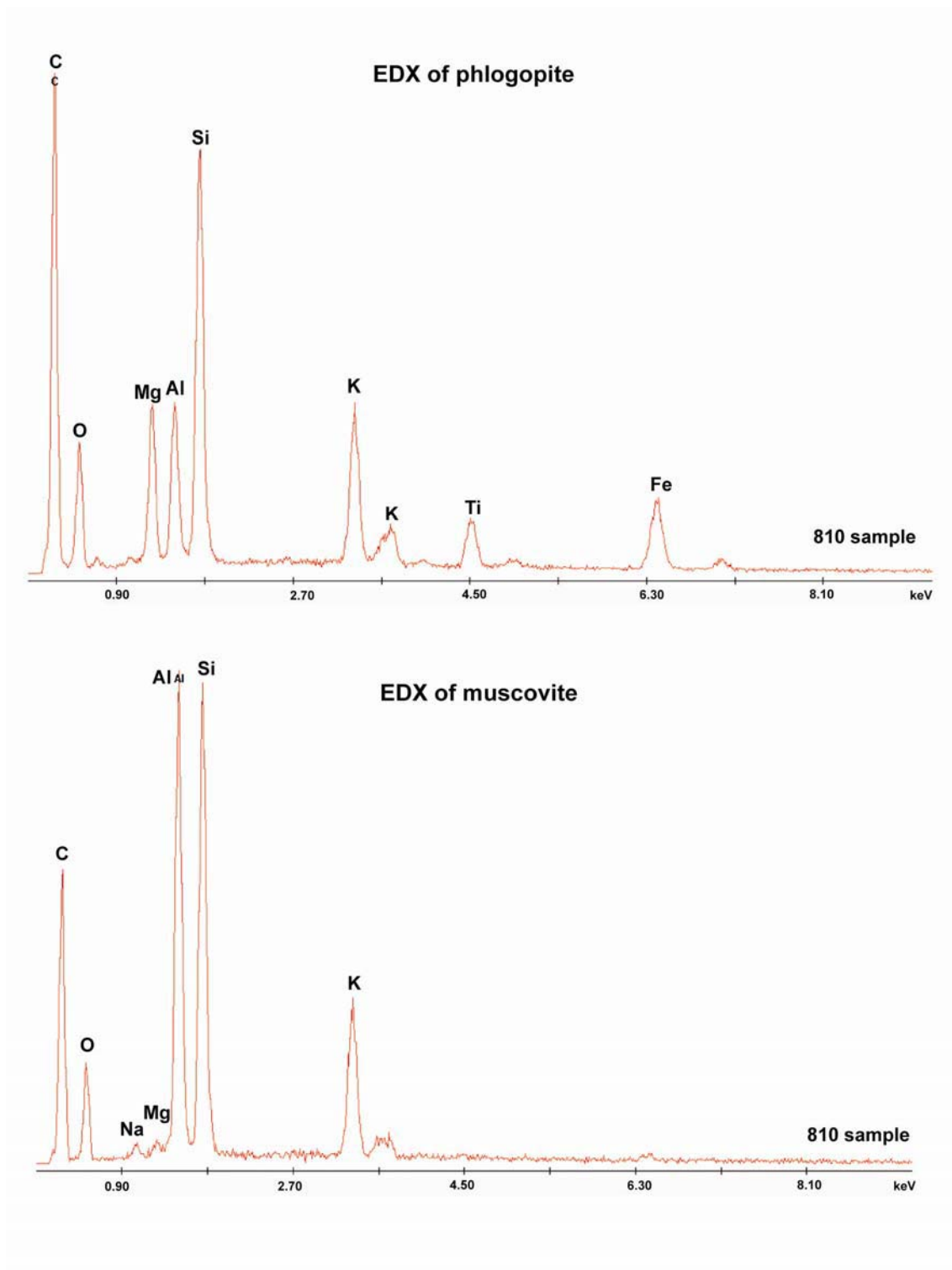
Figure 5.2b Typical EDX spectra of phlogopite and muscovite (sample 810) indentified in volcanic ash samples.

Table 5.1 Qualitative mineralogical composition by SEM-EDX of the supposed volcanic ash deposits in NW Argentina and Uruguay (x, detected; nd, not detected).

Sample	719	721	733	734	735	739	743	748
Glass	x	x	x	x	x	x	nd	nd
Quartz	x	x	x	nd	nd	nd	nd	nd
Mica	x	x	x	x	x	x	x	x
Biogenic Si	nd	nd	nd	x	x	x	x	x
Calcite	nd	nd	nd	nd	nd	nd	nd	nd
Clay	nd	nd	nd	x	x	nd	nd	nd
Classification	Ash	Ash	Ash	Mixed ash	Mixed ash	Mixed ash	No ash	No ash

Table 5.1 continuation.

Sample	753	754	785	808	809	810	AS-07
Glass	nd	x	nd	x	x	nd	nd
Quartz	nd	nd	nd	nd	x	nd	nd
Mica	x	x	nd	nd	x	x	x
Biogenic Si	x	x	x	nd	nd	nd	x
Calcite	nd	nd	nd	nd	nd	x	x
Clay	nd	nd	nd	nd	nd	nd	nd
Classification	No ash	Mixed ash	No ash	Ash	Ash	No ash	No ash

Table 5.1 continuation.

Sample	AS-08	AS-17	AS-21	AS-28	AS-29	AS-33
Glass	nd	nd	nd	x	x	x
Quartz	nd	nd	nd	x	x	x
Mica	x	nd	x	x	x	x
Biogenic Si	x	nd	x	nd	nd	nd
Calcite	nd	x	x	nd	nd	nd
Clay	nd	nd	nd	nd	nd	nd
Classification	No ash	No ash	No ash	Ash	Ash	Ash

Table 5.1 continuation.

Sample	UR-1	UR-2	UR-3	UR-4	UR-5	UR-6	UR-7	UR-8
Glass	x	nd	nd	nd	nd	nd	x	x
Quartz	x	x	nd	nd	nd	x	x	x
Mica	x	x	x	nd	x	x	x	nd
Biogenic Si	nd	nd	nd	nd	nd	nd	nd	nd
Calcite	nd	x	x	x	nd	nd	nd	x
Clay	nd	x	x	x	x	nd	nd	x
Classification	Ash	No ash	No ash	No ash	No ash	Ash	Ash	No ash

SEM images of selected volcanic ashes are reported in Figures 5.3a-e. Textural features of volcaniclastic materials may be used to interpret eruptive mechanisms, being intimately related to the degassing and fragmentation processes (Verhoogen, 1951).

Samples were finally classified as follows:

(1)   Samples UR-1, UR-6, UR-7, and 808 were almost fully glassy. Abundant Y-shaped, plate like, curved, and angular shards (typically from spherical vesicle wall breakage) were detected in samples UR-1, UR-6, and 808, whilst UR-7 presented also vesicular spongy particles.

(2)   Other glassy samples 719, 721, 733, 809, AS-28, CHA-1F, CHA-2R, CHA-G, CHA-E were characterized by irregular blocky fragments and, in some cases, highly elongated pipe-like vesicles parallel to the long axis of the pyroclast indicating the flow direction and a certain amount of crystalline phases. For these samples, the amount of particle size <5 µm was abundant.

(3)   Samples AS-29 and AS-33 consists of poorly vesicular equant blocky fragments (5-200 µm) of glass, high content of crystalline phases and rare fine grain-size particles.

(4)   Samples COP, LON, LLA, and HUD were poorly vesicular with equant blocky fragments (5-200 µm) of glass, scarce fine grain-size particles and relatively low crystal content. Rare Y-shard, platelike, curved and angular shards (vesicle wall breaking remains) occurred also in these samples. The blocky glass particle morphology of the Hudson ash is very similar to ash from the 2001 basaltic eruption of Mt. Etna (Scasso and Carey, 2005; Taddeucci et al., 2004) whereas vesicular and fluidal particles were observed in LON and LLA samples.

These groups likely fingerprint different explosive volcanic styles. The morphology of the particles from magmatic eruptions of high viscosity magma (rhyolitic, diacitic and some andesitic magmas) is entirely dependent on the shape of the vesicles in the rising magma before fragmentation (Wohletz et al., 1989). The concavities, grooves and tubes of particles correspond to broken vesicles. Elongate grain shapes are controlled by pipelike vesicles and equant grain by undeformed vesicles. Flat or slightly curved platy shards are from broken vesicle walls. This is the case of the ash groups 1 and 2. The high content of glass with practically no crystals in the group 1 indicates a very fast

ascent of magma to the surface, whereas the high content of fine grains in group 2 could indicate highly explosive eruptions.

The morphology of ash particles from phreatomagmatic eruptions is controlled by stresses within the chilled magma. The principal effects of water interaction are to promote quenching and inhibit vesiculation. Their shapes may indicate fragmentation by thermal fracturing (i.e., angular edges) and not by abrasion (i.e., rounded edges) (Heiken and Wohletz, 1992). Shards often have a particularly angular shape resulting from the violent explosive interaction between magma and water (Wohletz, 1986). These shapes include blocky, fusiform, mosslike, platey, as in the case of ash group 3. In these ashes, possible magma stagnation in the chamber during the ascent provide the crystallization of the observed crystalline phases (Ruggieri et al., 2010b). The same shape features was observed for Hudson, Copahue, Llaima, and Lonquimay ashes. Other works classified also these eruptions as phreatomagmatic (Kratzmann et al., 2009; Kratzmann et al., 2010; Naranjo and Moreno, 1991; Naranjo and Polanco, 2004; Naranjo et al., 1992; Naranjo and Stern, 1998).
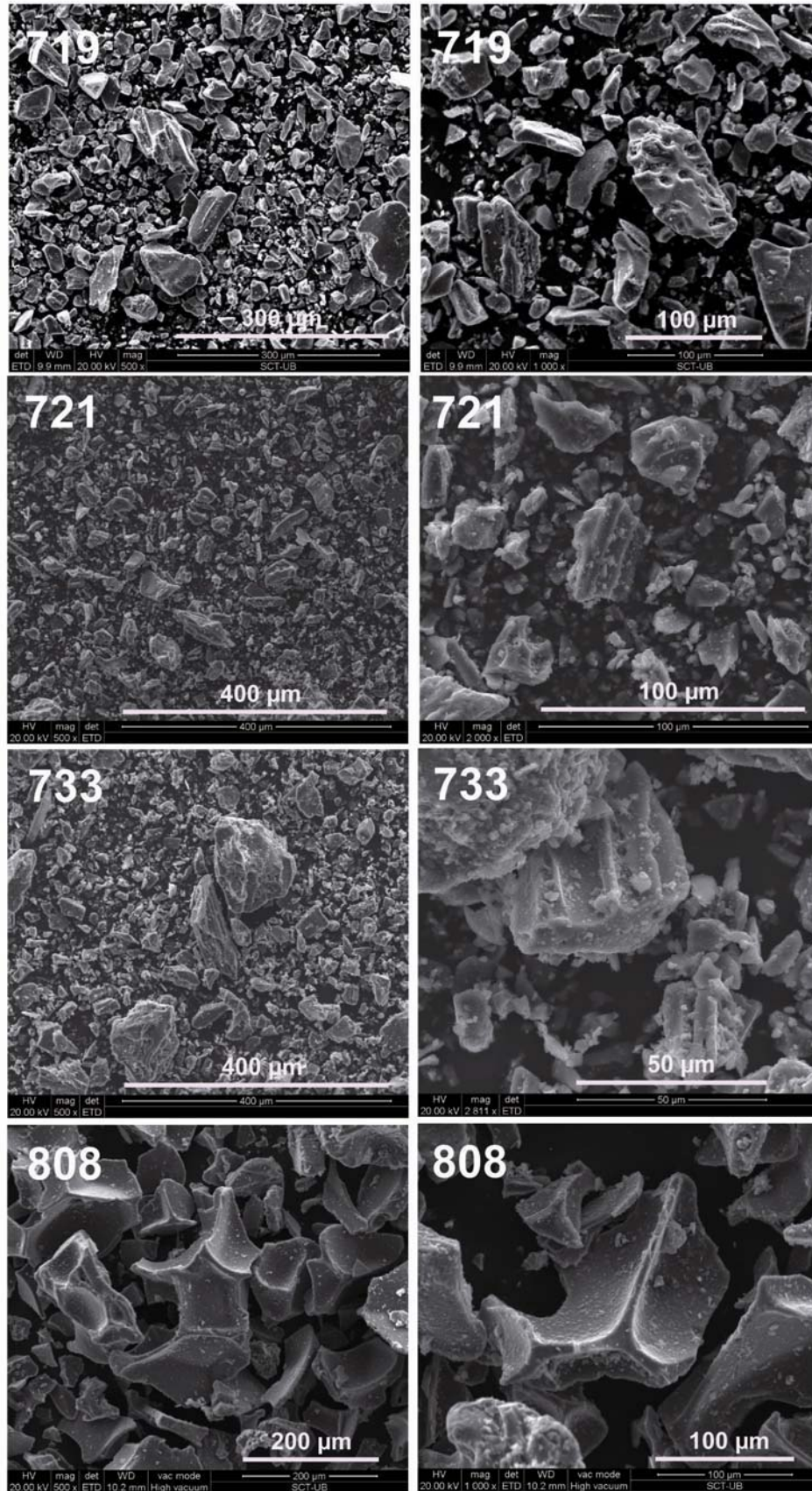
Figure 5.3a SEM images of ashes from the Puna and neighbouring area.
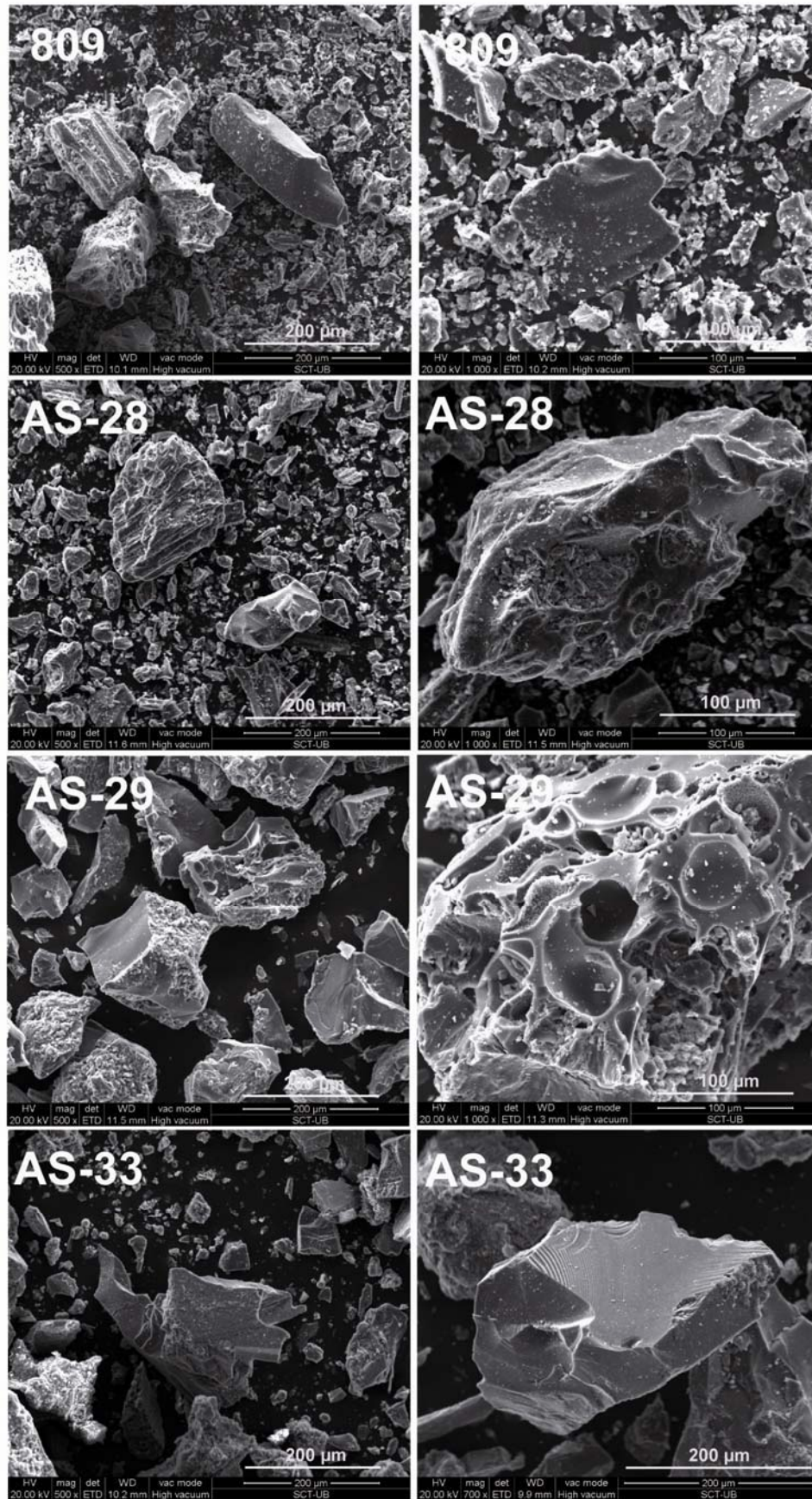
Figure 5.3b SEM of volcanic ashes from the Puna and neighbouring area.
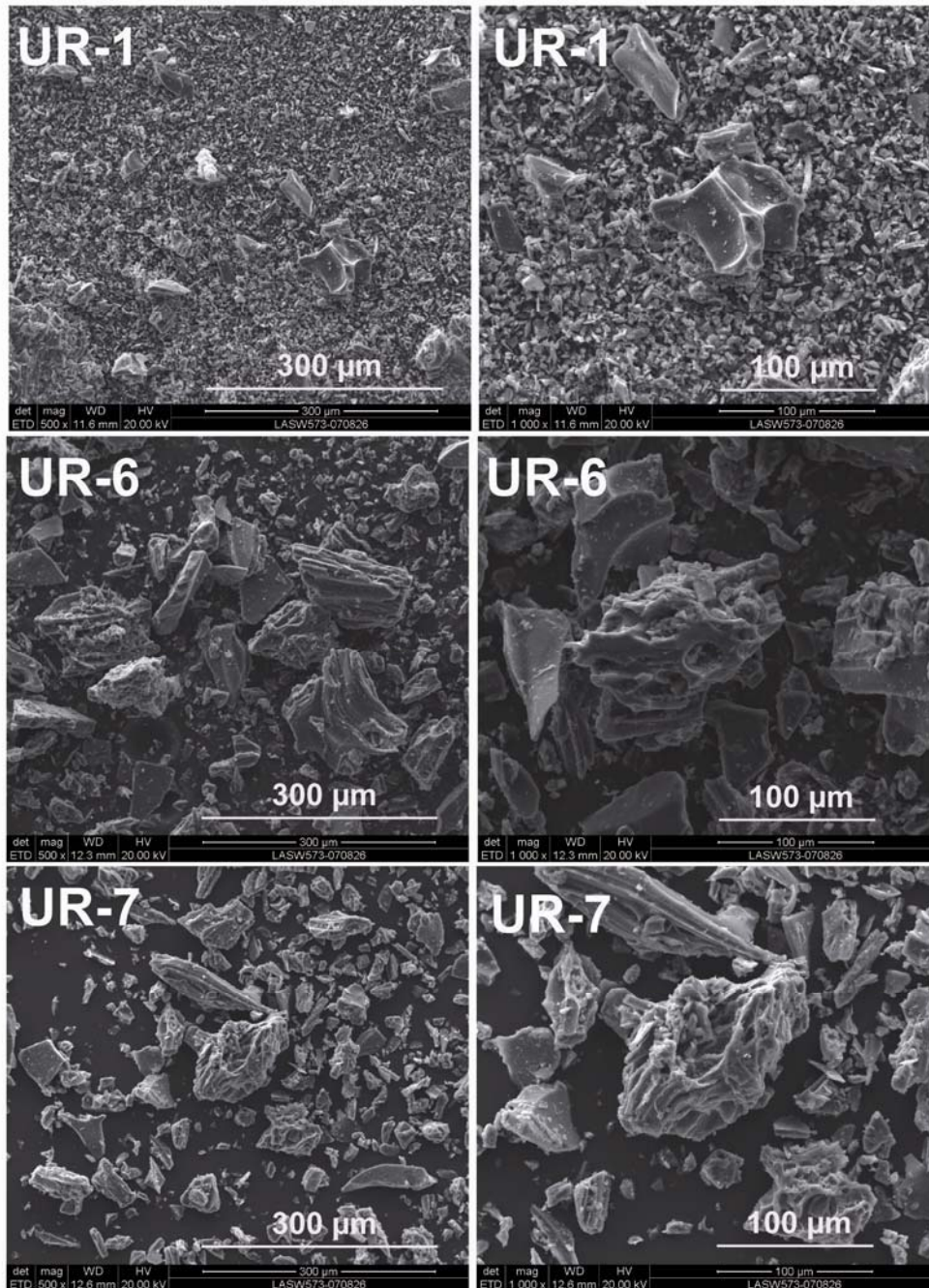
Figure 5.3c SEM images of volcanic ashes from Uruguay.
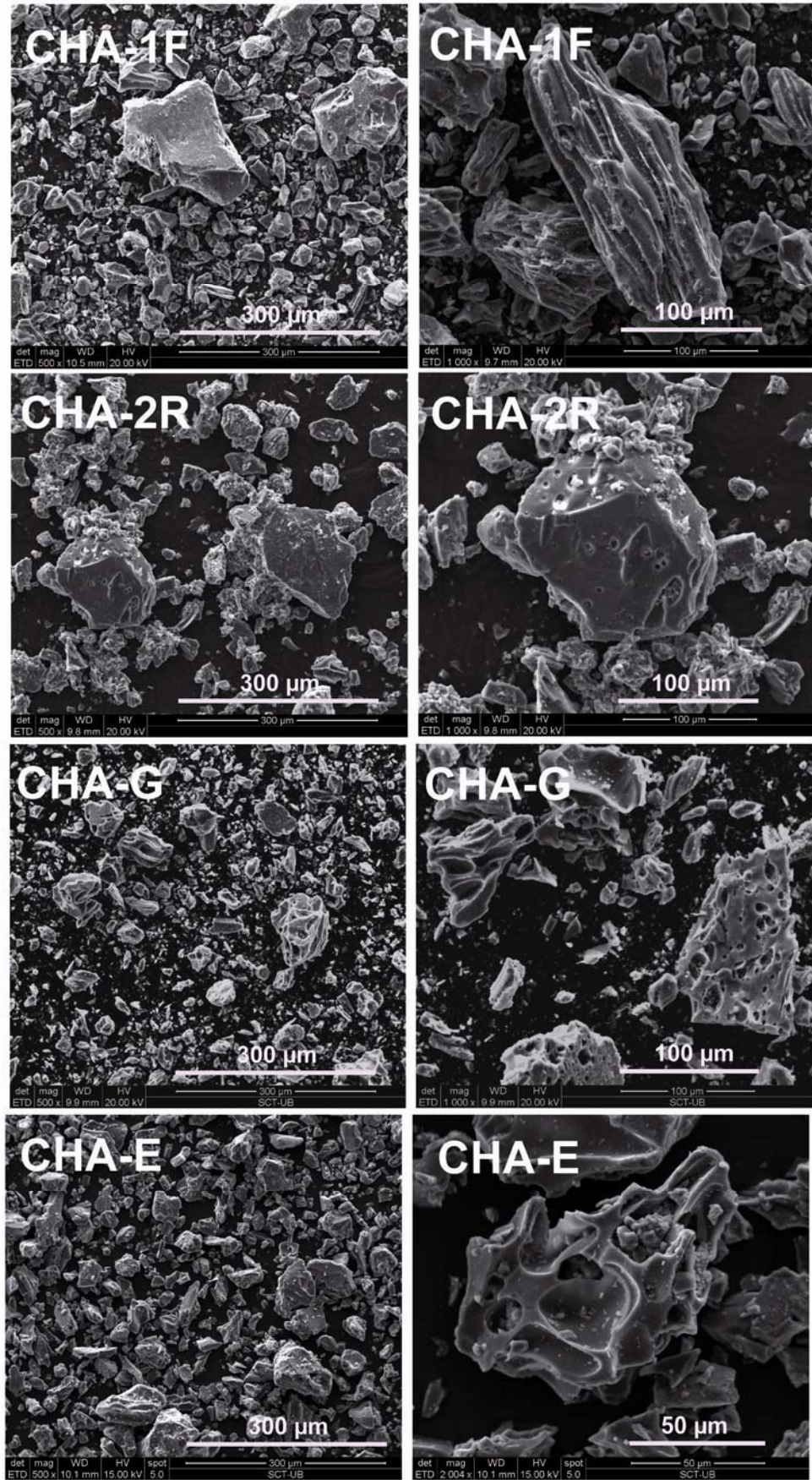
Figure 5.3d SEM images of ashes from 2008 Chaiten eruption.
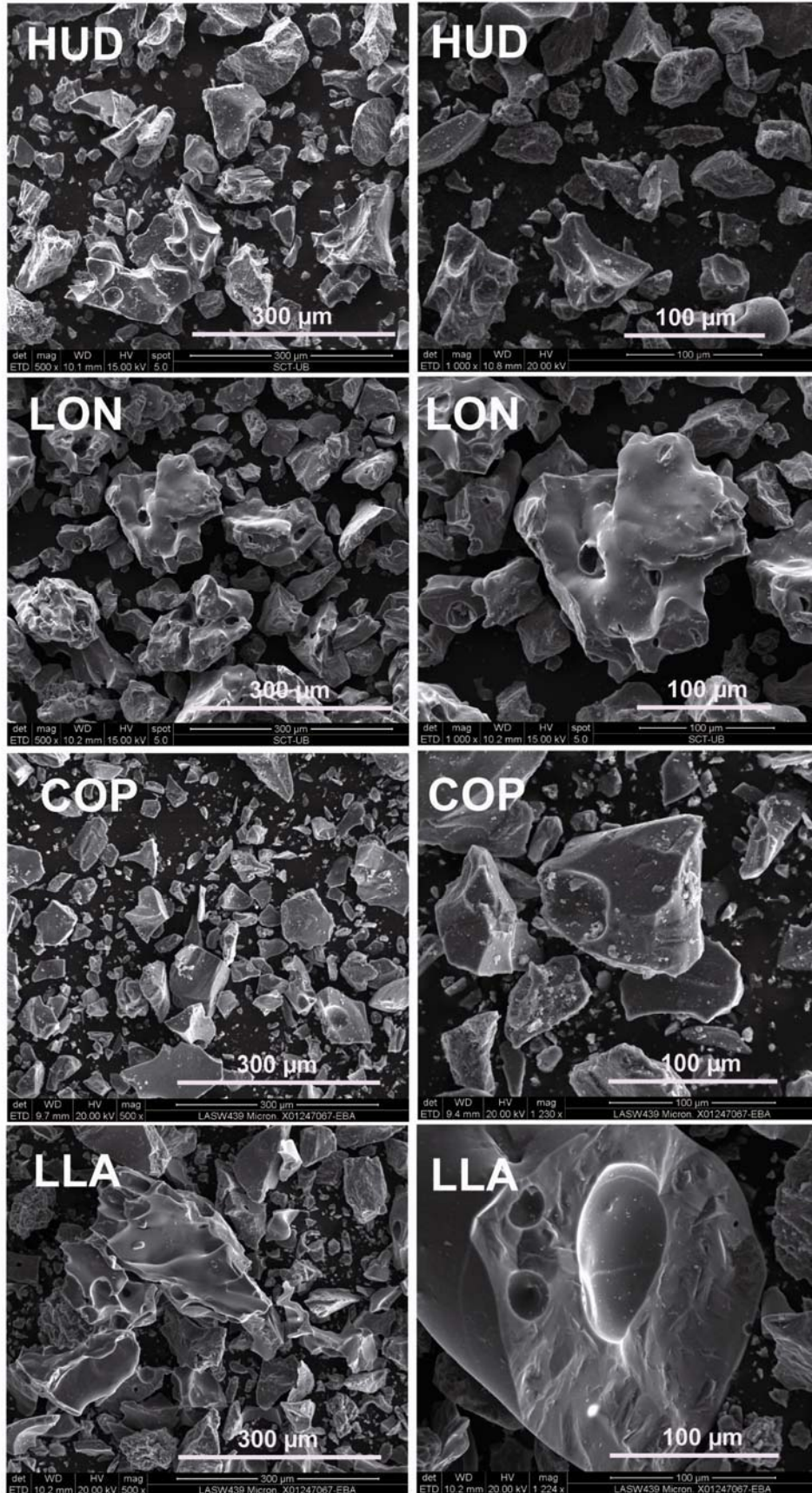
Figure 5.3e SEM images of ashes from eruption of Hudson, Lonquimay, Copahue, and Llaima volcanoes.

5.1.2 Specific surface area by the BET method

The Specific Surface Area (SSA) analysis was performed on the mixed and pure ashes from Puna and neighbouring area. In pure volcanic ash this parameter is principally function of particle size, decreasing with increasing the particle size (Horwell et al., 2003a). Pioneering study indicates that for particles larger than approximately 0.5 mm the SSA was independent of the particle size (Papelis et al., 2003). Literature values on pure ash fall in a very broad range. Andesitic ash from the Soufrière Hills volcano range from 2.8 to 7.5 m^2 g^{-1}, with the highest value observed for an ash sample that had been leached and weathered (Horwell et al., 2003a). Whilst ash sample from Mount St. Helens volcano range from 0.2 to 1.6 m^2 g^{-1} (Papelis et al., 2003). SSA results of our samples are given in Table 5.2. Pure volcanic ashes were between 0.55 - 7.74 m^2 g^{-1} with the lower value for pure 719 ash and the higher for the 808 sample.

Table 5.2 Specific Surface Area (SSA) of samples in ascending order.

Sample	Type	SSA m^2 g^{-1}
719	ash	0.55
AS-28	ash	0.99
721	ash	1.12
733	ash	1.31
809	ash	1.49
AS-29	ash	2.28
AS-33	ash	4.82
808	ash	7.74
754	mixed ash	16.3
735	mixed ash	16.9
739	mixed ash	33.7
734	mixed ash	45.2

This range shows very different SSA values among the samples. Ash particles retain valuable information regarding magma dynamics and vesiculation at the time of eruption (Proussevitch et al., 2011). In pure volcanic ash, the differences between the SSA values are related to the above mentioned size of the ash particles, but also to the morphology (e.g., characteristic vesicles) (Papelis et

al., 2003). These results were consistent with particle morphology based on SEM images. High internal porosity and significant surface roughness in AS-29 sample and the very well defined Y-shard in sample 808 explain their high SSA. Mixed ashes ranged from 16.3 to 45.2 $m^2 g^{-1}$. The high SSA values were due to the occurrence of clay minerals and/or biogenic silica, which typically develop large SSA (Fowler et al., 2004; Fubini, 1997).

5.1.3 Grain-size analysis by laser diffraction

5.1.3.1 Setting operating conditions

Laser diffraction analysis used in this research detects particle sizes in the range of 0.1–1000 µm using the Mie light scattering theory. Powders can be measured either in wet (i.e., water) or dry media (i.e., air). In every case, the ash composition (i.e., proportion of crystalline phases *vs.* volcanic glass) is may be important for this technique and a prior study of the optical properties (Absorption coefficient, AC, and Refractive index, RI) of the volcanic ash under study is advisable. Quantitative mineralogical composition was done by the XRD RockJock method (Andrews et al., 2006; Eberl, 2003). Then, we have tested the effect of varying RI in different operating conditions (in air, in water with and without ultrasonic bath) on GSA analysis using the 719 ash sample. The choice of this sample was because most of the samples under study were rhyolitic and the high amount available.

Previous study on several type of volcanic ashes shows that AC can be set between 0.1 and 1.0 without affect significantly the GSA, but a low value (AC= 0.1, close to transparent) assures a correct detection of the fine particles (Horwell, 2007). Taking into account that SEM analysis proves the occurrence of <5 µm particles, the recommended value (AC= 0.1) was used in this research. RI varies with the precise mineral composition of the sample and more accurate results could be obtained using the average RI estimated by summing the RIs of the component minerals, adjusted to reflect the proportion of the minerals in the ash being analysed (Horwell, 2007). RI values for individual minerals and volcanic glass are compiled in different sources (Kerr, 1977). For volcanic glass the RI range is 1.48-1.61, being the low value more

appropriate for basaltic glass and the high value for silicic glass. The average RIs obtained taking into account the mineralogical composition of ash (sample 719) are in Table 5.3.

Table 5.3 Calculation of the average Refractive index (RI) using three different RIs for volcanic glass (sample 719).

Mineral	wt %	RI	Proportional RI	wt %	RI	Proportional RI	wt %	RI	Proportional RI
Quartz	5.6	1.55	0.08	5.6	1.55	0.09	5.6	1.55	0.08
Sanidine	1.2	1.52	0.02	1.2	1.52	0.02	1.2	1.52	0.02
Albite	5.4	1.52	0.08	5.4	1.52	0.08	5.4	1.52	0.08
Glass	87.8	1.48	1.29	87.8	1.53	1.34	87.8	1.61	1.41
TOTAL	100.0		**1.49**	100.0		**1.53**	100.0		**1.60**

Comparison of GSA results using the three calculated RI values is reported in Figure 5.4. Results are obtained as volume percentages of grain size fractions and then were converted into cumulative volume (%). The first observation concerns the different results obtained with the dry method (i.e., in air). Generally, the dry method dispersion works well for large particles, where the interfacial contact area is small and the physical bonds holding together the individual particles are relatively weak. For relatively smaller particles, the higher surface to volume ratios produces numerous contact points and, thus, a greater driver force is needed to separate aggregated particles. Data obtained suggest that the dry method fails to disaggregate the particles lower than <100 µm, which are probably joined by electrostatic forces (Figure 5.4). Thus, a best dispersion is achieved in water medium. Not significant differences were shown using different RI values in water with or without ultrasonic bath. The intermediate value (1.53) is considered an adequate practical value because it cover different type of volcanic ashes (from basaltic to rhyolitic) and it is in agreement with the RI recommended by the equipment supplier for general application (Malvern Instruments). A standard operating procedure was used for each analysis (in water medium at 20 sec of measurement time, obscuration of 10-20%, and pump speed of 2500 rpm). Prior to analysis all the ash samples were dried in an oven at 40 °C for 24h. Three measurements were recorded for each sample and an average taken.
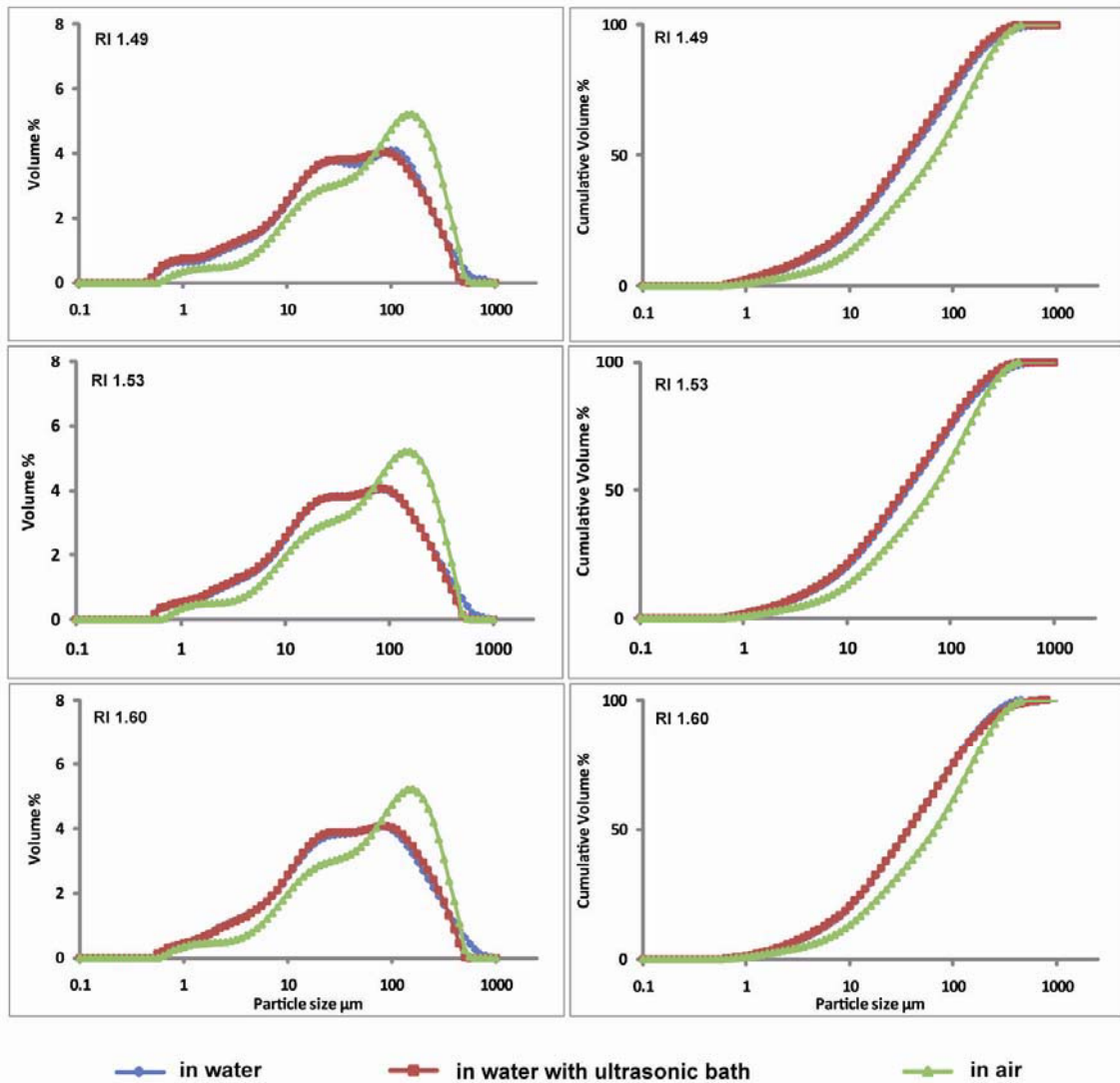
Figure 5.4 GSA data obtained varying the RI value in different operating conditions.

5.1.3.2 Grain-size analysis of bulk ashes

Grain-size analysis is an important tool in the study of volcanic ashes because it provides information for both eruptive and environmental concerns. It is well known that deposition and transport processes are strongly dependent on the particle size. Following the analysis of the grain size distribution, it is illustrative to compare the results among the different volcanic eruptions investigated. Results were obtained as volume percentages of grain size fractions and then were converted into cumulative volume (%) to assess the amount of material in
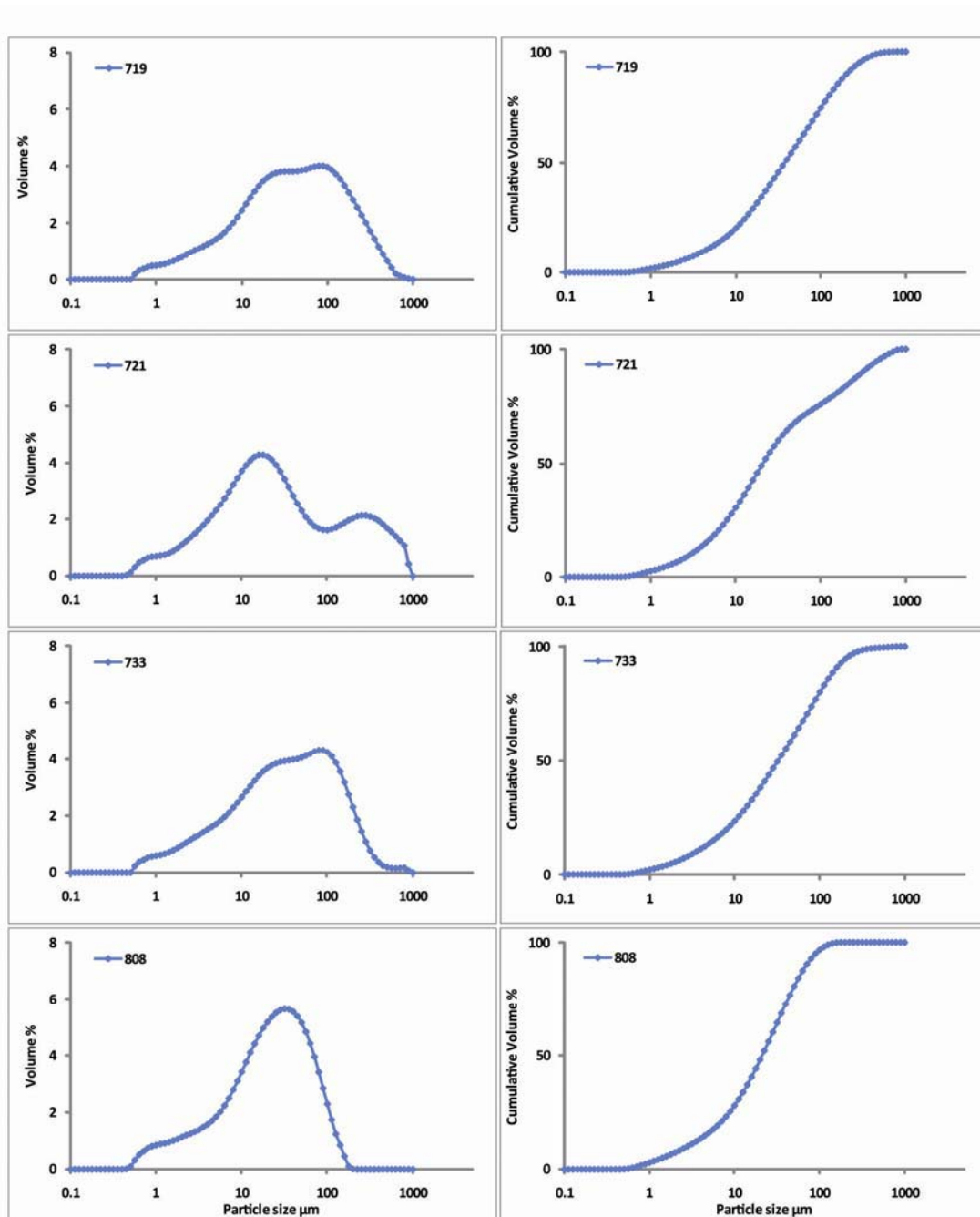
Figure 5.5a Average results (3 runs) of grain size distributions expressed as volume percentages of grain size fractions (left side) and cumulative volume (right side) in the Puna and neighbouring area samples.
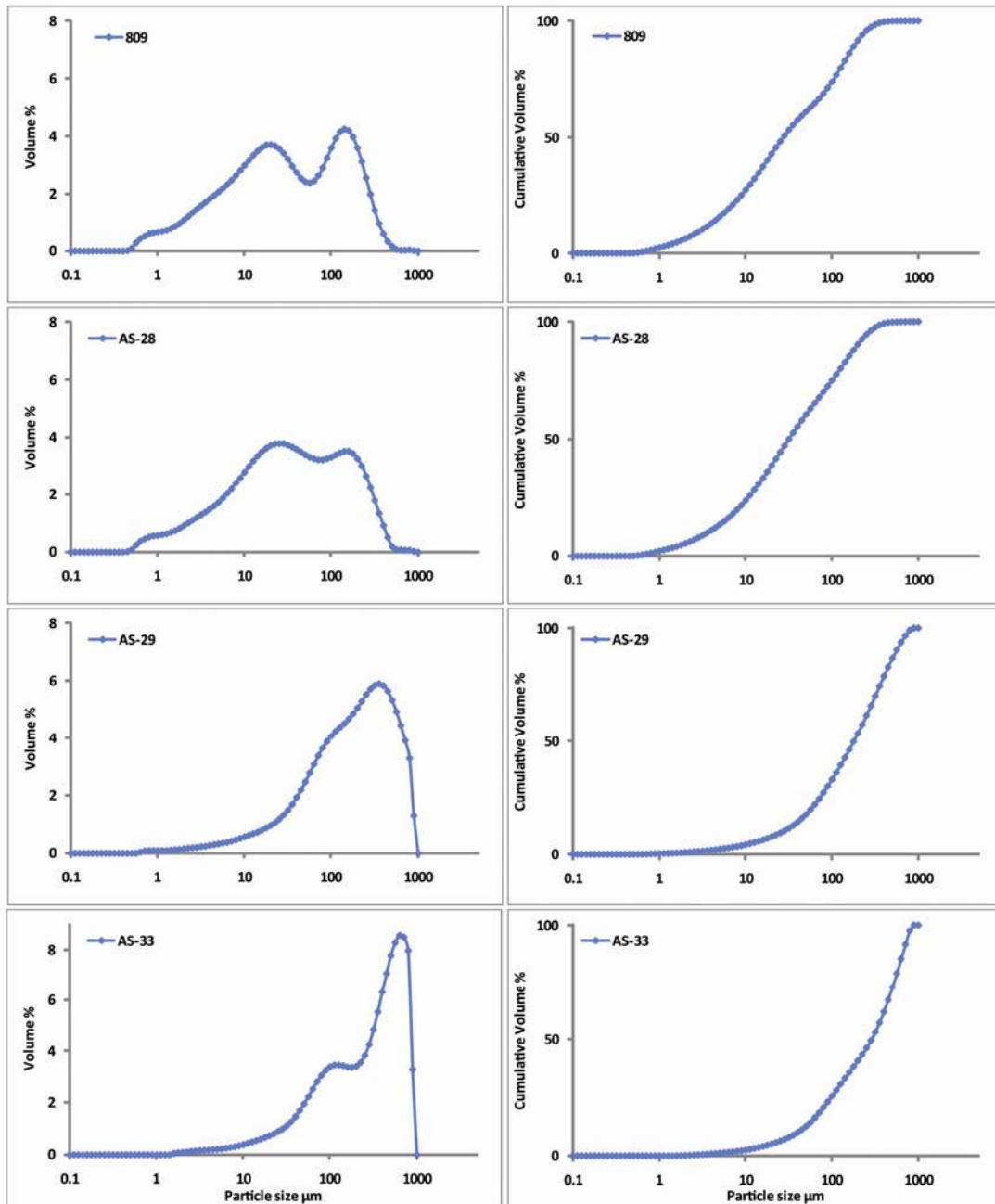
Figure 5.5b Average results (3 runs) of grain size distributions expressed as volume percentages of grain size fractions (left side) and cumulative volume (right side) in the Puna and neighbouring area samples.
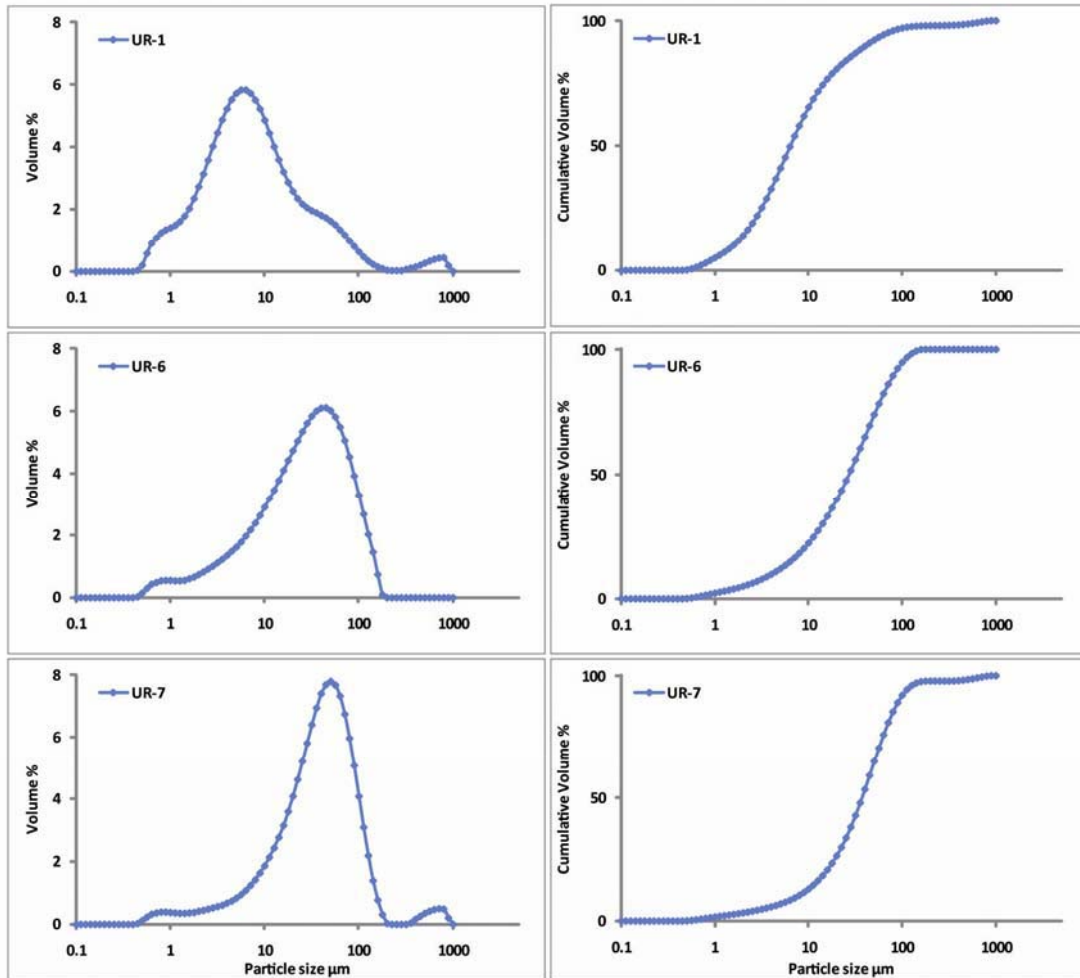
Figure 5.5c Average results (3 runs) of grain size distributions expressed as volume percentages of grain size fractions (left side) and cumulative volume (right side) in the Uruguay samples.
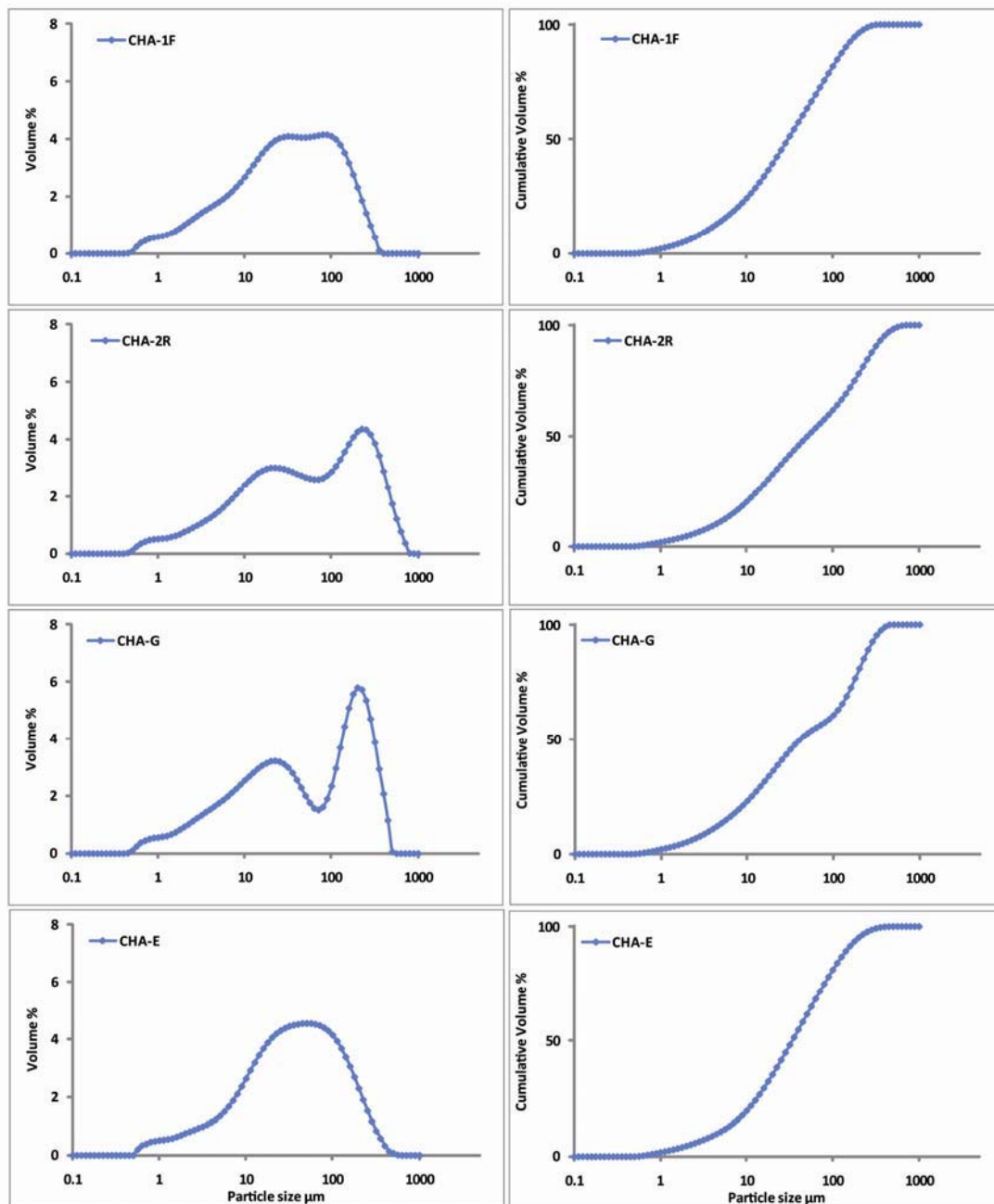
Figure 5.5d Average results (3 runs) of grain size distributions expressed as volume percentages of grain size fractions (left side) and cumulative volume (right side) in the Chaiten samples.
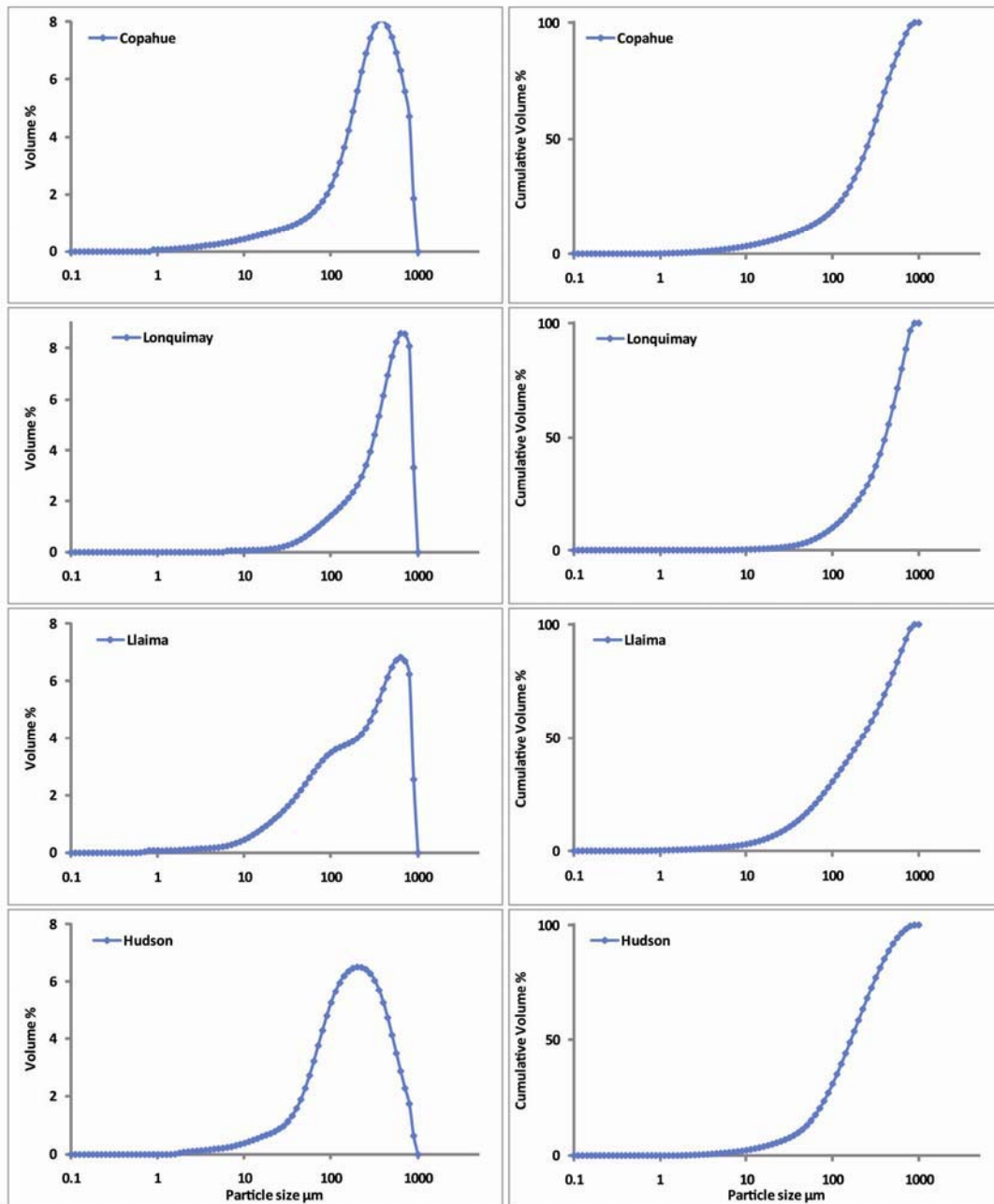
Figure 5.5e Average results (3 runs) of grain size distributions expressed as volume percentages of grain size fraction (left side) and cumulative volume (right side) in the SVZ (Copahue, Lonquimay, Llaima, and Hudson volcanoes) samples.

each fraction (Figures 5.5a-e). Table 5.4 shows the amount of material in six particle size fractions (<5, 5-10, 10-50, 50-100, 100-500, 500-1000 μm) expressed in percentage of volume.

The diagrams reported in Figures 5.5a-e are useful for identifying the frequency distributions of the samples. Any sample presents a normal distribution. However, some samples tended toward unimodal distributions, being composed mainly of a specific fraction. This is the case of the 808, AS-29, AS-33, UR-1, UR-6, UR-7, CHA-E, COP, LON, LLA, and HUD samples. These samples could be further grouped on the basis of the main fraction observed. High content of large particles (500-1000 μm) were reported in samples AS-29, AS-33, COP, LON, LLA, and HUD, in contrast to samples 808, UR-1, UR-6, UR-7, CHA-E which presented higher fine size (10-100 μm) content. Other samples (721, 809, CHA-2R, and CHA-G) presented clearly a bimodal distribution with two peaks at 10-50 μm and 50-100 μm. Finally, not significant differences among the size fractions in samples 719, 733, AS-28, and CHA-1F indicated a multimodal distribution.

Table 5.4 Amount of material in six particle size fractions (volume, %).

Sample	Grain-size fraction					
	< 5 μm	5-10 μm	10-50 μm	50-100 μm	100-500 μm	500-1000 μm
719	11.48	8.74	36.83	17.69	24.64	0.62
721	16.68	13.78	37.65	7.84	19.87	4.18
733	13.59	9.83	37.85	18.83	19.4	0.53
808	16.11	11.92	52.57	16.13	3.27	0.00
809	15.97	11.41	33.66	12.73	26.06	0.12
AS-28	13.41	10.3	36.8	14.54	24.67	0.24
AS-29	2.25	1.99	13.31	15.42	53.82	13.22
AS-33	1.16	1.35	10.2	12.84	47.27	27.18
UR-1	40.96	24.43	26.86	4.77	1.63	1.33
UR-6	12.03	10.26	51.71	20.85	5.18	0.00
UR-7	6.92	6.06	51.83	27.28	6.36	1.54
CHA-1F	14.28	10.11	39.11	18.32	18.17	0.0
CHA-2R	11.39	8.92	29.58	11.93	36.45	1.75
CHA-G	13.41	9.7	29.57	7.9	39.42	0.00
CHA-E	10.73	9.0	41.85	19.49	18.92	0.01
COP	1.69	1.64	8.02	7.65	62.17	18.81
LON	0.00	0.30	3.20	6.45	53.36	36.67
LLA	1.48	1.43	13.89	13.79	47.85	21.56
HUD	0.97	1.32	10.67	17.84	60.99	8.18

The amount of fine particles is important because reflect several features including: (1) style and dynamics of eruption; (2) geographical location, i.e., the distance from the volcano to the sampling site; and (3) environmental hazard assessment factors because high contents of small particles are potentially more dangerous than samples composed by larger particles.

In general, basaltic volcanoes produce relatively small amount of fine particles when compared with andesitic, dacitic and rhyolitic eruptions. This feature was visible in the ashes under study being the rhyolitic samples (including most of the ashes from Puna, Uruguay, and Chaiten volcano) much more fine-grained than the less silicic ashes (samples COP, LON, LLA, and HUD) (Table 5.4). The Chaiten ashes are the only samples collected in this study for which we could observe a possible increase of fine grain-size with the distance. However, the Chaiten ashes present similar fine grained content (<10 µm) in the closest ash to the vent (sample CHA-1F) than in the furthest samples (CHA-G and CHA-E), being 20-24 volume (%) (Table 5.4). These results corroborate those reported by Horwell et al., 2008. The grain size distribution in the Chaiten ash samples suggests a possible evolution during the 2008 eruption passing form a clear bimodal distribution in the first initial phase (sample CHA-G) to more homogeneous distribution (samples CHA-1F and CHA-E, collected only a few days later). Moreover, the sample CHA-2R collected on August 2008 (after dome collapse) presents the same distribution of the sample collected during the first fallout. Though dome-collapse eruptions not are, usually, highly explosive, they could generate large amounts of fine particles as in the case of the historic eruption of Soufrière Hills volcano and the more recent eruption of Chaiten volcano (Horwell, 2007; Horwell et al., 2010).

The amount of very fine materials (<5 µm) in the rhyolitic ashes under study varies from 1.16-40.96 volume (%), being the lower value for sample AS-33 and the higher for sample UR-1 (Table 5.4). The UR-1 ash distribution is coherent with its deposition at more than 1300 km of the source volcano of the Andes. In the latter the fine content implies a greater environmental and health assessment because particles with aerodynamic diameter less than 4 µm are considered "respirable fraction" (Horwell, 2007). Taking into account the fine materials lower than 10 µm, the environmental hazard posed by the ash under

study could be as follows: UR-1>721>808>809>CHA-1F>733>CHA-G>AS-28>
UR-6>719>CHA-2R>CHA-E>UR-7>AS-29>COP >LLA>AS-33>HUD>LON.

5.2 Mineralogical characterisation

5.2.1 XRD patterns of the bulk ashes

The X-ray diffraction (XRD) patterns show that glass is the main constituent of
all types of ash, except for AS-29 and AS-33 samples, though there are also
minor amounts of other crystalline mineral phases (Table 5.5). The XRD
patterns of all the ashes investigated are reported in Appendix 2.

Table 5.5 Mineral composition (***, common; **, frequent; *, scarce; w, rare; nd, not detected) of the volcanic ashes under study.

Sample	Qz	Ab	Sa	Bt	Glass	Crs	Di	An	Ad
719	**	***	**	*	***	nd	nd	nd	nd
721	***	*	*	**	***	w	nd	nd	nd
733	*	**	**	**	***	nd	nd	nd	nd
808	nd	nd	nd	nd	***	nd	nd	nd	nd
809	*	*	*	w	***	nd	nd	nd	nd
AS-28	**	**	**	**	***	w	nd	nd	nd
AS-29	**	**	*	w	w	*	nd	nd	nd
AS-33	**	**	*	w	w	*	nd	nd	nd
UR-1	nd	nd	nd	nd	***	nd	nd	nd	nd
UR-6	nd	nd	nd	nd	***	nd	nd	nd	nd
UR-7	nd	nd	*	nd	***	nd	nd	nd	nd
CHA-1F	w	nd	nd	nd	***	w	nd	nd	**
CHA-2R	*	nd	nd	nd	***	*	nd	nd	***
CHA-G	w	nd	nd	nd	***	w	nd	nd	**
CHA-E	w	nd	nd	nd	***	w	nd	nd	**
COP	nd	nd	nd	nd	***	nd	nd	*	nd
LON	nd	nd	nd	nd	***	nd	nd	*	nd
LLA	nd	nd	nd	nd	***	nd	nd	*	nd
HUD	nd	nd	nd	nd	***	nd	w	*	nd

Qz, Quartz; Ab, Albite; Sa, Sanidine; Bt, Biotite; Crs, Cristobalite; Di, Diopside; An, Anorthite; Ad, Andesite (mineral abbreviations from Whitney and Evans, 2010).

Mineralogical composition and the location of the ash samples allowed us to organize the samples into four broad groups:

(1) Ancient volcanic ash samples from southern Puna and neighbouring areas. The glass was accompanied by minor amounts of quartz, albite, sanidine, and biotite. Within this cluster, samples AS-29 and AS-33 show similar XRD patterns whereas samples 721 and AS-28 present scarce cristobalite. Sample 808 was made up only of volcanic glass.

(2) Ancient volcanic ash samples from Uruguay which were composed only by volcanic glass. Scarce sanidine was observed in sample UR-7.

(3) Recent volcanic ashes from the SVZ (samples COP, LON, LLA, and HUD), in which conspicuous amount of anorthite was detected.

(4) Volcanic ashes from Chaiten eruption, in which quartz, andesite, and remarkable amount of cristobalite were identified.

Cristobalite is a silica polymorph of priority environmental concern because of its acicular shape and fine grain size fall in the range of respirable fraction (<4 µm) (Horwell et al., 2010). In that work was exposed that ash erupted during the initial explosive phase (2–5 May 2008) contained lower amount of cristobalite than ash generated after dome growth began (from 21 May 2008). This feature was observed also in our samples, in which the qualitatively observation of the spectra highlights more cristobalite content in the ash sampled after dome collapse (sample CHA-2R). Moreover, Horwell et al, (2010) make a comparison with the cristobalite found in the andesite lava dome of the Soufriere Hills volcano, Montserrat (Baxter et al., 1999). These authors suggest that the high presence of cristobalite in the ash generated in the second phase of eruption was due to the breakage of small silica spherulites in the ancient dome during the initial stage of eruption (Horwell et al., 2010). Applying this hypothesis to our samples, the occurrence of cristobalite in an ash perhaps could help to fingerprint ancient explosive eruptions as in the case of samples 721 and AS-28.
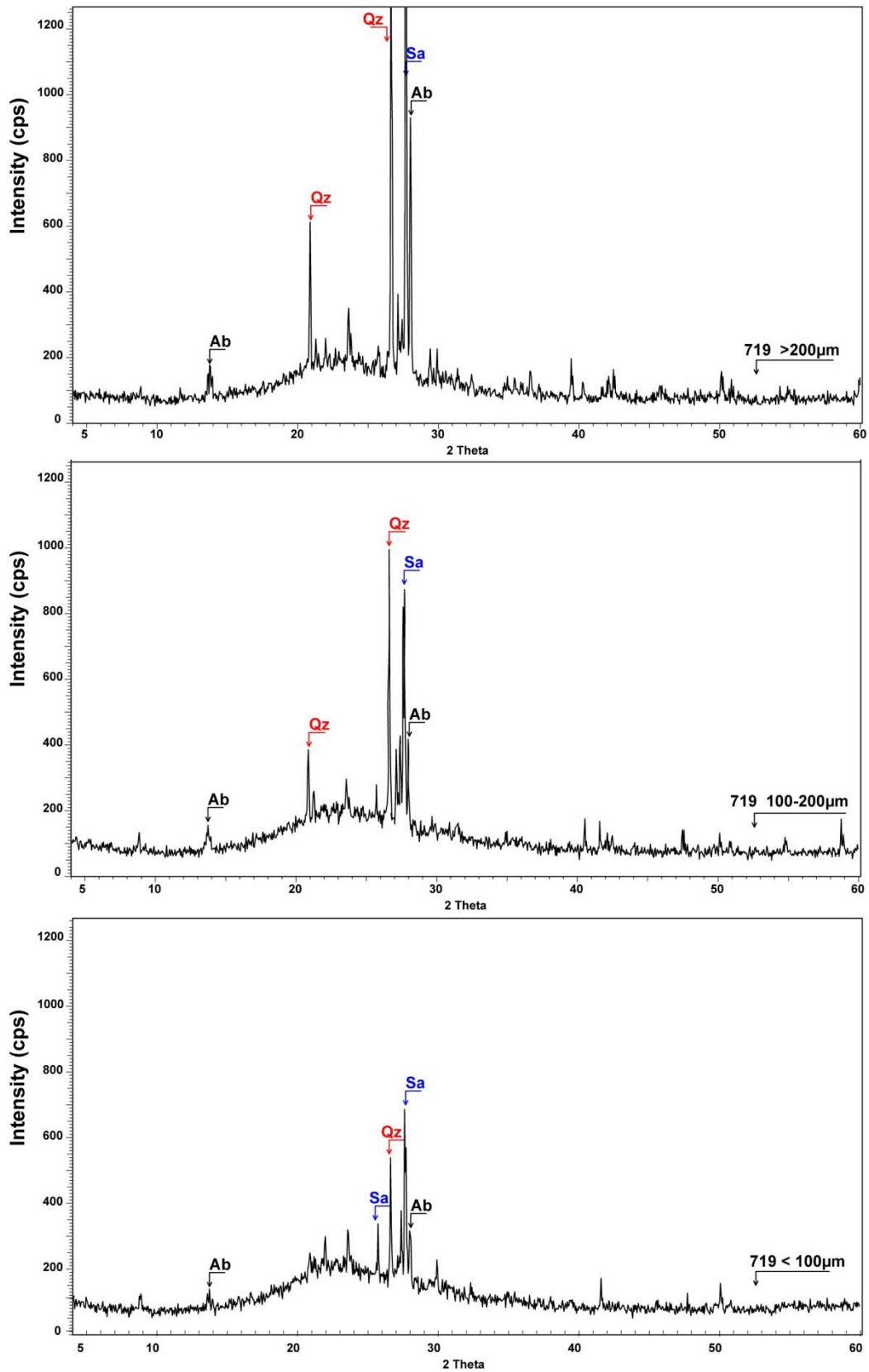
Figure 5.6 XRD patterns of the three grain size fractions studied in sample 719.

5.2.2 XRD patterns of the grain-size fractions of 719 volcanic ash

The aim of this part of research was to apply a simple grain-size fractionation procedure in order to verify possible differences in the mineralogical content. Sample 719 was selected due to the high amount of sample available. The dried ash

was sieved by mechanical separation in three particle size fractions: <100 μm, 100-200 μm, and >200 μm. XRD patterns are shown in Figure 5.6. The crystalline phase content of the sample decreases towards the finest size fraction (<100 μm). Crystals are more abundant in the grain size range <2 mm to 63 μm and are generally absent below 10 μm, whereas glass shards can be micrometric in size (Duggen et al., 2010). These results are useful for the interpretation of the results other methods (e.g., leaching test).

In addition, taking into account that volcanic eruptions are natural sources of continental particulate matter in the atmosphere, the mineralogical study of size fractionated ashes may be useful recognizing their effects on the environment (Duggen et al., 2010).

5.3 Bulk chemical analysis: major oxides and trace elements

Tables 5.6a and b present the original data of major oxides and trace elements. Major oxides compositions of ashes from the SVZ obtained in this study (Table 5.6b) are similar to those reported by previous authors (Bitschene et al., 1994; Moreno and Gardeweg, 1989; Naranjo and Stern, 2004; Watt et al., 2009). No previous published data were found for the Llaima ash erupted in 2008.

The studied volcanic ashes have been geochemically classified using the Total Alkali *vs.* Silica (TAS) diagram (Figure 5.7) (Le Bas et al., 1986; Le Maitre, 1989).
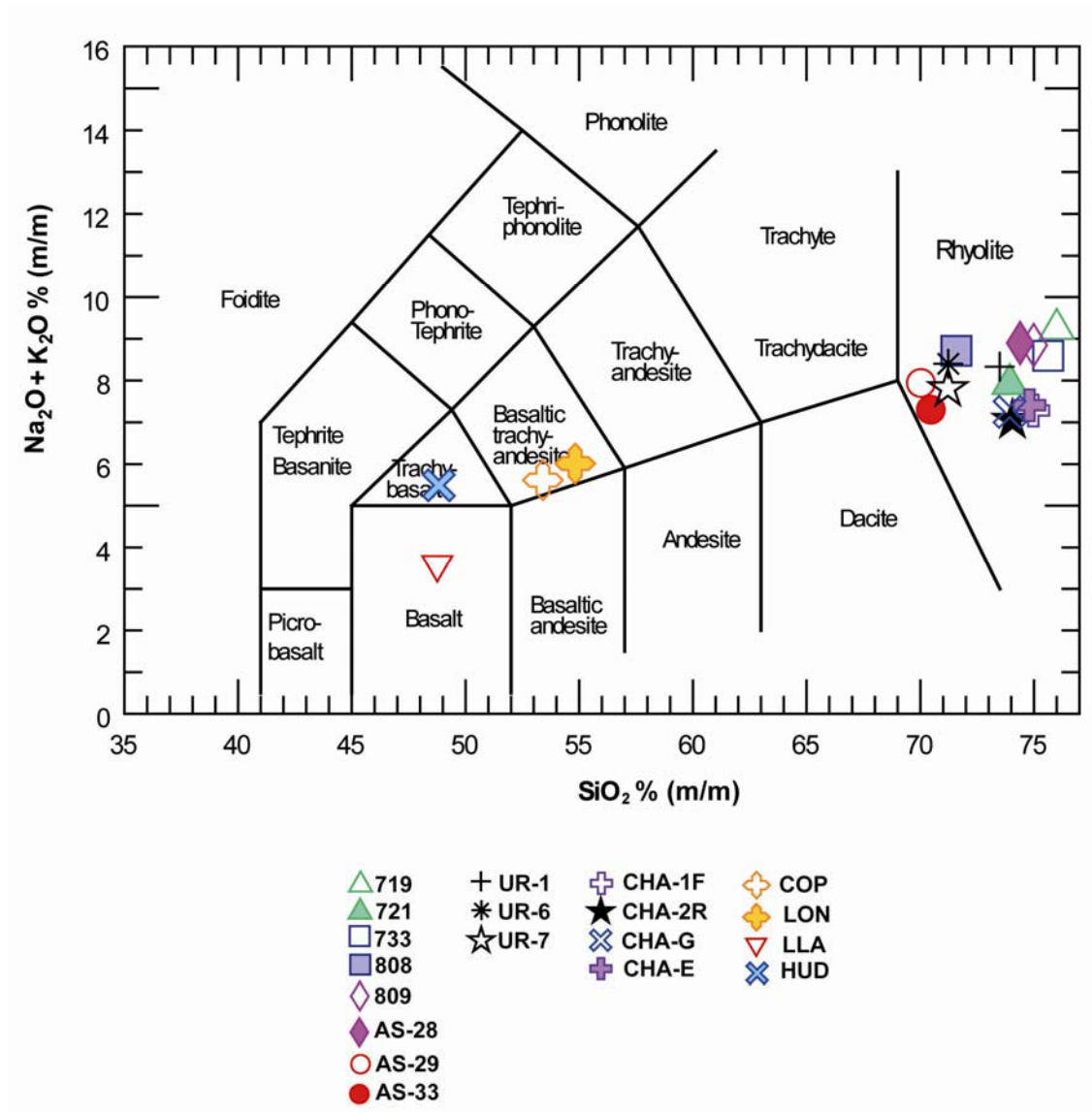
Figure 5.7 Total Alkali *vs*. Silica plot of volcanic ashes from this study.

For this diagram, major element concentrations were recalculated before plotting to sum 100 %, m/m on water and CO_2 free basis. The ashes are classified in the TAS diagram as follows:

(1) basalt: sample LLA;

(2) trachy-basalt: sample HUD;

(3) basaltic trachy-andesite: samples LON and COP;

(4) rhyolite: samples 719, 721, 733, 808, 809, AS-28, AS-29, AS-33, UR-1, UR-6, UR-7, CHA-1F, CHA-2R, CHA-G, and CHA-E.

Bulk major and trace elements chemistry unambiguously distinguish a diversity of magma genesis processes along the Andean cordillera. Several authors reported the difference between the more silicic volcanic rocks erupted in CVZ, including the Puna and neighbouring area, in contrast to the common presence of basalts and basaltic andesites in the volcanic centers of the SVZ (Lopez-Escobar et al., 1993; Stern, 2004, 2008).

Table 5.6a Bulk geochemistry of volcanic ashes from the Puna and Uruguay (major oxides as %, m/m); trace elements as µg g^{-1}. LOI, Loss on Ignition and LoD, Limit of Detection.

	719	721	733	808	809	AS-28	AS-29	AS-33	UR-1	UR-6	UR-7
SiO$_2$	74.55	72.08	73.72	69.79	73.10	72.52	68.30	68.74	71.88	70.05	69.51
Al$_2$O$_3$	12.45	12.61	12.77	14.25	12.82	13.26	14.92	14.52	12.80	13.62	13.81
Fe$_2$O$_{3\,t}$	0.81	2.01	0.93	0.99	0.89	1.08	2.87	3.15	1.09	1.57	1.87
MnO	0.08	0.10	0.08	0.09	0.09	0.10	0.07	0.06	0.06	0.07	0.13
MgO	0.16	0.77	0.32	0.42	0.22	0.32	0.92	0.92	0.24	0.37	0.44
CaO	0.89	1.65	0.92	0.81	0.71	1.03	2.82	2.99	0.88	1.00	0.99
Na$_2$O	3.92	3.60	3.68	4.20	4.18	4.22	4.23	4.03	2.62	3.12	2.90
K$_2$O	4.49	4.11	4.70	4.29	4.44	4.46	3.49	3.07	5.50	5.07	4.71
TiO$_2$	0.11	0.26	0.13	0.14	0.12	0.14	0.32	0.35	0.16	0.21	0.23
P$_2$O$_5$	0.02	0.06	0.03	0.05	0.01	0.02	0.10	0.08	0.05	0.08	0.09
LOI	2.53	2.71	2.73	4.94	3.39	2.85	1.89	2.00	4.63	5.03	5.37
Total	99.96	99.94	99.97	99.91	99.92	99.94	99.97	99.96	99.96	100.09	99.98

Table 5.6a continuation.

	719	721	733	808	809	AS-28	AS-29	AS-33	UR-1	UR-6	UR-7
Li	90.3	93.2	86.4	56.8	111	93.7	12.5	17.3	16.2	25.5	29.3
Be	6.35	6.39	6.52	3.31	6.75	6.29	2.35	2.02	2.86	3.05	3.07
V	6.60	33.1	8.84	8.19	6.17	8.59	53.0	62.59	6.75	12.2	16.0
Cr	4.49	21.24	11.17	4.44	3.73	6.95	17.2	21.2	3.88	6.45	8.34
Mn	593	695	572	661	652	667	464	451	443	457	894
Co	0.82	4.39	1.86	23.4	12.6	27.3	19.4	32.7	76.7	30.2	21.0
Ni	2.52	11.4	5.82	3.04	1.84	5.10	12.3	9.15	2.31	3.03	7.02
Cu	7.13	9.55	4.38	5.17	4.62	7.03	12.8	10.9	5.64	7.53	11.3
Zn	39.9	60.3	42.0	53.8	39.9	111.1	71.9	56.3	40.5	64.0	69.0
Ga	20.2	21.4	20.0	18.6	21.1	20.3	21.0	19.6	14.9	16.1	16.6
Ge	1.84	1.92	1.85	1.50	1.94	2.07	0.90	0.75	1.25	1.36	1.38
As	5.75	7.37	5.46	6.34	6.69	7.24	1.44	1.35	1.44	3.18	2.05
Rb	376	348	373	146	401	495	133	81	176	185	179
Sr	24.6	93.6	41.7	90.3	25.7	37.3	354	482	125	132	133
Zr	68.5	89.7	72.6	78.7	57.8	66.2	22.1	80.0	nd	nd	nd
Nb	33.0	33.3	30.0	10.3	27.8	27.1	14.8	7.8	nd	nd	nd
Mo	2.68	2.81	2.78	2.60	2.89	2.86	1.86	0.22	2.61	2.67	2.54
Cd	<LoD	<LoD	<LoD	<LoD	<LoD	0.15	0.10	0.10	0.17	0.17	0.28
Sn	2.71	6.91	3.63	2.34	3.61	3.71	2.24	1.81	2.40	2.50	2.54
Sb	1.13	1.20	1.14	0.31	1.18	2.40	9.11	2.71	0.77	0.68	0.69
Cs	25.1	24.4	25.3	5.0	27.8	26.9	6.78	2.71	7.22	8.40	8.37
Ba	34.9	152.7	61.9	820.0	41.3	69.6	439	578	539	530	536
La	14.5	22.1	18.0	17.7	18.7	17.5	73.8	50.9	46.3	49.0	48.2
Ce	33.7	45.8	37.9	37.1	39.8	37.3	113	84.0	82.9	88.7	92.5
Pr	10.7	5.40	4.42	4.23	4.64	4.24	10.8	8.46	8.86	9.49	9.47
Nd	12.7	19.3	15.3	14.5	16.0	14.7	33.4	27.9	28.1	30.0	30.8
Sm	5.26	4.00	3.18	3.12	3.36	3.10	4.82	4.30	4.43	4.78	5.00
Eu	0.79	0.48	0.30	0.56	0.26	0.29	1.23	1.07	0.70	0.82	0.86
Gd	2.48	3.96	3.17	3.16	3.33	3.07	6.08	4.79	4.43	4.80	5.19
Tb	0.96	0.60	0.49	0.52	0.52	0.48	0.65	0.54	0.55	0.61	0.65
Dy	2.39	3.57	2.98	3.13	3.18	2.97	3.52	2.99	3.07	3.45	3.64
Ho	1.00	0.67	0.57	0.57	0.63	0.58	0.55	0.47	0.51	0.58	0.61
Er	1.55	2.17	1.88	1.71	2.04	1.88	1.88	1.51	1.60	1.82	1.95
Tm	0.59	0.34	0.30	0.25	0.33	0.30	0.25	0.20	0.22	0.25	0.26
Yb	1.77	2.50	2.19	1.68	2.39	2.22	1.67	1.32	1.46	1.65	1.79
Lu	0.70	0.38	0.35	0.25	0.38	0.36	0.24	0.19	0.22	0.25	0.27
Hf	3.48	4.54	3.73	3.50	4.33	3.94	2.18	1.06	3.79	3.81	4.19
Tl	1.98	1.81	1.93	0.82	1.96	1.76	0.75	0.32	0.59	0.83	0.97
Pb	36.5	35.5	36.6	25.3	36.7	39.2	21.7	18.1	28.4	31.2	32.0
Bi	1.17	1.18	1.24	0.31	1.28	1.10	0.27	0.14	0.30	0.39	0.39
Th	29.1	27.0	28.2	13.2	29.3	31.9	32.2	19.2	32.7	34.6	32.8
U	18.3	17.3	18.4	4.2	19.9	24.4	6.08	4.05	9.04	9.30	8.54

Table 5.6b Bulk geochemistry of volcanic ashes from SVZ (major oxides as %, m/m); trace elements as µg g^{-1}. LOI, Loss on Ignition and LoD, Limit of Detection.

	CHA-1F	CHA-2R	CHA-G	CHA-E	COP	LON	LLA	HUD
SiO$_2$	73.62	72.35	71.88	73.41	53.36	54.45	47.53	49.91
Al$_2$O$_3$	14.41	14.61	14.65	14.42	17.43	16.82	18.50	16.35
Fe$_2$O$_{3t}$	1.57	1.88	1.88	1.59	8.28	9.96	10.18	11.48
MnO	0.07	0.07	0.07	0.07	1.40	2.32	1.71	1.96
MgO	0.35	0.56	0.60	0.36	4.39	2.49	6.93	4.37
CaO	1.57	2.04	1.99	1.62	7.09	5.64	9.65	8.23
Na$_2$O	4.07	4.08	4.18	4.20	3.60	4.88	2.93	4.08
K$_2$O	3.02	2.79	2.89	3.02	1.86	0.98	0.56	1.27
TiO$_2$	0.16	0.21	0.20	0.17	1.25	1.57	1.03	2.19
P$_2$O$_5$	0.08	0.09	0.08	0.10	0.28	0.37	0.18	0.74
LOI	1.06	1.43	1.57	0.96	0.79	-0.02	-0.56	-0.31
Total	99.52	99.99	100.26	99.58	98.91	98.47	98.64	97.95

Table 5.6b continuation.

	CHA-1F	CHA-2R	CHA-G	CHA-E	COP	LON	LLA	HUD
Li	48.4	46.1	41.1	45.5	11.7	12.8	6.96	7.59
Be	1.76	1.76	1.62	1.65	1.37	1.04	0.67	1.14
V	5.11	13.0	13.8	5.70	189	75.0	238	313
Cr	13.8	18.9	19.0	16.3	89.7	13.6	83.8	31.9
Mn	513	548	563	510	1082	1795	1324	1520
Co	1.41	2.81	2.57	1.52	24.3	13.1	36.8	26.3
Ni	1.67	3.68	4.31	1.56	29.2	1.30	55.0	8.28
Cu	6.41	10.5	8.45	5.90	52.6	41.1	109	53.7
Zn	51.0	54.1	51.2	53.3	103	153	107	141
Ga	14.1	14.5	14.1	14.0	18.8	21.0	17.8	19.7
Ge	1.21	1.21	1.07	1.13	0.91	1.15	0.88	1.10
As	18.1	47.8	38.4	15.1	7.60	8.27	4.65	0.92
Rb	105	98.4	98.8	103	53.8	18.6	10.8	30.0
Sr	151	173	167	154	505	472	472	535
Zr	104	93.2	93.2	100	204	112	72	178
Nb	7.37	7.17	7.17	7.27	6.97	2.57	1.97	8.12
Mo	0.91	0.75	1.02	0.80	1.05	0.06	< LoD	0.03
Cd	0.48	0.21	0.25	0.18	0.41	0.33	0.20	0.42
Sn	3.01	2.43	2.41	2.83	2.45	1.92	1.18	2.25
Sb	1.08	1.80	1.51	1.01	0.40	0.51	0.25	0.06
Cs	6.66	6.12	6.42	6.73	2.97	1.99	1.02	0.91
Ba	626	596	617	634	408	319	177	376
La	24.3	23.2	24.4	24.5	23.5	13.3	7.35	24.7
Ce	45.7	44.3	46.5	46.4	51.3	32.0	17.4	56.8
Pr	4.84	4.77	4.97	4.93	6.58	4.67	2.47	7.71
Nd	16.1	15.8	16.5	16.4	26.8	21.7	11.3	33.7
Sm	2.61	2.60	2.83	2.60	5.43	5.40	2.89	7.29
Eu	0.61	0.64	0.66	0.61	1.44	1.93	1.02	2.39
Gd	2.87	2.90	2.98	2.88	5.61	5.91	3.20	7.60
Tb	0.39	0.41	0.43	0.40	0.89	1.05	0.57	1.20
Dy	2.24	2.28	2.38	2.28	5.05	6.28	3.46	6.89
Ho	0.39	0.41	0.43	0.41	0.93	1.24	0.69	1.26
Er	1.25	1.26	1.37	1.30	2.75	3.58	2.06	3.68
Tm	0.19	0.19	0.20	0.19	0.39	0.52	0.30	0.50
Yb	1.37	1.31	1.44	1.36	2.51	3.40	1.96	3.17
Lu	0.22	0.21	0.23	0.22	0.38	0.52	0.31	0.49
Hf	3.42	3.98	3.18	3.40	5.48	3.38	2.31	4.46
Tl	0.65	0.65	0.64	0.67	0.65	0.16	0.08	0.32
Pb	20.7	19.6	22.4	25.6	14.3	13.5	6.73	7.52
Bi	0.24	0.28	0.30	0.27	0.33	0.07	0.03	0.06
Th	13.1	11.7	13.0	13.3	9.34	2.97	1.27	3.33
U	3.31	2.85	3.26	3.35	2.32	0.88	0.41	0.76

5.4 FTIR spectroscopy

In this study, FTIR was used to provide information on the water chemical bonds present in the volcanic ashes under study. The water content in volcanic glass has been worldwide studied by several techniques (i.e., ion microprobe, electron microprobe, and FTIR). Among these, the FTIR spectroscopic method presents excellent analytical sensitivity (Devine et al., 1995; Stolper, 1982). Figures 5.8a-c show the IR spectra of the studied ashes. Qualitative observations of the IR spectral line profiles allow us to classify the samples into two broad groups:

(1)   Samples from the southern Puna, Uruguay and Chaiten volcano with high water content. The typical peaks of H_2O_t, OH and H_2O_m were clearly observed.

(2)   Samples with low amount of water (COP, LON, LLA, and HUD) in which no noticeable peaks in their IR spectral line profiles were reported.

The IR spectra allow estimating the H_2O_t content by integration of the area under the peak at around 3612-3411 cm^{-1} wave number (Table 5.7). It is well known that rhyolitic magma may have a great amount of water if compared with less silicic magma. This feature explains the lower integrated area of water peaks in the IR spectral line profiles of the volcanic ashes from the SVZ, respect to the rhyolitic samples of Chaiten volcano. If the values of the area under the H_2O_t peak of rhyolitic ashes are compared, the ancient samples present high water content than the more recent ashes (i.e., Chaiten volcano).

An interesting study about the mechanism and rate of hydration of rhyolitic glass suggests that during weathering the water migrates into glass predominantly as H_2O_m (Yokoyama et al., 2008). The H_2O_m peaks are ca. 1600 and 5200 cm^{-1} in the IR spectral line profiles. These peaks are higher in the Puna and Uruguay rhyolitic ashes and could indicate that they are affected in some degree by weathering.
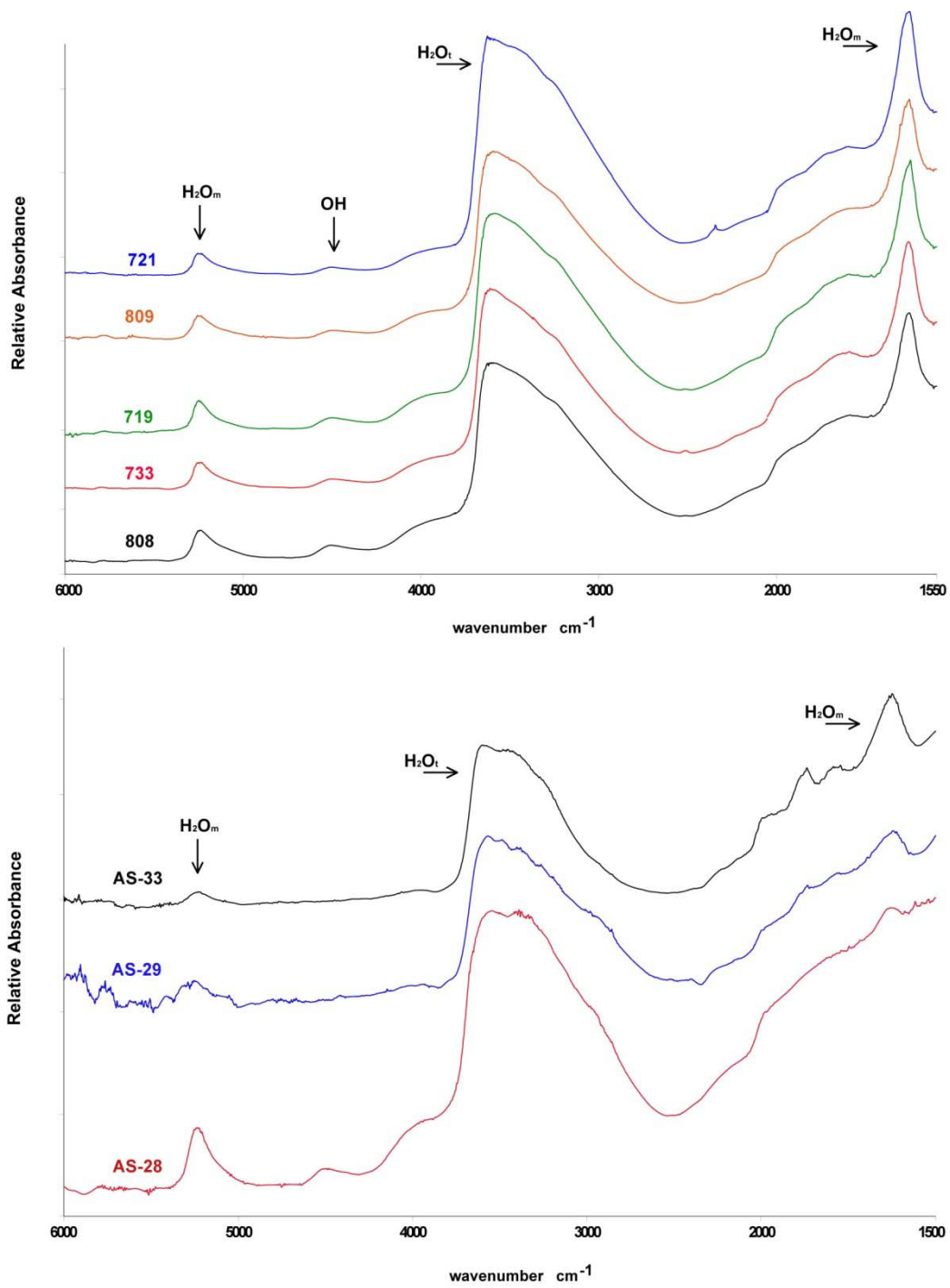
Figure 5.8a IR spectra of volcanic ashes from southern Puna and neighbouring area.

Table 5.7 Integrated area under the H_2O_t peak and LOI values by calcination of the samples.

Sample	Area H_2O_t IR peak	LOI
719	540	2.53
721	469	2.71
733	468	2.73
808	663	4.94
809	459	3.39
AS 28	687	2.85
AS 29	424	1.89
AS 33	367	2.00
UR-1	558	4.63
UR-6	460	5.03
UR-7	541	5.37
CHA-1F	354	1.06
CHA-2R	319	1.43
CHA-G	355	1.57
CHA-E	351	0.96
COP	250	0.79
LON	146	-0.02
LLA	53	-0.56
HUD	80	-0.31
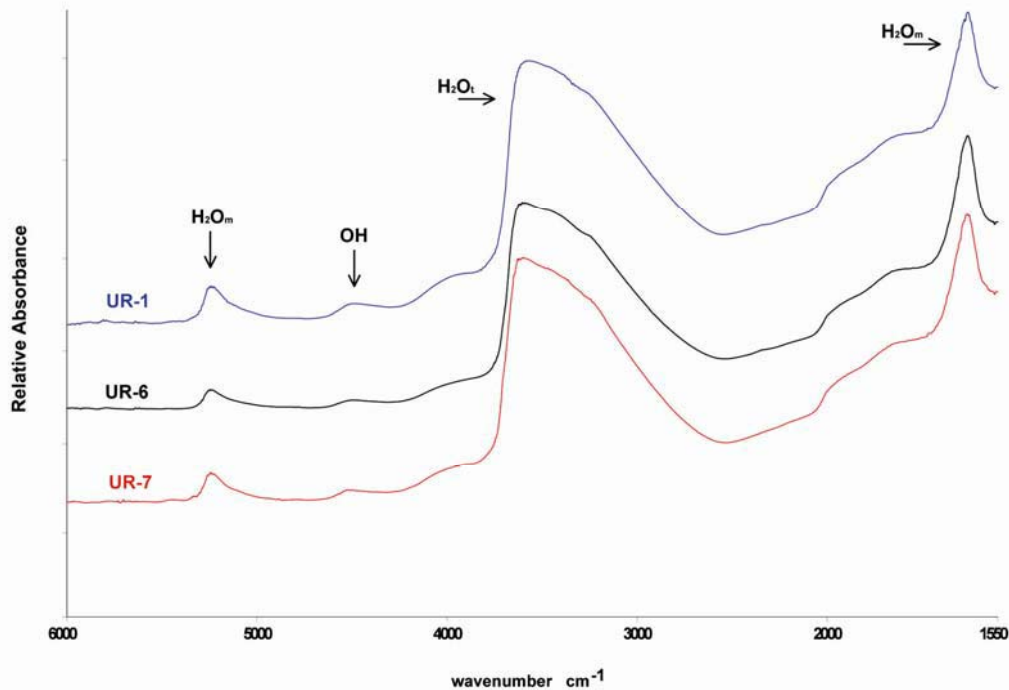
Figure 5.8b IR spectra of volcanic ashes from Uruguay.
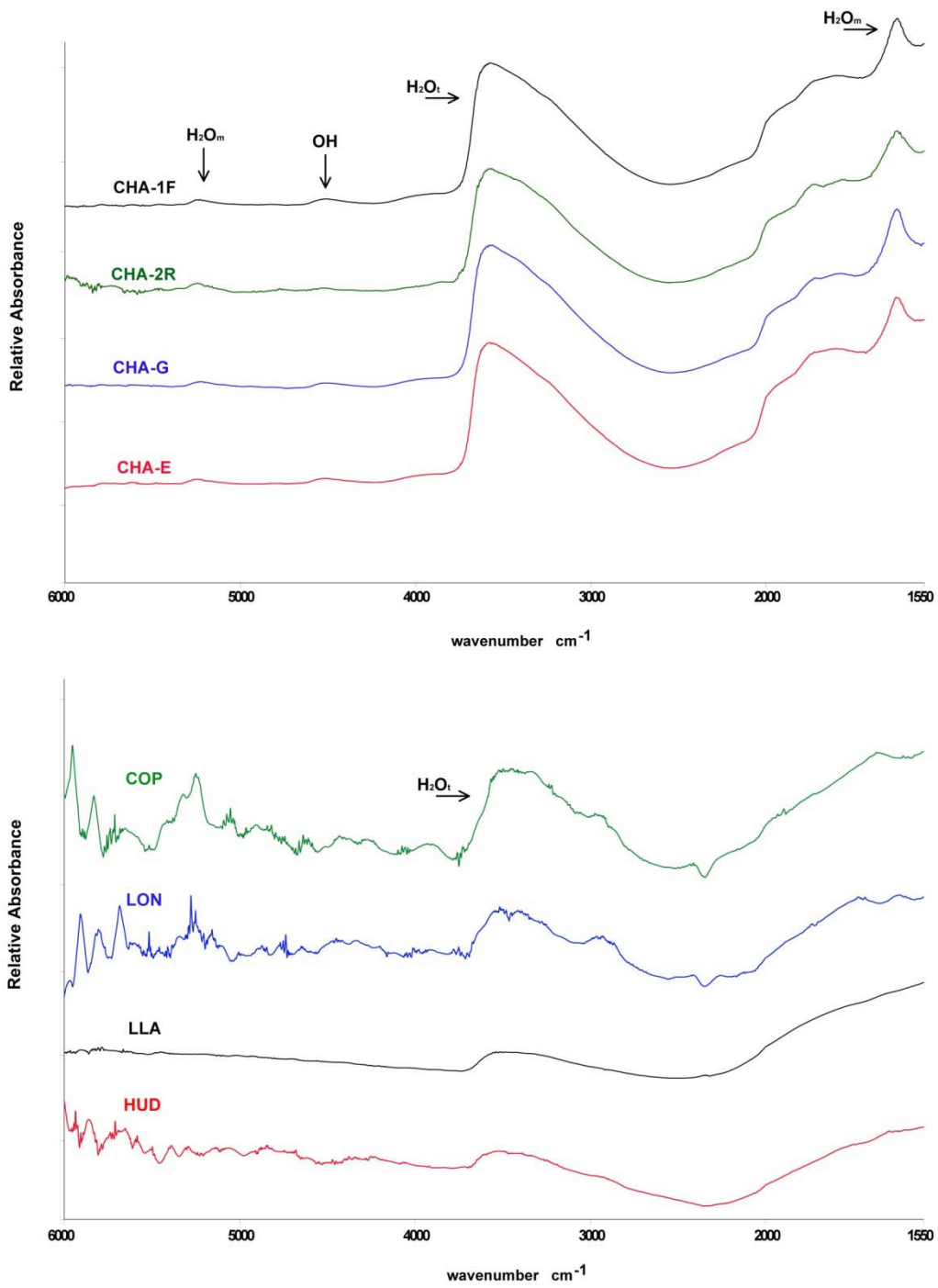
Figure 5.8c IR spectra of volcanic ashes from the SVZ.

5.4.1 Volatile content *vs*. integrated area of H_2O_t IR peak

Volatile content (i.e., H_2O, CO_2, F, Cl, S, etc.) are usually evaluated in whole rock analysis through the Loss on Ignition (LOI) content. This is a good approximation only for the samples in which weight gain does not occur during calcinations. LOI data reported in Table 5.7 indicate higher volatiles content in ashes from Puna and Uruguay than in the ashes from SVZ.
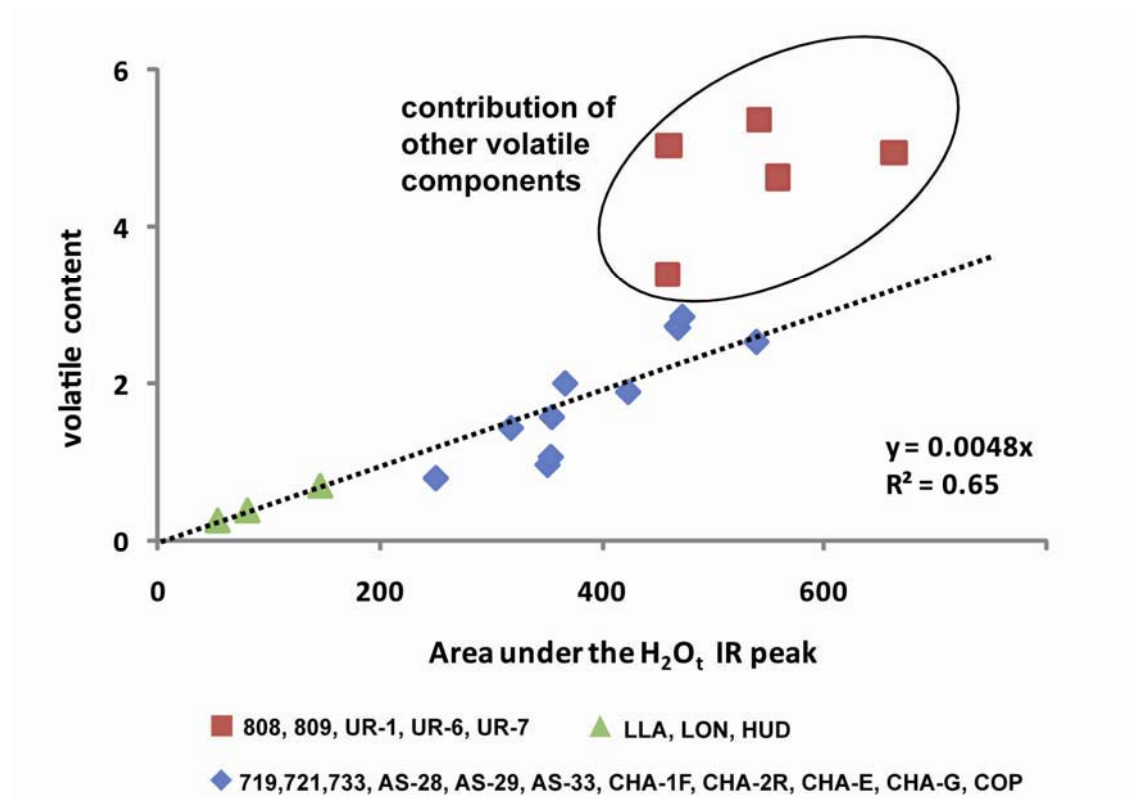
Figure 5.9 Correlation between the volatile content (estimated by LOI) *vs*. the area under the H_2O_t IR peak. In the LLA, LON, and HUD samples the volatiles content are inferred through this correlation.

The mineralogical and petrographic observations indicate that a significant portion of the ashes corresponds to anhydrous or slightly hydrated minerals. The biotite generally has less than 5% of H_2O, i.e., the whole rock equivalent content is very low in the most micaceous samples (Table 5.5). Consequently, water should concentrate in the glass. Nevertheless, although the glass may contain halogens in small quantities (Aiuppa et al., 2009), most of LOI is water and its content in glass should be somewhat higher than that indicated in Table

5.7 by LOI. A good correlation when the volatile content (estimated by LOI) is plotted against the value of the integrated area under the H_2O_t peak should be expected. Plot diagram in Figure 5.9 indicates best correlation when samples 808, 809, UR-1, UR-6, and UR-7 were considered separately from the other ashes, being $R^2 = 0.65$. A contribution of other volatile components besides the water (i.e., Cl, F, S, etc.) could take place in these samples.

On the other hand, knowing the value of the area under the H_2O_t peak, this diagram could be used as a calibration curve in order to check the volatile content of less silicic samples. The new volatile content addressed to LLA, LON, and HUD samples increases according to the corresponding silica content (LLA, 0.25; LON, 0.38; HUD, 0.70 %, m/m) and they appear more realistic than the values estimated by means of calcinations (Table 5.7).

5.4.2 Ash reactivity

It is well known that the structure of a silicate melt is modified with the dissolution of water such that the addition of small amounts of water can significantly change its physical and chemical properties. The presence of water in a magmatic system influences the viscosity of the liquid (Giordano et al., 2008; Stevenson et al., 1998), crystal nucleation rates (Davis et al., 1997), and the chemical diffusivities that control melt homogenization, crystal growth rates, and the degree of interaction with surrounding wall-rock (Zhang et al., 1991). It is generally accepted that in felsic liquids these effects are related to reactions that form hydroxyl groups (OH) from dissolved H_2O molecules (H_2O_m) and tetrahedral aluminosilicate units in the melt as follows:

$$H_2O_m + X—O—X \leftrightarrow X—OH + OH—X$$
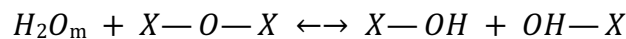
where X can be Si, Al, Na, etc., except H.

In essence, the dominant classical idea that water dissolves in silicate melts and reacts with the melts (highly polymerized) breaking the chains of the tetrahedral bonds (Si, Al)O_4 with oxygen, resulting two OH ends of two shorter chains by depolymerisation (Dingwell, 1998), implies that dissolved water

appears in the network as (Si–OH) groups in chains smaller than those originated in a more anhydrous media. This means that the fragility of volcanic glasses and melts depends on the degree of polymerisation, i.e., the fragility increases as the degree of depolymerisation increases (Giordano et al., 2009). From an environmental point of view, a high degree of depolymerisation of volcanic glass implies more ash reactivity (Ruggieri et al., 2010).

Pioneering studies show that the distribution of OH and water in the glass formed by melt quenching reflects their distribution on melt, except at very high temperatures (Ihinger et al., 1999; Stolper, 1982, 1989). These works quantify the H_2O_t, H_2O_m and OH in silicate glasses (natural and synthetic), cooled at high temperature, using IR spectroscopy and point out the following conclusions of their results:

(1) The H_2O_m appears at contents of $H_2O_t > 0.2\%$ showing a small increase up to 1% of H_2O_t, approximately, and grows more rapidly later, according to a regular variation. Probably, it is linked to the structure and is not a separate phase in inclusions or bubbles as indicates its presence in the studied spectra of rhyolitic ashes.

(2) The OH groups also grow regularly with the H_2O_t content. Unlike H_2O_m, the increase of OH content is very fast up to 2–3 % of H_2O_t, and then it slows down. Around 3 % H_2O_t water is distributed equally in H_2O_m and OH. Once these values have been reached, H_2O_m prevails increasingly over the OH content, although both increase (unevenly) with H_2O_t. That is, for low H_2O_t contents the hydroxyl groups are dominant over the H_2O_m.

(3) The ratio OH/ H_2O_m varies little with the chemical composition of glass from a melt cooled rapidly and varies nothing with pressure. However, this ratio increases moderately with the cooling temperature of glass (Stolper, 1989). As a guide, according to this author, the OH content in glasses with 2 % H_2O_t, cooled at temperatures of 1000–200 ºC, decreases steadily from 1.3 to 0.7 %.

Applying these conclusions to the present study and admitting cooling temperatures similar to those considered in that works (Ihinger et al., 1999; Stolper, 1982), although all H_2O_t is not used in the depolymerisation, most of it must be do because (H_2O_m/OH) <1. Only in the cases of samples 808, UR-1,

UR-6, and UR-7 the trend is reversed. In the other cases, the ratios are in the range of 0.1 to 0.8. This means that conspicuous OH groups are present in these samples, indicating relatively disruption of the silicate network, which in turn affects the chemical stability of the glasses. At lower cooling temperatures, the percentage of OH is smaller but, nevertheless, it is remarkable (as in the case of the ashes from the SVZ). This, together with the intrinsic metastable character of the glass, points out an increase in reactivity when compared with the crystalline phases, facilitating hydrolysis. In general, natural glasses are less stable than crystalline minerals because the glass retains more energy from its parent magma than the latter minerals (Stefánsson et al., 2001), being the dissolution rates significantly faster for Si-rich glasses than for their crystalline counterparts (Wolff-Boenisch et al., 2006). High ash reactivity not only depends on glass content but is particularly remarkable in ancient ashes, where the most labile elements, such as those showing preferential enrichment on tephra surfaces (e.g., SO_4^{2-}, Cl^- and F^-), were probably released during the early burial of the deposit (Ruggieri et al., 2010). As a result, the role of glass in the release of major, minor and trace elements is potentially greater in ancient ashes than in current ones. Following these observations it is possible to define an order of the ash reactivity degree: 809>719~721~733~AS-28>AS-29~AS-33>CHA-G~CHA-2R~CHA-1F~CHA -E>COP>LON>LLA~HUD. However, this classification must be taken with caution because many factors control the reactivity of a given ash in the environment (i.e., grain size particles, geological setting of the ash deposits, etc.).

5.5 Summary and conclusions

This part of research is important because allows achieving two important objectives of the research. Firstly, it has been identified which criteria are useful to distinguish between volcanic and non-volcanic products collected during a field campaign, and, then, the analytical methodology applied for the characterisation of volcanic ashes were exposed. Figure 5.10 summarises the established protocol.
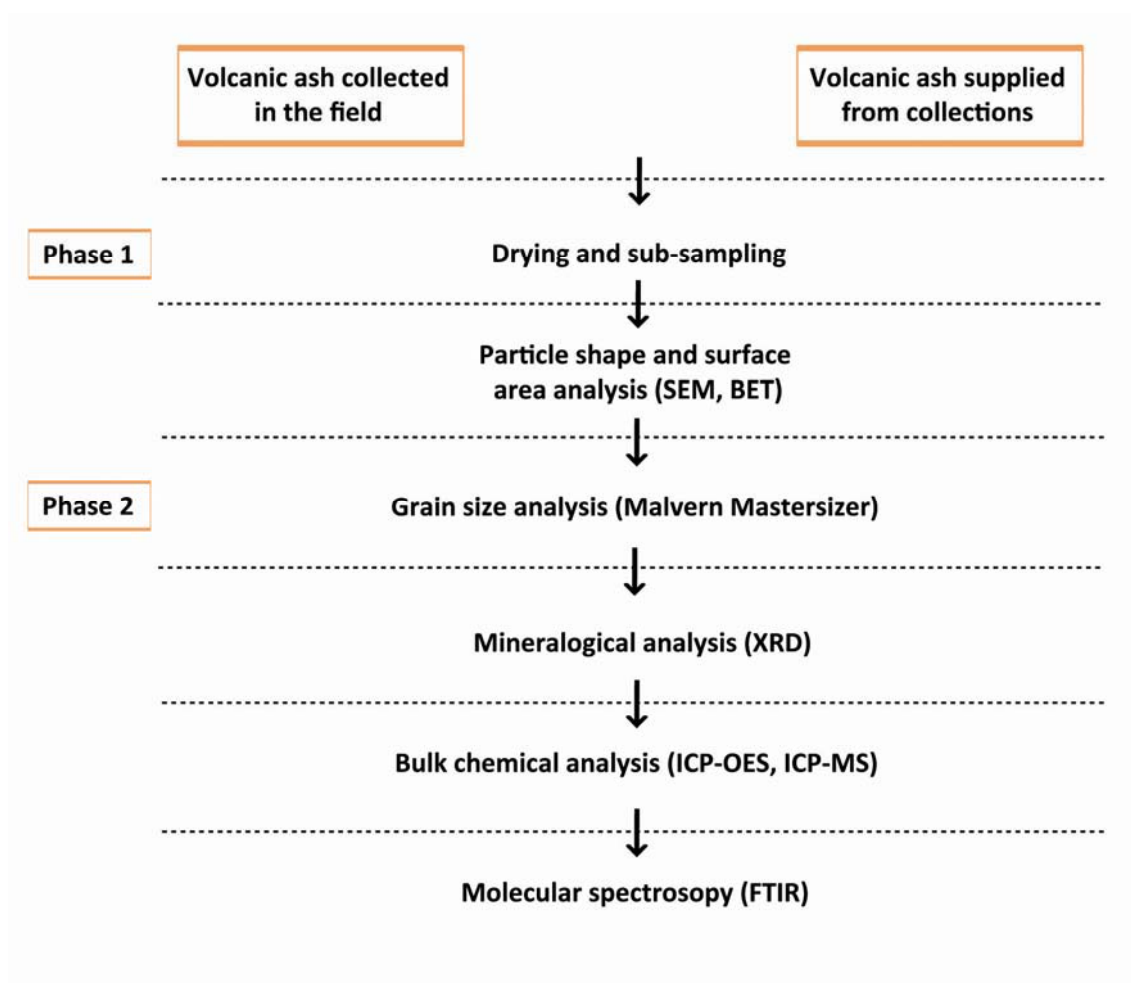
Figure 5.10 Sample analysis protocol carried out in this research.

From a methodological point of view, some considerations could be done based on the obtained results:

(1) Phase 1. The SEM examination allows recognizing the ash by the presence of the typical components as, primarily, glass, and the crystalline mineral phases and to make predictions on the eruptive style and dynamics of the investigated eruptive products, as well magmatic and phreatomagmatic activity. It makes available the identification of no volcanic minerals as clay, biogenic silica, calcite, etc.. In addition, the coupling with EDX spectrometry provides a complementary way correlating volcanic ashes in terms of qualitative composition of components. BET analysis allows determination of SSA values, corroborating the SEM analysis.

(2)   Phase 2. Grain-size analysis also is a crucial step in the assessment of the volcanic ash hazard, giving an idea of the total amount of fine ash produced by a given eruption or presented in a given volcanic ash deposit. Mineralogical characterisation is used to identify the crystalline components in a bulk powdered ash. This is an important step because small amounts of hazardous components (i.e., cristobalite) could be detected. The bulk chemical characterisation allows to classify the volcanic ash (according to the major element content) and to know the trace element concentrations, including the elements potentially toxic. Moreover, the study of molecular spectroscopy by FTIR provides information about the water chemical bonds (and therefore content) present in the ashes. This technique allows making important considerations on the chemical stability of the glass, which in turn has a fundamental importance on the environmental hazard posed by the ash deposition on the Earth surface. Concluding, the combination of these analytical techniques clearly highlights the main environmental concerns related to the studied ashes and it lays the foundation of the basic knowledge required to understand the ash leaching behaviour (issue of the following three chapters of this research).

Chapter 6. Design of a single batch leaching test (SBLT) with deionised water

6.1 State of art and objectives

Leaching tests are often designed to provide information about the constituent release from a specific specimen under conditions approximately close to the actual situation. In the case of volcanic ash, they have been widely used to simulate the release of potentially toxic trace elements (PTTEs) under laboratory conditions in order to assess the environmental impact of ash deposition. Most of the soluble constituents of ash are detected by one stage batch leaching tests (Armienta et al., 2002; Cronin et al., 2003; Cronin and Sharp, 2002; Delmelle et al., 2000; Edmonds et al., 2001; Frogner et al., 2001; Risacher and Alonso, 2001; Ruggieri et al., 2010, 2011; Smith et al., 1982; Smith et al., 1983; Taylor and Stoiber, 1973). Such tests consist of leaching in one step a fixed amount of ash with a fixed amount of leachant. A review of 55 studies reporting ash leachate data for 27 volcanoes concluded that the use of a wide range of methodological variable values (in leachant composition, contact time and liquid to solid or L/S ratio) makes the comparison between the different studies difficult (Witham et al., 2005). That review concludes that there is a great need for harmonization of leaching tests to characterise volcanic ash, recommending a batch leaching test method based on the most widely used values of the methodological variables, rather than on an exhaustive study to find the optimal experimental conditions.

The aim of this part of research is to propose a proved methodology for a single batch leaching test with deionised water in order to obtain information on short term leaching behaviour of volcanic ash identifying, qualitatively and quantitatively, the potentially hazardous elements being rapidly released from both recently erupted and ancient volcanic ashes. Moreover, the results obtained have been proposed to the scientific community in order to improve the need of harmonization previously commented by other authors (Duggen et al., 2010; Witham et al., 2005).
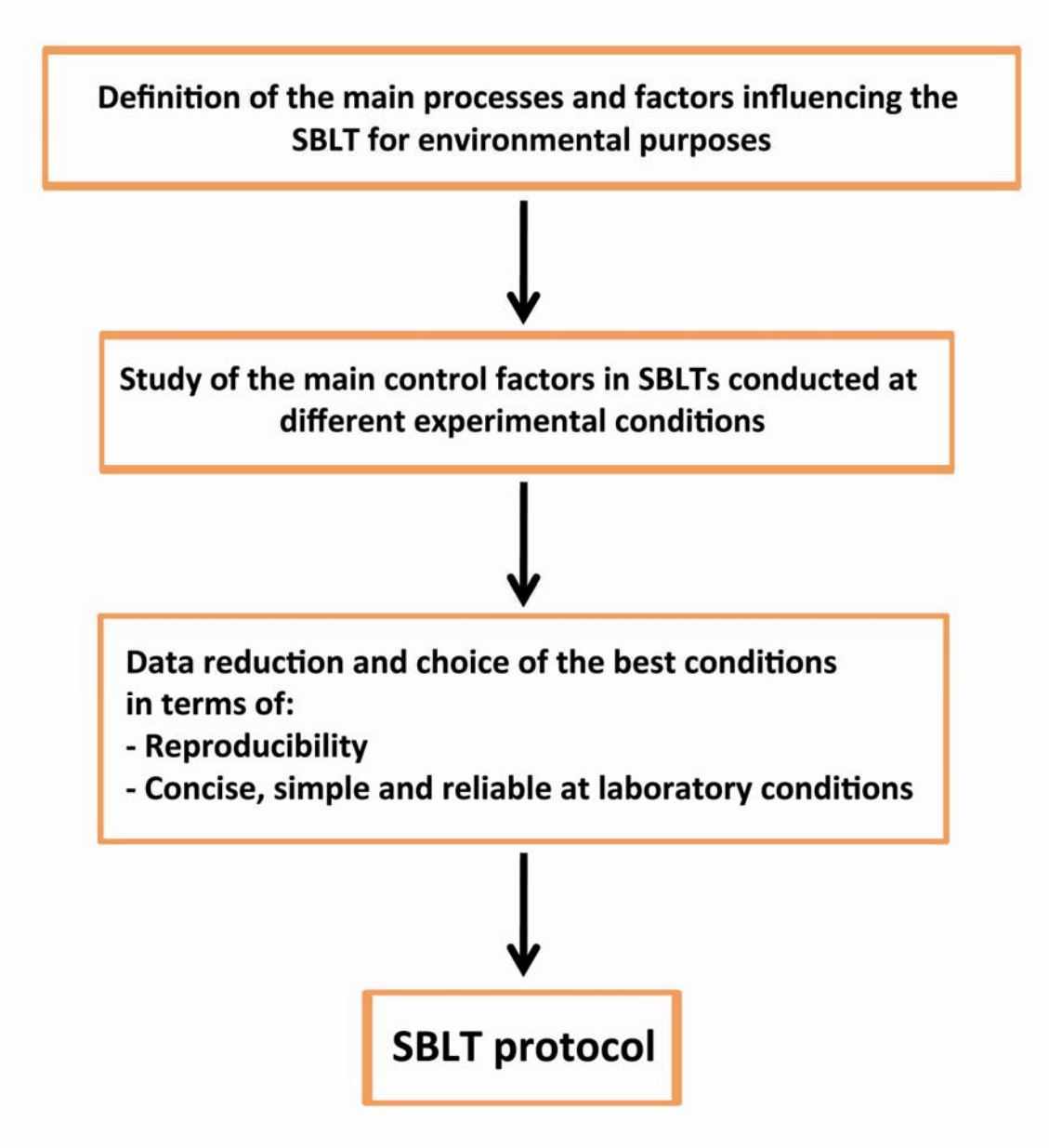
Figure 6.1 Methodological approach for designing a suitable Single Batch Leaching Test (SBLT) with deionised water.

6.2 Methodological approach for designing a suitable SBLT

The schematic methodological approach used for designing a suitable single batch leaching test (SBLT) with deionised water is shown in Figure 6.1. When a leaching test is designed it is very important to define the objective in order to select the appropriate experimental conditions. Consequently, designing more realistic and appropriate leaching tests will help to model more accurately the environmental behaviour of volcanic ash deposits. This requires a good understanding of all processes involved in the ash leaching. When the purpose is to determine the environmental impact, the major chemical processes involved in ash leaching are constituent solubility, metal complexation, sorption/desorption, dissolution/precipitation, and redox reactions (Figure 6.2).
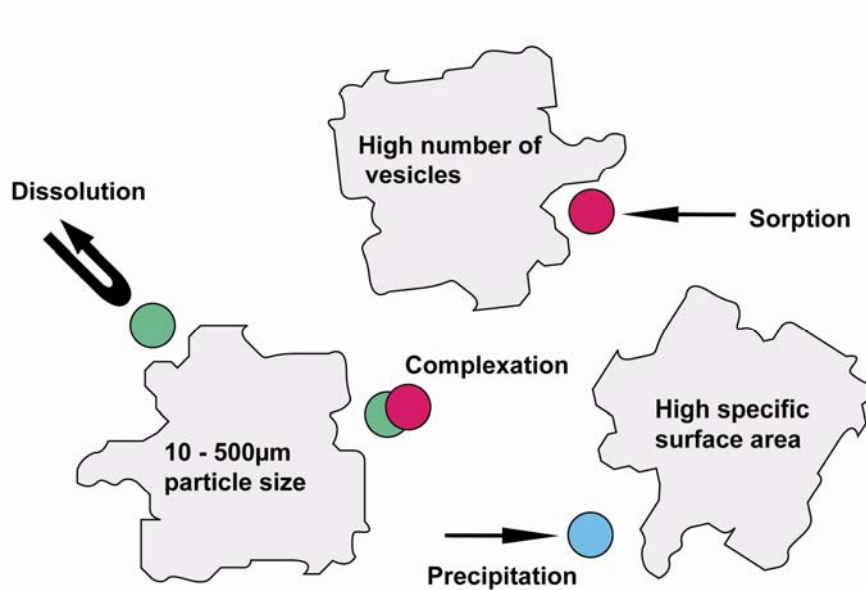
Figure 6.2 Some of the processes that take place in the batch leaching system.

Several factors can influence the rate at which constituents are dissolved from the matrix. The study of the influence of these factors in a batch leaching system is a critical issue for designing a suitable SBLT. They can be divided in

chemical (e.g., mineral composition) and physical factors (e.g., particle size) (Table 6.1). Among these factors, there is a group intrinsically linked to the properties and composition of ash (primary factors), whereas some others depend on leaching conditions that can be varied to design more suitable procedures (control factors). Among the control factors, pH is considered one of the most important because many chemical reactions are pH-dependent. Several leaching tests may be carried out varying pH. For example, very strong acidic conditions are used for the assessment of the maximum environmentally available contents of PTTEs (Papastergios et al., 2010). These SBLT types will be discussed in the following sections. However, if the purpose of the leaching test is a rapid and reproducible screening of soluble constituents simulating ordinary natural conditions, a non-aggressive leachant as deionized water is a good option.

Table 6.1 Physical and chemical factors affecting leachability of elements.

Physical factors	Chemical factors
Porosity of volcanic ash	Chemical composition of volcanic ash
Particle size	Phase composition
Leaching Time	Leachant type
Liquid to Solid (L/S) ratio	pH
Temperature	Redox Potential

Taking into account the previous considerations, it was previously decided to perform the SBLT under some fixed conditions. Namely, the water batch leaching tests were carried out:

(1)   using no ground and no sieved volcanic ash;

(2)   using a non-aggressive leachant as deionised water;

(3)   at room temperature.

6.3 Water batch leaching tests

6.3.1 Experimental design

Two rhyolitic volcanic ash samples have been selected to cover a wide range of ash ages: the pristine Chaiten volcanic ash (CHA-1F) and the ancient volcanic ash layer (719) of the southern Puna, Argentina.

The SBLTs were conducted at different conditions of L/S ratios, varying the amount of ash (0.1 and 1 g), leachant volume (1, 2.5, 10, 25, and 50 ml of deionized water) and contact time (1.5, 4 and 16 h) (Figure 6.3). MilliQ Q Plus deionized water type (18.2 MΩ cm^{-1}) was employed as leachant.
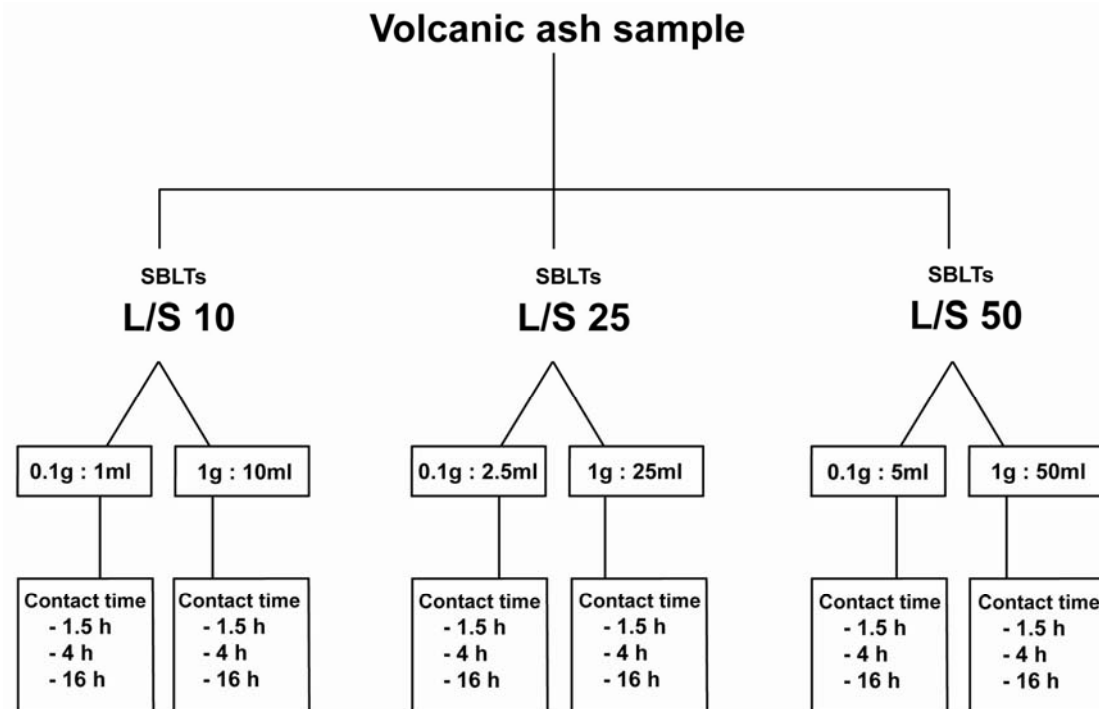
Figure 6.3 Series of SBLTs applied to the ancient and pristine volcanic ashes.

Four replicates were run for each batch leaching test to ensure the reproducibility of the experimental data conditions, resulting 18 tests by ash sample and a total of 72 leachate samples. The mixture of leachant and ash sample was shaken at 20 rpm at room temperature in polypropylene test tubes (14x100 mm) or polyethylene (HDPE) reactors (50 and 100 ml), depending on the leachate volume. Leachate solutions, previous centrifugation (3000 rpm) during 15 minutes, were filtered through Polyvinyledene Diflouride (PVDF) syringe filters with tube tip (Whatmann, 25 mm diameter and 0.45 μm pore size) and made up to 100 ml volume in 1% (v/v) HNO_3.

Concentration of major elements in the leachant solutions were analysed by inductively coupled plasma optical emission spectroscopy (ICP-OES, Optima 3100 X, PerkinElmer), and trace elements by inductively coupled plasma mass spectroscopy (ICP-MS, Elan 6000, PerkinElmer). Given the physico-chemical characteristics of the samples studied, Cl and S concentrations were expressed as Cl^- and SO_4^{2-}, respectively.

Element selection covers the geochemical behaviour range of the main groups of elements implied during leaching and takes into account:

(1)   the less mobile elements during the leaching processes (e.g., Si, Al, Mn, Fe, and Ca) (Chang, 1999; Gayer et al., 1958; Wollast and Chou, 1992);

(2)   highly soluble components (i.e., SO_4^{2-}, and Cl^-) with preferential enrichment on tephra surfaces (Delmelle et al., 2000; Delmelle et al., 2007);

(3)   trace elements dominantly combined with halogens and sulphate forming salts (e.g., Na, Mg, Ba, and Sr) and acid droplets on particle surfaces in pristine ashes or associated with the volcanic glass dissolution during weathering for ancient ashes (e.g., As, Ni, V, Mo, and Sb) (Hinkley, 1994; Hinkley, 1991; Hinkley et al., 1999; Symonds et al., 1992; Symonds et al., 1994; Symonds et al., 1987, Francisca and Perez, 2009; Nicolli et al., 2011; Nicolli et al., 2001).

Leaching concentrations have been expressed as mg kg^{-1} (major elements) or μg kg^{-1} (trace elements) of dry ash to compare directly the different experimental conditions tested (mean and relative standard deviation values are reported in the Appendix 4). The underlying assumption in this type of leaching tests is that the equilibrium condition is achieved at the end of the experiment. Thus, the constituent released in the leachate become constant. Data set was

statistically treated with the STATA 10.0 software. Hence, low dispersion of values involves a high reproducibility of the leaching tests. Box plots of selected elements are shown in Figures 6.4-6.8. Box represents the 25th and 75th percentiles and the solid line within the box is the median of the four replicates used for each experiment.

6.3.2 Factors controlling leachability

6.3.2.1 Amount of volcanic ash and L/S ratio

The first factor considered concerns the released amount of an element using different quantity of ash during the leaching tests. In general, higher concentrations were reported by the lowest amount of sample (0.1 g). Although it seems contradictory, a low amount of sample allows extracting more actively the species present in volcanic ash. This amount is a good option because it detects better the analytes under study. However, the box plots in Figures 6.4 – 6.8 clearly show that ash amounts of 0.1 g have a lower reproducibility of the leaching tests against 1 g of ash for all the leachant volumes tested. This aspect is clearly detectable for highly soluble compounds (as SO_4 and Cl) and the alkali elements (as Na, Ba, Sr, and K) and trace elements (as As, Ni, V, Mo, and Sb) dominantly combined with halogens and sulphate on tephra surfaces, whose concentrations are only theoretically limited by their available amount in the ash. Similar results were also observed for Si, the most abundant major element in rhyolitic volcanic ash, and other major elements as Al, Ca and Fe (Figure 6.4), mainly at high contact time (16 h). Leachability of the latter elements is not only limited by solubility, being also controlled by other chemical processes as dissolution of glass and crystalline phases and precipitation of secondary minerals. This aspect is evident in leaching tests performed with 0.1 g of sample where the released element concentrations decrease when the leachant volume increases, probably indicating the occurrence of precipitation processes (Figure 6.4). It is not dilution because all results are referred to the original sample as mg kg^{-1} or µg kg^{-1} for major and trace elements, respectively.
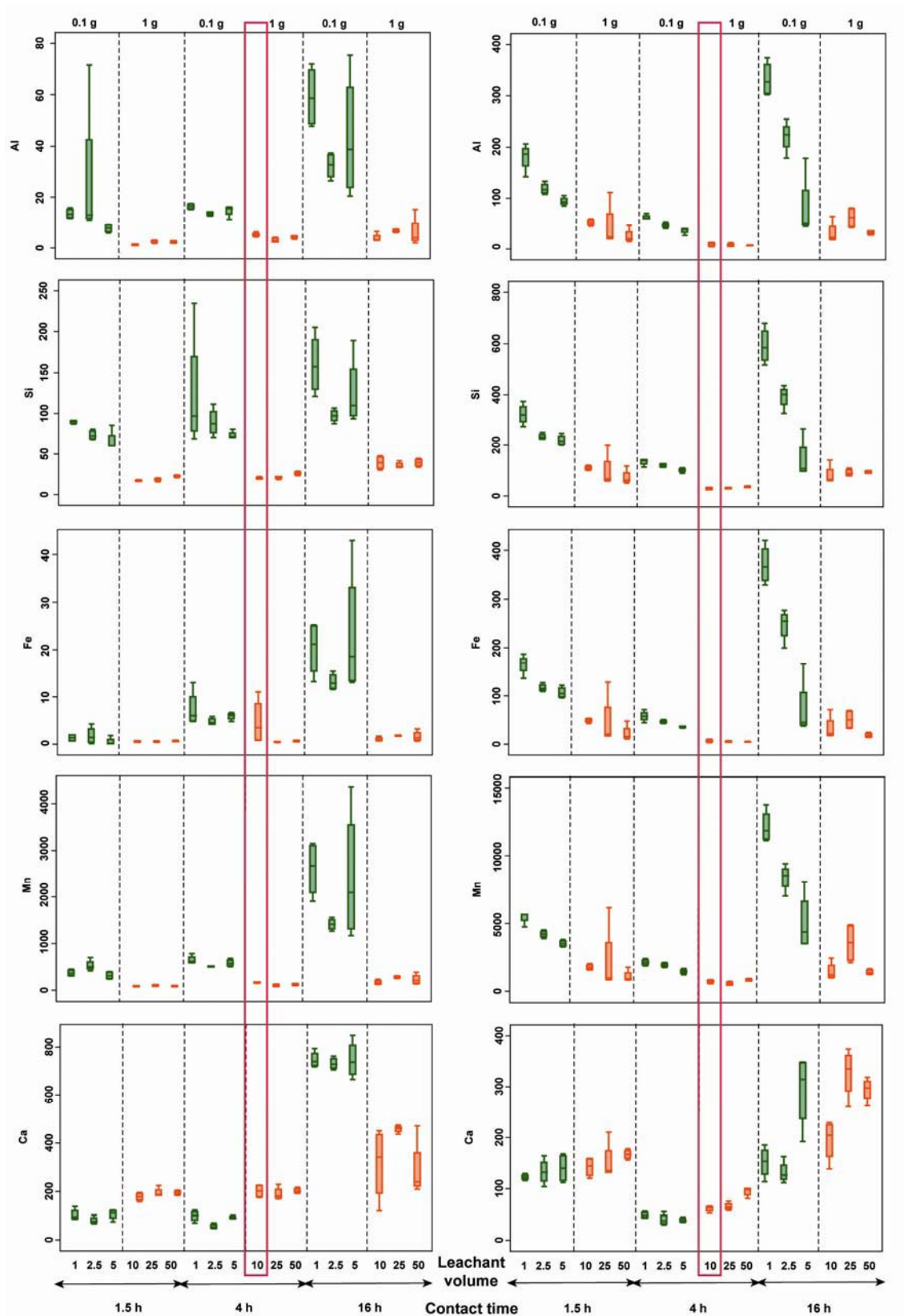
Figure 6.4 Box plots of the less mobile elements (Si, Al, Fe, Mn and Ca) for each one of the leaching tests carried out (n = 4 experiments). The left side the ancient ash (719) and the right side represent the pristine ash (CHA-1F).

These results indicate that a low amount of sample is not always representative of the ash under study, because it is more difficult to reach the chemical equilibrium in these experimental conditions.

In general, the leachant volume has a low influence on the element release when 1 g of sample is employed in the leaching tests. Lower reproducibility was obtained at high L/S ratio (mainly at high contact time). Furthermore, it is an interesting variable designing a leaching test due to analytical reasons. The choice of a high L/S ratio means a larger dilution, which could lead to the inconvenience of concentrations close or lower to the detection limits.
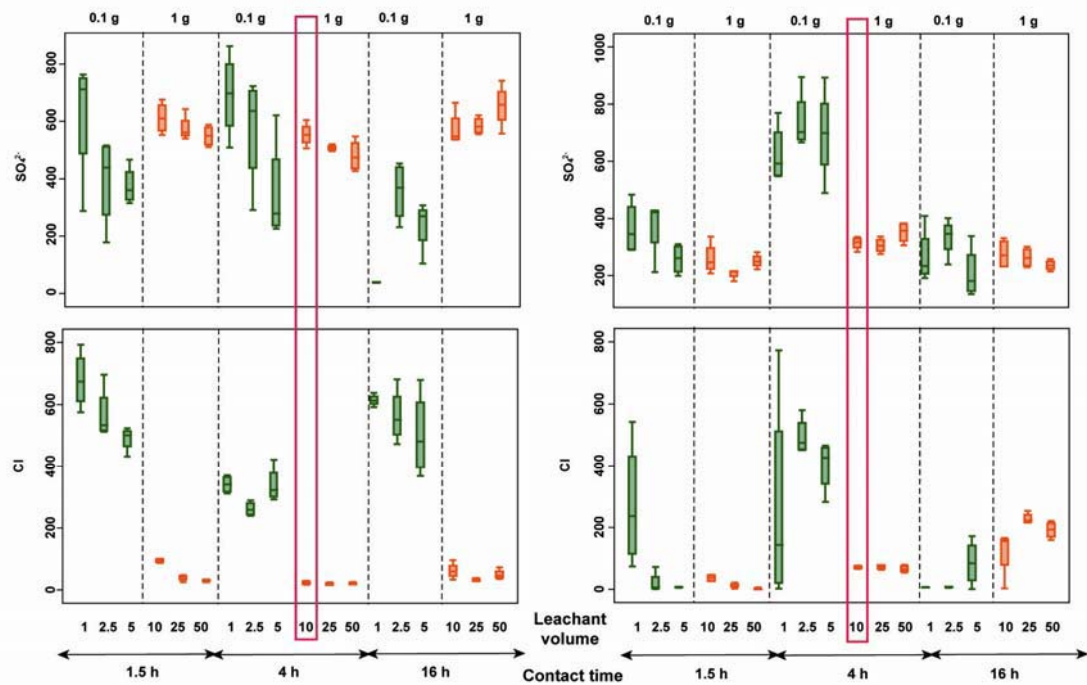
Figure 6.5. Box plots of SO_4^{2-} and Cl for each one of the leaching tests carried out (n = 4 experiments). The left side the ancient ash (719) and the right side represent the pristine ash (CHA-1F).

6.3.2.2 Contact time

Contact time is an important factor because it is directly associated with the heterogeneous chemical reactions occurring when the volcanic ash interacts with water. Median values of released concentrations reported in Figures 6.4 – 6.8 show that contact time affects the released fraction of many elements, especially when the low contact times (1.5 and 4 h) are compared with 16 h. However, highly soluble elements become mobile immediately after contact with water and reach the same leached fraction independently of this factor.

This is the case of compounds as SO_4^{2-} and Cl^- and the elements usually associated with them (i.e., elements forming halide and sulphate compounds as Mg) in the leaching tests performed with 1 g of sample (Figure 6.6). Leachability of other elements may be controlled by many other processes, some of them dependent of the contact time. Illustrative cases are Ca, Sr, Cu, and As where higher releases were reached at 16 h (Figures 6.4, 6.6-6.8). This feature may be due to several reactions occurring in solution. Dissolution of alkaline compounds occurring on the ash surfaces and acid-base or complexation reactions are usually fast, in the order of fractions of second to a few seconds (Oelkers et al., 2009; Toscano et al., 2008). Instead, surface sorption, precipitation, dissolution, and redox reactions involving solid phases are slow, in the order of hours to years (Stumm and Furrer, 1987). Finally, diagenetic changes and weathering are slower (Gislason and Oelkers, 2003; Oelkers and Gislason, 2001; Wolff-Boenisch et al., 2006; Wolff-Boenisch et al., 2004).

This aspect is complex in the ash leaching system because the solid phase is multicomponent, containing many discrete phases of different solubilities (mainly glass but also some crystalline minerals). The worst reproducibility was obtained at low (1.5 h) and high (16 h) contact times. Especially for the pristine ash CHA-1F leaching, the tests conducted at 1.5 h evidenced very inconsistent patterns probably due to the lack of enough time to reach the equilibrium. The dispersion of values at 16 h can be associated with the beginning of weathering processes. Therefore, leaching tests performed at 4 h produced the best results in terms of reproducibility.
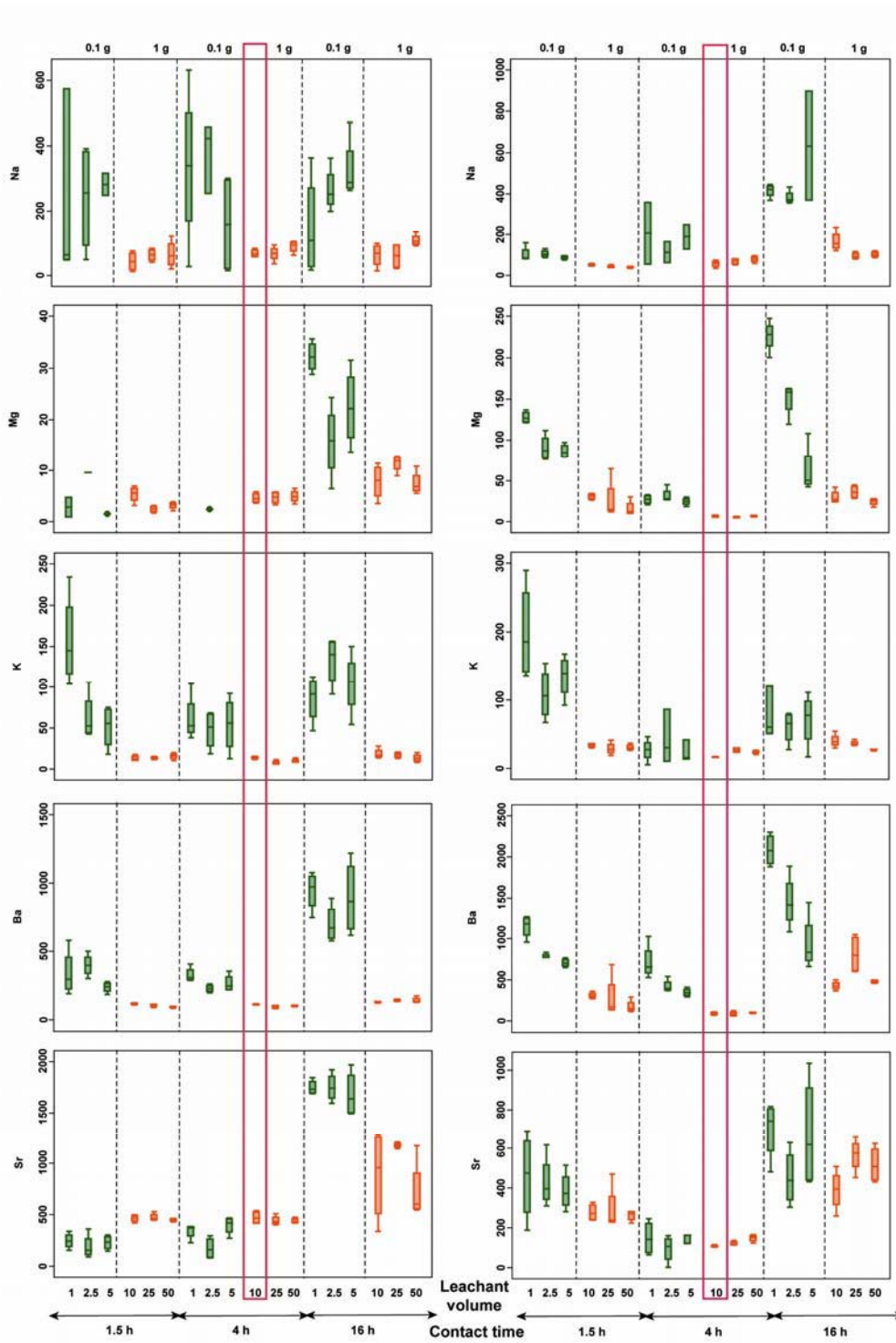
Figure 6.6 Box plots of Na, Mg, K, Ba, and Sr for each one of the leaching tests carried out (n = 4 experiments). The left side the ancient ash (719) and the right side represent the pristine ash (CHA-1F).
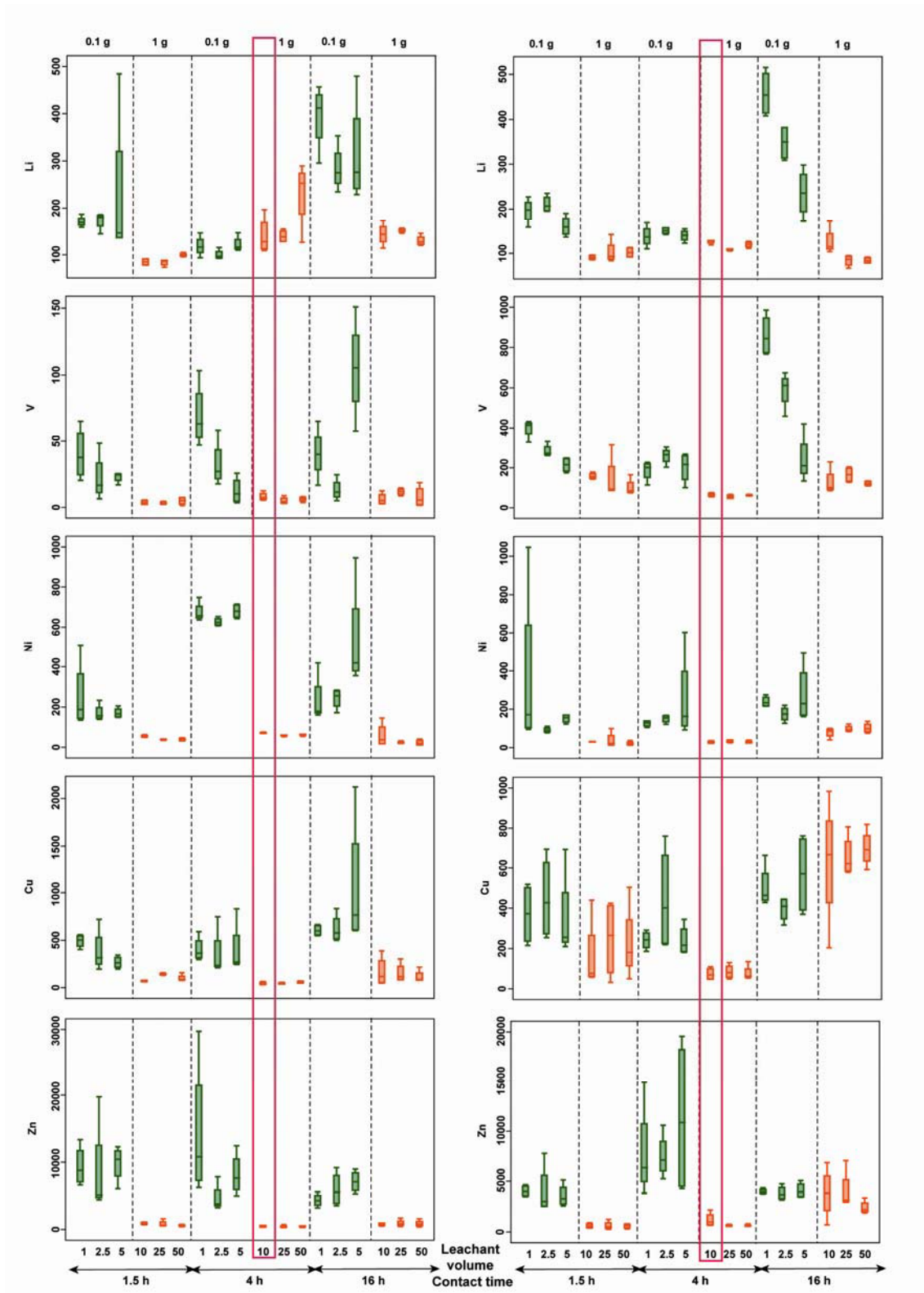
Figure 6.7 Box plots of Li, V, Ni, Cu, and Zn for each one of the leaching tests carried out (n = 4 experiments). The left side the ancient ash (719) and the right side represent the pristine ash (CHA-1F).
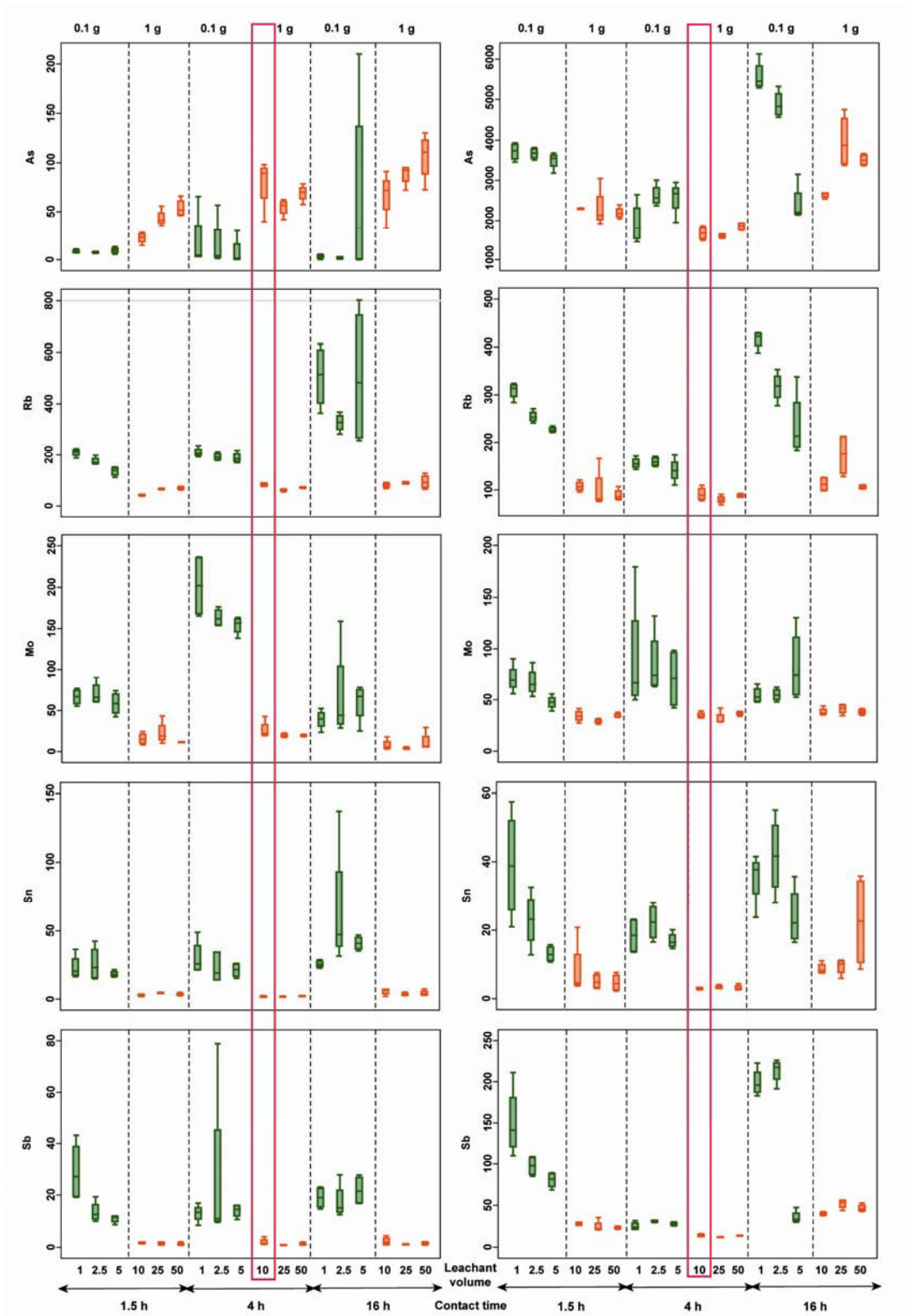
Figure 6.8 Box plots of As, Rb, Mo, Sn, and Sb for each one of the leaching tests carried out (n = 4 experiments). The left side the ancient ash (719) and the right side represent the pristine ash (CHA-1F).

.

6.4 Summary and conclusions

The potential geochemical impact of volcanic ash on the environment is frequently assessed using laboratory leaching tests. Most of the soluble constituents of volcanic ash have been detected by one stage batch leaching tests, but the existence of a multitude of leaching procedures may lead to confusion when a direct numerical comparison is carried out between the different studies. The batch leaching principles of volcanic ashes have been examined, being the robustness of leaching tests assessed in terms of reproducibility using 0.1 and 1 g of ash, 1, 2.5, 5, 10, 25 and 50 ml of deionised water, and a contact time of 1.5, 4 and 16 h.

A single standard leaching test on volcanic ash should have the following characteristics:

(1)   feasibility to determine the PTTEs that can be leached and their concentrations (i.e., if a hazard is posed);

(2)   suitable for general application to ashes of different composition, provenience and geological age; and

(3)   a simple design easily applicable and standardizable (reproducible, inexpensive and fast in laboratory conditions).

Batch leaching tests are based on the assumption that chemical equilibrium is reached during the test. Thus, the choice of the L/S ratio and contact time is important because:

(1)   they must be high enough to prevent saturation of the solution, but chemical equilibrium or semi-equilibrium must be reached;

(2)   they must ensure sufficient amount of leachate (in volume) to perform the chemical analysis; and

(3)   they must guarantee that most of the analytes are present in detectable concentrations.

Results from this study led to the development and application of a batch leaching test which can be used to evaluate the PTTEs release in the context of volcanic ashes. The physico-chemical background information (SEM, GSA, PTTE identification and quantification) should be known prior the application of

a SBLT. In this way, considering the experimental results obtained in this study, the proposed procedure is as follows:

(1)   Unground and unsieved volcanic ash must be used in batch leaching tests to know the leachable loadings in the closest conditions to those occurring in the environment.

(2)   Use deionized water as leachant because although pH is a major control factor affecting the release of many constituents from ash, deionised water is an excellent leachant if the purpose of the leaching test is the accurate, reproducible and rapid screening of soluble constituents. It is worldwide available and allows comparing the results among different laboratories.

(3)   Use a L/S ratio of 10, which must be reached by the mixture of 1 g of volcanic ash and 10 ml of deionised water. A split of 1 g is representative of the ash. This mixture produces a leachate with PTTE concentrations generally higher than the respective limits of detection whereas the reproducibility is high.

(4)   Determine the leachate pH immediately after the contact between the ash and water and at the end of the experiment.

(5)   Shake the mixture for 4 h in polypropylene or polyethylene reactors. This contact time is enough to reach reproducible values, as indicate by the obtained results. Agitation ensures a homogeneous mixture, promotes the contact between the ash and the leachant, and increases the leaching rate.

(6)   Filter mixture using 0.45 μm surfactant-free cellulose acetate membrane filters. Centrifuging samples prior to filtration will prevent clogging of the membranes facilitating ash sample recovery.

(7)   Leaching test results must be expressed either as leachate concentration (mg l^{-1}) or as release of constituent (mg kg^{-1} of dry material). The basis selected for expressing results depends on the type of data which is desired to be compared. Results expressed as leachate concentrations allow a comparison of constituents/compounds solubility in the specific leaching conditions (e.g., contact time, L/S ratio, etc.). The mass leached data allow determining the fraction available for leaching and it makes the comparison between samples easier.

Chapter 7. Single Batch Leaching Tests (SBLTs)

7.1 Objectives and brief description of the SBLTs methodology

The aim of this part of research is to apply the methodology proposed (in the latter chapter) for a single batch leaching test (SBLT) with deionised water and to introduce the results obtained throughout the SBLT with nitric acidic solution. The developed protocols for the different chemical analysis and experimental methodologies are reported in Appendix 1 and 5. However, a brief description of the SBLT experimental methodology is reported below. Thereafter, the structure of this chapter is as follows:

(1)   In the first part are reported the geochemical data of SBLT with deionised water;

(2)   In the second part are described the results obtained by the acidic SBLTs;

(3)   Finally, the summary and conclusions section gives the main remarks of the results (including the environmental concern).

In the present study, two batch leaching tests were performed using deionised water and nitric acid as leachants. The former leachant is less aggressive and its slightly acid pH allows a rapid screening of the potentially hazardous elements that can be leached from the ashes. Nitric acid extraction is useful for the assessment of the maximum load of PTTEs environmentally available (Papastergios et al., 2009, 2010; Sastre et al., 2002). This method has been modified from the method proposed by USEPA for sediments, sludges, and soils (USEPA, 1998). Among the acids proposed in the USEPA method concentrated HNO_3 has been selected because it produces extreme pH conditions and maintains, at the same time, the compatibility of the leachate with the input solution for chemical analysis by ICP-OES and ICP-MS (direct determination after dilution). This type of leaching test allows us to understand the elements involved during glass and mineral dissolution. In addition, the acid

leaching is a very useful tool because it reproduces environmental circumstances in which very acidic conditions occur. For example, very acidic waters in the Andean SVZ region can find in the Copahue Volcano area (Varekamp et al., 2009). The pH of water of Caviahue Lake ranges between 2.1 and 2.7; pH of Agrio River is lower than 3 before this lake. The most hyperacid conditions are observed in the Copahue hot springs where there are values of pH as low as 0.2.

Following the recommendation reported in the last chapter unground and unsieved ashes were employed, except for the Llaima sample. It was composed by coarse ash and lapilli and sieving (< 2 mm fraction) was necessary to homogenize the leaching tests. For water leaching tests, 1 g of ash was mixed with 10 ml Milli Q Plus deionized water type (18.2 Ω cm^{-1}) in 14x100 mm polypropylene test tubes. After 4 h of stirring at 20 rpm at room temperature, the water leachates, previous centrifugation, were filtered through Polyvinyledene Diflouride (PVDF) syringe filters with tube tip (Whatmann, 25 mm diameter and 0.45 µm pore size). The water leachate pH and the specific conductivity (SC) was monitored in duplicate batches immediately after ash–water mixing (pH_0 and SC_0) and at the end of the experiment (pH_f and SC_f), without filtering by means of specific electrodes (Crison Multimeter MM40). Fluoride concentration was determined using an ion selective electrode (ISE) for fluoride (Orion, Thermo Scientific). Finally, the volume was made up to 100 ml in 1% (v/v) HNO_3.

Following this methodological approach, new batch leaching tests were performed using 1 ml of analytical grade HNO_3 (65 %) and 0.1 g of sample. The mixture was shaken for 12 h. In these batch leaching tests, deionised water was added to the resulting leached solution to facilitate centrifugation and then filtering. The final solution had a volume of 100 ml with 1% (v/v) HNO_3. The developed protocols for the different chemical analysis and experimental methodologies are reported in Appendix 1 and 5.

7.2 Data presentation

Geochemical data of leaching tests are presented as mg kg^{-1} (major elements) and µg kg^{-1} (trace elements) (water ash leachates in Tables 7.1-7.2 and nitric ash leachates in Tables 7.7-7.8). A comparison of ancient *vs.* recent water leaching results by statistical treatment of the data set using the R software package (R, Development Core Team 2010) is also reported (Figures 7.1-7.4 and Table 7.4). For both leaching tests the relative mass leached factors (RML) were calculated (the results are displayed in Appendix 6). The RML is defined as the fraction, expressed as %, of leached element (element/solid by weight) obtained from the batch leaching tests (i.e., water batch test and nitric acid batch tests) over the total element concentration (element/solid by weight) (Georgakopoulos et al., 2002b; Papastergios et al., 2009).

Once determined the RMLs for each element and for each leaching method, the elements were grouped according to their mobility expressed by their RML. High mobility was assumed for elements showing RML >5%, moderate mobility for elements with RML between 0.5 and 5%, and low mobility for those elements having RML <0.5%. The low mobility group shows a low potential hazard for the environment (Georgakopoulos et al., 2002a).

The RML values were used to predict the amount of the elements easily transferable to the environment through the water pathway from each one of the ashes investigated (the results are displayed in Appendix 6). Moreover, an estimation of the amount of major and trace elements environmentally available from each eruption (i.e., entire ash deposits) under study is also inferred (Tables 7.5-7.6 and Figures 7.7-7.9).

7.3 SBLTs with deionised water

The ash–water interaction in SBLTs was incipient but significant. The results should be taken as a model of a typical field scenario in which ash-water interaction produces the release of the most soluble constituents. The dissolution of volcanic glass in natural conditions occurs at rates several orders of magnitude lower than in ash-leachate dissolution according to several

experimental works (Gislason and Oelkers, 2003; Jones and Gislason, 2008; Witham et al., 2005; Wolff-Boenisch et al., 2004). These works found that the dissolution of glasses and other compounds occurring in volcanic ashes is remarkable even within the 4 h considered here (Witham et al., 2005). These results could be interpreted as typical of a very early stage of weathering.

7.3.1 pH and specific conductivity

The pH data of leachates suggests that immediately after adding deionised water (with a pH slightly acid) to the ash and before beginning the agitation process for 4 h, the pH was alkaline for ancient ashes, except samples from Uruguay (Table 7.1). Instead, the pH_0 of recent ashes was acid, except for Chaiten samples CHA-G (Table 7.2). After 4 h of shaking, the leachates increase the pH. Exceptions are samples 808 and 809 suggesting that the slow geochemical processes (e.g., hydrolysis) which decrease pH have started. Reactions of minerals with water and their thermodynamic fundamentals highlighted as pH changes are very common when mineral phases are contacted with water (Holdren and Speyer, 1985). This increase is due to both a fast and large dissolution of alkaline compounds and a release into solution of hydroxyl ions from the oxo-groups (MxO) present on the particle ash surface. In the case of silica, the main constituent of glass, H^+ and $(OH)^-$ diffuse in the three spatial dimensions, even through the solid surface, charging it. In these active interfaces, the $(OH)^-$ are linked to Si and the H^+ to O, promoting the dissociation of water (the water dissociation constant, K_w, changes by several orders of magnitude in these conditions). This explains because the suspended solids in natural waters are often negatively charged at pH close to neutrality (6-8) (Oelkers et al., 2009). These negative charges surrounding the solid tend to attract H^+ by raising the pH of the closest solution until the equilibrium is obtained. For more details on the temporal pH behaviour and the chemical reactions involved during the ash leaching other kind of leaching tests would be carried out. These are dynamic leaching tests and they will be developed in the following chapters.

Table 7.1 Geochemical data of major elements (mg kg^{-1}) and trace elements (µg kg^{-1}) in water ash leachates of ashes from Puna and neighbouring area and Uruguay. The pH and the specific conductivity (SC) was monitored in duplicate batches at the beginning (pH$_0$ and SC$_0$), immediately after ash–water mixing, and at the end of the experiment (pH$_f$ and SC$_f$), without filtering. SCs are in µS cm^{-1}.

	719	721	733	808	809	AS-28	AS-29	AS-33	UR-1	UR-6	UR-7
pH$_0$	8.93	8.64	9.57	9.18	10.03	7.86	8.55	9.09	6.78	6.73	7.64
pH$_f$	8.93	8.93	9.67	8.97	10.02	8.85	9.80	9.84	7.76	7.40	7.76
SC$_0$	35.9	53.6	75.9	147	250	70.1	33.8	59.6	10.7	9.23	13.6
SC$_f$	141	131	120	860	432	146	135	214	31.3	19.9	33.6
Ca	228	147	30.5	55.1	29.8	104	20.9	24.7	13.8	11.0	9.8
Mg	4.21	6.48	1.47	4.35	1.10	4.09	19.9	13.4	2.08	1.72	2.35
Na	35.1	58.7	168	1293	796	146	209	415	37.2	22.0	57.6
K	16.9	25.1	50.0	49.8	19.7	16.8	18.9	21.0	13.6	18.1	15.7
Si	22.5	39.6	46.0	78.1	64.9	36.3	248	263	13.2	34.5	83.4
Cl	21.8	29.8	80.2	1376	459	242	16.5	81.5	22.8	19.6	20.0
SO$_4^{2-}$	429	355	60.1	853	266	58.9	13.8	46.1	30.9	9.45	23.4

Specific conductivity (SC) increases after 4 h of ash-water interaction (Tables 7.1 and 7.2). SC is a good approximation to the concentration of total dissolved solids (TDS) and the ionic constituents in solution. In the ancient ashes the final SC$_f$ values were twice or much higher than the initial SC$_0$ (Table 7.1). Lower increments were observed in the recent ash leachates than in the ancient ash leachates (Table 7.2). HUD sample behaviour was the most similar to the ancient ashes, whilst LON sample presented similar SC$_0$ and SC$_f$. These features suggest a low amount of readily soluble materials in the recent ashes than in the ancient ashes, as well as in the rhyolitic ashes than in the basaltic ones.

Table 7.1 continuation. LoD, Limit of Detection.

	719	721	733	808	809	AS-28	AS-29	AS-33	UR-1	UR-6	UR-7
Li	78.2	187	62.3	180	1956	259	83.8	119	30.8	32.1	46.0
Be	<LoD	<LoD	<LoD	<LoD	<LoD	<LoD	<LoD	<LoD	<LoD	<LoD	<LoD
F⁻	5065	5385	1334	3123	48343	2968	2129	2339	2042	3587	6392
B	1913	3209	<LoD	5719	335	3882	<LoD	<LoD	<LoD	<LoD	<LoD
Al	6068	3670	2114	12807	4051	4479	58074	30831	1870	3242	9235
P	241	218	518	365	1282	477	553	6356	343	297	515
Sc	27.3	43.5	48.8	72.7	63.9	44.8	206	214	17.8	33.1	63.3
Ti	98.6	90.1	81.8	185	85.7	106	889	2136	54.6	160	338
V	4.90	12.1	60.3	65.0	347	36.5	8.37	116	39.8	40.0	89.7
Cr	14.2	10.8	10.02	5.99	7.29	10.6	11.5	31.8	7.03	7.74	8.80
Fe	<LoD	<LoD	<LoD	142	<LoD	<LoD	32297	52100	<LoD	118	3542
Mn	74.1	50.8	36.4	57.6	66.6	76.5	957	634	104	26.7	70.2
Co	<LoD	<LoD	<LoD	<LoD	<LoD	20.8	8.66	10.7	<LoD	<LoD	<LoD
Ni	19.2	17.8	45.7	16.6	31.3	20.6	38.3	61.7	26.8	21.3	20.0
Cu	41.4	26.4	39.9	25.4	73.5	63.0	50.1	85.1	29.7	20.2	24.1
Zn	<LoD	<LoD	11.50	<LoD	<LoD	51.5	606	933	<LoD	<LoD	<LoD
Ga	2.35	<LoD	<LoD	<LoD	<LoD	<LoD	17.4	21.9	<LoD	<LoD	<LoD
Ge	<LoD	<LoD	<LoD	<LoD	<LoD	<LoD	<LoD	<LoD	<LoD	<LoD	<LoD
As	15.8	23.4	35.3	74.3	195	79.7	6.54	45.9	8.52	6.21	15.2
Se	<LoD	<LoD	<LoD	<LoD	<LoD	<LoD	<LoD	<LoD	<LoD	<LoD	<LoD
Br	228	272	282	363	1918	395	331	337	233	255	296
Rb	51.3	44.7	39.7	47.4	17.4	23.8	22.3	92.4	7.9	20.1	18.7
Sr	738	818	136	440	132	268	74.3	139	80.4	62.0	69.8
Y	1.37	<LoD	2.46	3.19	21.8	1.90	3.66	20.3	3.37	3.15	7.23
Zr	46.1	47.0	14.4	26.9	8.88	100	68.7	53.3	11.4	13.9	24.9
Nb	3.62	2.42	2.65	5.32	5.29	3.04	22.1	50.2	61.3	62.5	50.0
Mo	2.45	3.77	3.73	7.15	59.0	6.18	1.44	2.63	3.56	1.15	3.23
Ag	<LoD	<LoD	<LoD	<LoD	<LoD	<LoD	<LoD	<LoD	<LoD	<LoD	<LoD
Cd	<LoD	<LoD	<LoD	<LoD	<LoD	<LoD	<LoD	<LoD	<LoD	<LoD	<LoD
Sb	<LoD	<LoD	1.97	<LoD	1.50	1.43	2.21	2.82	<LoD	<LoD	1.37
Cs	1.96	1.45	1.77	1.55	1.60	1.43	1.35	7.50	<LoD	<LoD	1.56
Ba	93.7	61.1	43.6	37.4	46.9	48.0	59.6	170	55.8	50.2	72.5
La	<LoD	<LoD	<LoD	<LoD	16.5	<LoD	15.4	47.4	4.75	6.11	13.8
Ce	21.9	20.9	7.86	11.6	9.98	21.0	18.0	84.4	7.53	10.5	18.6
Pr	<LoD	<LoD	1.08	<LoD	3.99	<0.01	2.02	7.99	1.09	1.34	2.93
Nd	<LoD	<LoD	<LoD	<LoD	13.5	<LoD	<LoD	17.43	<LoD	<LoD	8.90
Sm	<LoD	<LoD	<LoD	<LoD	3.69	<LoD	<LoD	3.80	<LoD	<LoD	1.96
Eu	<LoD	<LoD	<LoD	<LoD	<LoD	<LoD	<LoD	<LoD	<LoD	<LoD	<LoD
Gd	<LoD	<LoD	<LoD	<LoD	3.69	<LoD	1.06	4.48	<LoD	<LoD	2.15
Tb	<LoD	<LoD	<LoD	<LoD	<LoD	<LoD	<LoD	<LoD	<LoD	<LoD	<LoD
Dy	<LoD	<LoD	<LoD	<LoD	3.89	<LoD	<LoD	3.60	<LoD	<LoD	1.66
Ho	<LoD	<LoD	<LoD	<LoD	<LoD	<LoD	<LoD	<LoD	<LoD	<LoD	<LoD
Er	<LoD	<LoD	<LoD	<LoD	2.30	<LoD	<LoD	2.34	<LoD	<LoD	<LoD
Tm	<LoD	<LoD	<LoD	<LoD	<LoD	<LoD	<LoD	<LoD	<LoD	<LoD	<LoD
Yb	<LoD	<LoD	<LoD	<LoD	1.50	<LoD	<LoD	2.43	<LoD	<LoD	<LoD
Lu	<LoD	<LoD	<LoD	<LoD	<LoD	<LoD	<LoD	<LoD	<LoD	<LoD	<LoD
Hf	<LoD	<LoD	<LoD	<LoD	<LoD	<LoD	<LoD	<LoD	<LoD	<LoD	<LoD
Ta	<LoD	<LoD	<LoD	<LoD	<LoD	<LoD	<LoD	<LoD	<LoD	<LoD	<LoD
Tl	<LoD	<LoD	<LoD	<LoD	<LoD	<LoD	<LoD	<LoD	<LoD	<LoD	<LoD
Pb	56.3	59.7	29.3	81.2	21.7	85.3	161	238	18.3	18.8	18.5
Bi	<LoD	<LoD	<LoD	<LoD	<LoD	<LoD	<LoD	<LoD	<LoD	<LoD	<LoD
Th	<LoD	<LoD	<LoD	<LoD	<LoD	1.24	26	76.9	<LoD	2.10	<LoD
U	<LoD	<LoD	<LoD	<LoD	<LoD	1.90	28	46.9	<LoD	<LoD	<LoD

Table 7.2 Geochemical data of major elements (mg kg^{-1}) and trace elements (μg kg^{-1}) in water ash leachates of ashes from SVZ. The pH and the specific conductivity (SC) was monitored in duplicate batches at the beginning (pH$_0$ and SC$_0$), immediately after ash–water mixing, and at the end of the experiment (pH$_f$ and SC$_f$), without filtering. SCs are in μS cm^{-1}.

	CHA-1F	CHA-2R	CHA-G	CHA-E	COP	LON	LLA	HUD
pH$_0$	6.54	6.98	8.30	5.47	4.75	5.39	5.72	5.76
pH$_f$	8.64	8.60	9.07	7.85	4.98	5.84	6.29	6.64
SC$_0$	52.2	48.6	109	24.7	606	10.5	15.6	47.5
SC$_f$	96.6	94.1	154	86.1	861	11.2	79.5	245
Ca	79.9	130	138	105	351	15.9	70.6	149
Mg	6.57	5.49	7.14	4.84	595	2.58	16.4	18.8
Na	64.2	28.8	88.0	29.5	277	8.9	52.7	214
K	14.2	18.2	21.4	14.0	20.4	10.0	11.2	23.3
Si	18.4	20.4	28.1	24.0	3.74	5.73	5.00	3.64
Cl	148	16.8	126	35.1	561	14.1	71.8	337
SO$_4{}^{2-}$	153	226	198	107	3142	10.6	94.4	295

Table 7.2 continuation. LoD, Limit of Detection.

	CHA-1F	CHA-2R	CHA-G	CHA-E	COP	LON	LLA	HUD
Li	95.5	88.4	185	75.8	192	9.93	69.4	26.3
Be	<LoD	<LoD	<LoD	<LoD	<LoD	<LoD	<LoD	<LoD
F$^-$	6803	7011	10301	2731	20717	1021	29722	204399
B	<LoD	<LoD	<LoD	<LoD	<LoD	<LoD	<LoD	<LoD
Al	4954	4821	5251	6487	20305	1420	2229	8006
P	373	404	427	1251	139	192	216	316
Sc	21.1	22.3	27.6	24.6	10.7	12.2	11.5	10.4
Ti	93.9	99.2	104	93.3	160	114	92.9	77.3
V	10.2	35.0	59.8	17.3	2.11	1.91	17.9	15.9
Cr	7.24	8.58	7.81	6.72	6.42	5.44	6.03	5.51
Fe	<LoD	1150	48.0	2.67	<LoD	<LoD	<LoD	<LoD
Mn	473	209	145	110	12415	277	345	1725
Co	<LoD	<LoD	29.9	<LoD	567	5.44	11.69	<LoD
Ni	49.0	28.2	65.7	31.8	726	27.8	34.2	24.0
Cu	39.5	37.2	41.9	47.5	126	30.8	104	345
Zn	168	295	509	49.4	779	450	237	3476
Ga	4.19	3.49	4.86	2.67	<LoD	<LoD	<LoD	<LoD
Ge	<LoD	<LoD	<LoD	<LoD	<LoD	<LoD	<LoD	<LoD
As	352	726	3009	130	6.51	2.96	19.61	9.16
Se	<LoD	<LoD	<LoD	<LoD	<LoD	<LoD	<LoD	<LoD
Br	198	165	252	195	769	136	155	239
Rb	26.7	41.6	48.9	24.6	85.2	7.74	7.45	22.8
Sr	146	182	296	409	1471	73.6	251	543
Y	<LoD	1.90	1.14	1.88	8.62	<LoD	<LoD	<LoD
Zr	14.1	14.3	58.3	37.8	11.2	17.6	30.8	15.3
Nb	46.9	47.4	39.8	40.3	44.9	28.8	32.2	47.3
Mo	16.1	31.9	44.6	9.00	<LoD	1.15	4.90	2.95
Ag	<LoD	<LoD	<LoD	<LoD	<LoD	<LoD	<LoD	<LoD
Cd	31.5	<LoD	271	10.3	72.7	35.3	69.5	12.4
Sb	4.48	8.38	9.33	2.37	<LoD	<LoD	1.04	1.97
Cs	2.10	2.20	3.33	1.58	1.15	<LoD	<LoD	<LoD
Ba	85.2	107	90.3	201	33.0	44.9	33.6	85.3
La	<LoD	<LoD	<LoD	<LoD	28.5	<LoD	<LoD	<LoD
Ce	4.19	5.29	4.09	6.13	89.7	<LoD	<LoD	<LoD
Pr	<LoD	<LoD	<LoD	<LoD	12.9	<LoD	<LoD	<LoD
Nd	<LoD	<LoD	<LoD	<LoD	43.7	<LoD	<LoD	<LoD
Sm	<LoD	<LoD	<LoD	<LoD	6.03	<LoD	<LoD	<LoD
Eu	<LoD	<LoD	<LoD	<LoD	<LoD	<LoD	<LoD	<LoD
Gd	<LoD	<LoD	<LoD	<LoD	6.51	<LoD	<LoD	<LoD
Tb	<LoD	<LoD	<LoD	<LoD	<LoD	<LoD	<LoD	<LoD
Dy	<LoD	<LoD	<LoD	<LoD	3.16	<LoD	<LoD	<LoD
Ho	<LoD	<LoD	<LoD	<LoD	<LoD	<LoD	<LoD	<LoD
Er	<LoD	<LoD	<LoD	<LoD	<LoD	<LoD	<LoD	<LoD
Tm	<LoD	<LoD	<LoD	<LoD	<LoD	<LoD	<LoD	<LoD
Yb	<LoD	<LoD	<LoD	<LoD	<LoD	<LoD	<LoD	<LoD
Lu	<LoD	<LoD	<LoD	<LoD	<LoD	<LoD	<LoD	<LoD
Hf	<LoD	<LoD	<LoD	<LoD	<LoD	<LoD	<LoD	<LoD
Ta	<LoD	<LoD	<LoD	<LoD	<LoD	<LoD	<LoD	<LoD
Tl	<LoD	<LoD	<LoD	<LoD	<LoD	<LoD	<LoD	<LoD
Pb	348	155	2015	257	102	392	1071	24.1
Bi	<LoD	<LoD	<LoD	<LoD	<LoD	<LoD	<LoD	<LoD
Th	<LoD	<LoD	<LoD	<LoD	<LoD	<LoD	<LoD	<LoD
U	<LoD	<LoD	<LoD	<LoD	<LoD	<LoD	<LoD	<LoD

7.3.2 Comparison of ancient *vs.* recent ash water leachates

The leaching behaviour of a recently erupted volcanic ash (pristine) is different from an ancient ash. The surfaces of pristine ash particles were argued to host soluble salts formed through gas-particle interaction in the plume of volcanic eruptions (Delmelle et al., 2007; Duggen et al., 2007; Frogner et al., 2001; Jones and Gislason, 2008). An ancient volcanic ash has long been deposited on land and is continuously subject to hydrological and soil processes, which effectively remove any soluble salts attached to the surface of ash particles. Ancient ash particles may be remobilised by wind and become a component of the aeolian mineral dust load but, in general, the readily soluble salts adsorbed onto pristine ash are washed away during exposure to water (e.g., meteoric water) (Duggen et al., 2010). Therefore, ancient ash should not exhibit the same behaviour as pristine ash when exposed to water.

Water ash leachate data set was statistical analysed with the R software package (R, Development Core Team, 2010). Box plots of the element distributions were used in order to compare the element release of ancient *vs.* recent ashes (Figurer 7.1). Box represents the 25th and 75th percentiles and the horizontal solid line within the box is the median of the element range concentrations in the different ashes. Median values show that some elements (i.e., Ca, Mg, Cl, SO_4^{2-}, F^-, Mn, Ni, Cu, As, Sr, Mo, Ba, and Pb) presented higher values in the recent ash leachates, whereas some others (i.e., Na, Si, Al, P, Ti, V, Fe, Zr, and U) showed higher concentrations in the ancient ash leachates. The latter elements have usually a wider range of concentrations in ancient that in recent ashes. It is interesting to note that the elements enriched in recent ash leachates were usually implicated in the chemical reactions occurred in volcanic plumes. The elements with preferential enrichment on ash compared to its bulk composition are sulphur, chlorine, and fluorine (Delmelle et al., 2000; Delmelle et al., 2007). Generally, up to 10-20% of HCl and 30-40% of SO_4 can be scavenged by ash in the eruptive column (Delmelle et al., 2000; Jones and Gislason, 2008; Oskarsson, 1980). Cations as calcium (Ca^{2+}), sodium (Na^+) and magnesium (Mg^{2+}) also occur at high concentrations during the first exposure to water (Wilson et al., 2010; Witham et al., 2005). Independently of the magma silica content, sulphates and chlorides are the major compounds observed in
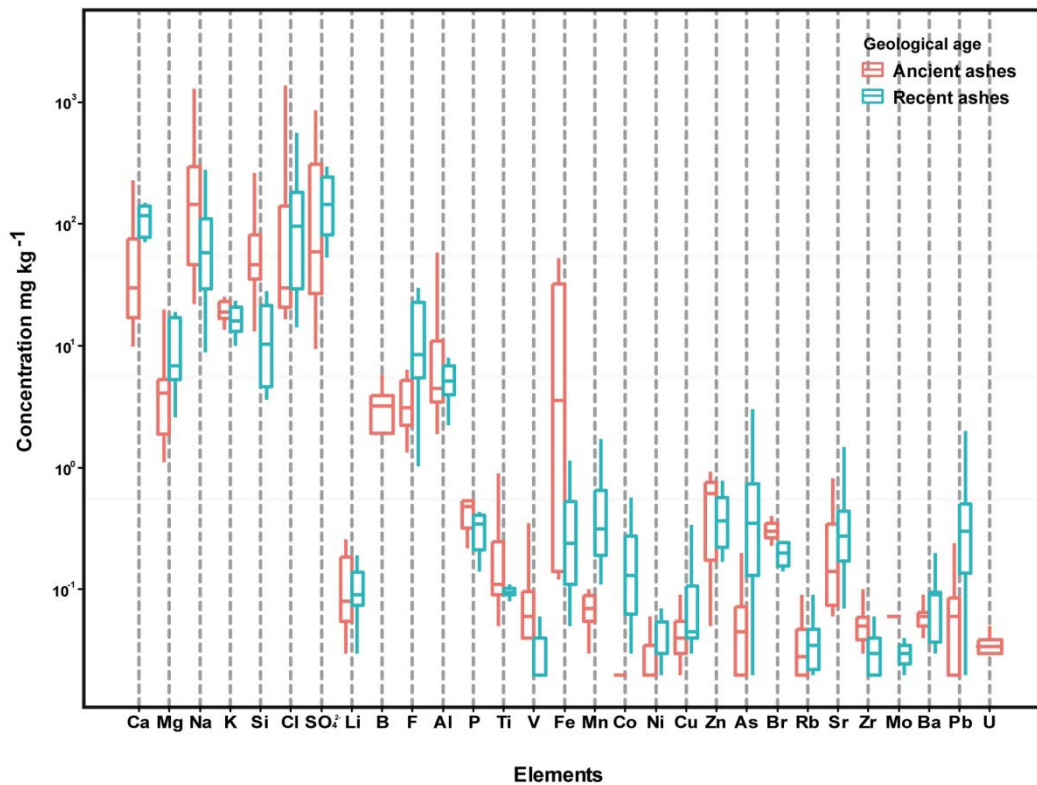
Figure 7.1 Box plots of the water ash leaching data from ancient vs. recent ashes.

Chaiten, Hudson and Copahue ash water leaching tests, with particular emphasis for the latter sample. Negligible values of these compounds reported for Lonquimay ash water leachate confirm its no pristine character, while the low content of sulphate compounds onto particle surfaces could explain this feature in Llaima water leachate (Table 7.2). The F^- release from the Hudson ash is far greater than for any other sample. Early ash analysis revealed high levels of fluoride after the 1991 eruption (Inbar et al., 1995; Rubin et al., 1994). Comparing to the other samples, F^- concentration in Hudson ash leachate (204399 µg kg^{-1}) is over 20 times more than in the Chaiten ash and nearly 200 times more than in the Lonquimay ash (Table 7.2). Copahue and Llaima water leachates have also a notable fluoride concentration (20717 and 29722 µg kg^{-1}, respectively). The trace elements (e.g., Ni, Cu, As, Sr, Ba, and Pb) enriched in the pristine water leachates correspond to the elements dominantly combined with halogens and sulphate forming salts and/or acid droplets coating the ash-grain surfaces. The latter process involves the partial dissolution of the ash

through reactions with the acidic gases (i.e., mainly SO_2, HCl, HF) and aerosols (i.e., H_2SO_4) of the plume, followed by precipitation at the ash-liquid interface being responsible of the enrichment of elements with low volatility (lithophilic element as Ba and Sr) (Delmelle et al., 2007). This is supported by volcanic gas measurements that indicate lithophilic element enrichment in the gaseous and particulate phases emitted during magma degassing processes and volcanic eruptions (Hinkley, 1994; Hinkley, 1991; Hinkley et al., 1999; Symonds et al., 1992; Symonds et al., 1994; Symonds et al., 1987).

The elements with preferential enrichment (i.e., Na, Si, Al, P, Ti, V, Fe, and Zr) in the ancient ash leachates should come from different origin than ash-acidic gases interaction in the volcanic plume. Some of these are termed as rock forming mineral elements (e.g., Si, Al, Ti, and Fe) which are usually defined as the less mobile elements during the weathering processes. For example, the solubility product, K_s, of Al and Fe hydroxides are extremely low, 10^{-33} and 10^{-39}, respectively (Chang, 1999; Gayer et al., 1958). If the molar ratio Si/Al in rock and water ash leachates are compared, the low solubility assumed usually for these elements should be reconsidered in the studied samples. The molar ratio Si/Al in rock was clearly lower than in the aqueous leachate (Table 7.3), except for samples 808, AS-29, and AS-33, which was only slightly lower, and sample 719, where the terms was reversed and Si/Al was higher in rock than in water. This implies that Al dissolves more readily than Si in these ashes.

Table 7.3 Si/Al molar ratio in rock and in water ash leachates of samples from Puna and neighbouring area, Uruguay and SVZ.

	719	721	733	808	809	AS-28	AS-29	AS-33	UR-1	UR-6	UR-7
Si/Al rock	5.08	4.86	4.90	4.16	4.84	4.64	3.89	4.02	4.76	4.37	4.29
Si/Al water leachate	3.57	10.4	20.9	5.86	15.4	7.79	4.11	4.19	6.76	10.2	8.67

Table 7.3 continuation.

	CHA-1F	CHA-2R	CHA-G	CHA-E	COP	LON	LLA	HUD
Si/Al rock	4.33	4.21	4.16	4.28	2.59	2.76	2.20	2.55
Si/Al water leachate	3.57	4.06	5.14	3.56	0.18	3.88	2.15	0.44

However, the same feature was observed also in the recent ash leachates, being especially noticeable for Copahue, Hudson and Chaiten ash samples. Some relatively high values for Mn, Ti, and geochemically analogous elements were also observed in concentrations with orders of magnitude of hundreds to thousands of µg kg^{-1} (Tables 7.1 and 7.2). The explanation of these behaviours features is related to the presence of stable complexes which may be dissolved in these conditions. Such complexes are clearly dependent on pH (Ruggieri et al., 2010). Moreover, a high iron release was observed in the Chaiten ash leachates, confirming deposition of airborne ash from volcanic eruptions is a way to inject significant amounts of bio-available Fe into both continental and ocean waters (Duggen et al., 2010; Langmann et al., 2010).

7.3.4 Principal component and cluster analyses

Principal Component analysis (PCA) performed on the water ash leachate data allows to split the samples by geological age. The first three principal components explain 46.2% of the total variance (Table 7.4). Figure 7.2 shows the distribution of the samples in the PC1 and PC2 axes.

PC1 axis, essentially, recounts the variability among the ancient ash leachates. Some of the elements enriched in the ancient ash leachates (in descending order: Fe, B, Zn, Ti and Al) are the main constituents of the PC1 (Table 7.4), and their relative content is responsible of the location of the ancient samples along the PC1 axis. For example, AS-29 and AS-33 samples (on the right side of the diagram) presented higher concentrations of Al, Fe and Ti, whilst the samples on the left side of the diagram (719, 721, AS-28, 808 and 809) were largely defined by B concentration. Finally, samples 733, UR-1, UR-6, and UR-7 were not suitable explained only by the PC1 component.

The PC2 was mainly produced by positive weights of Mn, Zn, Mg, SO$_4^{2-}$, F, Ca (more abundant in recent ash leachates) and negative contribution of B, Si, Fe, V, and Ti (more abundant in the ancient ash leachates), corroborating the observations reported in the latter paragraph (Table 7.4 and Figure 7.3).
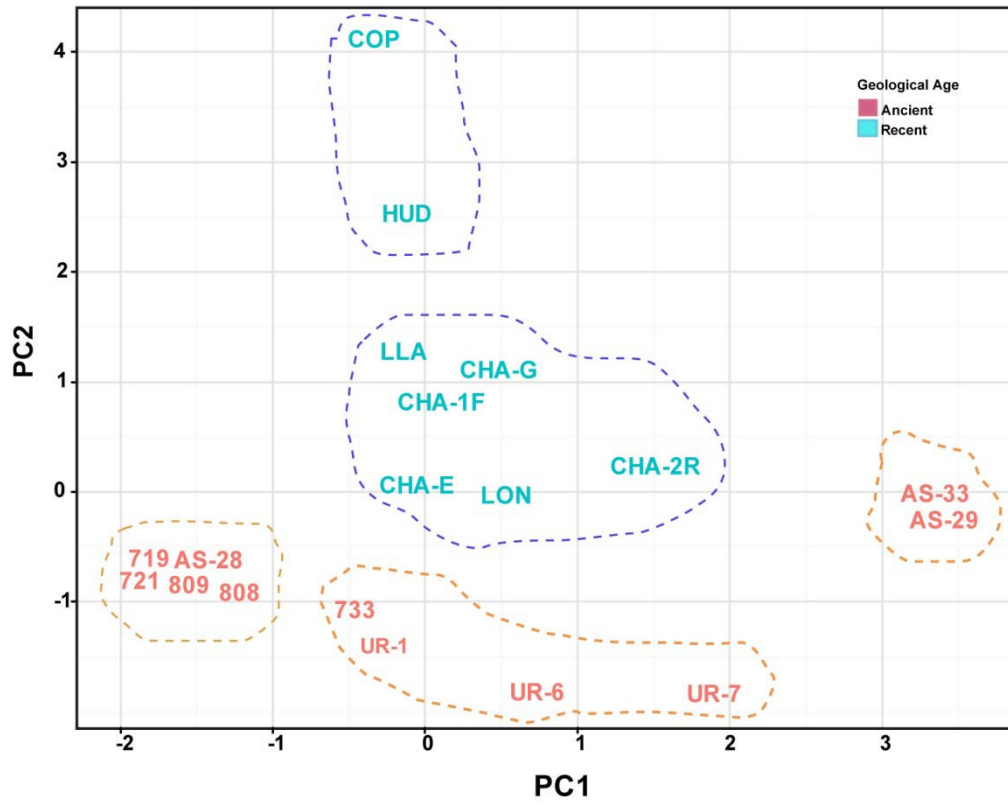
Figure 7.2 Principal component analysis (PCA) of ashes. The projection in the PC1-PC2 axes split the ancient and recent ashes.

Table 7.4 The first three principal components of the PCA analysis.

	PC1	PC2	PC3
Ca	-0.138	0.210	0.099
Mg	0.068	0.355	0.098
Na	-0.010	0.060	0.356
K	-0.019	-0.014	0.077
Si	0.146	-0.228	0.245
Cl	-0.151	0.175	0.267
SO_4^{2-}	-0.220	0.245	0.268
Li	-0.095	0.014	0.280
B	-0.433	-0.234	0.473
F	-0.085	0.224	0.065
Al	0.144	0.074	0.214
P	0.108	-0.066	0.121
Ti	0.197	-0.021	0.144
V	0.024	-0.120	0.132
Fe	0.690	-0.187	0.375
Mn	0.141	0.393	0.023
Co	-0.028	0.193	0.051
Ni	0.034	0.172	0.029
Cu	-0.001	0.155	0.041
Zn	0.270	0.467	-0.027
As	-0.026	0.017	0.154
Br	-0.032	0.008	0.123
Rb	0.010	0.053	0.146
Sr	-0.141	0.160	0.116
Zr	0.018	-0.016	0.104
Mo	-0.014	0.009	0.039
Ba	0.049	-0.010	0.018
Pb	0.081	0.163	-0.025
U	0.074	-0.013	0.081
Variance (%)	16.9	15.6	13.7
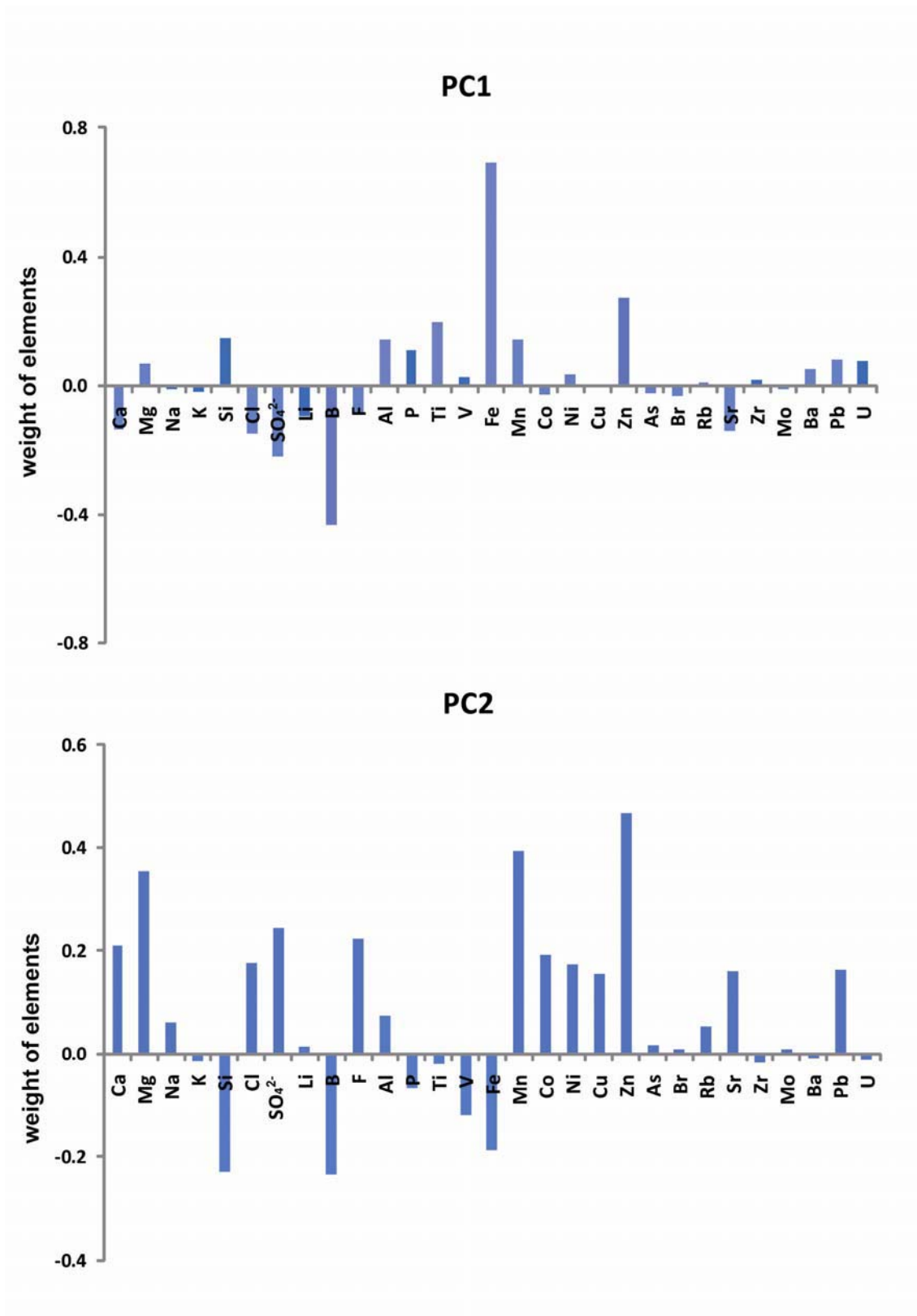
Figure 7.3 Composition of the first two PCA components which could explain the difference among the ancient ash leachates (PC1) and the variability between ancient and recent ash leachates (PC2).

In order to assess the statistical separability of the two types of ash leachates, the Jeffries-Matusita (JM) distance was inferred. JM distance ranges from 0 to 2 and it is calculated assuming a multi-gaussian distribution of the classes (Richards, 1986). A value of JM = 0 implies that the two distributions are completely correlated whilst JM = 2 implies that the distributions are completely uncorrelated. In our case, the JM values proved high separability (JM = 1.99), implying great difference in terms of leachate composition.
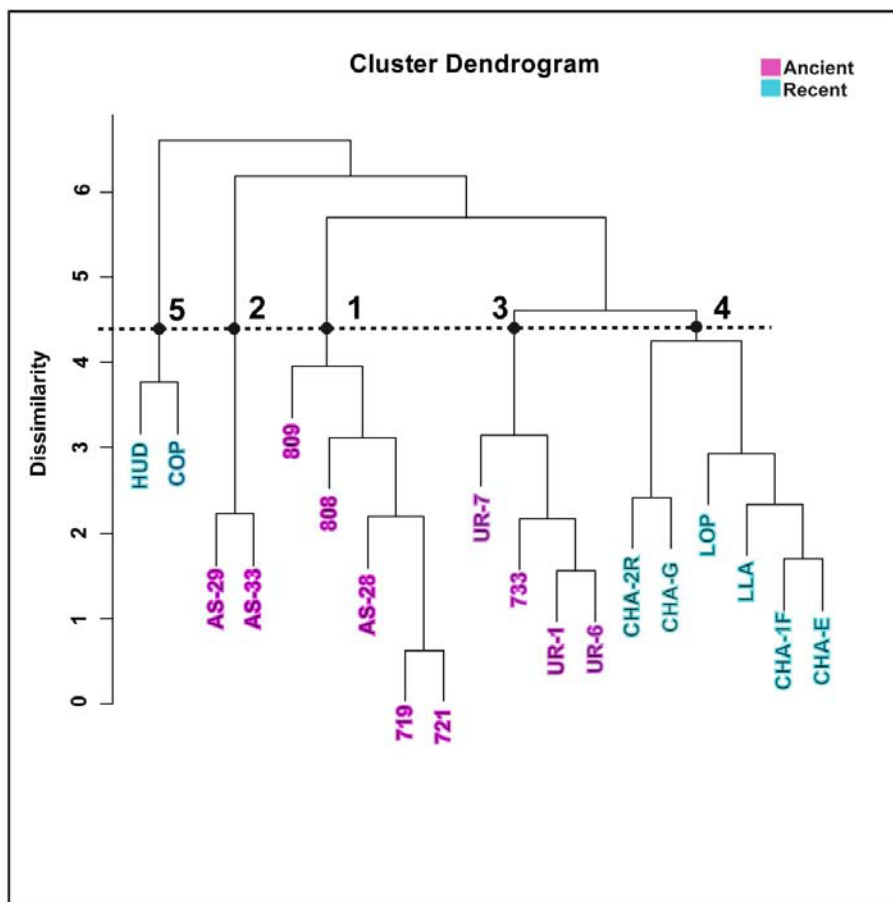
Figure 7.4 Hierarchical clustering obtained with the volcanic ashes investigated.

Hierarchical clustering (i.e., dendogram cluster) was performed on the data set in order to define the association of the ash leachates (Figure 7.4). In the hierarchical clustering the groups are listed along the x-axis whereas the y-axis measures the dissimilarity of the groups obtained cutting the dendrogram at a certain level. In this case the cutting level at 4.5 was chosen as a compromise between complexity of the classification and internal homogeneity of the groups and keeping coherent with the diagram obtained projecting the samples by geological age (Figure 7.2). This selection involves a robust observation of the data set for which the same groups were obtained throughout two different statistical treatments (principal component analysis and cluster dendogram). These groups were as follows:

(1)   Group 1: 719, 721, AS-28, 808 and 809 samples.

(2)   Group 2: AS-29 and AS-33 samples.

(3)   Group 3: 733, UR-1, UR-6, and UR-7 samples.

(4)   Group 4: CHA-1F, CHA-2R, CHA-G, CHA-E, LON, and LLA samples.

(5)   Group 5: COP and HUD samples.

These groups were created based on the similar behaviour of the ash leachates, and it will be discussed in the following sections.

7.3.4 Relative mass leached in ash water leachates

Appendix 6 reports the Relative Mass Leached (RMLs, %) data obtained throughout the water ash leaching tests. Although, Be, Ge, Se, Ag, Cd, Tl, Bi and many of the REE elements were analysed, they could not be included in the RML data because their concentrations were below or very close to the respective detection limits. Moreover, RMLs were not determined for Cl, SO_4^{2-}, B, F, Br, and Hg because these elements were not analysed in bulk ashes. Only in the Uruguay bulk ashes Zr and Nb were not determined. Any element showed RML>5%, indicating that in a deionised water system high element mobilization is low. However, some elements presented moderate mobility (i.e., RML between 0.5 and 5 %) in these leaching conditions. For the ash leachates carried out with the ancient ashes moderate mobility was shown by Ca, Na, Li, P, V, Ni, Cu, Zn, As, Sr, Nb, Mo, and U. This classification is a generalization. In

a more detailed observation of results, some elements appear in more than one class depending of the considered ash. In the case of the recent ashes, moderate mobility were achieved by Ca, Mg, Na, Li, Mn, Co, Ni, Cu, Zn, As, Nb, Mo, Sb, and Pb. Again this is a generalization. For example Mg, Na, Li, Co, and Mn occur with moderate mobility only in COP samples.

7.3.5 Contribution to the regional geochemical balance

The RML values were used to predict the amount of the elements easily transferable to the environment through the water pathway. Knowing the RML (%) and the bulk composition (BC_X mg kg^{-1}) for an element X in a given ash, the content environmentally available of an element X (EA_X mg kg^{-1}) in a given ash was calculated as follows:

$$EA_x = BC_x \times RML_x$$

The EA values obtained from the ashes investigated are displayed in Appendix 6. Major elements (i.e., Ca, Mg, Na, Si, K, and Al) present the higher concentration potentially releasable in the environment for both ancient and recent ashes. Figures 7.5 and 7.6 show the environmental availability of trace elements. The samples were organized according to groups observed by the statistical treatment. Puna and Uruguay ashes could release in the environment the same trace elements, however, in different concentrations. Those mainly involved were P, Ti, Fe, Mn, Zn, and Sr. Some of these are rock forming mineral elements supporting the idea that once deposited, the volcanic ash undergoes irreversible geochemical weathering reactions (e.g., oxidation followed by slow dissolution), causing destabilization of the silicate framework and release of the elements associated with it. More variability was observed in the recently erupted ashes. Chaiten ashes showed high EA values for As, Pb, Fe, and Zn, whilst the other samples (i.e., COP, LON, LLA, and HUD) could release principally P, Ti, Mn, Zn, Ni, and Pb.
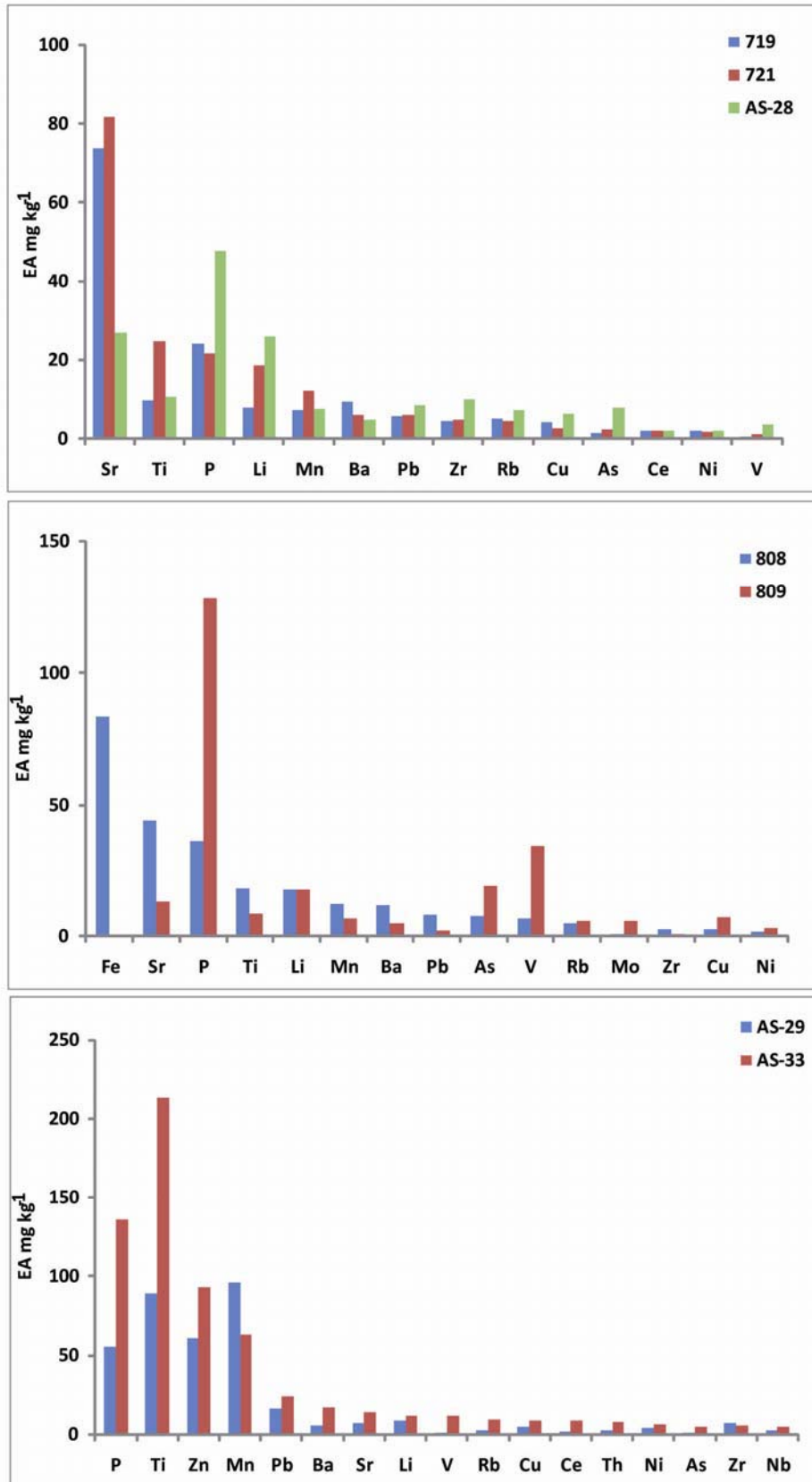
Figure 7.5a Environmental available (EA) content of trace elements in descending order from ash of Puna and neighbouring area.
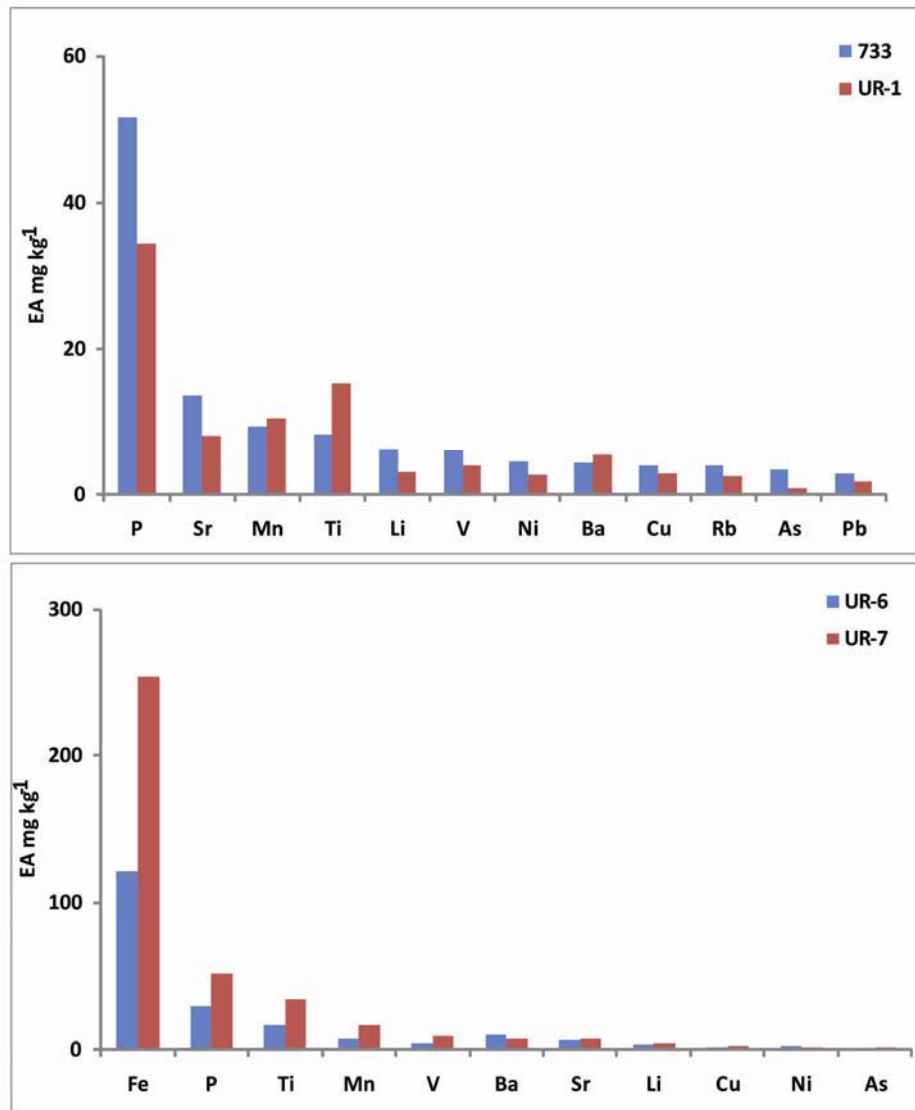
Figure 7.5b Environmental available (EA) content of trace elements in descending order from ash of Uruguay and sample 733.
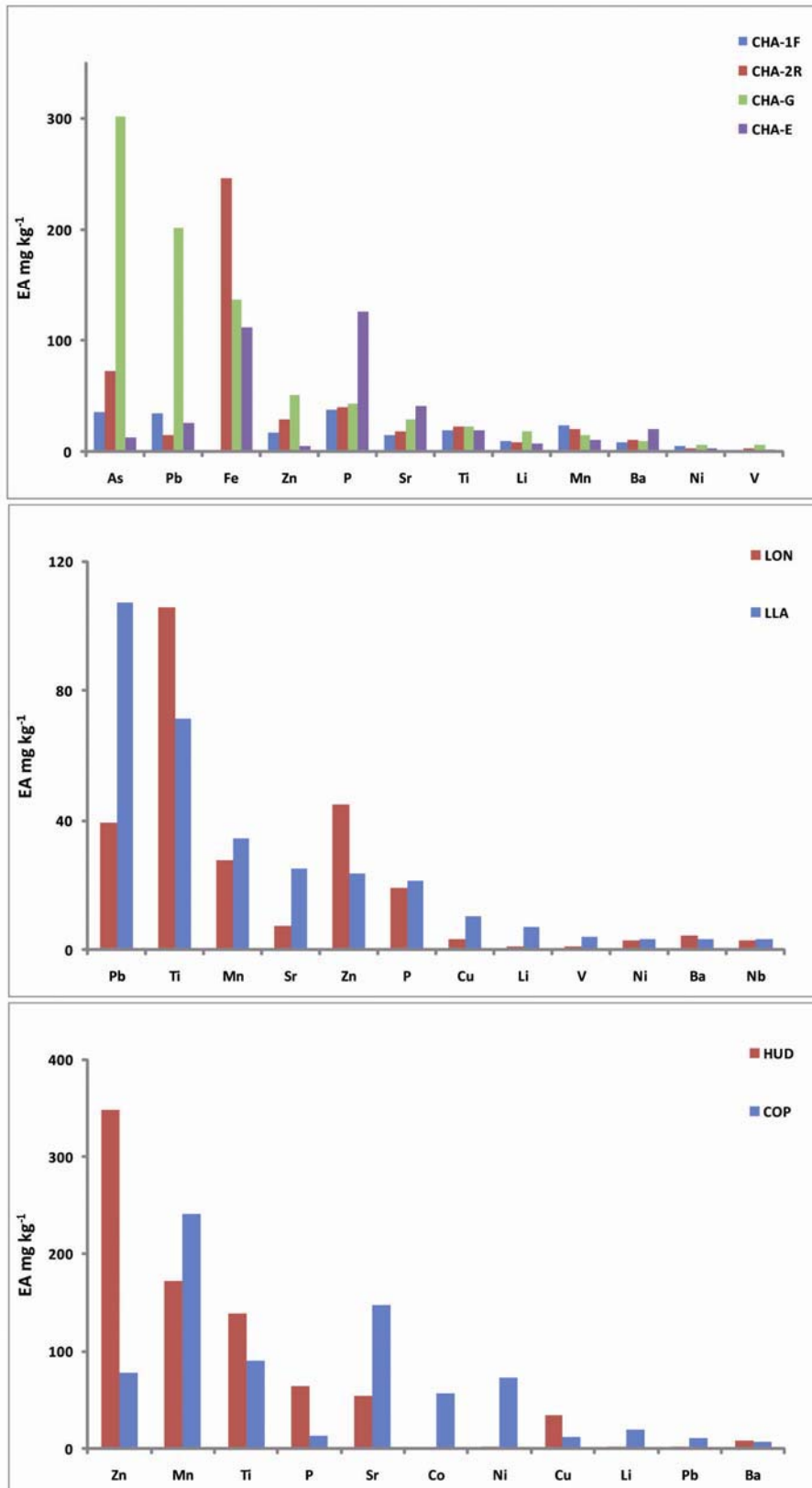
Figure 7.6 Environmental available (EA) content of trace elements in descending order from ash of SVZ.

The estimation of the element amount that each eruption under study could potentially transfer to the environment through the water pathway was inferred. This modelling requires some additional information as the volume of the pyroclastic materials ejected during each eruption and the density of the samples. Tephra volume is usually expressed as dense-rock equivalent volume (V_{DRE}, km^3), i.e., without the void spaces of the ash particles (vesicles). This correction can be inferred comparing the bulk volume of the tephra deposit (V_{bulk}) with the vesicle volume fraction (ω) following the equation (Harris et al., 2007):

$$V_{DRE} = V_{bulk} * (1 - \omega)$$

In the absence of directly measured values for vesicularity, ω has been taken from the literature (Harris et al., 2007). In this study, the value reported for the correction of the andesitc tephra volume erupted from Soufriere Hills during the 1995-1997 eruption (Montserrat) was used (Sparks et al., 1998). The vesicle volume fraction was in the range from 8 to 21 %, being the latter more appropriate for highly vesicular tephra.

In the case of the ashes from Puna and Uruguay, the V_{DRE} of the Plinian eruption of Quizapu, 1932 was used as reference. The Quizapu eruption has been one of the largest explosive eruptions of the 20th century which sent ~9.5 km^3 of ash (V_{DRE}= 4.05 km^3) into the atmosphere. The similarity of the ash layer deposits and the very distal ash deposit (isopach map extended to Uruguay) makes this eruption a good candidate for our model (Hildreth and Drake, 1992).

The V_{DRE} of some of the historical eruptions under study were previously addressed by other authors. This, was the case of Chaiten 2008 eruption (Watt et al., 2009), Hudson 1991 eruption (Kratzmann et al., 2010b), and Lonquimay 1988 eruption (Naranjo et al., 1992). Volume of bulk tephra deposited by Copahue 2000 and Llaima 2008 eruptions was supposed to be 10^{-2} and 10^{-3} km^3, respectively. These assumptions were based on a pioneering study which allows estimate the volume of bulk ejecta knowing the Volcanic Explosivity Index (VEI) (Newhall and Self, 1982). For Copahue and Llaima eruptions a VEI

2 and a VEI 1 was respectively inferred (Naranjo and Polanco, 2004; Venzke et al., 2009). Then, the V_{DRE} was estimated applying the above mentioned equation, in which ω was chosen based on SEM observations. Both ashes were poorly vesicular with equant blocky fragments of glass, therefore, a low value of vesicle volume fraction (ω=8 %) was employed. Density (d, kg m^{-3}) of the ash samples was calculated with the KWare geological software (Wohletz, 2010). Then, the maximum amount of each element that could be easily transferred to the environment through the water pathway was calculated following the equation:

$$X = V_{DRE} * d * EA$$

where X is the maximum element amount (expressed as tonnes), d is the density in kg m^{-3} and EA the amount of element environmentally available of ash in mg kg^{-1}. The values obtained are reported in Tables 7.5 and 7.6. Both ancient and recent ashes could transfer to the environment high amount of major elements, mainly Ca and Na. Some of the elements available from these ash deposits are macro- and micronutrients (e.g., Mn, Fe, and P), evidencing the fertilizing potential of the ashes. Many others are potentially toxic trace elements (PTTEs). Figures 7.7-7.9 show the amount (in per cent, %) of the PTTEs (i.e., As, Cu, Mo, Ni, Pb, Zn, and U) available to move easily in the environment through water in each one of the ash deposits investigated. Substantial variability of the PTTEs implied was observed. Puna ash deposits of samples 719, 721, 808, 809 and AS-28 showed high environmental available content of Pb, As, and Cu. Lead, Cu, and Ni were enriched in 733 and Uruguay ash deposits. High content of available Zn was displayed for AS-29 and AS-33 ash deposits. Chaiten, Llaima, and Lonquimay tephra deposits might release mainly Pb. The Chaiten deposit could considered also a reservoir of As. Finally, Hudson and Copahue might release mainly Ni and Cu in the environment. These observations are coherent with the results of the statistical treatment of the data set and are the basis for the environmental monitoring of these ash deposits.

Some of the latter elements (As, Cu, F, Mo, Ni, Pb, and Zn) are included in the drinking water guidelines (ANMAT, 2007; INN, 2006; WHO, 2008) due to their potential toxicity even at very low concentrations and must be especially monitored in the environmental assessment of these ashfall deposits. This aspect is very important if we take into account the environmental conditions in which the ash deposits occurred. The leachate drainage in small and closed hydrographic basins such in the Puna and surrounding regions can greatly affect the geochemical fluxes of streams and lakes, especially immediately after the scarce rainfalls, because the process is very fast (Ruggieri et al., 2010). On the contrary, the high rainfall on the western flanks of the Andean Cordillera in the SVZ implies a constant leaching (and therefore weathering) of the ash deposits.

Table 7.5 Prediction of the element amount available (expressed as tonnes, t) that might easily move in the environment by water in the studied ash deposits from Puna and neighbouring area and Uruguay. d, ash density; V_{DRE}, dense rock equivalent volume of the corresponding deposit; nd, not determined.

	719	721	733	808	809	AS-28	AS-29	AS-33	UR-1	UR-6	UR-7
d kg m^{-3}	2.32	2.34	2.33	2.39	2.32	2.33	2.39	2.39	2.37	2.37	2.34
V$_{DRE}$ km^3	4.05	4.05	4.05	4.05	4.05	4.05	4.05	4.05	4.05	4.05	4.05
Ca	214497	139639	28694	53354	28055	98586	20211	23975	13234	10562	9269
Mg	3955	6147	1388	4212	1032	3857	19279	13026	1999	1653	2225
Na	32929	55690	158000	1251852	747902	137428	201827	402293	35799	21124	54595
K	15912	23762	47113	48206	18484	15878	18255	20388	13044	17450	14923
Si	53877	37525	43318	75632	60988	34267	240479	254666	44997	33156	79066
Li	73.5	177	58.7	174	1838.4	244	81.1	116	29.6	30.9	43.7
Al	11889	9805	8358	12402	10188	10855	56212	29880	8319	10028	8756
P	226	207	488	354	1205	450	535	6160	330	286	488
Ti	92.6	235	77.1	179	80.6	100	860	2070	146	154	321
V	4.6	11.5	56.8	62.9	326.1	34.4	8.1	112	38.3	38.5	85.0
Cr	13.3	10.3	9.4	5.8	6.8	10.0	11.1	30.9	6.8	7.4	8.3
Fe	nd	nd	nd	809	nd	nd	31262	50494	nd	1167	3358
Mn	69.6	114	88.2	120	62.6	72.2	926	615	100	69.5	151
Co	1.7	1.4	2.0	3.6	2.1	19.6	8.4	10.4	nd	nd	nd
Ni	18.0	16.9	43.0	16.1	29.5	19.5	37.1	59.7	25.8	20.5	19.0
Cu	38.9	25.0	37.6	24.6	69.1	59.5	48.5	82.5	28.6	19.4	22.8
Zn	nd	nd	10.8	nd	nd	48.6	586	903	nd	nd	nd
As	14.8	22.2	33.2	72.0	183	75.3	6.3	44.5	8.19	5.97	14.4
Rb	48.2	42.4	37.4	45.9	54.0	69.1	21.6	89.6	24.6	19.3	17.7
Sr	693	776	128	426	124	253	71.9	135	77.3	59.6	66.2
Zr	43.3	44.6	13.6	26.0	8.35	94.4	66.5	51.6	nd	nd	nd
Nb	3.40	5.45	5.32	5.15	4.97	2.87	21.4	48.6	nd	nd	nd
Mo	2.30	3.58	3.52	6.93	55.5	5.83	1.4	2.55	3.43	1.10	3.06
Sb	nd	nd	1.9	nd	1.41	1.35	2.1	2.74	nd	nd	1.30
Cs	4.20	3.69	4.05	1.50	4.12	3.88	1.3	7.27	nd	nd	1.48
Ba	88.0	57.9	41.1	116	44.1	44.9	57.7	164	53.6	99.3	68.8
La	nd	nd	nd	nd	15.5	nd	14.9	46.0	4.57	5.88	13.1
Ce	20.6	19.8	7.40	11.2	9.38	19.5	17.4	81.8	15.2	10.1	17.6
Pb	52.9	56.6	27.6	78.6	20.4	80.6	155	230	17.6	18.1	17.5
Th	nd	nd	nd	nd	nd	4.18	24.8	74.6	nd	5.35	nd
U	nd	nd	nd	nd	nd	4.10	26.9	45.5	nd	nd	nd

Table 7.6 Prediction of the element amount available (expressed as tonnes, t) that might easily move in the environment by water in the studied ash deposits from the SVZ. d, ash density; V_{DRE}, dense rock equivalent volume of the corresponding deposit; nd, not determined.

	CHA-1F	CHA-2R	CHA-G	CHA-E	COP	LON	LLA	HUD
d kg m^{-3}	2.344	2.359	2.359	2.345	2.638	2.598	2.757	2.695
V$_{DRE}$ km^3	0.17	0.17	0.17	0.17	0.0092	0.1	0.00092	2.7
Ca	3185	5204	5532	4170	853	412	179	108171
Mg	262	220	286	193	1444	67.0	41.6	13683
Na	2559	1157	3528	1175	673	231	134	155810
K	566	729	859	560	49.5	261	28.5	16978
Si	2104	2171	2474	2325	69.8	813	69.7	19345
Li	3.80	3.55	7.43	3.02	0.47	0.26	0.18	19.13
Al	502	503	522	565	49.28	268	30.5	12121
P	14.9	16.2	17.1	49.9	0.34	4.98	0.55	464
Ti	7.58	9.07	8.95	7.76	2.20	27.40	1.81	1010
V	0.41	1.41	2.40	0.69	0.05	0.24	0.11	34.3
Cr	0.29	0.34	0.31	0.27	0.04	0.14	0.04	4.01
Fe	nd	98.7	54.7	44.3	nd	nd	nd	nd
Mn	18.8	8.38	5.81	4.38	30.1	7.19	0.88	1255
Co	nd	nd	1.20	nd	1.38	0.14	0.03	nd
Ni	1.95	1.13	2.63	1.27	1.76	0.72	0.09	17.5
Cu	1.58	1.49	1.68	1.89	0.31	0.80	0.26	251
Zn	6.71	11.8	20.4	1.97	1.89	11.7	0.60	2529
As	14.0	29.1	121	5.18	0.02	0.08	0.05	6.66
Rb	1.06	1.67	1.96	0.98	0.21	0.20	0.02	16.6
Sr	5.83	7.30	11.9	16.3	3.57	1.91	0.64	395
Zr	0.56	0.57	2.34	1.51	0.08	0.46	0.08	24.0
Nb	1.87	1.90	1.60	1.61	0.11	0.75	0.08	34.4
Mo	0.64	1.28	1.79	0.36	nd	0.03	0.00	2.15
Sb	0.18	0.34	0.37	0.09	nd	nd	0.00	1.43
Cs	0.08	0.09	0.13	0.06	0.00	nd	nd	nd
Ba	3.39	4.27	3.62	7.99	0.18	1.17	0.09	62.0
La	nd	nd	nd	nd	0.07	nd	nd	nd
Ce	0.35	0.21	0.35	0.24	0.22	nd	nd	nd
Pb	13.9	6.20	80.8	10.2	0.25	10.2	2.72	17.6
Th	nd	nd	nd	nd	nd	nd	nd	nd
U	nd	nd	nd	nd	nd	nd	nd	nd
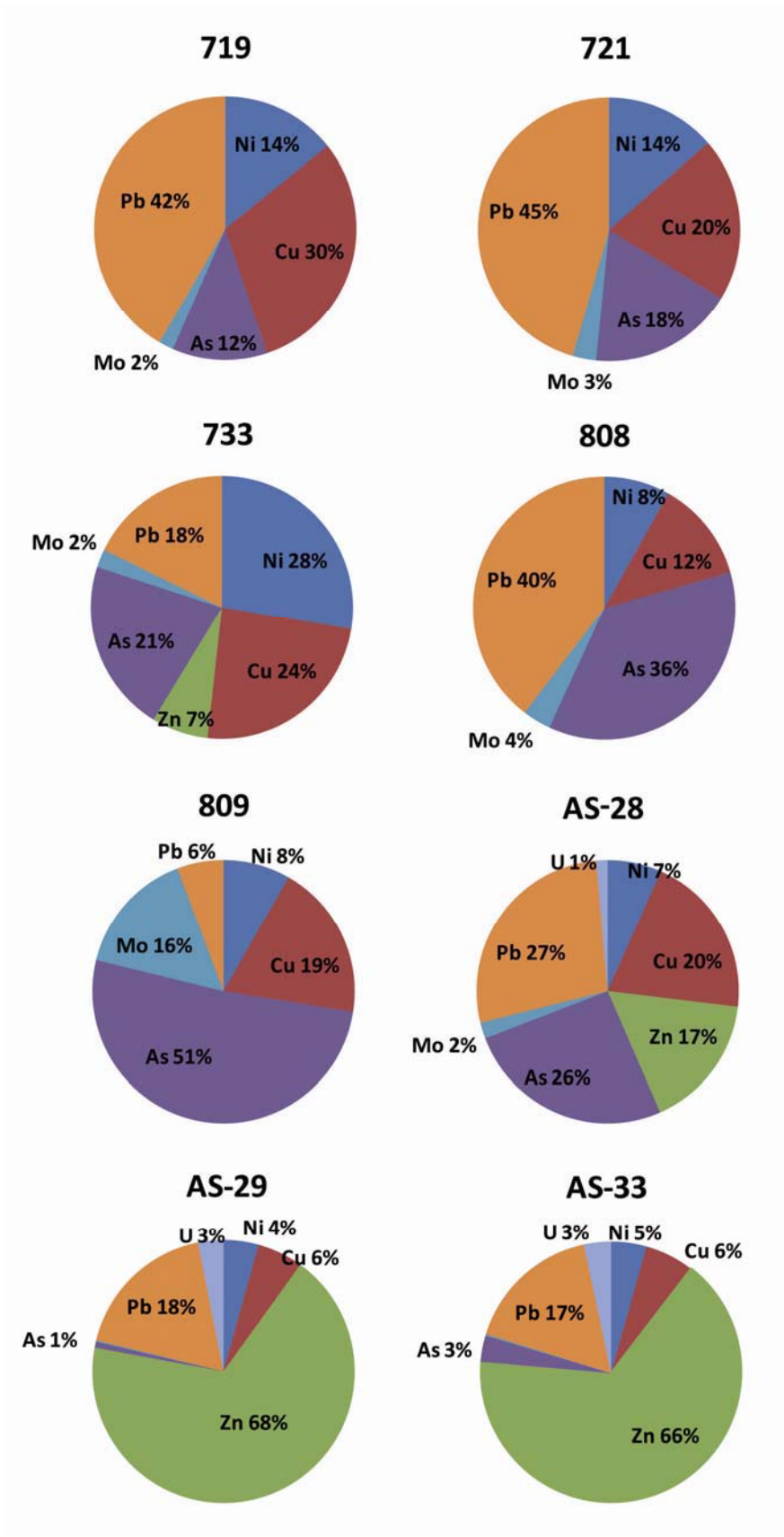
Figure 7.7 Percentages of the main environmental available PTTEs in each one of the Puna and neighbouring area ash deposits.
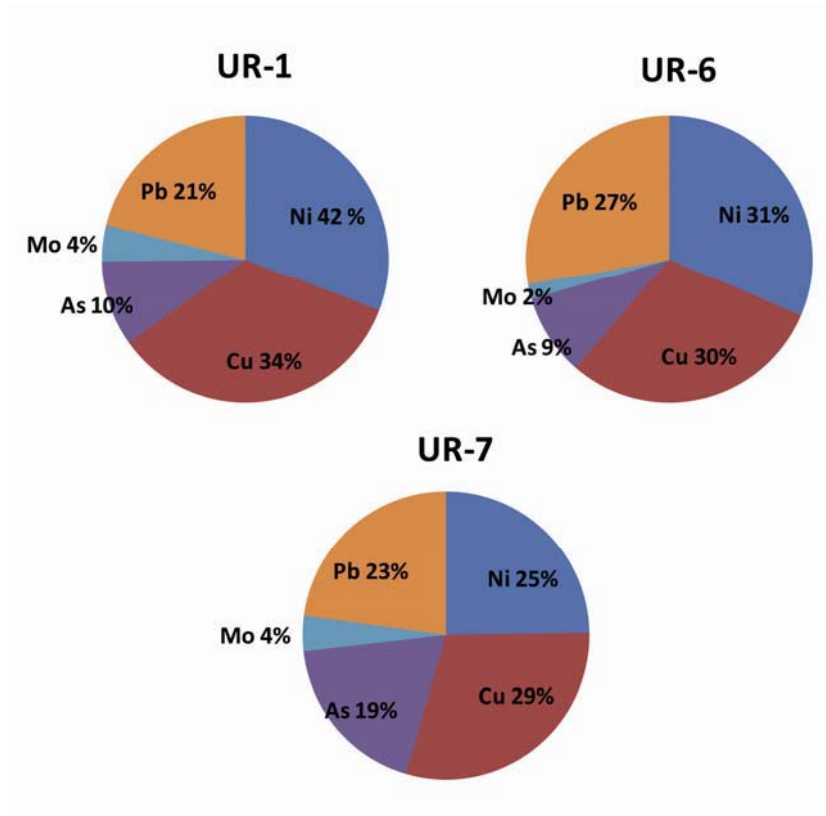
Figure 7.8 Percentages of the main environmental available PTTEs in the Uruguay ash deposits.
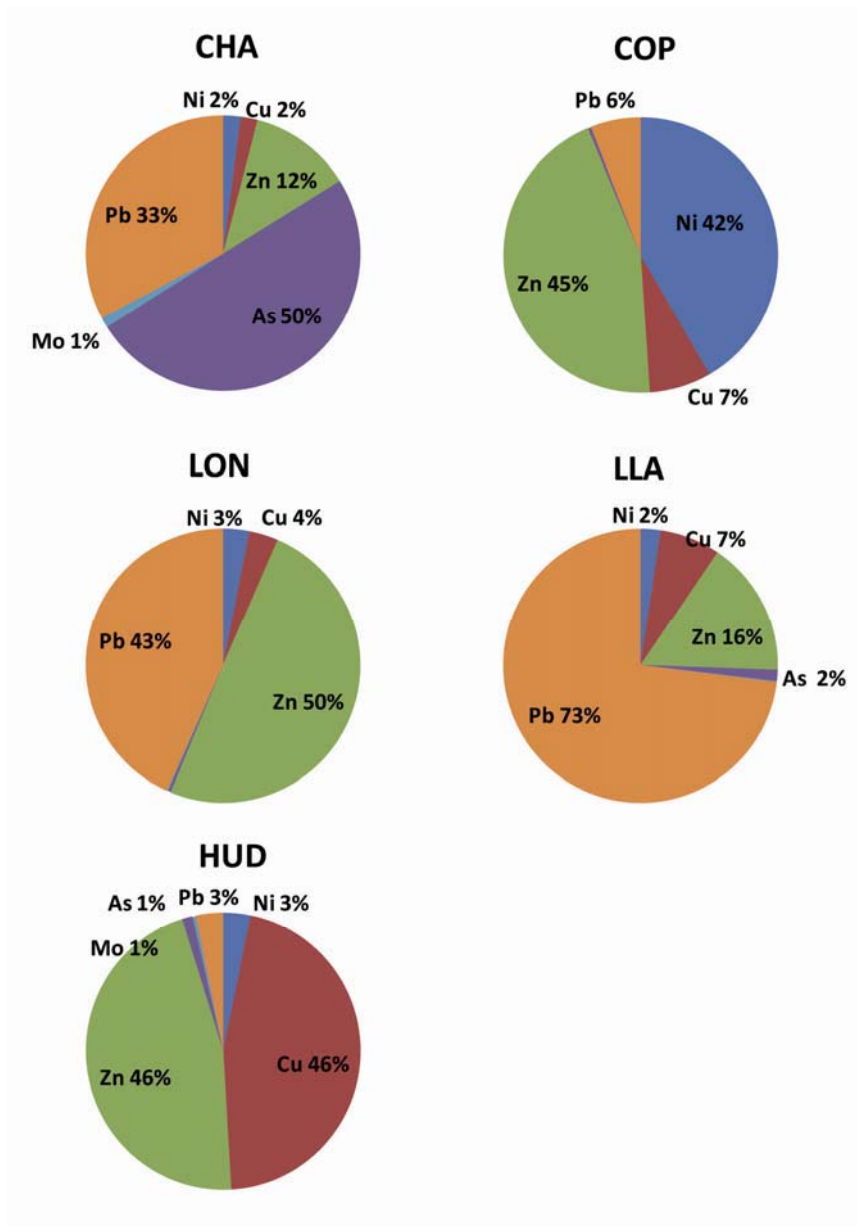
Figure 7.9 Percentages of the main PTTEs environmental available in the SVZ ash deposits.

7.4 SBLTs with nitric acid

Acid leach treatments generally remove larger amounts of material from ash than water leaches (Ruggieri et al., 2010, 2011; Smith et al., 1982; Smith et al., 1983). Deionised water is an extractant without buffering capacity that leaches primarily the easily soluble salts adsorbed on ash particle surfaces (incorporated in volcanic plume for the pristine ashes or during the weathering environment for the ancient ashes), while the acid leach continues this process, including dissolution of volcanic glass and mineral components. Therefore, this type of leaching tests were useful because allows to complement the water leachate information about the elements potentially mobilisable from the ashes investigated. Geochemical data obtained through nitric ash leaching tests are shown in Tables 7.7-7.8. As in the case of the water ash leaching tests, the first general observation is related to the higher capability of the dissolution of ancient ashes respect to recent ashes. This feature suggests that the residence time of the volcanic ash in the environment have a critical reflection on the element leachability. Once deposited, the volcanic ash undergoes irreversible geochemical weathering reactions (e.g., oxidation followed by slow dissolution), causing destabilization of the silicate framework and release of the elements associated with it.

Table 7.7 Geochemical data of major elements (mg kg^{-1}) and trace elements (µg kg $^{-1}$) in nitric ash leachates of ashes from Puna and neighbouring area and Uruguay.

	719	721	733	808	809	AS-28	AS-29	AS-33	UR-1	UR-6	UR-7
Ca	2447	5073	2192	1929	1722	2101	2878	2379	1628	1141	1889
Mg	166.0	894.3	326.0	384.3	350.2	592.3	196.2	582.0	316.6	410.8	822.7
Na	524.4	626.2	709.8	3263	1383	441.7	917.5	3455	738.9	179.0	275.0
K	252.4	404.5	409.9	636.1	372.9	519.7	500.8	2734	513.7	399.9	403.6
Si	101.4	164.1	137.0	170.7	297.7	208.0	150.9	354.4	38.0	64.9	73.5
Cl	166.4	178.0	171.0	625.4	518.3	434.8	246.5	270.4	1745	179.3	<LoD
SO$_4^{-2}$	3698	3743	3004	4060	4181	2991	3534	3019	148.8	170.9	284.1

Table 7.7 continuation.

	719	721	733	808	809	AS-28	AS-29	AS-33	UR-1	UR-6	UR-7
Li	1.51	2.62	1.49	5.19	9.85	2.83	0.95	3.32	0.31	0.55	1.08
Be	0.05	0.07	0.05	0.34	0.05	0.09	0.15	0.07	0.02	0.13	0.27
B	5.00	4.29	4.50	5.95	8.42	8.25	5.17	6.39	4.99	2.80	5.38
Al	361	540	274	1649	543	701	479	2049	478	870	1634
P	86.2	163	130	109	61.7	63.6	340	354	60.2	109	119
Ti	12.7	15.4	10.4	4.56	39.4	53.5	21.4	82.7	15.8	22.1	14.4
V	0.35	1.49	0.70	1.04	1.68	1.75	1.09	2.71	0.71	1.09	2.08
Cr	0.26	0.85	0.40	0.87	0.95	1.19	0.39	0.86	0.48	0.18	0.60
Fe	248	802	332	288	599	1091	321	1097	229	507	830
Mn	23.6	53.2	17.3	87.0	41.0	53.3	20.5	37.9	18.5	19.3	39.3
Co	0.19	0.78	0.86	20.8	0.32	0.56	11.9	25.5	0.27	0.35	0.54
Ni	2.27	5.57	3.39	2.29	2.41	2.70	2.18	2.79	2.06	1.09	1.28
Cu	1.27	2.34	1.10	1.09	1.98	1.88	0.77	2.09	9.04	5.71	2.67
Zn	38.5	46.1	52.3	33.6	92.9	43.1	24.1	34.9	42.2	16.7	9.66
Ga	0.14	0.23	0.12	0.28	0.25	0.34	0.20	0.81	0.12	0.30	0.50
As	0.98	1.75	0.91	1.18	0.52	2.06	0.83	1.05	0.27	0.22	0.06
Br	9.79	8.66	7.53	0.68	1.13	15.89	11.67	11.48	<LoD	<LoD	<LoD
Rb	2.79	4.02	2.35	2.69	3.21	5.24	6.42	15.19	1.68	4.97	5.61
Sr	4.86	11.9	5.01	16.4	4.46	3.68	3.80	21.36	7.87	7.28	15.39
Y	0.39	1.39	0.55	1.41	0.71	0.83	1.01	1.33	0.74	2.19	4.04
Zr	0.38	0.69	0.31	0.83	0.64	0.54	0.75	1.17	0.30	0.82	2.30
Nb	0.05	0.04	0.03	0.08	0.11	0.13	0.08	0.05	0.01	0.02	0.02
Mo	0.44	0.40	0.35	0.30	0.44	0.40	0.31	0.22	0.13	0.05	0.04
Cd	0.02	0.03	0.02	0.02	0.01	0.02	0.01	<LoD	0.04	0.01	0.01
Sn	<LoD	<LoD	<LoD	0.06	0.06	0.02	<LoD	<LoD	0.08	0.05	0.04
Sb	0.13	0.08	0.08	0.13	0.16	0.11	0.11	0.10	<LoD	<LoD	<LoD
Cs	0.23	0.34	0.40	0.37	0.17	0.37	0.45	1.36	0.09	0.24	0.55
Ba	6.57	18.4	9.82	46.0	5.11	3.42	4.78	23.6	23.2	21.1	31.9
La	0.55	2.19	1.15	1.47	1.17	1.37	5.29	9.56	1.33	4.21	7.08
Ce	1.14	4.44	2.36	3.55	2.24	2.84	8.05	15.05	2.36	8.43	9.97
Pr	0.14	0.59	0.30	0.39	0.28	0.35	0.82	1.39	0.29	1.02	1.68
Nd	0.56	2.32	1.14	1.42	1.06	1.36	2.45	4.35	1.06	3.78	6.18
Sm	0.11	0.45	0.21	0.31	0.19	0.27	0.30	0.57	0.17	0.65	1.11
Eu	0.02	0.07	0.03	0.05	0.03	0.04	0.04	0.08	0.04	0.13	0.21
Gd	0.10	0.45	0.21	0.31	0.20	0.25	0.36	0.64	0.17	0.67	1.13
Tb	0.01	0.06	0.02	0.05	0.03	0.03	0.03	0.06	0.02	0.09	0.15
Dy	0.08	0.31	0.13	0.28	0.14	0.18	0.19	0.30	0.12	0.48	0.86
Ho	0.01	0.05	0.02	0.05	0.02	0.03	0.03	0.04	0.01	0.07	0.14
Er	0.04	0.14	0.05	0.14	0.07	0.08	0.10	0.13	0.06	0.21	0.42
Tm	0.01	0.02	0.01	0.02	0.01	0.01	0.01	0.01	<LoD	0.02	0.05
Yb	0.03	0.10	0.04	0.14	0.05	0.06	0.09	0.10	0.04	0.16	0.34
Lu	<LoD	0.01	0.01	0.02	0.01	0.01	0.01	0.02	<LoD	0.02	0.05
Hf	0.03	0.05	0.02	0.21	0.34	0.07	0.05	0.07	0.23	0.08	0.21

Table 7.7 continuation.

	719	721	733	808	809	AS-28	AS-29	AS-33	UR-1	UR-6	UR-7
Ta	<0.01	<0.01	<0.01	0.02	0.02	<0.01	<0.01	0.01	0.02	0.01	0.01
Hg	0.01	0.01	0.01	0.44	0.03	0.01	0.40	0.31	0.01	0.01	0.01
Tl	0.01	0.04	0.02	0.02	0.03	0.06	0.02	0.07	0.01	0.03	0.04
Pb	0.88	1.28	0.78	2.91	1.02	1.27	0.40	2.86	1.37	1.32	1.73
Bi	0.03	0.03	0.02	0.02	0.03	0.03	0.02	0.03	0.01	0.01	0.01
Th	0.31	0.52	0.19	0.54	0.35	0.35	2.05	1.39	0.01	0.50	1.76
U	0.08	0.18	0.05	0.09	0.13	0.08	0.43	0.24	0.08	0.12	0.35

Table 7.8 Geochemical data of major elements (mg kg^{-1}) and trace elements (µg kg^{-1}) in nitric ash leachates of ashes from SVZ.

	CHA-1F	CHA-2R	CHA-E	CHA-G	COP	LOP	LLA	HUD
Ca	867	1847	768	2153	806	327	985	1143
Mg	289.1	978.1	192.9	1086	2695	710.0	19	1983
Na	220.5	112.9	157.7	307	361.9	46.4	148.4	346.6
K	103.7	129.3	59.7	194	227.0	5.3	21.0	69.8
Si	38.5	45.9	31.0	36.0	82.4	83.2	155.4	70.2
Cl	<LoD	26.3	<LoD	<LoD	92.9	<LoD	<LoD	83.2
SO$_4^{-2}$	230.5	1729	73.0	1529	5235	<LoD	<LoD	163.4

Table 7.8 continuation.

	CHA-1F	CHA-2R	CHA-E	CHA-G	COP	LOP	LLA	HUD
Li	0.60	1.25	0.44	1.73	0.46	0.29	0.22	0.57
Be	0.03	0.07	0.02	0.07	0.02	0.01	0.02	0.01
B	1.02	9.43	1.82	6.65	9.22	4.42	5.76	7.19
Al	441	1099	343	1211	694	248	864	221
P	33.8	81.7	29.2	96.2	47.6	29.7	4.26	157
Ti	7.59	41.5	9.42	14.1	11.8	48.3	20.5	85.0
V	1.00	4.01	0.75	4.30	2.11	0.28	1.44	3.52
Cr	0.46	1.99	0.26	2.27	0.69	<LoD	0.93	0.45
Fe	707	2700	496	2601	4262	1731	1749	3607
Mn	24.6	86.7	15.8	89.5	56.4	46.6	31.1	69.3
Co	0.25	1.18	0.25	1.08	3.10	0.64	1.67	2.01
Ni	1.08	2.18	0.95	2.39	5.55	0.77	5.07	1.79
Cu	2.29	3.13	1.66	3.15	14.6	4.72	5.04	16.2
Zn	9.75	13.7	14.0	22.9	12.3	11.7	6.80	32.3
Ga	0.20	0.52	0.13	0.63	0.19	0.07	0.15	0.11
As	7.14	25.9	3.20	23.9	2.74	0.35	0.60	0.20
Br	<LoD	<LoD	<LoD	0.19	<LoD	<LoD	<LoD	<LoD
Rb	0.77	1.26	0.61	1.51	0.36	0.04	0.02	0.20
Sr	1.74	3.54	2.04	3.52	7.85	1.24	5.11	3.02
Y	0.29	1.03	0.37	0.90	0.46	0.37	0.11	0.97
Zr	0.17	0.36	0.20	0.18	0.29	0.41	0.15	1.81
Nb	<LoD	<LoD	<LoD	<LoD	<LoD	<LoD	<LoD	0.02
Mo	0.21	0.23	0.16	0.31	0.18	0.10	0.13	0.14
Cd	0.01	0.02	0.00	0.09	0.04	0.02	0.01	0.08
Sn	0.07	0.07	0.07	0.07	0.08	0.02	0.01	0.13
Sb	<LoD	<LoD	<LoD	<LoD	<LoD	<LoD	<LoD	<LoD
Cs	0.14	0.33	0.11	0.37	0.01	0.01	0.00	0.01
Ba	3.73	5.63	5.67	5.40	9.74	3.08	1.32	2.79
La	0.25	0.55	0.22	0.61	0.66	0.15	0.06	0.79
Ce	0.52	1.25	0.49	1.39	1.46	0.37	0.12	1.80
Pr	0.06	0.16	0.06	0.18	0.19	0.05	0.02	0.24
Nd	0.27	0.70	0.27	0.78	0.80	0.23	0.07	1.01
Sm	0.05	0.16	0.06	0.17	0.15	0.06	0.01	0.22
Eu	0.01	0.03	0.01	0.03	0.02	0.02	0.01	0.05
Gd	0.05	0.16	0.06	0.18	0.15	0.06	0.02	0.22
Tb	0.01	0.03	0.01	0.03	0.02	0.01	<LoD	0.03
Dy	0.05	0.16	0.06	0.16	0.10	0.06	0.02	0.18
Ho	0.01	0.03	0.01	0.03	0.01	0.01	<LoD	0.03
Er	0.02	0.08	0.03	0.08	0.05	0.04	0.01	0.09
Tm	<LoD	0.01	<LoD	0.01	<LoD	<LoD	<LoD	0.01
Yb	0.02	0.07	0.02	0.07	0.04	0.03	0.01	0.08
Lu	<LoD	0.01	<LoD	0.01	<LoD	<LoD	<LoD	0.01
Hf	0.07	0.11	0.07	0.05	0.10	0.03	0.04	0.31

Table 7.8 continuation.

	CHA-1F	CHA-2R	CHA-E	CHA-G	COP	LOP	LLA	HUD
Ta	<LoD	0.01	0.01	<LoD	<LoD	<LoD	<LoD	<LoD
Hg	<LoD	0.01	0.01	0.01	<LoD	<0.01	0.01	0.01
Tl	<LoD	0.01	<LoD	0.01	0.03	<0.01	0.01	0.11
Pb	0.59	1.48	2.00	1.40	1.21	0.33	0.16	1.92
Bi	0.01	0.05	<LoD	0.14	0.08	<LoD	<LoD	<LoD
Th	0.04	0.30	<LoD	0.04	0.06	<LoD	<LoD	0.06
U	0.02	0.04	0.02	0.04	0.02	0.01	0.01	0.02

As in the case of the water batch tests, once determined the RMLs for each element, they were grouped according to their mobility. The RML values are reported in Appendix 6.

For ancient volcanic ash the results were as follows:

(1) High mobile elements (RML > 5%): Ca, Mg, Fe, Mn, P, As, Ba, Co, Cu, Mo, Ni, Sb, Sr, V, Y, Zn, and REE.

(2) Moderate mobile elements (RML between 0.5 and 5%): Na, K, Al, Ti, Be, Bi, Cr, Cs, Ga, Hf, Li, Nb, Pb, Rb, Sn, Ta, Th, Tl, U, and Zr.

(3) Low mobile elements (RML < 0.5%): Si.

The elements with a very high RML were Zn and P. The high concentration extracted for Zn, in many cases with a recovery of close to 100 % (i.e., 733 and 809 samples), suggests that this element is more associated with sulphides (probably adsorbed on particle surfaces), which are more easily weathered, than with silicates (Ruggieri et al., 2010). The difference of Zn with Cu and Pb, with which it is often associated, seems to indicate that the latter are related to the silicates. Also P reaches a very high mobilization in the acidic condition, approaching 100% in samples 809 and AS-33. This element typically concentrates as phosphate in a single mineral —apatite— in high silica igneous rocks, although it can occasionally appears in others (monazite, xenotime, Li phosphates, etc.), and also within the network of alkali aluminium silicates. It has long been established that P is somewhat easily mobilized in the weathering of rocks considered here, according to their mineralogical composition (Middelburg et al., 1988; Rice, 1973). Its dissolution at different pH values has been investigated experimentally (Nickel, 1973). The behaviour of apatite in the weathering of igneous rocks with high silica content was studied in detail by electron microscopy by Banfield et al., 1989, who found that

weathering mobilized early not only around 85% of the existing P of the original rock, but also REE and Y (Banfield and Eggleton, 1989). The high mobilization of REE in AS-33 confirms this hypothesis. However, only a P fraction were solubilised in the others samples suggesting that P is also in a more resistant network of silicate. The presence of phosphorus in the feldspar network is well known. This element displays an affinity for alkalis and Al, not for Si, in water saturated rhyolitic melts (London et al., 1993). The accumulation of P in alkali feldspar increases with the excess of Al, expressed by the alumina saturation index A/CNK. The sample with lower leachable P in HNO_3, sample 808, is the only of peraluminous composition, with an A/CNK index of 1.09. Therefore, almost 50 % of P must be in the silicate network.

The trace elements with high RML in all the ashes investigated (e.g., As, Co, Mo, Ni, and V) could indicate glass dissolution. Also the REE show high mobilization in acidic leaching conditions, mainly in the samples AS-29 and AS-33. This is probably due to the fractionation of REE during hydrolysis (see above the case of P). These elements, besides appearing in apatite in rocks derived from high silica magmas, can concentrate also in allanite, titanite, zircon, monazite and xenotime. As these five minerals are much more resistant to weathering, the apatite is probably the main mineral controlling the leaching of REE (Ruggieri et al., 2010, 2011).

The elements with moderate mobility in all the ancient ashes (i.e, Ti, Be, Cs, Ga, Nb, Pb, Rb, Th, Tl, U, and Y) present high mobility in AS-29 and AS-33 samples. These elements are well characterised as less mobile in weathering processes. These ancient ashes correspond to the most ferromagnesian and lower silica content ashes. Therefore, this behaviour must be related to: 1) a better feasibility for hydrolysis of these ashes compared with those with higher silica and lower ferromagnesian contents (a well known feature); and 2) a lower retention capacity, either produced by the lack of external ions that could improve solubility and/or by the not yet well-developed surface features that facilitate the adsorption of the most favourable elements (with high-alkali ionic radius and low charge, among others) (Ruggieri et al., 2010).

For more recent volcanic ashes the RML values are given below:

(1) High mobile elements (RML > 5 %): Ca, Mg, Fe, P, Co, Ni, Cu, Zn, As, Mo, V, Cd, and Pb.

(2) Moderate mobile elements (RML between 0.5 and 5 %): Na, K, Mn, Li, Be, Al, Ti, V, Cr, Fe, Ga, Rb, Sr, Y, Sn, Ba, Hf, Tl, Bi, U, and REE.

(3) Low mobile elements (RML < 0.5 %): Si, Mn, Zr, Nb, Sb, Cs, Ta, and Th.

The trace elements with higher mobility (e.g., Ni, Zn, As, Mo, Cd, and Pb) confirm that they are dominantly combined with halogens and sulphate as metal salts adsorbed on particle surfaces (Africano et al., 2002; Bernard and Leguern, 1986; Delmelle et al., 2007; Jones and Gislason, 2008). Remarkable high mobility was reported for Ni, As, and Mo in Chaiten ash nitric leachate.

Again the case of P is paradigmatic, with high mobility in Chaiten and Hudson nitric acid leachates. As mentioned above, P usually occurs as apatite. The presence of this mineral in Hudson ash is well documented by mineralogical and petrographic observations (Kratzmann et al., 2010a). Furthermore, in most natural systems, apatite usually contains fluorine instead of the hydroxyl groups forming fluorapatite although it can be also found in some silicates as in the feldspar network (Valsami-Jones et al., 1998). Though fluorapatite ($K_s = 10^{-60.6}$) is less soluble than hydroxylapatite ($K_s = 10^{-58.3}$), its solubility increases when pH decreases (Driessens, 1982; McDowell et al., 1977). The presence of F in Hudson water ash leachate and the REE-enriched trend depicted nitric acid leachate could indicate the P mobilisation by fluorapatite dissolution. In the Chaiten ashes, feldspars seem to be the surce to P, because as in the case of the 808 ancient ash, it is peraluminous with a A/CNK index of 1.09. Finally, the enrichment of the LREE (Light REE as La and Ce) in Copahue ash nitric leachate agrees with the mineral and volcanic glass dissolution occurring during the intrusion of a new magma in the hydrothermal system of the Copahue area (Varekamp et al., 2009).

7.5 Summary and conclusions

Figure 7.10 shows the main information available from SBLTs. The application of the SBLT (with deionised water) method developed in this chapter defines the potential geochemical impact of the volcanic ashes investigated on the environment. Through the statistical treatment of the data set it was demonstrated a clear difference between the ancient and recent ash leaching

behaviours. Ancient volcanic ashes were deposited long time ago on land and they were subjected to hydrological and soil processes, which effectively removed any soluble salts attached to the surface of the original pristine ash particles.
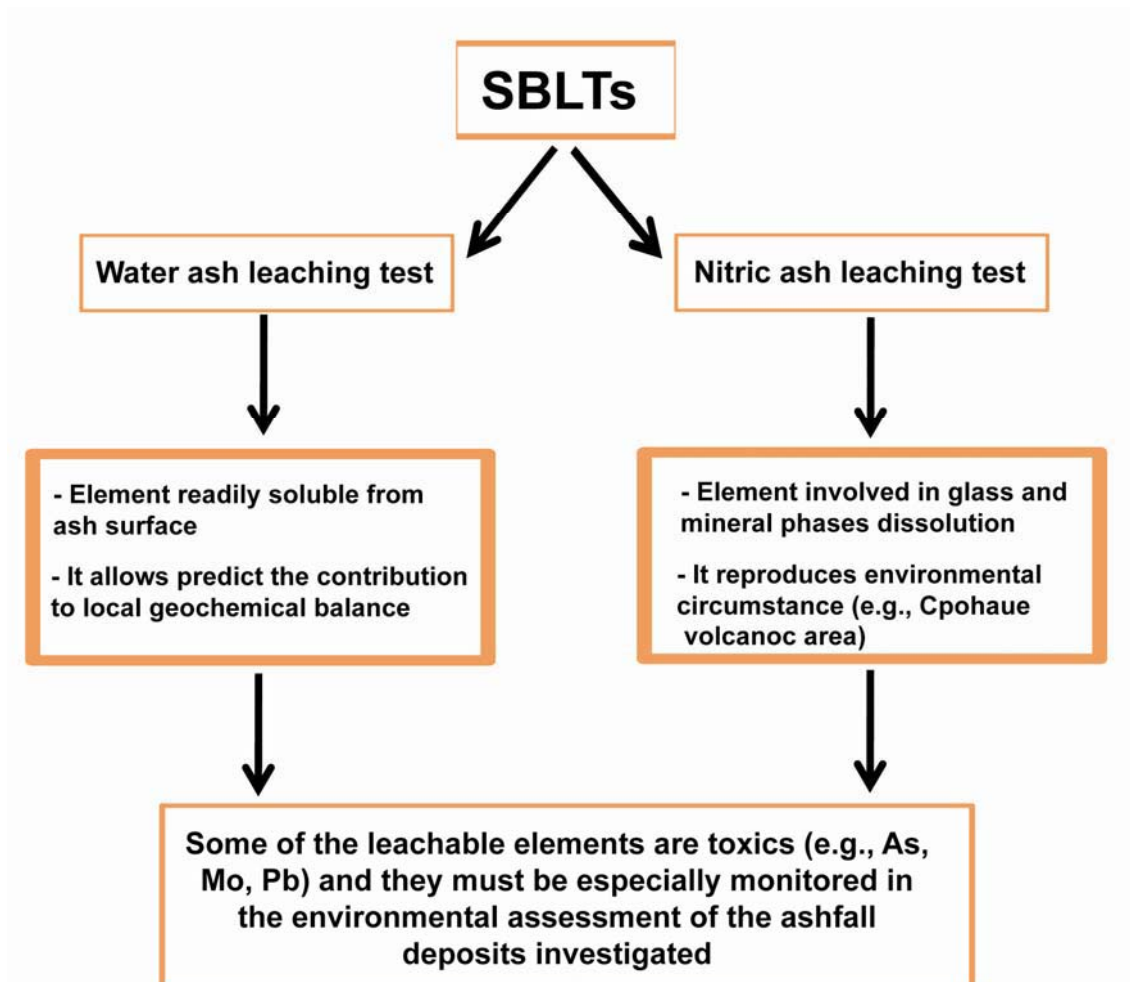
Figure 7.10 Information available from Single Batch Leaching Tests with desionised water and nitric acid (HNO_3).

Specific conductivity values and the geochemical data of ash water leachates show that ancient ashes have a higher dissolution capability. This suggests that the residence time of a volcanic ash in the environment seems to have a reflection on the element leachability. Once deposited, a volcanic ash

undergoes irreversible geochemical weathering reactions (e.g., oxidation followed by slow dissolution), causing destabilization of the silicate framework and release of the elements associated with it. Water ash leachate data were also used to estimate the environmental available amount of each element in each one of the volcanic ashes investigated when ash-water interaction occurs. These features allowed to estimate the contribution to regional geochemical balance of the entire ashfall deposits. Both ancient and recent ashes could transfer to the environment high amount of major elements, mainly Ca and Na. Some of the elements available from these ash deposits are macro- and micronutrients (e.g., Fe, Mn, and P), evidencing the fertilizing potential of the ashes. Many others are potentially toxic trace elements (PTTEs) even at very low concentrations. These are As, Cu, F, Mo, Ni, Pb, and Zn. Some of the latter elements are included in the drinking water guidelines (ANMAT, 2007; INN, 2006; WHO, 2008) due to their potential toxicity and must be especially monitored in the environmental assessment of these ashfall deposits.

Finally, nitric ash leachates allow to understand the elements involved during the glass and crystalline phases dissolution, as well as, they reproduces environmental circumstances in which very acidic conditions occur (e.g., acidic surface water in the Copahue volcano area). Acid leach tests remove more amount of material from ash than water leach tests and allow mobilising also the release of more immobile elements, as REE.

Chapter 8. Column leaching tests

8.1 Objectives

The aim of this part of research is to present the results obtained through the application of column leaching tests to the different types of volcanic ashes under study. The SBLTs reported in the latter chapter play an important role, although they do not represent the full complexity of a natural system, allow knowing the total leachable loads of a specific ash. Moreover, the development of a standardised and rapid screening tool as a SBLT is a significant topic of environmental research (Witham et al., 2005). The main restriction of the SBLT is the lack of information about the temporal behaviour of the leachate. The rainwater percolation into a layer of volcanic ash dissolves glass and several mineral phases mobilizing different species which may arrive to surface and groundwater. Therefore, a dynamic test as a column leaching test can be designed to evaluate the release of species as a function of time, giving information on the breakthrough of the leached compounds and their potential mobility. In a column leaching test, the leachant is typically passed through a vertical column of fine-grained material in up-flow or down-flow, and the resulting leachate is collected in discrete fractions and analyzed. The underlying assumption in this type of leaching tests (as well as for single batch tests) is that the equilibrium condition is achieved. In the case of a column leaching test, the assumed equilibrium condition corresponds to a local equilibrium assumption (LEA) when the rate of percolation is sufficiently slow (Meza et al., 2008; Seaman et al., 2005). Column tests are more suitable for prediction purposes because provides a closer approximation to the leaching processes occurring under actual conditions, without compromising the reproducibility of the experiments. The column test design for a PTTE leaching study is far less straightforward making it difficult to compare results for studies conducted using, for example, different leachant volumes passed through the sample, column lengths, and flow rates. Moreover, it is time consuming, ranging the experiment duration from several days to weeks or years. Previous studies

carried out with environmental purposes have, however, demonstrated the utility of this kind of experiments (Van der Sloot et al., 1997).

Three volcanic ashes were employed in this study: samples 719 and 808 (ancient ashes from the Puna region) and sample CHA-1F (pristine ash collected during the 2008 eruption of Chaiten volcano). Three column leaching tests were carried out being the main objectives:

(1)   To understand the differences in mobility of PTTEs between ancient and pristine volcanic ashes. In this way, the results of column leaching tests performed on the raw ashes were compared.

(2)   To know the mobility difference of PTTEs in grain-size fractions of ash. In this case, a simple fractionation procedure was carried out on sample 719 and the experiments run with such fractions. Moreover, the results are discussed taking into account the XRD analysis carried out on the size fractions.

After a brief description of the column experimental methodology, the structure of this chapter is as follows:

(1)   in the first part are reported the column leaching data obtained using the raw ash samples;

(2)   in the second part are described the results obtained by the column leaching tests with the ancient ash grain-size fractions;

(3)   finally, the summary and conclusions section gives the recount of the observed remarks (including the environmental concern).

8.2 Column leaching test methodology

The developed protocols for the different chemical analysis and experimental methodologies are reported in Appendixes 1 and 5. Figure 8.1 shows a schematic diagram of the column experimental set-up. A vertical column (Teledyne ISCO Ref. 69-3873-140) of 8 cm height and a cross-sectional area of 2.5 cm^2 was employed. The column was filled with 10 g of sample and 1 L of deionised water (MilliQ Q Plus type, 18.2 MΩ cm^{-1}) was employed as leachant. Loading of column was carried out gradually, under mild shaking in order to
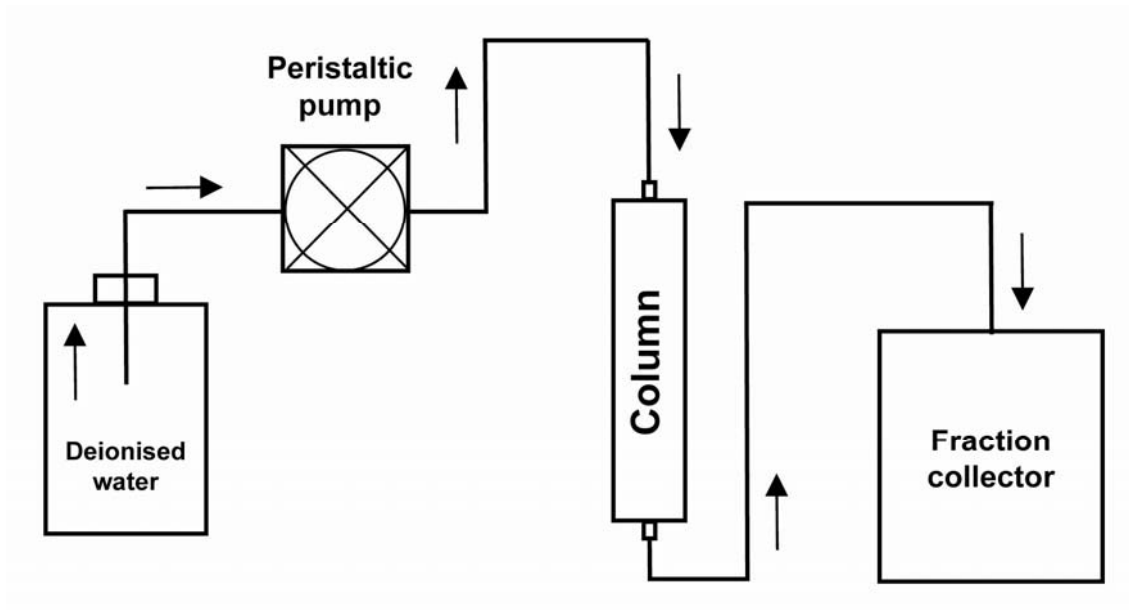
Figure 8.1 Schematic diagram of the column experimental set-up.

Table 8.1 Water flows of the column experiments carried out with raw (unsieved) ashes and 719 size fractions.

Volcanic ash	Water flow ml min^{-1}
719	0.25
808	0.22
CHA-1F	0.24
719 <100µm	0.12
719 100-200 µm	0.12

compact the ash specimen. This filling process prevents the entrapment of air bubbles and grain size fractionation and avoids the unnatural channelling of water and clogging by very fine material when the flow through. A silica filter with average pore size of 60 Å was attached at the column inlet and outlet. A peristaltic pump (Minipuls 3, Gilson) at the head of the column assured the constant, stable and low water flow from top to bottom (15 rpm). Due to different size and physical properties of the samples, each column presented different water flows (Table 8.1). A fraction collector at the column outlet took samples from the leaching solution (FC 204, Gilson) in 14x100 mm polypropylene test tubes. The drop mode collection has been employed, counting 400 drops per

tube of leachate solution from the column outlet. Leachate solution was collected in about 6 days resulting in a set of 100 test tube samples.

A subset of 40 samples (acidified with 1% HNO_3) was analysed for major and trace elements by HR-ICP-MS. Another subset of 40 samples was removed for pH determination (Crison Multimeter MM40). Samples were stored at 4 ºC until analysis.

8.3 Column leaching tests on bulk ashes

For each experiment, the results are reported as breakthrough curves of major and trace element concentration *vs.* accumulated volume of the percolate solution; experimental values of pH variation are also reported (Figures 8.2-8.4). Only selected elements are reported here because a lot of them presented negligible concentrations (in some cases, as REE, below to 0.01 µg l^{-1}).

8.3.1 pH and hydrolysis

The pH value rises quickly upon leachant contacts with ash in all the experiments (Figure 8.2). This feature has been commonly reported for volcanic ash leachates, also when seawater was used as leachant (Jones and Gislason, 2008; Rango et al., 2010; Smith et al., 1982; Smith et al., 1983). This initial increase was observed also in SBLTs and is due to both a fast and large dissolution of alkaline compounds and a release into solution of hydroxyl ions from the oxo-groups (MxO) present on the particle ash surface (Oelkers et al., 2009).

Early stages of the contact of minerals with water are usually highlighted by pH changes (Luce et al., 1972; Parks, 1990; Petrovic et al., 1976). In the case of silica, the main constituent of glass, H^+ and $(OH)^-$ diffuse in the three spatial dimensions, even through the solid surface, charging it. In these active interfaces, the $(OH)^-$ are linked to Si and the H^+ to O, promoting the dissociation of water (the water dissociation constant, K_w, changes by several orders of

Figure 8.2 Behaviour of pH and major elements (Ca, Mg, Na, K, Si, Cl, and SO_4^{2-}) (mg l^{-1}) in the column leaching tests.

Figure 8.3 Behaviour of trace elements Li, B, Al, P, V, and Fe (µg l^{-1}) in the column leaching tests.

Figure 8.4 Behaviour of trace elements Mn, As, Br, Rb, Sr, Mo, Ba, and U (µg l^{-1}) in the column leaching tests.

magnitude in these conditions). This explains because the suspended solids in natural waters are often negatively charged at pH close to neutrality (6-8) (Oelkers et al., 2009).

Although only at the beginning of the process, these negative charges surrounding the solid tend to attract H^+, raising the pH of the closest solution until the equilibrium is obtained. Thereafter, the slower processes of dissolution, hydrolysis, and buffering power of the solid phase by progressive acid-base interaction proceed, decreasing the pH (Toscano et al., 2008). However, in a volcanic ash the process is more complex due to the occurrence of other silicates of Na, Ca, K and Mg (i.e., alkali feldspars as albite, anorthite, and sanidine). According to several studies on aluminosilicate dissolution, the process develops in three stages: (1) virtually instantaneous exchange of the alkaline ion (Na^+, K^+, Mg^{2+}, Ca^{2+}) by H^+ (or as H_3O^+), i.e., with increase of pH; (2) generation and fast growth of a residual layer poor in that alkalis and rich in Si; and (3) interaction of feldspar-solution through the residual layer and beginning of an incongruent dissolution (process necessarily slower, at pH lower than in previous steps) (Oelkers and Gislason, 2001; Oelkers et al., 2009; Schott and Oelkers, 1995; Wollast and Chou, 1992). The first stage involves a reversible reaction where H^+ forms the feldspar $HAlSi_3O_8$ when Na^+ is released. At the end of the second stage, a layer of this compound is developed by incongruent dissolution. The third stage, the slow one, controls the process of aqueous dissolution. These are the processes (together with volcanic glass dissolution) taking place on the column leaching tests studied here explaining the variation of pH. The pH diagram in Figure 8.2 indicates that among the volcanic ashes the sharpest pH was shown for sample 808, which is practically made up only of volcanic glass (see § 5.4.1 XRD patterns of the bulk ashes).

8.3.2 Silica and aluminium dissolution

The rate of silicate glass dissolution in the aqueous phase can be reasonably described in terms of pH and aluminium dependencies, although the presence of other components (e.g., fluoride and sulphate) in the system can dramatically

increase glass dissolution rates (Flaathen et al., 2010; Wolff-Boenisch et al., 2004).

Volcanic ash could be defined as formed by amorphous-crystalline silicates (including volcanic glass and quartz) and minor amount of aluminosilcates (i.e., principally alkali feldspars in our samples). Although in rhyolitic samples the mineral content is relatively low, their presence could affect the leaching behaviour of some elements as Al, Fe, and P related to rock forming minerals.

It is well established that the solubility of amorphous silica, the most abundant constituent of volcanic ash, is higher than for crystalline silica (quartz) (Alexander et al., 1954). In every case, the different forms of silica have the same fundamental structure. They are highly polymerized chains of SiO_4 in which the silicate group (Si—O—Si) is the reactive group. This group could be broken by water in two steps: (1) the absorption of water near a Si—O—Si group; and (2) the formation of a new Si—O bond by the oxygen of the adsorbed water and the cleavage of the Si—O—Si group (Schott and Oelkers, 1995). Dissolution is associated with the latter step, which at 25 ºC involves an equilibrium between the solid phase and a monomeric form of silica ($Si(OH)_4$) in solution (Alexander et al., 1954). The increase in total dissolved silica at basic pH is well established, but it is possible that at very low pH the solubility increases by reaction of $Si(OH)_4$ with acids (Alexander, 1957). According to pH variation, it was observed a higher solubility of Si at more basic pH conditions (Figure 8.2).

The structure of aluminosilicates (e.g., alkali feldspar) contains exchangeable cations (e.g., Na^+, Ca^{2+}) along two hydrolysable sites in the polymer: silicate groups (Si—O—Si) and aluminate groups (Al—O—Si). As explained above their dissolution can be considered as a three step process. Here it is briefly explained in terms of Al concentration. The first of these steps is the relatively rapid equilibration between hydrogen and alkali ions on the mineral surface (causing an increase of pH) (Wollast and Chou, 1992). The second step is the reversible exchange of hydrogen with aluminium on the mineral surface involving the breaking of Al—O bonds of Al—O—Si groups and leaving the surface of the minerals enriched in silica both at acidic (Casey et al., 1989) and basic conditions (Hellmann et al., 1990). This mechanism indicates that within the tetrahedral framework, Al—O—Si bonds are weaker than Si—O—Si bonds.

Therefore, Al undergoes dissolution as depicted in the 719 and CHA-1F ashes (in which the XRD patterns have demonstrated noticeably presence of alkali feldspars). The final and rate limiting step of these compound dissolutions is the hydrolysis of Si—O—Si bonds. The complete absence of aluminosilicate minerals in the sample 808 could explain the difference of the Al behaviour of this sample respect to the other ashes (Figure 8.3).

8.3.3 Other major and trace element behaviours

The geochemical composition of leachates in the column experiments was predominantly controlled by incongruent dissolution of glass and crystalline phases (if present) and dissolution of coatings on the ash particle surfaces. Therefore, we should discriminate between the elements rapidly released from the ash surface and those related to more complex processes as dissolution.

The initial dissolution of ash compounds in deionised water shows that those elements removed at the beginning of the experiment were Ca, Mg, Na, Cl, SO_4^{2-}, Li, B, V, Mn, Rb, Sr, Mo, Ba, and U. Sharp variations in concentrations of these elements occur between 0-200 ml of accumulated volume of the percolate solution. Smooth element concentration variations define the second stage (from 200 to 1000 ml accumulated volume of the percolate solution). The rapid increase of pH (i.e., rapid consumption of H^+) was accompanied by the release of alkali ions (i.e., Ca^{2+}, Mg^{2+}, Na^+, and Li^+), which suggest a rapid equilibration between hydrogen and alkali ions on the silicate surface.

However, the time required for passing 200 ml along the column (i.e., ~26 hours) was considered enough for begin the chemical weathering and a rapid incongruent dissolution of volcanic glass (that is the reactive phase) by cation-exchange processes that could be also the source of the aforementioned elements (Rango et al., 2010).

Differences in the order of magnitude of the component concentrations were detected among the ashes under study. The higher initial concentrations depicted for Cl^- (300 mg l^{-1}) and SO_4^{2-} (250 mg l^{-1}) in CHA-1F experiment confirm the presence of soluble compounds rapidly leachable (as chlorides and sulfates) onto pristine ash particle surfaces. The same feature was reported for

Li, B, P, Mn, Rb, Br, V, and Mo, indicating soluble salts on the surfaces which were formed in the plume of the volcanic eruption through gas-particle interaction or the partial dissolution of the ash with acidic gases (i.e., mainly SO_2, HCl, HF) and aerosols (i.e., H_2SO_4), followed by precipitation at the ash-liquid interface, specially for elements with a low volatility in magma (lithophilic elements) (Delmelle et al., 2007).

In contrast, some other metals (Ca, Sr, Ba) present higher concentrations in the ancient ashes (Figures 8.2-8.4). In these samples, the most mobile elements showing preferential enrichment on tephra surfaces were probably released during the early burial of the deposit.

Some element concentrations (P, Fe, As, and to a lesser extent Br) do not show a very sharp decrease during the leaching time. This feature enhances the relation to glass dissolution processes. If we take into account the leaching behaviour of the CHA-1F pristine ash, also B, and V are associated with the glass dissolution in these experimental conditions. It is very well known that the latter elements (including As) are normally enriched in rhyolitic melts due to their incompatibility.

8.4 Column leaching tests on grain-size fractions

Sample 719 was sieved by mechanical separation in two grain-size fractions (<100 µm; 100-200 µm) and the column experiments carried out with each one of these fractions. Then, the results were reported as breakthrough curves of major and trace element concentration *vs.* accumulated leachate volume and compared with the raw ash data (Figures 8.5-8.8). As in the previous column tests on raw ashes only selected elements are reported here, because a lot of them presented concentrations too low (in some cases, as REE, below to 0.01 µg l^{-1}). The aim of these leaching tests is to know the mobility of PTTEs in different grain size-fractions of ancient ash. The specific mechanism by which the pH quickly increases when ash-water interaction occurs has been previously exposed and it not will repeated here. An interesting consideration
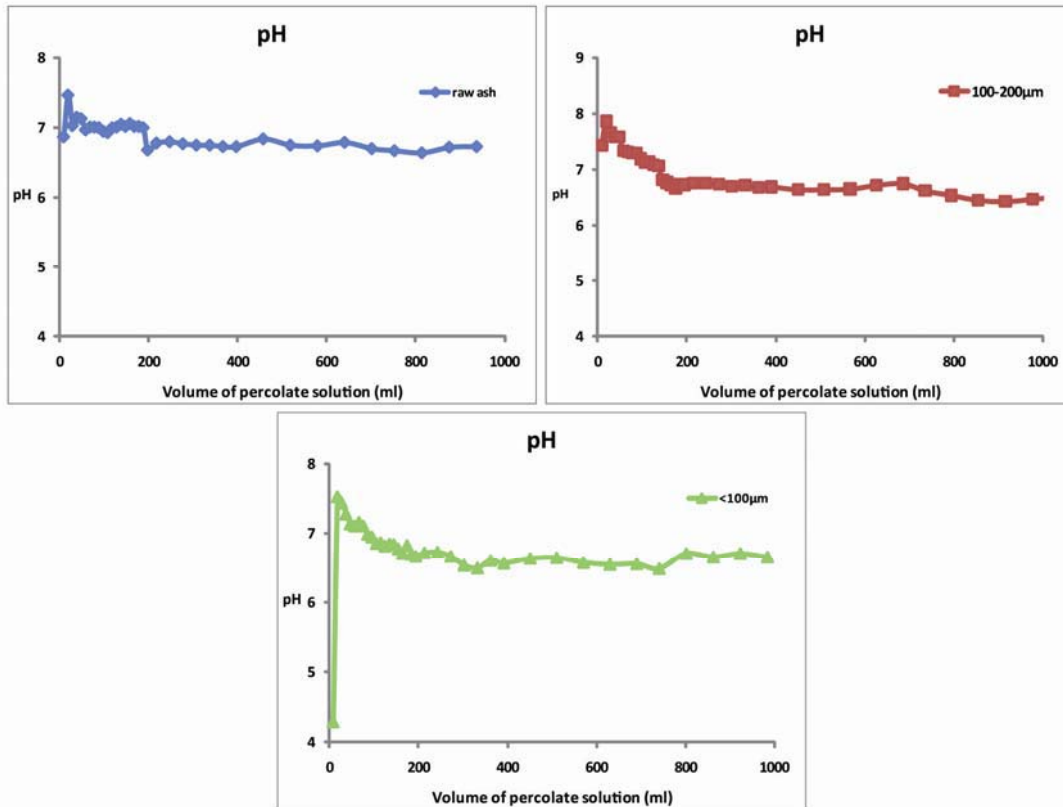
Figure 8.5 Variation of pH during the column leaching experiments of 719 raw ash (unsieved) and <100 and 100-200 μm fractions.

must be made on the different pH variation among the grain-size fractions (Figure 8.5). Very rapid increase was detected in the lower fraction (<100 μm), i.e., the fraction with the highest amount of volcanic glass. This feature has been previously determined by the qualitative observation of XRD analysis (*see* § 5.2.2 XRD patterns in grain-size fractions of 719 volcanic ash). Therefore, a very rapid incongruent dissolution of volcanic glass by cation-exchange processes is suggested to explain this behaviour. This aspect was confirmed by the higher Si concentration observed in that fraction (Figure 8.6). Aluminium concentration was reversed, with the lower concentration in the smalles size. It is well known that crystalline minerals are more abundant in the grain-size
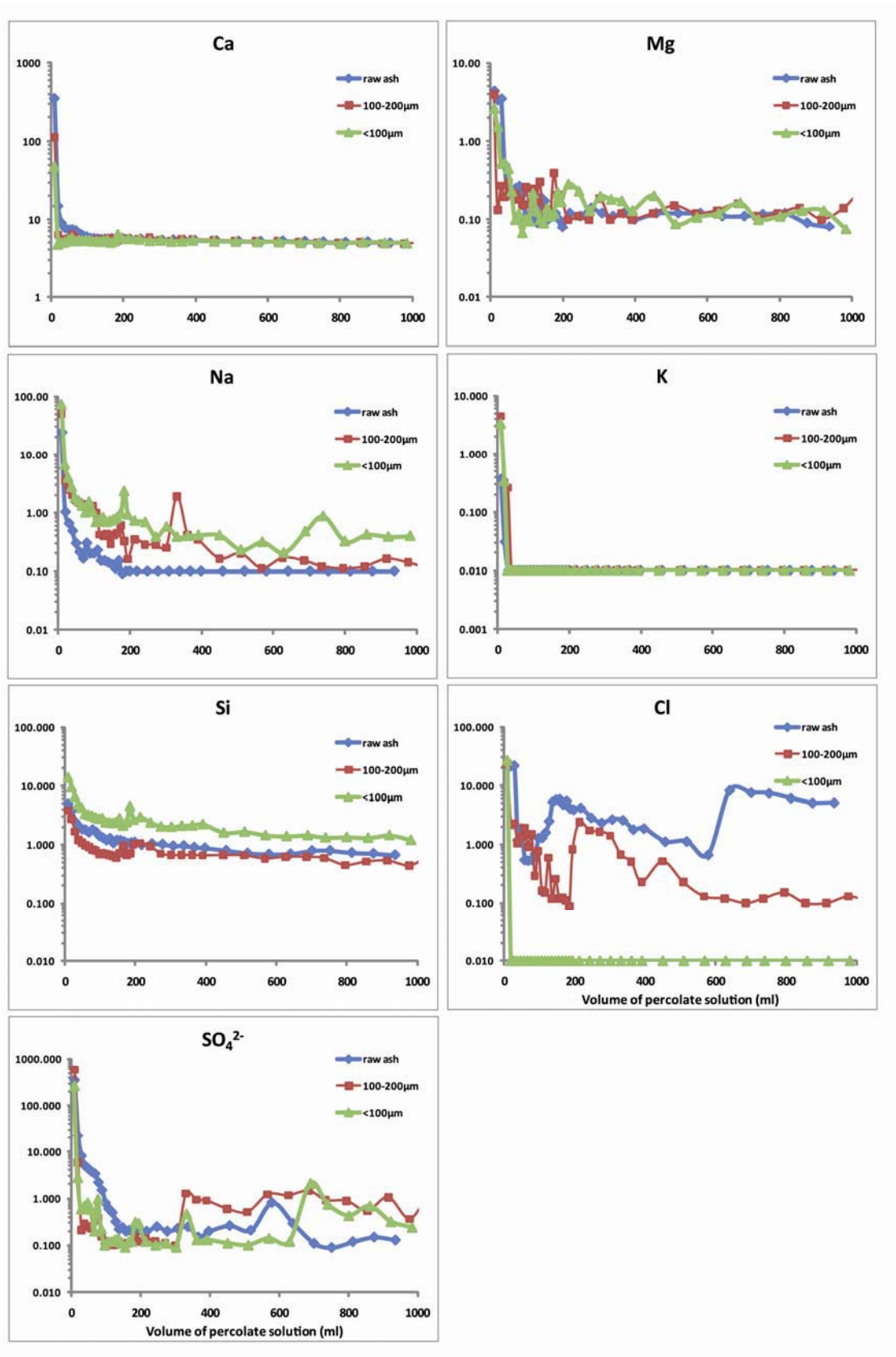
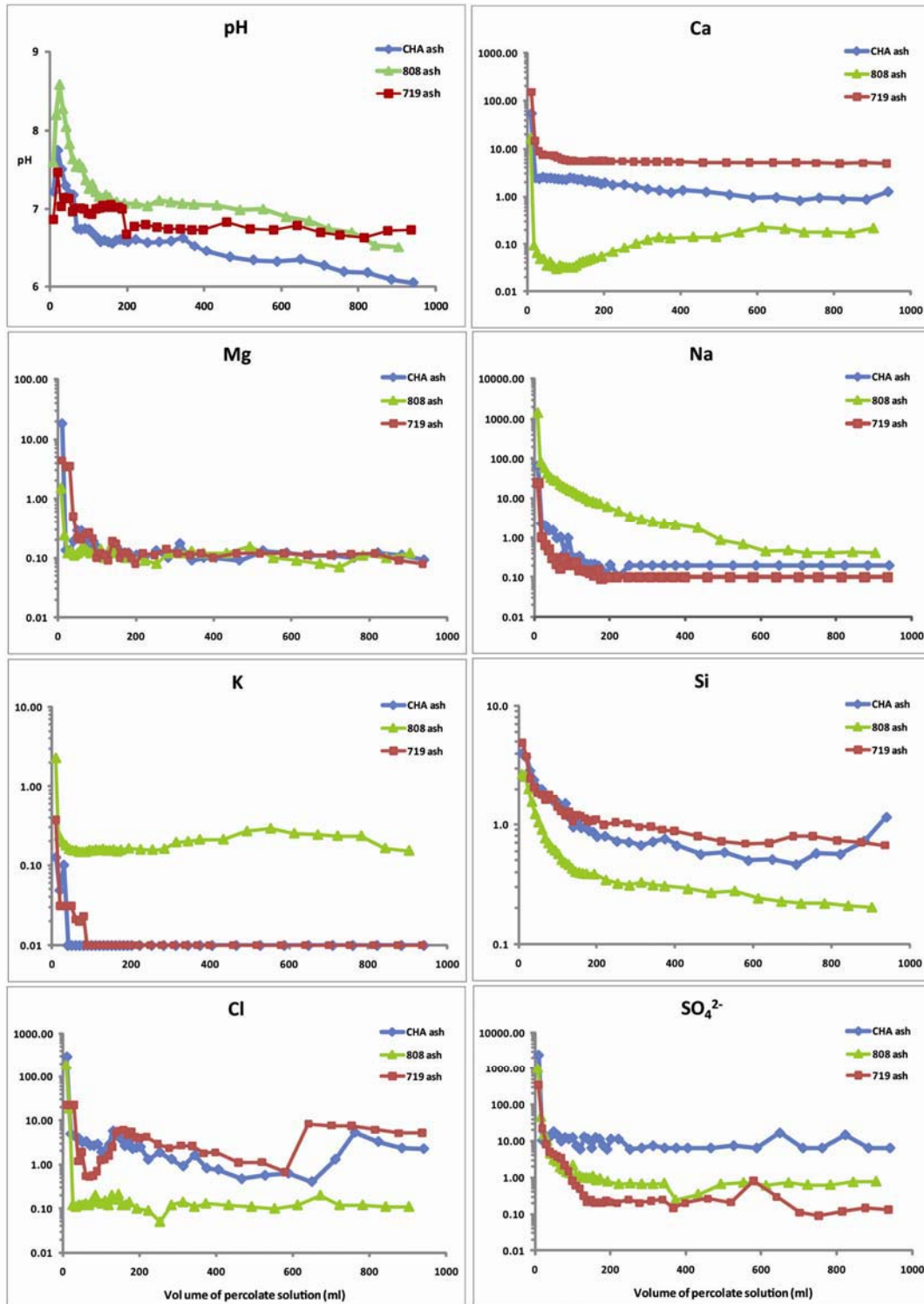**Figure 8.6** Behaviour of major elements Ca, Mg, Na, Si, Cl, SO_4^{2-} (mg l^{-1}) in column leaching tests.
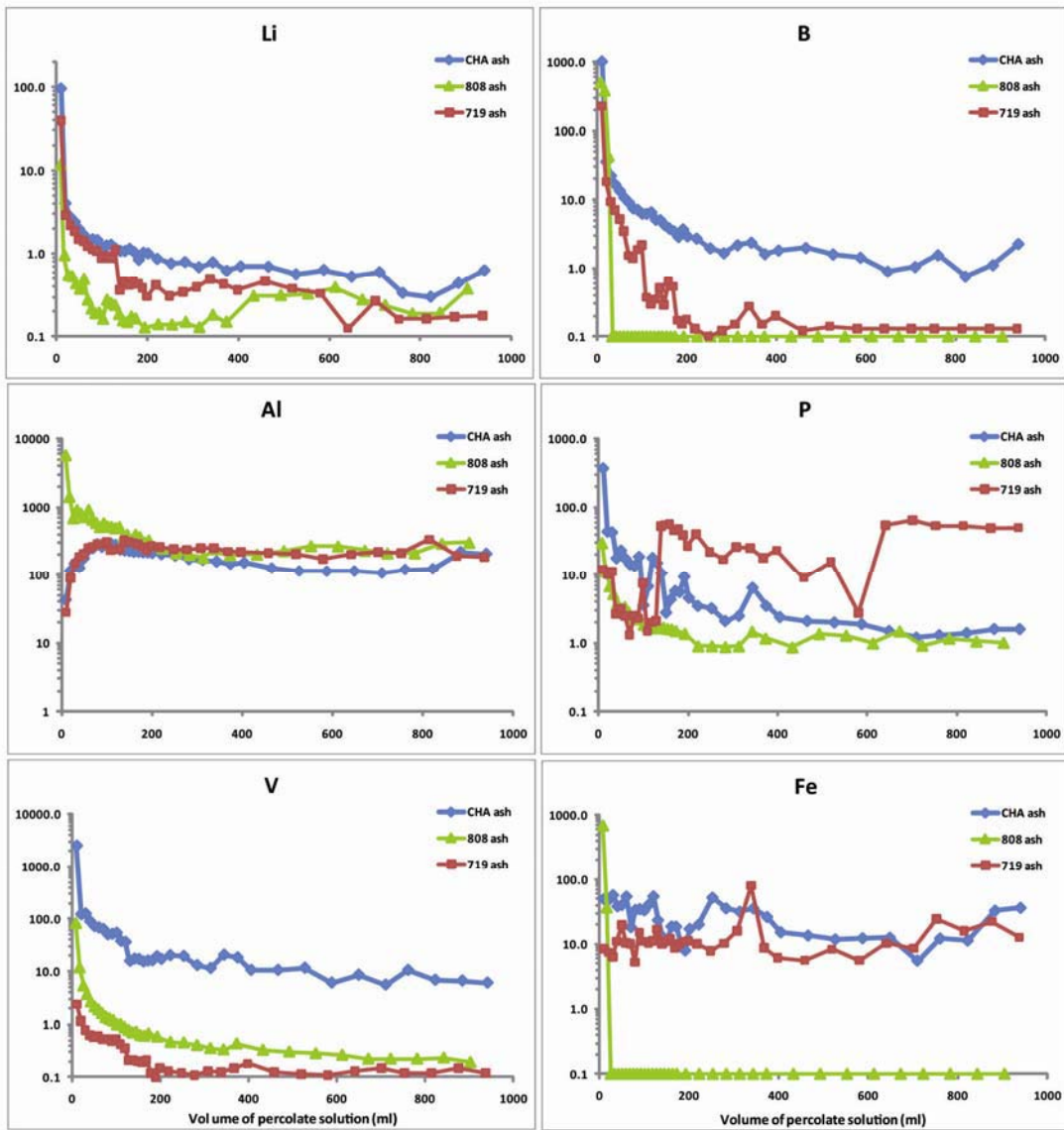
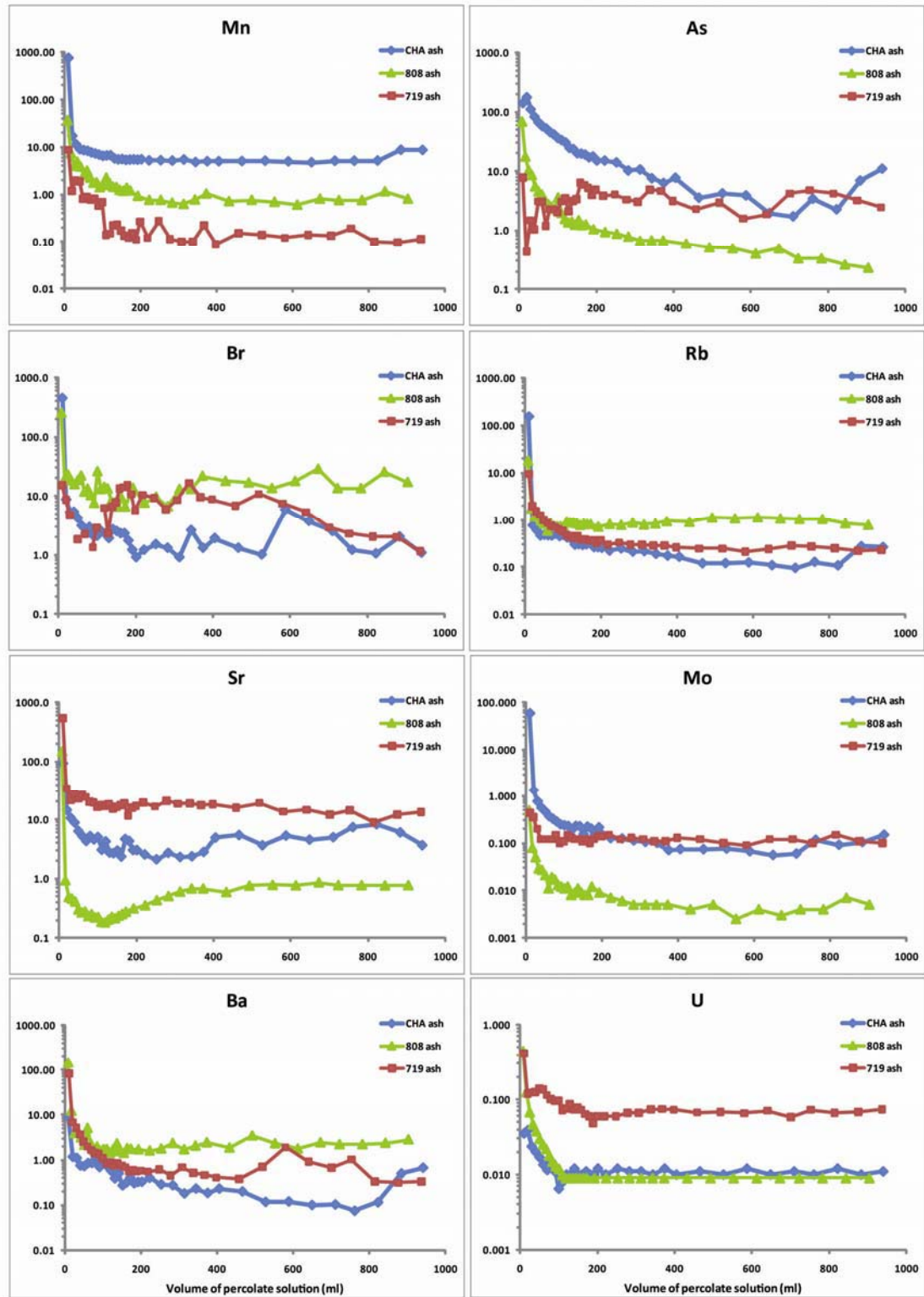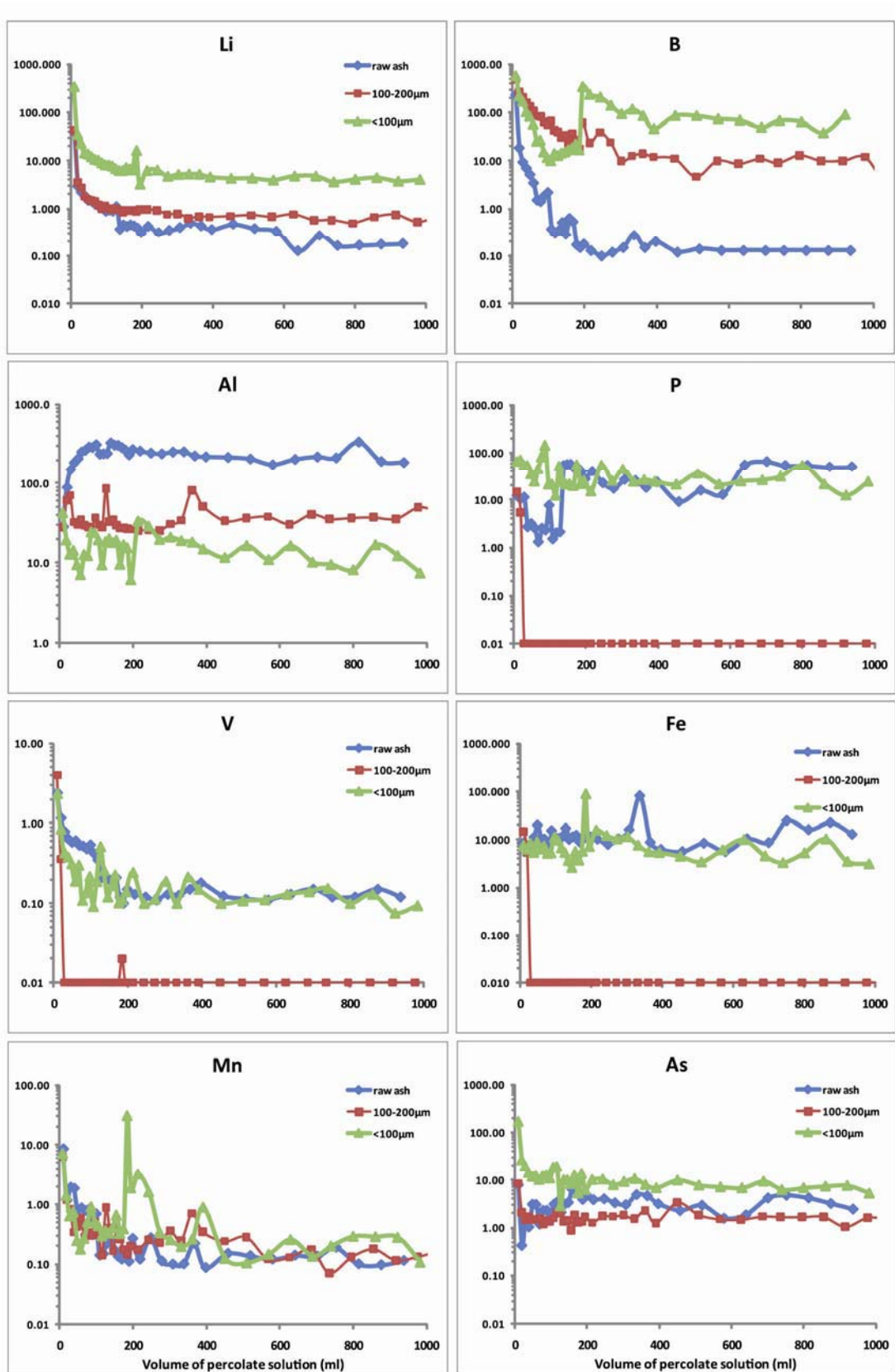**Figure 8.7** Behaviour of trace elements Li, B, Al, P, V, Fe, Mn, As ($\mu g\ l^{-1}$) in column leaching tests.
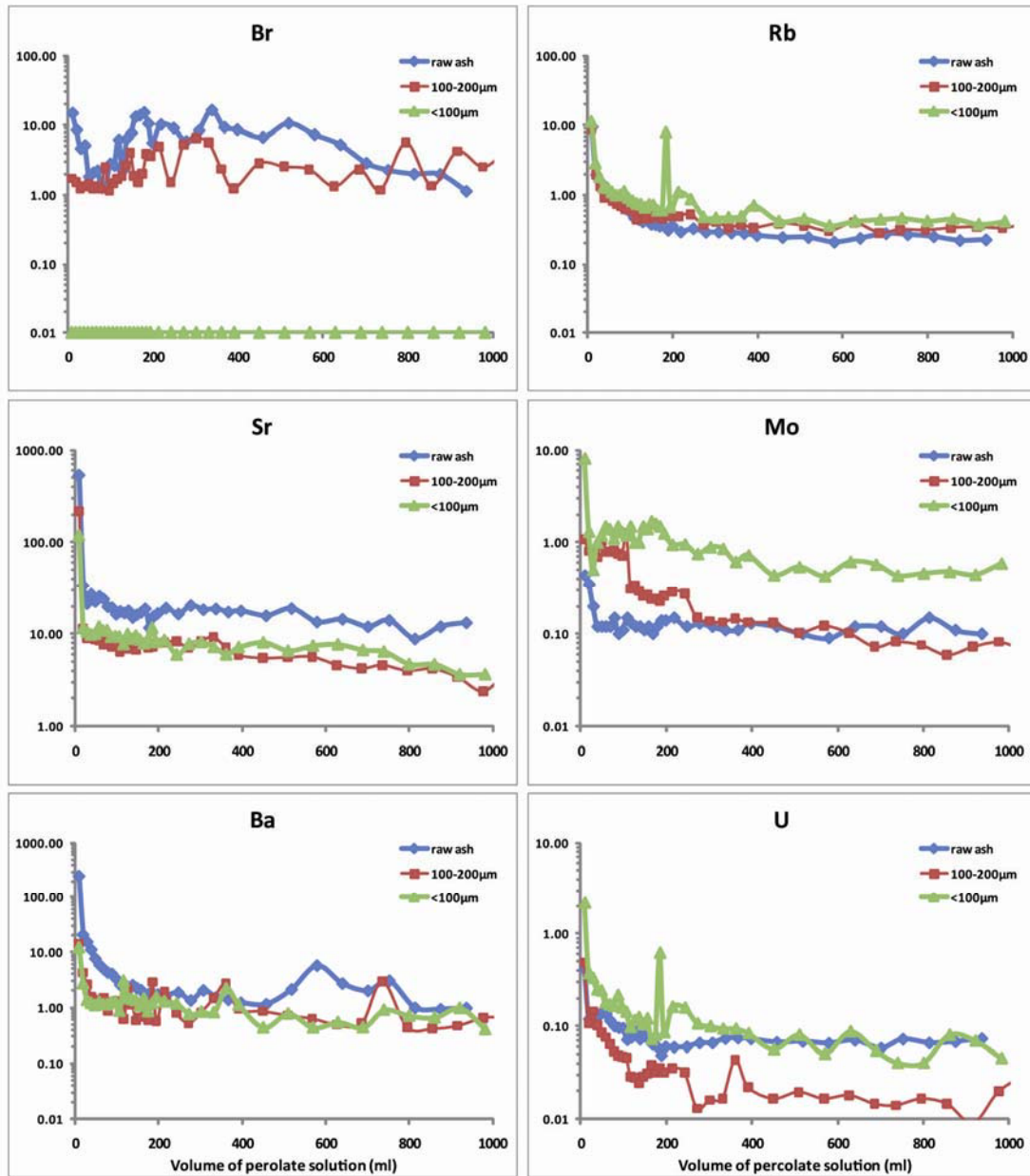
Figure 8.8 Behaviour of trace elements Rb, Sr, Mo, Ba, U ($\mu g\ l^{-1}$) in column leaching tests.

range 63 µm to <2 mm and are generally absent below 10 µm, whereas glass shards can be micrometric in size (Duggen et al., 2010).

The breakthrough curves of major and trace element concentrations *vs.* accumulated volume of percolate solution are shown in Figures 8.6-8.8. The elements rapidly released within the first stage of leaching were Ca, Na, Mg, SO_4^{2-}, Rb, Sr, and Ba. This behaviour was similar in the three run experiments indicating a weak association on the ash particle surfaces independently of the grain-size fraction. Combination of two processes (i.e., incongruent dissolution of volcanic glass and dissolution of coating on ash particles) could be the sources of these elements. As already mentioned, an ash very fast loss the coating associated with the original volcanic gas-ash interaction during and the very labile elements extracted form an ancient ash should be sourced from transformation processes during the weathering (i.e. hydrological and soil processes as oxidation and washing by meteoric water) (Kawano et al., 1997).

Those trace elements enriched in the <100 µm fraction were Li, B, P, V, Fe, As, Mo, and U, suggesting a volcanic glass dissolution source. Phosphorous and Fe could have a controversial origin. The column leaching tests conducted on the raw ashes show that they were less leached (or directly not leached as in the case of Fe) in the sample 808 (made up practically only by volcanic glass). The presence of P in the alkali feldspar network is a featur well known (Middelburg et al., 1988). More probably their source is from both glass and crystal dissolution.

Several studies on the very high concentrations of some of the above mentioned elements (As, Mo, V, B, and U) in groundwater of northwestern Argentine (this area lies to the Puna region) are associated with the presence of high contents of volcanic glasses in the loess of the aquifer sediments. These studies show that arid and/or semiarid (i.e., dry) climate and the basic pH found in many basins of this region favour the glass dissolution and leaching of elements as As, Mo, V, B, and U (Francisca and Perez, 2009; Nicolli et al., 2010). Therefore, this study confirms through laboratory experiments the association and the aforementioned trace elements with glass dissolution.

8.5 Summary and conclusions

Column leaching tests can be considered one of the best tools to assessing the geochemical impact of ash fallout, providing a fundamental basis to estimate the temporal behaviour of released elements (Figure 8.9). Dynamic leaching tests allow discrimination between the element weakly associated with the ash particle surfaces and those involved in more complex chemical reactions. In the experiments on the raw ashes, the elements can be grouped according to their temporal behaviour in:

(1) Elements with clear relationship with pH variation: Si and Al.

(2) Elements with high solubility during the first stages of the experiment: Ca, Na, Si, Cl⁻, SO_4^{2-}, Li, B, V, Mn, Rb, Sr, Mo, Ba, and U.

(3) Elements involved in other processes (e.g., hydrolysis): P, Fe, and As.

This classification shows general trends and some elements may be in one or other group depending of the considered sample. For example, Fe concentration presents high solubility in the first stages of the column experiment for the sample 808 whilst in the rest seems to be involved in other chemical reactions. However, the elements released during the first stages of the experiment (until to 200 ml of percolate, i.e., ~26 hours) indicate a rapid incongruent dissolution of volcanic glass by cation-exchange processes.

In the same way, column experiments carried out with the grain-size fractions could be used for grouping the elements according to their behaviour in:

(1) elements with similar behaviour in the three run experiments: (Ca, Na, Mg, SO_4^{2-}, Rb, Sr, Mo, and Ba);

(2) elements with a clearly enrichment in the <100 μm fraction and for which volcanic glass dissolution is the source: Si, Li, B, P, V, Fe, As, Mo and U.
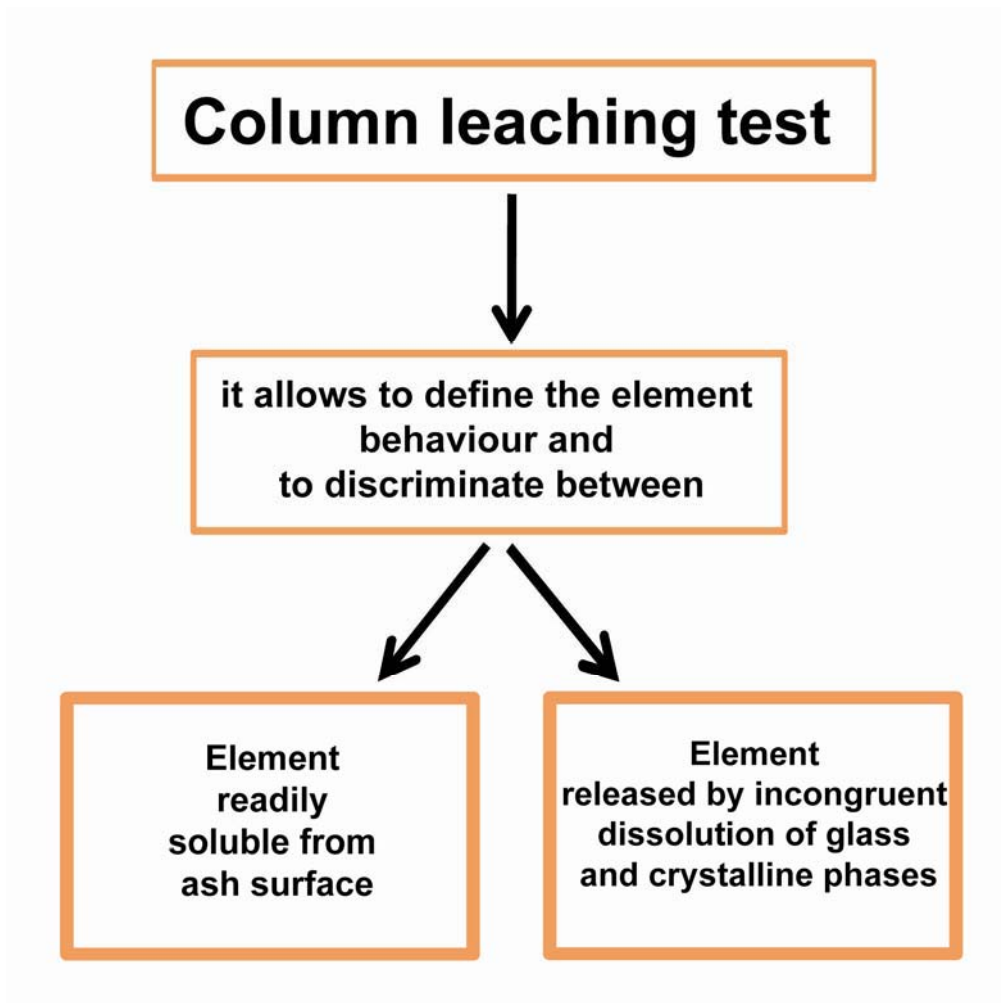
Figure 8.9 Information available from column leaching test.

Chapter 9. Sequential Extraction Scheme (SES)

9.1 Overview on sequential extraction procedures

Sequential extraction procedures have been designed to remove the most mobile elements in a first step or fraction and continue the fractionation in order of decreasing mobility. Various sequential extraction protocols have been proposed allowing the element fractionation into operationally defined geochemical phases for the environmental assessment basically of soils and sediments (Chao and Zhou, 1983; Hall et al., 1996; Sondag, 1981; Tessier et al., 1979; Ure et al., 1993). More recently, several sequential extraction procedures have been proposed for other solid samples of environmental interest such as fly ashes, sewage sludges and mining wastes (Fernandez-Turiel et al., 1994; Perez-Lopez et al., 2008; Zemberyova et al., 2010). Very few works have been addressed to the application of sequential extraction to volcanic ash (Bhattacharya et al., 2006).

The basic concept of the sequential extraction procedure is that the mobility of elements in the environment depends not only on their total concentrations but also on the chemical form in which they are bound in the solid phase (Filgueiras et al., 2002). From a practical point of view, element fractionation is achieved by treatments involving the use of selective chemical reagents, which are sequentially applied to the solid sample aliquot. In all schemes, extractants are applied in order of increasing reactivity so that the successive fractions obtained correspond to element association forms with lesser mobility. The extractants more commonly used in sequential extraction schemes fall generally within the following groups: unbuffered salts; weak acids; reducing agents; oxidising agents; and strong acids (Rauret, 1998). The choice of the extractant type is related to the matrix from which the compounds must be extracted. A suitable sequential extraction procedure is dependent on the main characteristics of the solid sample (e.g., physico-chemical and mineralogical features). The use of this procedure involves the chemical separation into element soluble in neutral and acid medium, exchangeable, reducible or associated with Fe and Mn

oxides, oxidisable or associated with organic matter and sulphur, and residual or associated with silicates. The latter includes the element fraction which can only be mobilised as a result of weathering, causing long-term effects on the environment (Filgueiras et al., 2002).

9.2 Methodological approach for designing a suitable SES

The schematic methodological approach used for designing a suitable SES is shown in Figure 9.1. After definition of the chemical fractions present in volcanic ash, the possible candidates as chemical reagents were suggested. Each one of these fractions was studied by leaching experiments in order to find the best chemical reagent in terms of extraction efficiency and to set the best operating conditions (e.g., leaching time).

9.2.1 Definition of chemical fractions of interest in volcanic ash

A rhyolitic volcanic ash (>70 % SiO_2) is composed mainly by volcanic glass although there are also common crystals as pure SiO_2 (quartz) and aluminosilicates (i.e., albite, sanidine, andesine and biotite). Therefore, the lack of oxidisable phases associated with organic matter and sulphur in rhyolitic volcanic ashes reduces the number of stages of the typical sequential extraction procedures normally performed on soils and sediments (Rauret et al., 2000; Tessier et al., 1979).

For rhyolitic volcanic ashes, four basic chemical fractions may be considered:

(1) F1: elements non-specifically adsorbed on the ash particle surfaces and easily releasable by ion-exchange processes.

(2) F2: elements associated with the amorphous oxides;

(3) F3: elements associated with the crystalline oxides;

(4) F4: Residual phase.

This scheme has been applied in several works (Kersten and Forstner, 1986; Krishnamurti et al., 1995; Usero et al., 1998; Wenzel et al., 2001).
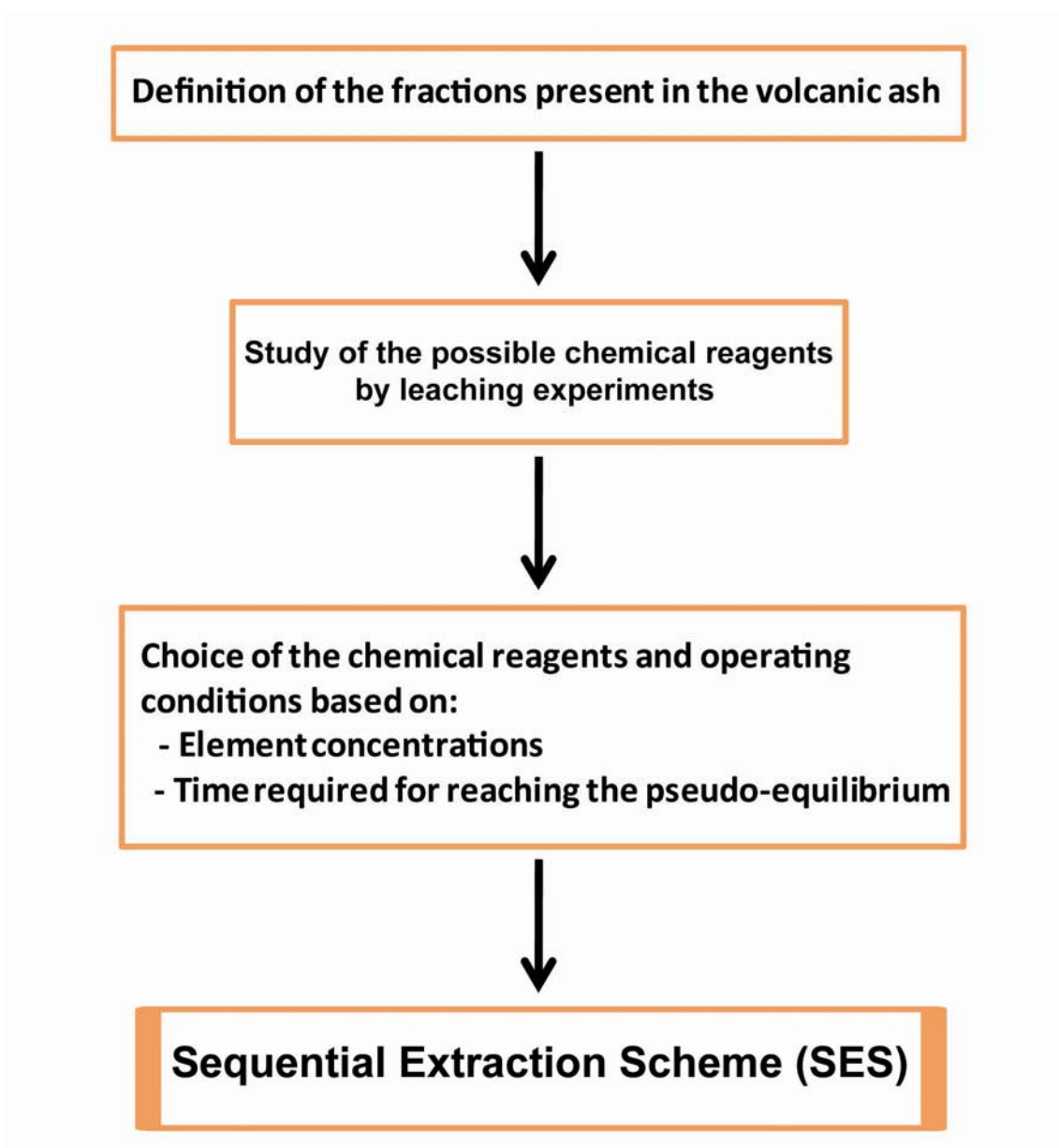
Figure 9.1 Methodological approach for designing a suitable sequential extraction scheme (SES).

9.2.2 Possible candidates as chemical reagents

Several chemical reagents have been used for releasing the chemical fractions reported above. In this research, the chemical extractants were chosen after a meticulous literature research and based on theoretical and practical considerations. Table 9.1 shows the possible candidates of chemical reagents for the SES.

Table 9.1 Chemical reagents studied by leaching experiments before the SES application.

Chemical fraction		Chemical reagent
F1 Easily exchangeable	E1a	deionised water
	E1b	NH_4NO_3-$(NH_4)_2SO_4$ 10^{-4}M adjusted to pH 7 with NaOH
F2 Amorphous Al, Fe, Mn oxides	E2a1	NH_4Ac 0.25M adjusted to pH 4.5 with HNO_3
	E2a2	NH_4Ox 0.25M adjusted to pH 4.5 with HNO_3
	E2a3	NH_4Cit 0.25M adjusted to pH 4.5 with HNO_3
F3 Crystalline Al, Fe, Mn oxides	E3	NH_4Ox 0.25M adjusted to pH 4.5 with HNO_3 + ascorbic acid 0.1M

9.2.2.1 Reagent for easily exchangeable fraction (F1)

Many sequential extraction procedures use deionised water as first extractant for quantifying the most mobile and potentially most available elements, including the weakly adsorbed elements retained on the ash particle surfaces (i.e., elements that can be easily released by ion-exchange processes). In this study the data obtained throughout the Single Batch Leaching Test (SBLT) with deionised water reported in the chapter 6 were compared with the results obtained using the NH_4NO_3 - $(NH_4)_2SO_4$ 10^{-4} M (E1b). The latter chemical reagent has been used by several studies in order to simulate better the environmental condition when interaction with rainwater occurs (Wenzel et al., 2001). Terrestrial rain compositions vary significantly because the regional geology can greatly affect the types of particulates that could be added to the atmosphere. The rainwater composition in the Andes cordillera contains H^+,

NH_4^+, NO_3^-, SO_4^{2-}, and a very low content of salts (Beiderwieden et al., 2005; Grau, 2001; Niello et al., 1999). Therefore, this extractant was tested at 10^{-4} M concentration with adjusted pH 7 by adding NaOH (Table 9.1).

9.2.2.2 Reagents for amorphous and crystalline oxides (F2 and F3)

A selective leaching of amorphous Al, Fe and Mn oxides fraction (F2) from soils has been proposed with acid ammonium organic extraction, such as NH_4-Acetate (E2a$_1$), NH_4-Oxalate (E2a$_2$), and NH_4-Citrate (E2a$_3$) in different operating conditions (Chao and Zhou, 1983; Rauret et al., 2000; Usero et al., 1998; Wenzel et al., 2001). A pioneering comparative study of extraction techniques of amorphous iron oxides from soils and sediments suggested the use of acid ammonium oxalate extraction 0.25 M at adjusted pH 4.5 (Chao and Zhou, 1983). In this research, the effects of three acid organic solutions (E2a$_1$, E2a$_2$, E2a$_3$) at 0.25 M concentration and pH 4.5 (adjusted adding HNO_3) were compared through leaching experiments.

Several authors proposed the acid ammonium oxalate extraction adding ascorbic acid (0.1 M) in darkness at 70 ºC (30 min shaking) to release the elements associated with the well crystallized Al and Fe hydrous oxides (Krishnamurti et al., 1995; Wenzel et al., 2001). The main advantage of this reagent over other reducing reagents is due to the high purity degree and its inactivity on silicates (Krishnamurti et al., 1995). Following these observations, this solution was used in this study.

9.2.3 Setting the operating conditions for sequential extraction

The influence of operation conditions (such as pH, temperature, leaching time, reagent concentration, stirring system, particle size of the solid and ratio of solid to extractant volume) become a critical issue when a new SES is proposed. In this study, the easily exchangeable and the amorphous oxides fraction were studied by leaching experiments in order to:

(1) choose the best reagent in terms of extraction efficiency, which was examined by comparing the element concentrations; and

(2) define the time necessary to achieve the pseudo- equilibrium condition; this factor was defined by recording the amount of leached element*s vs.* leaching time.

9.2.3.1 Methodology

For the leaching experiments an ancient volcanic ash (sample 808) was employed. Some of the experimental conditions were previously fixed. They include:

(1) use of no ground and no sieved volcanic ash;

(2) use the same solid/liquid (1g in 10ml) than for the single batch experiments with deionised water;

(3) at controlled pH;

(4) at room temperature.

The same methodology was applied for each one of the chemical reagents (E1b, E2a$_1$, E2a$_2$, and E2a$_3$) under study. The experiments were performed through a battery of batch leaching tests in order to give information on the breakthrough of the leached compounds. A series of batch tests were carried out by mixing and shaking at 20 rpm the same aliquot of sample (1 g of volcanic ash) with 10 ml of each leachant at different contact times (ranging from 0.5 to 24 h) in polyethylene test reactors. Two replicates were performed for each experiment. Leachate solutions, once centrifugated (3000 rpm) during 15 minutes, were filtered through Polyvinyledene Diflouride (PVDF) syringe filters with tube tip (Whatmann, 25 mm diameter and 0.45 μm pore size) and made up to 100 ml volume in 1% (v/v) HNO$_3$, and, finally, stored in polypropylene test tubes until the analysis.

Element selection covers:

(1) the less mobile major elements during the leaching processes (Al, Mn, and Fe) (Chang, 1999; Gayer et al., 1958; Wollast and Chou, 1992);

(2) trace elements (Zn, As, V, and Pb) dominantly combined with halogens and sulphate forming salts and/or acid droplets coating the ash-grain surfaces (Delmelle et al., 2007; Hinkley, 1991; Hinkley et al., 1994; Symonds et al., 1992; Symonds et al., 1994; Symonds et al., 1987) and associated with volcanic glass dissolution in a dry weathering environment of Argentina (i.e., As and V) (Francisca and Perez, 2009; Nicolli et al., 2011; Nicolli et al., 2001).

Aluminum, Fe and Mn concentrations were determined by inductively coupled plasma optical emission spectrometry (ICP-OES, Optima 3100 X, Perkin Elmer) and the trace elements (Zn, As, V, Pb) were determined by inductively coupled plasma mass spectrometry (ICP-MS, Elan 6000, Perkin Elmer). Individual calibration was used for each extractant solution and the Limits of Detection and Limits of Quantification were calculated based on the standard deviation (sd) of 10 replicates of the blank and the slope of the calibration curve (S) of each reagent according to the formula: LoD = 3(sd/S) and LoQ = 10(sd/S) (Table 9.2). These LoD and LoQ calculations are different than those calculated for the bulk chemical and ash leachates analyses (reported in the methodological chapter). This apparent discrepancy is due to the use of solutions broadly different than the deionised water solution normally employed in the conventional chemical analyses. In this case the variability of the instrument sensitivity (i.e., LoD and LoQ values) was evaluated taken in consideration the extractant used in the leaching experiments.

Table 9.2 Analytical performance achievable for quantification of major and trace elements in extractant solutions by ICP-OES and ICP-MS (10 replicates); LoD, Limit of Detection and LoQ, Limit of Quantification.

Extractant	Al		Mn		Fe		Zn		V		As		Pb	
solution	LoD	LoQ	LoD	LoQ	LoD	LoQ	LoD	LoQ	LoD	LoQ	LoD	LoQ	LoD	LoQ
E1b	0.004	0.053	0.002	0.09	0.008	0.016	0.021	0.070	0.006	0.021	0.008	0.027	0.003	0.009
E2a1	0.091	0.303	0.006	0.010	0.005	0.016	0.098	0.187	0.011	0.036	0.010	0.034	0.018	0.060
E2a2	0.060	0.211	0.005	0.012	0.003	0.012	0.090	0.134	0.001	0.021	0.009	0.015	0.009	0.031
E2a3	0.002	0.045	0.003	0.098	0.007	0.019	0.010	0.032	0.002	0.006	0.003	0.010	0.001	0.002

Mn, Fe, Al: mg l^{-1}

Zn, As, V, Pb: µg l^{-1}

9.2.3.2 Leaching data for the easily exchangeable fraction (F1)

Leaching data obtained using the E1b extractant expressed as the amount of leached elements *vs.* time are reported in Figure 9.2. Manganese, Fe, Al and Pb concentrations were below to the respective detection limits (Table 9.2). Appreciable content was verified only for As, V, and Zn, which present similar temporal profiles. Comparing these results with those obtained by the SBLT with deionised water higher concentrations were obtained with the latter reagent. The hypothesis drawn is that some of these elements (i.e., Mn, Fe, and Al) precipitated during the treatment with E1b. In order words, the E1b reagent is not suitable in the case of volcanic ash and following the results of the SBLT reported in the chapter 6, the easily exchangeable fraction was extracted shaking the sample with deionised water for 4 hours at room temperature. Moreover, the worldwide availability of deionised water allows comparing the results among different laboratories, it is fast in laboratory conditions and relatively inexpensive.

9.2.3.3 Leaching data for the amorphous oxides fraction (F2)

The leaching data obtained with the ammonium reagents are reported in Figure 9.3. Extraction efficiency for the E2a$_1$ acid solution is very poor (below to the respective detection limits) for all the elements analysed, except Al. The E2a$_2$ extraction exhibits a considerable higher leaching capability for Al, Mn, Fe, Zn, and V than the other two reagents (E2a$_1$ and E2a$_3$). Leaching curves obtained in the case of As and Pb extracted with E2a$_2$ and E2a$_3$ follow similar temporal trend and concentration. Most of the temporal behaviour shows the pseudo-equilibrium between 2 and 4 hours, but relatively higher element concentrations were observed with E2a$_2$ extraction. Taking into account that a suitable SES has to be fast and reliable in laboratory conditions and in agreement with the suggestion proposed by Chao and Zhou (1983), the amorphous oxides extraction was performed with E2a$_2$ 0.25 M solution at pH 4.5 (2 h shaking).
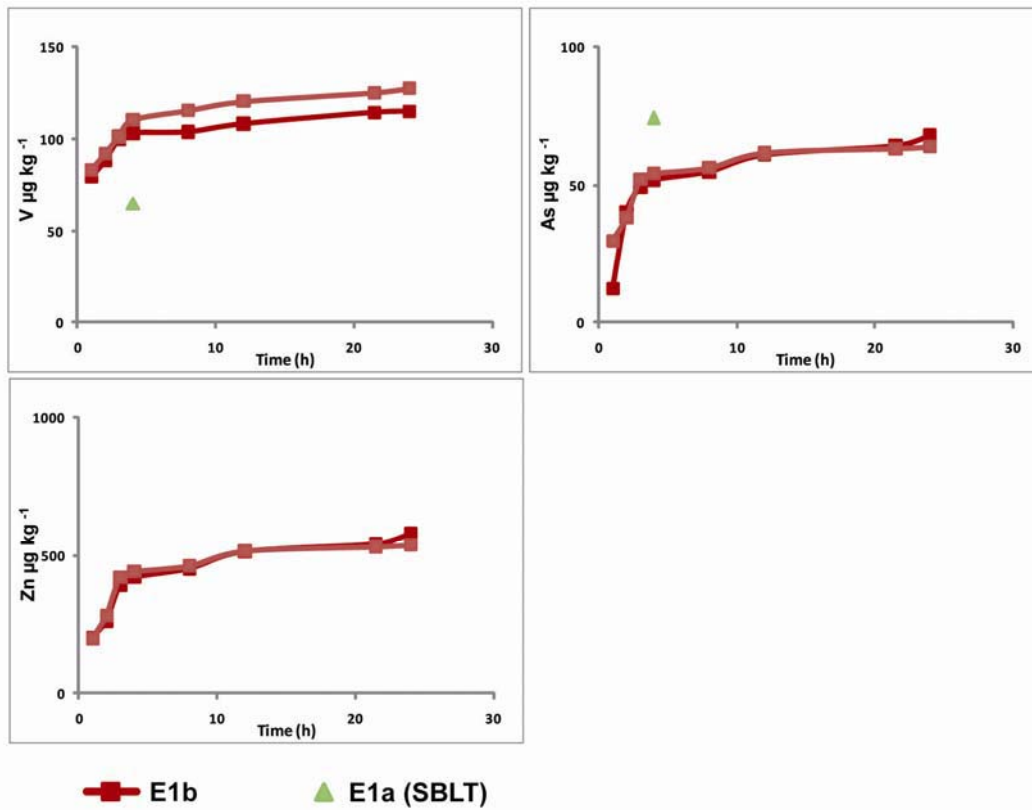
Figure 9.2 Two replicates of leaching data obtained with NH_4NO_3 $(NH_4)_2SO_4$ 10^{-4} M at pH 7 adjusted adding NaOH (extractant E1) with 808 rhyolitic ash compared with the value obtained throughout the Single Batch Leaching Test (SBLT) with deionised water.
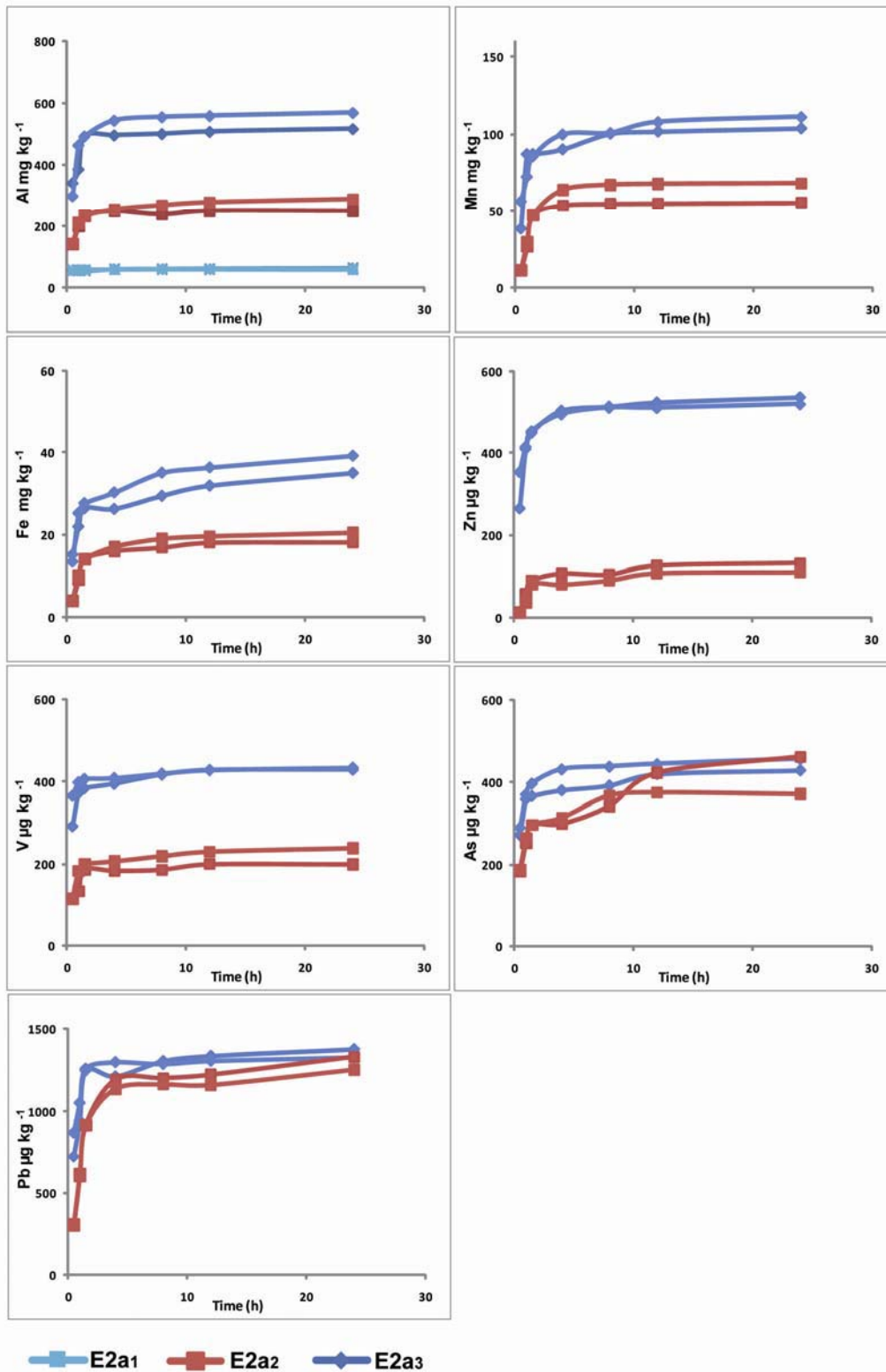
Figure 9.3 Comparative leaching results obtained with ammonium reagents (E2a$_1$, NH$_4$-Acetate; E2a$_2$ NH$_4$-Oxalate; and E2a$_3$ NH$_4$-Citrate) 0.25M at pH 4.5 adjusted adding HNO$_3$ with 808 rhyolitic ash (2 replicates).

192

9.3 Application of the proposed SES

9.3.1 Methodology

The proposed SES, including the operating conditions, is summarised in Table 9.3.

Table 9.3 Sequential Extraction Scheme (SES) proposed for volcanic ashes.

Fraction	Extractant	Extraction conditions
F1 Easily exchangeable	Deionised water	4 h shaking, 20 °C
F2 Amorphous oxides	NH_4-oxalate 0.25 M at pH 4.5 adjusted with HNO_3	2 h shaking, 20 °C
F3 Crystalline oxides	NH_4-oxalate 0.25 M+ ascorbic acid 0.1 M at pH 4.5 adjusted with HNO_3	30 min in water basin, 70 °C

Two rhyolitic volcanic ashes were used in this study: the Chaiten volcanic ash (CHA-2R) and the ancient volcanic ash (808) of the southern Puna. Following the same methodological approach of leaching experiments, 1 g of ash was shaken with 10 ml of each extractant solution. After each step the extracts were separated from the solid residue by centrifugation at 3500 rpm for 15 minutes. The extract solutions were filtered through Polyvinyledene Diflouride (PVDF) syringe filters with tube tip (Whatmann, 25 mm diameter and 0.45 μm pore size) and stored in polypropylene test tubes until the analysis.

The residue was washed adding 10 ml of deionised water, shaking for 10 minutes and centrifuged as before. Three replicates were performed for each step.

The element concentrations in the three fractions of the SES are reported in Table 9.4. The residual fraction (F4) was calculated by subtracting the bulk values to the sum of the three fractions extracted. The element partitioning (expressed in per cent) is shown in Figures 9.4 and 9.5.

Table 9.4 Element concentrations in the four fractions of the sequential extraction scheme and Bulk element concentrations (n=3 replicates, except for F1 and the bulk value where n=1).

Fraction	Unit	808		CHA-2R	
		mean	rsd%	mean	rsd%
		Al			
F1	mg kg^{-1}	12.8	-	5.25	-
F2	mg kg^{-1}	2368	48.2	533	24.7
F3	mg kg^{-1}	4030	44.7	1103	22.6
F4	mg kg^{-1}	65435	4.50	66328	0.57
Bulk	mg kg^{-1}	71847	-	67970	-
Extractable (%)		8.92	-	2.42	-
Residual (%)		91.1	-	97.6	-
		Mn			
F1	mg kg^{-1}	0.06	-	0.20	-
F2	mg kg^{-1}	166	30.7	27.5	13.2
F3	mg kg^{-1}	38.3	14.5	47.1	6.04
F4	mg kg^{-1}	385	12.8	367	1.68
Bulk	mg kg^{-1}	590	-	442	-
Extractable (%)		34.7	-	16.9	-
Residual (%)		65.3	-	83.1	-
		Fe			
F1	mg kg^{-1}	0.14	-	1.15	-
F2	mg kg^{-1}	79.5	30.7	272	10.8
F3	mg kg^{-1}	778	27.4	1989	7.9
F4	mg kg^{-1}	5669	4.19	8817	2.1
Bulk	mg kg^{-1}	6527	-	11079	-
Extractable (%)		13.1	-	20.4	-
Residual (%)		86.9	-	70.6	-

Table 9.4 Continuation

Fraction	Unit	808		CHA-2R	
		mean	rsd%	mean	rsd%
		Zn			
F1	µg kg^{-1}	0.01	-	295	-
F2	µg kg^{-1}	1631	12.7	5394	13.1
F3	µg kg^{-1}	4359	7.5	7842	10.9
F4	µg kg^{-1}	47814	1.1	40618	3.71
Bulk	µg kg^{-1}	53804	-	54149	-
Extractable (%)		11.1	-	24.9	-
Residual (%)		88.9	-	75.1	-
		V			
F1	µg kg^{-1}	65.0	-	59.8	-
F2	µg kg^{-1}	355	11.9	210	1.65
F3	µg kg^{-1}	886	8.50	1039	20.7
F4	µg kg^{-1}	6885	1.30	11686.2	1.9
Bulk	µg kg^{-1}	8192	-	12996	-
Extractable (%)		15.6	6.85	10.1	-
Residual (%)		84.1	1.30	89.9	-
		As			
F1	µg kg^{-1}	74.3	-	726	-
F2	µg kg^{-1}	646	1.6	6205	2.55
F3	µg kg^{-1}	1235	2.35	3828	4.55
F4	µg kg^{-1}	4387	0.46	37074	0.54
Bulk	µg kg^{-1}	6342	-	47833	--
Extractable (%)		30.8	-	22.5	-
Residual (%)		69.2	-	77.5	-
		Pb			
F1	µg kg^{-1}	81.2	-	155	-
F2	µg kg^{-1}	2695	8.26	2321	10.6
F3	µg kg^{-1}	2851	5.80	1585	7.20
F4	µg kg^{-1}	19654	1.96	15515	2.29
Bulk	µg kg^{-1}	25281	-	19576	-
Extractable (%)		22.3	-	20.7	-
Residual (%)		77.7	-	79.3	-

9.3.2 Extractable fractions

9.3.2.2 F1: easily exchangeable

Deionised water allows release the elements associated with the ash particle surfaces. The common elements of the rock-forming minerals were present at very low values in the solution at the end of this extraction step (Table 9.4). Among the trace elements under study only As and V present appreciable mobility (about 3 % in pristine ash) indicating the association with a very labile form on the ash particle surfaces (Figure 9.5). In pristine Chaiten ash sample, these compounds are mainly related to the volcanic gas-ash particle interaction in volcanic plume, in which many volatile elements, such as As and V, are also released (Allard et al., 2000; Mambo and Yoshida, 1993; Symonds et al., 1987). These elements present the same geochemical behaviour and usually have close relation with sulphur (Mambo and Yoshida, 1993). Therefore, in volcanic plume they could co-precipitate with elemental sulphur in the acid condensate on the ash particle surfaces (Symonds et al., 1994).

9.3.2.2 F2: amorphous oxides

Ammonium oxalate extractable concentrations of Mn are higher than concentrations of Fe and Al. For both volcanic ashes these elements were extracted in the following order Mn >> Al ≈ Fe. However, Mn was three times more extracted in the ancient ash than pristine ash (Figure 9.4). This imply that (1) for both volcanic ashes the amorphous oxides and hydroxides of Mn are more abundant and potentially of greater importance for trace element adsorption than those of Al and Fe, and (2) the ancient volcanic ash was undergone irreversible geochemical weathering reactions.

Several studies provide that, in general, the weathering processes of volcanic glass can be simply divided into two fundamental reactions: (1) dissolution of starting materials by interaction with water and (2) precipitation of hydrous silicates, including non-crystalline oxi-hydroxide compounds (Casey and Bunker
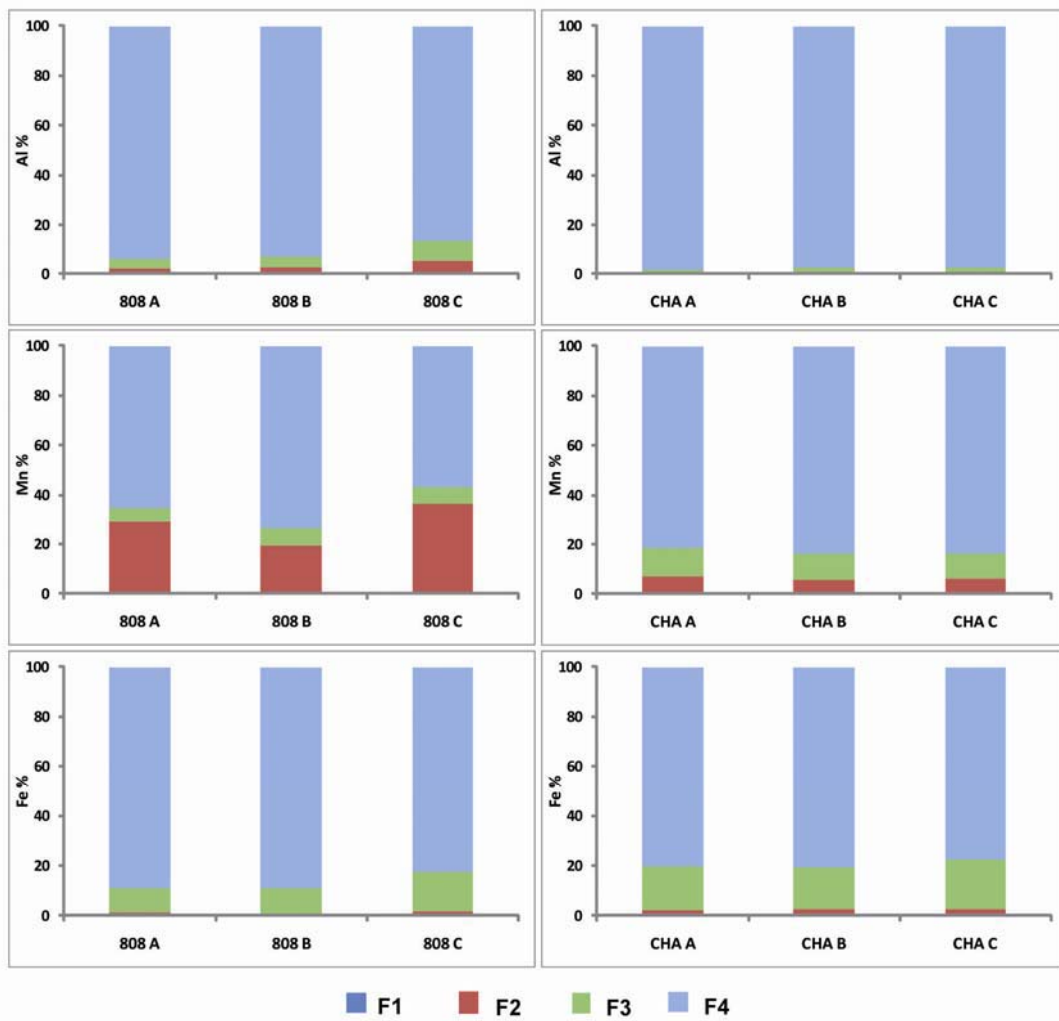
Figure 9.4 Partiotining of Al, Mn, and Fe among the four fractions in the Sequential Extraction Scheme (SES) proposed.
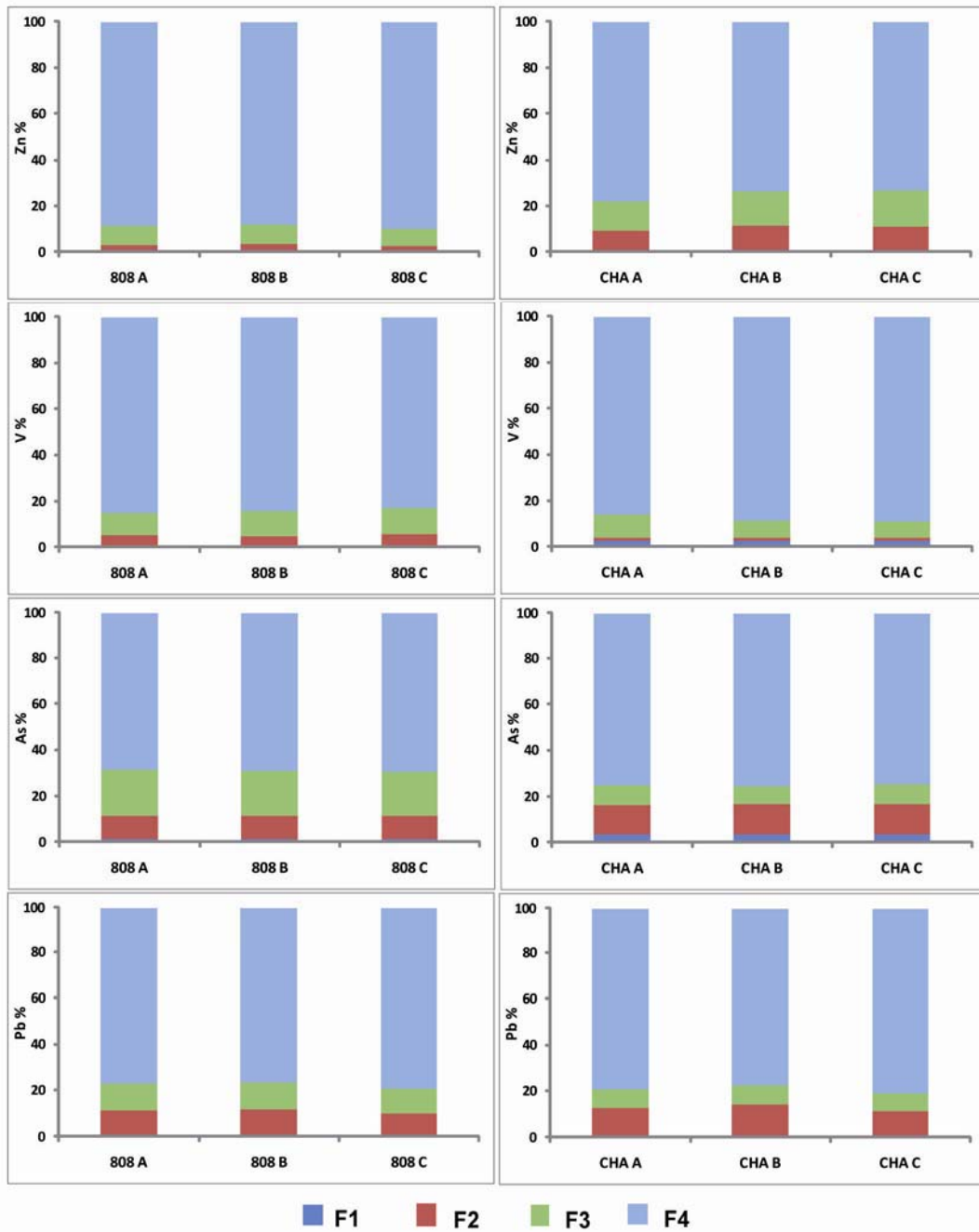
Figure 9.5 Trace elements (Zn, V, As, and Pb) partiotining among the four fractions in the Sequential Extraction Schem (SES) proposed.

1990; Casey et al., 1993; Kawano et al., 1997). A complex study about the weathering of a dacitic tephra deposit, conducted during 10 yr period under field conditions in cryic-udic climate regime examines the forms of active Al and Fe by selective dissolution techniques (i.e., the oxalate extractable fraction) during the time. This study verifies a relatively large increase of Al and Fe fraction in the weathered tephra respect to the unweathered counterpart concluding that active Al and Fe were accumulated during the weathering period as non-crystalline oxy-hydroxides (e.g., ferrihydrite and Al-hydroxide polymers) (Dahlgren et al., 1997). Similar processes could explain the observation in the ancient ash. The trace elements associated with the oxy-hydroxide compounds were extracted in order: Pb ≈ As > V > Zn in both ashes (Figures 9.4 and 9.5).

9.3.2.3 F3: crystalline oxides

Mixture of NH_4-oxalate and ascorbic acid promotes the release of elements associated with crystalline oxides (Wenzel et al., 2001). About 10-20 % of Fe and Mn were extracted in this step in both ash samples (Figures 9.4 and 9.5). Studies about the reference European volcanic soils show that for large contents of Fe the ammonium oxalate extraction procedure (i.e., the F2 in the current study) underestimates the amorphous fraction (Hernandez-Moreno et al., 2007; Meijer et al., 2007). These works also suggest that multiple oxalate extractions remove the amorphous hydroxides and the associated trace elements 2-10 times more than a single oxalate extraction. Thus, part of the amorphous fraction is probably included in the third step, explaining the high percentage of Fe extracted.

Considering the operating conditions of the third step, the trace element release was affected by other factors. This step has been conducted (1) in the presence of ascorbic acid and (2) at high temperature (70 ºC). The ascorbic acid acts as a reducing agent, whilst the latter enhances the reaction rate. Pioneering studies on dissolution of silica species in presence of organic acids suggest the occurrence of an activated complex surface that increases the dissolution rate in aqueous reducing conditions between 10 and 60 ºC (Bennett and Siegel,

1987; Bennett and Siegel, 1989). These reactions increase the destabilization of framework Si-O bonds increasing the solubility of silica compounds and the mobility of the trace elements associated with the Si-O framework.

The Si–O tetrahedra are considered the building blocks of the structure in the crystalline silicate and volcanic glass. Within the crystalline phases they are attached to other tetrahedra by bridging oxygens to form a regular, geometrically repeating pattern, over a large scale of unit cells (Oelkers et al., 2009; Wolff-Boenisch et al., 2006). In contrast, the silicate glass does not exhibit the typical large-scale regularity of minerals (White, 1984). Volcanic glass may be viewed as a metastable super-cooled liquid in which the rapid quenching inhibits the ordered arrangement of the typical three-dimensional Si–O network of minerals, involving a faster dissolution in our experimental conditions. The mobility of the trace elements follows the order: As > Pb > Zn > V in the pristine ash and As > Pb > V ≈ Zn in the ancient ash.

9.3.2.4 F4: Residual phase

Rhyolitic volcanic ash consists mainly of silicate compounds (including volcanic glass and crystalline phases). Hence, most of the elements under study are associated with the residual fraction. This fraction includes the elements strongly bounded to the silicate matrix, and for which only long term weathering could cause mobilization (Filgueiras et al., 2002). As expected, high residual fractions were verified for the elements of the rock forming minerals. Alluminium showed a very low mobility, being associated for more of 90% to the F4. Among the trace elements under study, As and Pb presented significant mobility.

9.4 Summary and conclusions

The sum of the amounts (expressed as percent of the total) of an element extracted in the first three steps (excluding the residual fraction) can be considered a potentially mobile fraction susceptible of environmental changes such as redox potential or pH (Filgueiras et al., 2002; Hernandez-Moreno et al.,

2007). The values reported in Table 9.4 show a general low element mobilization for both ashes. However, ancient ash showed higher element mobility than pristine ash. This study demonstrates that after the fast release of the soluble compounds present on the particle surfaces of pristine ash, the weathering of glass and crystalline components causes a very slow release of the elements in the environment. Therefore, the residence time of the volcanic ash in the environment seems to have a reflection on the element leachability. Once deposited, the volcanic ash undergoes irreversible geochemical weathering reactions (e.g., oxidation followed by slow dissolution), causing destabilization of the silicate framework and release of the elements associated with it.

From a methodological point of view, the sequential leaching approach is a powerful tool to evaluate the element mobility from both ancient and pristine volcanic ashes. The proposed SES provides reliable information on the elements released in the different chemical fractions of volcanic ashes. These operationally defined fractions represent non-specifically bound, specifically bound as amorphous hydrous oxide-bound, crystalline hydrous oxide-bound and, finally, the residual. Fraction 1 can be used for predicting the most mobile and potentially the most environmentally available elements, including the weakly adsorbed elements that can be easily released by ion-exchange processes. Such information is useful to assess the readily bio-available fraction. Fractions 2-3 may provide information on potential lability from the different solid phases as a result of weathering and change of environmental factors (i.e., redox, pH). Within the inherent limitations of the chemical fractionation, the reagents used are fairly powerful for the determination of the chemical form in which the element occurs and this study should be considered a good promising start for a further development and application of this methodology to volcanic ash.

PART 5. CONCLUSIONS

10. Conclusions

The study of the geochemical environmental hazard posed by different types of volcanic ashes from the Andes has been carried out through a multi-analytical approach. This approach has allowed:

(1) to identify which criteria are useful to distinguish between volcanic and non-volcanic products collected during a field campaign;

(2) to develop a specific analytical methodology for the whole rock characterization of ashes;

(3) to propose a new ash leaching methodology that can be useful both for recent and ancient volcanic ashes.

(4) to recognize the geochemical impact occurring after the deposition of volcanic ash on the environment through leaching experiments.

The main conclusions extracted from this research can be summarised as follows:

• SEM examination allows recognizing the ash by the presence of the typical components as, primarily, glass, and the crystalline mineral phases. It makes available the identification of no volcanic compomnents in supposed ash deposits as clay, biogenic silica, calcite, etc. Among 29 samples collected during the field campaign in the southern Puna and neighbouring areas (Catamarca and Salta provinces, Argentina) and Uruguay only 11 were found to be pure volcanic ashes. Once identified pure volcanic ashes a combination of different analytical techniques performed on the bulk ashes highlights the main environmental concerns related to these. The physical properties (i.e., SEM, BET, GSA) allowed describing the shape morphology of ash particles, the amount of specific surface area and the grain size distribution. The results allowed making predictions on the eruptive style and dynamics of the investigated eruptive products, as well as to predict the environmental and health hazard associated with the fine particle content (respirable fraction, <15 µm).   The order is as follows: UR-1> 721> 808> 809> CHA-1F> 733> CHA-G> AS-28> UR-6> 719> CHA-2R> CHA-E> UR-7> AS-29> COP >LLA> AS-33> HUD> LON. The relative content of glass and crystalline phases on the samples

was also determined by XRD analysis complementing previous SEM analyses. This is an important step because a small amount of hazardous components (i.e., cristobalite) in AS-28, AS-29, and Chaiten ashes has been detected. The bulk chemical characterisation allows to classify the volcanic ash (according to the major element content) and to know the trace element concentrations, including those potentially toxic. Moreover, the study of molecular spectroscopy by FTIR provides information about the water chemical bonds (and therefore qualitatively estimation of volatile content) present in the ashes. High ash reactivity not only depends on glass content but it is a particularly remarkable feature in ancient ashes, where the most labile elements, such as those showing preferential enrichment on tephra surfaces (e.g., SO_4^{2-}, Cl^- and F^-), were probably released during the early burial of the deposit. As a result, this study demonstrates that the role of glass in the release of major, minor and trace elements is potentially greater in ancient ashes than in current ones.

- The main body of this research has been to propose a proved methodology for a single batch leaching test (SBLT) with deionised water in order to obtain information on short term leaching behaviour of volcanic ash identifying, qualitatively and quantitatively, the potentially hazardous elements being rapidly released from both recently erupted and ancient volcanic ashes. Batch leaching principles of volcanic ashes have been examined, being the robustness of leaching tests assessed in terms of reproducibility. The recommended methodology for batch leaching tests of volcanic ashes is based on the use of a L/S ratio of 10, using 1 g of ash and 10 ml of deionised water, shaking the mixture during 4 hours. Entire procedure is completed within few hours and its design is simple, concise and reliable.

- The application of the SBLT (with deionised water) method developed in this research have allowed to define the potential geochemical impact of the volcanic ashes investigated on the environment. Through the statistical treatment of the data set it was demonstrated a clear difference between the ancient and recent ash leaching behaviour. Ancient volcanic ashes have long been deposited on land and were subject to hydrological and soil processes,

which effectively removed any original soluble salt attached to the surface of pristine ash particles. Specific conductivity values and the geochemical data of water ash leachates show that ancient ashes have a larger dissolution capability. This suggests that the residence time of the volcanic ash in the environment have a reflection on the element leachability. Once deposited, the volcanic ash undergoes irreversible geochemical weathering reactions (e.g., oxidation followed by slow dissolution), causing destabilization of the silicate framework and release of the element associated with it. Water ash leachate data were also used to estimate the amount of each element environmentally available in each one of the investigated volcanic ashes when ash-water interaction occurs. These features allowed model the contribution to regional geochemical balance of the entire ashfall deposits. Both ancient and recent ashes could transfer to the environment high amount of major elements, mainly Ca and Na. Some of the elements available from these ash deposits are macro- and micronutrients (e.g., Fe, Mn, and P), evidencing the fertilizing potential of the ashes. Many others are potentially toxic trace elements (PTTEs) even at very low concentrations. These are As, Cu, F, Mo, Ni, Pb, and Zn. Some of the latter elements are included in the drinking water guidelines due to their potential toxicity and must be especially monitored in the environmental assessment of these ashfall deposits. Among the ash deposits substantial variability was observed. Puna ash deposits of the samples 719, 721, 808, 809 and AS-28 show high Pb, As, and Cu environmental available concentrations. Lead, Cu, and Ni are enriched in 733 and Uruguay ash deposits. AS-29 and AS-33 ash deposits have the higher contents of available Zn. Chaiten, Llaima, and Lonquimay tephra deposits could release mainly Pb (even the Chaiten deposit could be considered also a reservoir of As). Finally, Hudson and Copahue might release mainly Ni and Cu in the environment.

Finally, nitric acid leachates allow understanding the behavior of the elements involved during the glass and mineral phase dissolution. Acid leach tests remove larger amounts of material from ash than water tests and allow mobilising also the less mobile element, as REE, in the AS-29, AS-33, COP, and HUD ashes. In addition, they reproduce environmental circumstances in which very acidic conditions occur (e.g., acidic surface water in the Copahue

volcano area). For ancient volcanic ashes, high mobile elements (RML > 5%) in the nitric acid leachates are: Ca, Mg, Fe, Mn, P, As, Ba, Co, Cu, Mo, Ni, Sb, Sr, V, Y, Zn, and REE. For more recent volcanic high mobile elements (RML > 5 %) are: Ca, Mg, Fe, P, Co, Ni, Cu, Zn, As, Mo, V, Cd, and Pb.

- Dynamic leaching tests have been performed in order to estimate the temporal behaviour of element release. They allow distinguish between the elements weakly associated with the ash particle surfaces and those involved in more complex chemical reactions (i.e., weathering). Two types of leaching tests have been carried out. In the first type, column leaching tests of raw ashes (ancient vs. recent) allowed to group the elements according to their temporal behaviour in:

(1) Elements with clear relationship with pH variation: Si and Al.

(2) Elements with high solubility during the first stages of the experiment: Ca, Na, Si, Cl⁻, SO_4^{2-}, Li, B, V, Mn, Rb, Sr, Mo, Ba, and U.

(3) Elements involved in other processes (e.g., hydrolysis): P, Fe, and As.

However, the time required for passing 200 ml along the column (i.e., ~26 hours) was considered enough for begin the chemical weathering and a rapid incongruent dissolution of volcanic glass (that is the reactive phase) by cation-exchange processes that could be also the source of the aforementioned elements.

In the same way, the second column experiment has been carried out with two size-fractions (<100 μm; 100-200 μm) of the 719 ancient ash in order to distinguish the mobility of PTTEs in that fractions. The elements have been grouped according to their behaviour and content in:

(1) Elements with similar behaviour in the three run experiments (Ca, Na, Mg, SO_4^{2-}, Rb, Sr, Mo, and Ba);

(2) Elements with a clearly enrichment in the fine fraction (<100 μm) and for which volcanic glass dissolution was inferred (Si, Li, B, P, V, Fe, As, Mo and U). From the data nowadays available on the temporal leaching of rhyolitic ashes collected along the Andean cordillera (from CVZ to SVZ), the association through laboratory experiments of some trace elements (As, Mo, V, B, and U) and glass dissolution have been inferred.

- Design of a suitable sequential extraction scheme (SES) for volcanic ash has been other objective of this research. The methodological approach for a suitable SES has been, first, to define the chemical fractions present in a volcanic ash and, then, to set the best chemical reagents in terms of extraction efficiency (e.g., leaching time) throughout leaching experiments. The proposed SES provides reliable information on the elements released in the different fractions of volcanic ash. These operationally defined fractions can represent non-specifically bound (F1), specifically bound as amorphous hydrous oxide-bound, crystalline hydrous oxide-bound and (F2 and F3), finally, the residual fraction (F4). Fraction 1 (extracted by deionised water) can be used for predicting the most mobile and potentially the most environmentally available elements, including the weakly adsorbed metals retained on the ash particle surfaces (i.e., elements that can be easily released by ion-exchange processes). Such information is useful to assess the readily bio-available fraction. Fractions 2-3 (extracted by NH_4-oxalate 0.25 M at pH 4.5 adjusted with HNO_3, NH_4-oxalate 0.25 M+ ascorbic acid 0.1 M at pH 4.5 adjusted with HNO_3, respectively) may provide information on potential lability from the different solid phases as a result of volcanic ash weathering and change of environmental factors (i.e., redox, pH). The residual fraction (F4) includes the element fraction which can only be mobilised as a result of weathering causing long-term effects on the environment. Within the inherent limitations of the chemical fractionation, the reagents used are fairly powerful for the determination of the chemical form in which the element occurs and this study should be considered a good promising start for a further development and application of this methodology to volcanic ash.

Concluding remarks and future perspective

This study represents a great advance on the knowledge of the geochemical environmental hazard posed by volcanic ashes, in general, and from the Andes, in particular. Explosive volcanic eruptions may have significant environmental repercussions for many Earth system cycles, particularly the water cycle. This research investigate the potential contribution to local geochemical fluxes

through water of ancient ash deposits erupted to hundreds of thousands to several million years ago and five historical eruptions that occurred over a 20-year period in the Andes. The major potentially toxic trace elements were arsenic, fluoride, molybdenum, nickel, lead and zinc.

The developed method of Single Batch Leaching Test (SBLT) is a very important contribution of this research because there is a need to harmonize the batch leaching tests applied to volcanic ash. The physico-chemical information of ashes (mainly the morphological features, grain-size distribution and PTTE identification and quantification) should be known prior the application of a SBLT. A recommended method has been outlined here with a view to standardising the reporting of leachate results and enhancing their application. This will hopefully prove a valuable addition to volcano monitoring efforts. In addition, use of the recommended method will be particularly beneficial for environmental and health applications where concentration data are required. Further works are needed to advance in the understanding of the elements implied to weathering of glass and mineral phases (which should be recognized by dynamic leaching tests). The results reported in this research could consider as basis for further developments.

REFERENCES

Abbey, S., 1978, Calibration standards .4. studies in standard samples - for use in general analysis of silicate rocks and minerals .5. 1977 edition of usable values, *X-Ray Spectrometry*, **7**(**2**), 99-121.

Africano, F., G. Van Rompaey, A. Bernard, and F. Le Guern, 2002, Deposition of trace elements from high temperature gases of Satsuma-Iwojima volcano, *Earth Planets and Space*, **54**(**3**), 275-286.

Aguilar, C. G., 2006, Aspectos sedimentologicos y estratigraficos de los depositos cuaternarios de la costa platense del departamento de canelones (uruguay), *Latin american journal of sedimentology and basin analysis*, **13**(**1**), 77-89.

Aiuppa, A., D. R. Baker, and J. D. Webster, 2009, Halogens in volcanic systems, *Chemical Geology*, **263**, 1-18.

Alexander, G. B., 1957, The effect of particle size on the solubility of amorphous silica in water, *Journal of Physical Chemistry*, **61**(**11**), 1563-1564.

Alexander, G. B., W. M. Heston, and R. K. Iler, 1954, The solubility of amorphous silica in water, *Journal of Physical Chemistry*, **58**(**6**), 453-455.

Allard, P., A. Aiuppa, H. Loyer, F. Carrot, A. Gaudry, G. Pinte, A. Michel, and G. Dongarra, 2000, Acid gas and metal emission rates during long-lived basalt degassing at Stromboli volcano, *Geophysical Research Letters*, **27**(**8**), 1207-1210.

Andrews, J. T., D. D. Eberl, and G. B. Kristjansdottir, 2006, An exploratory method to detect tephras from quantitative XRD scans: examples from Iceland and east Greenland marine sediments, *Holocene*, **16**(**8**), 1035-1042.

ANMAT, Administración Nacional de Medicamentos Alimentos y Tecnología Médica. 2007, Código Alimentario Argentino (CAA) -Capitulo XII—Bebidas Hídricas, Agua y Agua Gasificada—Agua Potable.

Armienta, M. A., S. De la Cruz-Reyna, O. Morton, O. Cruz, and N. Ceniceros, 2002, Chemical variations of tephra-fall deposit leachates for three eruptions from Popocatepetl volcano, *Journal of Volcanology and Geothermal Research*, **113**(**1-2**), 61-80.

Armienta, M. A., A. L. Martin-Del-Pozzo, R. Espinasa, O. Cruz, N. Ceniceros, A. Aguayo, and M. A. Butron, 1998, Geochemistry of ash leachates during the 1994-1996 activity of Popocatepetl volcano, *Applied Geochemistry*, **13**(**7**), 841-850.

Arunachalam, J., H. Emons, B. Krasnodebska, and C. Mohl, 1996, Sequential extraction studies on homogenized forest soil samples, *Science of the Total Environment*, **181**(**2**), 147-159.

Axerold, D. I., 1981, Role of volcanism in climate and evolution, *Geological Society of America-Special Paper*, **185**(**59**), 1-23.

Baker, M. C. W., and P. W. Francis, 1978, Upper cenozoic volcanism in central andes - ages and volumes, *Earth and Planetary Science Letters*, **41**(**2**), 175-187.

Banfield, J. F., and R. A. Eggleton, 1989, Apatite replacement and rare-earth mobilization, fractionation, and fixation during weathering, *Clays and Clay Minerals*, **37**(**2**), 113-127.

Barclay, J., D. S. Riley, and R. S. J. Sparks, 1995, Analytical models for bubble growth during decompression of high viscosity magmas, *Bulletin of Volcanology*, **57**(**6**), 422-431.

Bardintzeff, J. M., 2000, Eruptive styles and pyroclastic deposits. , in *Volcaniclastic Rocks from Magmas to Sediments.* , pp. 33–50., Leyrit H. and Montenat C. (eds), ed., Gordon and Breach Science Publishers., Amsterdam, The Netherlands.

Baxter, P. J., C. Bonadonna, R. Dupree, V. L. Hards, S. C. Kohn, M. D. Murphy, A. Nichols, R. A. Nicholson, G. Norton, A. Searl, R. S. J. Sparks, and B. P. Vickers, 1999, Cristobalite in volcanic ash of the Soufriere Hills Volcano, Montserrat, British West Indies, *Science*, **283**(**5405**), 1142-1145.

Beiderwieden, E., T. Wrzesinsky, and O. Klemm, 2005, Chemical characterization of fog and rain water collected at the eastern Andes cordillera, *Hydrology and Earth System Sciences*, **9**(**3**), 185-191.

Bennett, P., and D. I. Siegel, 1987, Increased solubilty of quartz in water due to complexing by organic compounds, *Nature*, **326**(**6114**), 684-686.

Bennett, P. C., and D. I. Siegel, 1989, Silica-organic complexes and anhanced quartz dissolution in water by organic acids, in *Water-rock interaction*, Miles, ed., Rotterdam.

Bernard, A., and F. Leguern, 1986, Condensation of volatile elements in high-temperature gases of mount St Helens., *Journal of Volcanology and Geothermal Research*, **28**(**1-2**), 91-105.

Bethke, C. M., 2008, Geochemical and biochemical reaction modeling: New York, Cambridge University Press.

Bhattacharya, P., M. Claesson, J. Bundschuh, O. Sracek, J. Fagerberg, G. Jacks, R. A. Martin, A. D. Storniolo, and J. M. Thir, 2006, Distribution and mobility of arsenic in the Rio Dulce alluvial aquifers in Santiago del Estero Province, Argentina, *Science of the Total Environment*, **358**(**1-3**), 97-120.

Bitschene, P. R., M. Fernandez, N. Arias, A. Arizmendi, M. Grizinik, and A. Nillni, 1994, Volcanology and environmental impact of the august 1991 eruption of the Hudson volcano (Patagonian andes, Chile), in *Zentralblatt Fur Geologie Und Palaontologie, Teil I: Allgemeine, Angewandte, Regionale Und Historische Geologie, 1993, Heft 1/2 - 13. Symposium on Latin-American Geosciences, Munster 1992*, 165-177, H. Miller, U. Rosenfeld, and K. WeberDiefenbach, eds., Zentralblatt Fur Geologie Und Palaontologie, Teil 1 : Allgemeine, Angewandte, Regionale Und Historische Geologie.

Blisniuk, P. M., L. A. Stern, C. P. Chamberlain, B. Idleman, and P. K. Zeitler, 2005, Climatic and ecologic changes during Miocene surface uplift in the Southern Patagonian Andes, *Earth and Planetary Science Letters*, **230**(**1-2**), 125-142.

Bundschuh, J., B. Farias, R. Martin, A. Storniolo, P. Bhattacharya, J. Cortes, G. Bonorino, and R. Albouy, 2004a, Groundwater arsenic in the Chaco-Pampean Plain, Argentina: Case study from Robles County, Santiago del Estero Province, *Applied Geochemistry*, **19**(**2**), 231-243.

Bundschuh, J., B. Farias, R. S. Martin, A. Storniolo, P. Bhattacharya, J. Cortes, G. Bonorino, and R. Albouy, 2004b, Groundwater arsenic in the Chaco-Pampean Plain, Argentina: case study from Robles county, Santiago del Estero Province, *Applied Geochemistry*, **19**(**2**), 231-243.

Bursik, M. I., R. S. J. Sparks, J. S. Gilbert, and S. N. Carey, 1992, Sedimentation of tephra by volcanic plumes .1. Theory and its comparison with a study of the Fogo-A Plinian deposit, Sao-Miguel (Azores), *Bulletin of Volcanology*, **54**(**4**), 329-344.

Buttner, R., P. Dellino, and B. Zimanowski, 1999, Identifying magma-water interaction from the surface features of ash particles, *Nature*, **401**(**6754**), 688-690.

Calarge, L. M., A. Meunier, B. Lanson, and M. L. L. Formos, 2006, Chemical signature of two Permian volcanic ash deposits within a bentonite bed from Melo, Uruguay, *Anais Da Academia Brasileira De Ciencias*, **78**(**3**), 525-541.

Carey, S., and M. I. Bursik, 2000, Volcanic plumes, in *Encyclopedia of volcanoes*, 527-545, H. Sigurdsson, B. F. Houghton, S. R. McNutt, H. Rymer, and J. Stix, eds., Academic Press, San Diego.

Carey, S., and H. Sigurdsson, 1989, The intensity of Plinian eruption, *Bulletin of Volcanology*, **51**, 28-40.

Carey, S. N., and H. Sigurdsson, 1982, Influence of particle aggregation on deposition of distal tephra from the may 18, 1980, eruption of Mount St Helens volcano, *Journal of Geophysical Research*, **87**(**NB8**), 7061-7072.

Cas, R. A. F., and J. V. Wright, 1988, Volcanic Successions: Modern and Ancient.

Casey, W. H., and B. Bunker, 1990, Leaching of mineral and glass surfaces during dissolution, *Mineral-Water Interface Geochemistry*, **23**, 397-426.

Casey, W. H., H. R. Westrich, J. F. Banfield, G. Ferruzzi, and G. W. Arnold, 1993, Leaching and reconstruction at the surfaces of dissolving chain silicate minerals, *Nature*, **366**(**6452**), 253-256.

Casey, W. H., H. R. Westrich, T. Massis, J. F. Banfield, and G. W. Arnold, 1989, The surface of labradorite feldspar after acid-hydrolysis, *Chemical Geology*, **78**(**3-4**), 205-218.

Cashman, K. V., B. Sturtevant, P. Papale, and O. Navon, 2000, Magmatic fragmentation, in *Encyclopedia of volcanoes*, 421-431, H. Sigurdsson, B. F. Houghton, S. R. McNutt, H. Rymer, and J. Stix, eds., Academic Press, San Diego.

Clapperton, C., 1993, Quaternary Geology and Geomorphology of South America: Amsterdam, Elsevier Science Publishers, 779 p.

Colin, N., B. F. Houghton, and W. Houghton, 2000, Pyroclats trasportation and deposition, in *Encyclopedi of volcanoes*, 545-555, H. Sigurdsson, B. F. Houghton, S. R. McNutt, H. Rymer, and J. Stix, eds., Academic Press, San Diego.

Cronin, S. J., V. E. Neall, J. A. Lecointre, M. J. Hedley, and P. Loganathan, 2003, Environmental hazards of fluoride in volcanic ash: a case study from Ruapehu volcano, New Zealand, *Journal of Volcanology and Geothermal Research*, **121**(**3-4**), 271-291.

Cronin, S. J., and D. S. Sharp, 2002, Environmental impacts on health from continuous volcanic activity at Yasur (Tanna) and Ambrym, Vanuatu, *International Journal of Environmental Health Research*, **12**(**2**), 109-123.

Crovisier, J. L., T. Advocat, and J. L. Dussossoy, 2003, Nature and role of natural alteration gels formed on the surface of ancient volcanic glasses (Natural analogs of waste containment glasses), *Journal of Nuclear Materials*, **321**(**1**), 91-109.

Chadwick, O. A., R. T. Gavenda, E. F. Kelly, K. Ziegler, C. G. Olson, W. C. Elliott, and D. M. Hendricks, 2003, The impact of climate on the biogeochemical functioning of volcanic soils, *Chemical Geology*, **202**(**3-4**), 195-223.

Chang, J. C., 1999, Solubility product constants, in *CRC Handbook of Chemistry and Physics*, D. R. Lide, ed., The Chemical Rubber Co., Boca Raton.

Chao, T. T., and L. Zhou, 1983, Extraction techniques for selective dissolution of amorphous iron-oxides from soils and sediments, *Soil Science Society of America Journal*, **47**(**2**), 225-232.

Chou, L., and R. Wollast, 1984, Study of the weathering of albite at room-temperature and pressure with a fluidized-bed reactor, *Geochimica Et Cosmochimica Acta*, **48**(**11**), 2205-2217.

Dahlgren, R. A., J. P. Dragoo, and F. C. Ugolini, 1997, Weathering of Mt. St. Helens tephra under a cryic-udic climatic regime, *Soil Science Society of America Journal*, **61**(**5**), 1519-1525.

Dahlgren, R. A., F. C. Ugolini, and W. H. Casey, 1999, Field weathering rates of Mt. St. Helens tephra, *Geochimica Et Cosmochimica Acta*, **63**(**5**), 587-598.

Davis, M. J., P. D. Ihinger, and A. C. Lasaga, 1997, Influence of water on nucleation kinetics in silicate melt, *Journal of Non-Crystalline Solids*, **219**, 62-69.

de Hoog, J. C. M., G. W. Koetsier, S. Bronto, T. Sriwana, and M. J. van Bergen, 2001, Sulfur and chlorine degassing from primitive arc magmas: temporal changes during the 1982-1983 eruptions of Galunggung (West Java, Indonesia), *Journal of Volcanology and Geothermal Research*, **108**(**1-4**), 55-83.

De Silva, S. L., and P. E. Francis, 1991a, Volcanoes of the Central Andes: New York, Springer-Verlag, 216 p.

De Silva, S. L., and P. W. Francis, 1991b, Volcanoes of the Central Andes: New York, Springer-Verlag, 216 p.

Delmelle, P., P. Gerin, and N. Oskarsson, 2000, Surface and bulk studies of leached and unleached volcanic ashes: AGU Fall Meeting abstracts.

Delmelle, P., M. Lambert, Y. Dufrene, P. Gerin, and N. Oskarsson, 2007, Gas/aerosol-ash interaction in volcanic plumes: New insights from surface analyses of fine ash particles, *Earth and Planetary Science Letters*, **259**(**1-2**), 159-170.

Delmelle, P., F. Villieras, and M. Pelletier, 2005, Surface area, porosity and water adsorption properties of fine volcanic ash particles, *Bulletin of Volcanology*, **67**(**2**), 160-169.

Dellino, P., and L. LaVolpe, 1996, Image processing analysis in reconstructing fragmentation and transportation mechanisms of pyroclastic deposits. The case of Monte Pilato-Rocche Rosse eruptions, Lipari (Aeolian islands, Italy), *Journal of Volcanology and Geothermal Research*, **71**(**1**), 13-29.

Devine, J. D., J. E. Gardner, H. P. Brack, G. D. Layne, and M. J. Rutherford, 1995, Comparison of microanalytical methods for estimating h2o contents of silicic volcanic glasses, *American Mineralogist*, **80**(**3-4**), 319-328.

Dijkstra, J. J., H. A. van der Sloot, and R. N. J. Comans, 2002, Process identification and model development of contaminant transport in MSWI bottom ash, *Waste Management*, **22**(**5**), 531-541.

Dingwell, D. B., 1998, Recent experimental progress in the physical description of silicic magma relevant to explosive vulcanism, in *The Physics of Explosive Volcanic Eruption*, 9-26, J. S. a. S. Gilbert, R.S.J., ed., Geological Society, Special Publications, London.

Driessens, F. C. M., 1982, Mineral Aspects of Dentistry: Basel, Krager S.

Duggen, S., P. Croot, U. Schacht, and L. Hoffmann, 2007, Subduction zone volcanic ash can fertilize the surface ocean and stimulate phytoplankton growth: Evidence from biogeochemical experiments and satellite data, *Geophysical Research Letters*, **34**(**1**).

Duggen, S., N. Olgun, P. Croot, L. Hoffmann, H. Dietze, P. Delmelle, and C. Teschner, 2010, The role of airborne volcanic ash for the surface ocean biogeochemical iron-cycle: a review, *Biogeosciences*, **7**(**3**), 827-844.

Duhart, P., H. Moreno, D. Basualto, M. Mella, and J. Muñoz, 2009a, Erupción en curso del Vólcan Chaitén: produstos, impactos y colapso parcila de domos del 19 de febrero de 2009, in *XII Congreso Geologico chileno*, Santiago de Chile.

Duhart, P., H. Moreno, D. Basualto, M. Mella, and J. Muñoz, 2009b, Erupción en curso del Vólcan Chaitén: produstos, impactos y colapso parcila de domos del 19 de febrero de 2009, in *XII Congreso Geologico chileno*, Santiago de Chile.

Eberl, D. D., 2003, User's guide to RockJock - A program for determining quantitative mineralogy from X-ray diffraction data, Open-File Report 03-78: Boulder, U.S. Geological Survey, 47 p.

Edmonds, M., C. Oppenheimer, D. M. Pyle, and R. A. Herd, 2001, Rainwater and ash leachate analysis as proxies for plume chemistry at Soufriere Hills Volcano, Montserrat: Flagship Meeting of the Geological-Society-of-London on Origins, Emissions and Impacts of Volcanic Gases, p. 203-218.

Edmonds, M., C. Oppenheimer, D. M. Pyle, and R. A. Herd, 2003, Rainwater and ash leachate analysis as proxies for plume chemistry at Soufrie`re

Hills volcano, Montserrat, in *Volcanic Degassing.*, G. Society, ed., London.

Elmer, T. H., and M. E. Nordberg, 1958, Solubility of silica in nitric acid solutions, *Journal of the American Ceramic Society*, **41**(**12**), 517-520.

Ersoy, O., G. Chinga, E. Aydar, A. Gourgaud, H. E. Cubukcu, and I. Ulusoy, 2006, Texture discrimination of volcanic ashes from different fragmentation mechanisms: A case study, Mount Nemrut stratovolcano, eastern Turkey, *Computers & Geosciences*, **32**(**7**), 936-946.

Fagents, S. A., and L. Wilson, 1993, Explosive volcanic-eruptions .7. the ranges of pyroclasts ejected in transient volcanic explosions, *Geophysical Journal International*, **113**(**2**), 359-370.

Fallman, A. M., and B. Aurell, 1996, Leaching tests for environmental assessment of inorganic substances in wastes, Sweden, *Science of the Total Environment*, **178**(**1-3**), 71-84.

Farmer, V. C., 1974, The Infrared spectra of minerals: Mineralogical Society monograph: London, 539 p.

Fernandez-Turiel, J. L., W. Decarvalho, M. Cabanas, X. Querol, and A. Lopezsoler, 1994, Mobility of heavy metals from coal fly ash, *Environmental Geology*, **23**(**4**), 264-270.

Fernandez-Turiel, J. L., A. López, J. F. Llorens, X. Querol, P. Aceñolaza, F. Durand, J. P. López, M. E. Medina, J. N. Rossi, A. J. Toselli, and J. Saavedra, 1995, Environmental monitoring using surface water, riversediments, and vegetation: a case study in the Famatina Range, La Rioja, NW Argentina, *Environment International*, **21**(**6**), 807-820.

Fernandez-Turiel, J. L., J. F. Llorens, M. Carnicero, and F. Valero, 2000a, Application of ICP-MS to outlet water control in the Llobregat and Ter drinking water treatment plants, *Quimica Analitica*, **19**(**4**), 217-224.

Fernandez-Turiel, J. L., J. F. Llorens, F. Lopez-Vera, C. Gomez-Artola, I. Morell, and D. Gimeno, 2000b, Strategy for water analysis using ICP-MS, *Fresenius Journal of Analytical Chemistry*, **368**(**6**), 601-606.

Filgueiras, A. V., I. Lavilla, and C. Bendicho, 2002, Chemical sequential extraction for metal partitioning in environmental solid samples, *Journal of Environmental Monitoring*, **4**(**6**), 823-857.

Fischer, C., A. F. White, and A. Luttge, 2009, From field to lab: Glass dissolution rates and sub-micron topography, *Geochimica Et Cosmochimica Acta*, **73**(**13**), A379-A379.

Fischer, R., 1961, Proponed classification of volcaniclastic sediments and rocks, *Geological Society American Bulletin*, **72**, 1409-1414.

Flaathen, T. K., and S. R. Gislason, 2007, The effect of volcanic eruptions on the chemistry of surface waters: The 1991 and 2000 eruptions of Mt. Hekla, Iceland, *Journal of Volcanology and Geothermal Research*, **164**(**4**), 293-316.

Flaathen, T. K., S. R. Gislason, and E. H. Oelkers, 2010, The effect of aqueous sulphate on basaltic glass dissolution rates, *Chemical Geology*, **277**(**3-4**), 345-354.

Folch, A., O. Jorba, and J. Viramonte, 2008, Volcanic ash forecast - application to the May 2008 Chaiten eruption, *Natural Hazards and Earth System Sciences*, **8**(**4**), 927-940.

Fowler, C. E., Y. Hoog, L. Vidal, and B. Lebeau, 2004, Mesoporosity in diatoms via surfactant induced silica rearrangement, *Chemical Physics Letters*, **398**(**4-6**), 414-417.

Francisca, F. M., and M. E. C. Perez, 2009, Assessment of natural arsenic in groundwater in Cordoba Province, Argentina, *Environmental Geochemistry and Health*, **31**(**6**), 673-682.

Frogner, P., S. R. Gislason, and N. Oskarsson, 2001, Fertilizing potential of volcanic ash in ocean surface water, *Geology*, **29**(**6**), 487-490.

Fubini, B., 1996, Surface reactivity in the pathogenic response to particulates: 6th International Meeting on the Toxicology of Natural and Man-Made Fibrous and Non-Fibrous Particles, p. 1013-1020.

Fubini, B., 1997, Surface reactivity in the pathogenic response to particulates, *Environmental Health Perspectives*, **105**, 1013-1020.

Gangale, G., A. J. Prata, and L. Clarisse, 2010, The infrared spectral signature of volcanic ash determined from high-spectral resolution satellite measurements, *Remote Sensing of Environment*, **114**(**2**), 414-425.

Garcia-Vallés, M., J. L. Fernandez-Turiel, D. Gimeno, S. J., and F. Ruggieri, 2008, Los yardangs del Campo de Piedra Pómez, Catamarca, Argentina, *Geo-Temas*, **10**, 1353-1356.

Garreaud, R., M. Vuille, and A. C. Clement, 2003, The climate of the Altiplano: observed current conditions and mechanisms of past changes, *Palaeogeography Palaeoclimatology Palaeoecology*, **194**(**1-3**), 5-22.

Gayer, K. H., L. C. Thompson, and O. T. Zajicek, 1958, The solubility of aluminum hydroxide in acidic and basic media at 25ºC, *Canadian Journal of Chemistry-Revue Canadienne De Chimie*, **36**(**9**), 1268-1271.

Georgakopoulos, A., A. Filippidis, and A. Kassoli-Fournaraki, 2002a, Leachability of major and trace elements of fly ash from Ptolemais power station, Northern Greece, *Energy Sources*, **24**(**2**), 103-113.

Georgakopoulos, A., A. Filippidis, A. Kassoli-Fournaraki, A. Iordanidis, J. L. Fernandez-Turiel, J. F. Llorens, and D. Gimeno, 2002b, Environmentally important elements in fly ashes and their leachates of the power stations of Greece, *Energy Sources*, **24**(**1**), 83-91.

Getahun, A., M. H. Reed, and R. Symonds, 1996, Mount St Augustine volcano fumarole wall rock alteration: Mineralogy, zoning, composition and numerical models of its formation process, *Journal of Volcanology and Geothermal Research*, **71**(**2-4**), 73-107.

Gèze, B., 1964, Sur la classification des dynamismes volcaniques *Bulletin of Volcanology*, **27**(**1**), 237-257.

Giggenbach, W. F., 1996, Chemical composition of volcanic gases, in *Monitoring and Mitigation of Volcano Hazards*, 221-256, R. Scarpa, and R. I. Tilling, eds., Spinger-Verlag, Berlin.

Giordano, D., P. Ardia, C. Romano, D. B. Dingwell, A. Di Muro, M. W. Schmidt, A. Mangiacapra, and K. U. Hess, 2009, The rheological evolution of alkaline Vesuvius magmas and comparison with alkaline series from the Phlegrean Fields, Etna, Stromboli and Teide, *Geochimica Et Cosmochimica Acta*, **73**(**21**), 6613-6630.

Giordano, D., J. K. Russell, and D. B. Dingwell, 2008, Viscosity of magmatic liquids: A model, *Earth and Planetary Science Letters*, **271**(**1-4**), 123-134.

Gislason, S. R., and E. H. Oelkers, 2003, Mechanism, rates, and consequences of basaltic glass dissolution: II. An experimental study of the dissolution rates of basaltic glass as a function of pH and temperature, *Geochimica Et Cosmochimica Acta*, **67**(**20**), 3817-3832.

Goryniuk, M. C., B. A. Rivard, and B. Jones, 2004, The reflectance spectra of opal-A (0.5-25 mu m) from the Taupo Volcanic Zone: Spectra that may identify hydrothermal systems on planetary surfaces, *Geophysical Research Letters*, **31**(**24**).

Grau, H. R., 2001, Regional-scale spatial patterns of fire in relation to rainfall gradients in sub-tropical mountains, NW Argentina, *Global Ecology and Biogeography*, **10**(**2**), 133-146.

Gregg, S. J., and k. S. W. Sing, 1982, Adsorption, surface area, and porosity: London, 2 ed. Academic Press.

Haflidason, H., J. Eiriksson, and S. Van Kreveld, 2000, The tephrochronology of Iceland and the North Atlantic region during the Middle and Late Quaternary: a review, *Journal of Quaternary Science*, **15**(**1**), 3-22.

Hall, G. E. M., J. E. Vaive, R. Beer, and M. Hoashi, 1996, Selective leaches revisited, with emphasis on the amorphous Fe oxyhydroxide phase extraction, *Journal of Geochemical Exploration*, **56**(**1**), 59-78.

Harris, A. J. L., J. Dehn, and S. Calvari, 2007, Lava effusion rate definition and measurement: a review, *Bulletin of Volcanology*, **70**(**1**), 1-22.

Hefflin, B. J., B. Jalaludin, E. McClure, N. Cobb, C. A. Johnson, L. Jecha, and R. A. Etzel, 1994, Surveillance for dust storms and respiratory-diseases in Washington-state, 1991, *Archives of Environmental Health*, **49**(**3**), 170-174.

Heiken, G., 1972, Morphology and petrography of volcanic ashes, *Geological Society of America Bulletin*, **83**(**7**), 1961-&.

Heiken, G., and K. H. Wohletz, 1992, Volcanic ash. 2nd ed.: Berkeley, California, University of California Press, 245 p.

Helffrich, G. R., and B. J. Wood, 2001, The Earth's mantle, *Nature*, **412**(**6846**), 501-507.

Hellmann, R., C. M. Eggleston, M. F. Hochella, and D. A. Crerar, 1990, The formation of leached layers on albite surfaces during dissolution under hydrothermal conditions, *Geochimica Et Cosmochimica Acta*, **54**(**5**), 1267-1281.

Hernandez-Moreno, J. M., J. I. Rodriguez-Gonzalez, and M. Espino-Mesa, 2007, Evaluation of the BCR sequential extraction for trace elements in

European reference volcanic soils, *European Journal of Soil Science*, **58**(**2**), 419-430.

Hickei-Vargas, R., M. Sun, L. López-Escobar, H. Moreno-Roa, M. K. Reagan, J. D. Morris, and J. G. Ryan, 2002, Multiple subduction components in the mantle wedge: Evidence from eruptive centers in the Central Southern volcanic zone, Chile *Geology*, **30**(**3**), 199-202.

Hildreth, W., and R. E. Drake, 1992, Volcan Quizapu, Chilean Andes, *Bulletin of Volcanology*, **54**(**2**), 93-125.

Hinkley, T., Le Cloarec, M.F. Lambert, G., 1994, Fractionation of families of major, minor, and trace metals across the melt-vapor interface in volcanic exhalations, *Geochimica Et Cosmochimica Acta*, **58**(**15**), 3255-3263.

Hinkley, T. K., 1991, Distribution of metals between particulate and gaseous forms in a volcanic plume, *Bulletin of Volcanology*, **53**(**5**), 395-400.

Hinkley, T. K., P. J. Lamothe, S. A. Wilson, D. L. Finnegan, and T. M. Gerlach, 1999, Metal emissions from Kilauea, and a suggested revision of the estimated worldwide metal output by quiescent degassing of volcanoes, *Earth and Planetary Science Letters*, **170**(**3**), 315-325.

Hobbs, P. V., D. A. Hegg, and L. F. Radke, 1983, resuspension of volcanic ash from mount St-Helens, *Journal of Geophysical Research-Oceans and Atmospheres*, **88**(**NC6**), 3919-3921.

Holdren, G. R., and P. M. Speyer, 1985, pH dependent changes in the rates and stoichiometry of dissolution of an alkali feldspar at room-temperature, *American Journal of Science*, **285**(**10**), 994-1026.

Horwell, C. J., 2007, Grain-size analysis of volcanic ash for the rapid assessment of respiratory health hazard, *Journal of Environmental Monitoring*, **9**(**10**), 1107-1115.

Horwell, C. J., and P. J. Baxter, 2006, The respiratory health hazards of volcanic ash: a review for volcanic risk mitigation, *Bulletin of Volcanology*, **69**(**1**), 1-24.

Horwell, C. J., I. Fenoglio, and B. Fublni, 2007, Iron-induced hydroxyl radical generation from basaltic volcanic ash, *Earth and Planetary Science Letters*, **261**(**3-4**), 662-669.

Horwell, C. J., I. Fenoglio, K. V. Ragnarsdottir, R. S. J. Sparks, and B. Fubini, 2003a, Surface reactivity of volcanic ash from the eruption of Soufriere Hills volcano, Montserrat, West Indies with implications for health hazards, *Environmental Research*, **93**(**2**), 202-215.

Horwell, C. J., J. S. Le Blond, S. A. K. Michnowicz, and G. Cressey, 2010a, Cristobalite in a rhyolitic lava dome: evolution of ash hazard, *Bulletin of Volcanology*, **72**(**2**), 249-253.

Horwell, C. J., S. Michnowicz, and J. Le BLond, 2008, Report on the mineralogical and geochemical characterization of Chaitén ash for the assessment of respiratory health hazard, International Volcanic Health Hazard Network (IVHNN) (available from www.ivhhn.org).

Horwell, C. J., R. S. J. Sparks, T. S. Brewer, E. W. Llewellin, and B. J. Williamson, 2003b, Characterization of respirable volcanic ash from the Soufriere Hills volcano, Montserrat, with implications for human health hazards, *Bulletin of Volcanology*, **65**(**5**), 346-362.

Horwell, C. J., G. W. Stannett, D. Andronico, A. Bertagnini, I. Fenoglio, B. Fubini, J. S. Le Blond, and B. J. Williamson, 2010b, A physico-chemical assessment of the health hazard of Mt. Vesuvius volcanic ash, *Journal of Volcanology and Geothermal Research*, **191**(**3-4**), 222-232.

Houghton, B. F., C. J. N. Wilson, and D. M. Pyle, 2000, Pyroclastic fall deposits, in *Encyclopedia of volcanoes*, 555-571, H. Sigurdsson, B. F. Houghton, S. R. McNutt, H. Rymer, and J. Stix, eds., Academic Press, San Diego.

Houston, J., and A. J. Hartley, 2003, The central andean west-slope rainshadow and its potential contribution to the origin of HYPER-ARIDITY in the Atacama desert, *International Journal of Climatology*, **23**(**12**), 1453-1464.

Hsu, C. N., J. C. Chen, and K. S. Ho, 2000, Geochemistry of Cenozoic volcanic rocks from Kirin Province, northeast China, *Geochemical Journal*, **34**(**1**), 33-58.

Ihinger, P. D., Y. X. Zhang, and E. M. Stolper, 1999, The speciation of dissolved water in rhyolitic melt, *Geochimica Et Cosmochimica Acta*, **63**(**21**), 3567-3578.

Iler, R. K., 1980, Isolation and characterization of particle nuclei during the polymerization of silicic-acid to colloidal silica, *Journal of Colloid and Interface Science*, **75**(**1**), 138-148.

Imai, N., S. Terashima, S. Itoh, and A. Ando, 1995, 1994 Compilation values for GSJ reference samples, igneous rock series, *Geochemical Journal*, **29**(**1**), 91-95.

Imai, N., S. Terashima, S. Itoh, and A. Ando, 1999, 1998 compilation of analytical data for five GSJ geochemical reference samples: The "Instrumental analysis series", *Geostandards Newsletter-the Journal of Geostandards and Geoanalysis*, **23**(**2**), 223-250.

Inbar, M., H. A. Ostera, C. A. Parica, M. B. Remesal, and F. M. Salani, 1995, Environmental assessment of 1991 Hudson volcano eruption ashfall effects on southern Patagonia region, Argentina, *Environmental Geology*, **25**(**2**), 119-125.

INN, 2006, Norma Chilena Oficial NCh409/1. Of2005 - Agua Potable - Parte 1 - Requisitos, pp. 9, Instituto Nacional de Normalización.

IRUG, 2000, Spectral Database Edition.

James, D. E., 1971, Plate tectonics and structure of central andean orogenic belt, *Transactions-American Geophysical Union*, **52**(**4**), 351-&.

Jones, M. T., and S. R. Gislason, 2008, Rapid releases of metal salts and nutrients following the deposition of volcanic ash into aqueous environments, *Geochimica Et Cosmochimica Acta*, **72**(**15**), 3661-3680.

Jones, M. T., R. S. J. Sparks, and P. J. Valdes, 2007, The climatic impact of supervolcanic ash blankets, *Climate Dynamics*, **29**, 553-564.

Kawano, M., K. Tomita, and Y. Shinohara, 1997, Analytical electron microscopic study of the noncrystalline products formed at early weathering stages of volcanic glass, *Clays and Clay Minerals*, **45**(**3**), 440-447.

Kerr, P. F., 1977, Optical mineralogy: New York, London, 4th edn, McGraw-Hill Book Company.

Kersten, M., and U. Forstner, 1986, Chemical farctionation of heavy-metals in anoxic estaurinw and costal sediments, *Water Science and Technology*, **18**(**4-5**), 121-130.

Kohler, S. J., D. Bosbach, and E. H. Oelkers, 2005, Do clay mineral dissolution rates reach steady state?, *Geochimica Et Cosmochimica Acta*, **69**(**8**), 1997-2006.

Kokelaar, P., 1986, Magma-water interactions in subaqueous and emergent basaltic volcanism, *Bulletin of Volcanology*, (**48**), 275-279.

Koltay, E., I. Rajta, Z. Kertesz, I. Uzonyi, J. R. Morales, and A. Z. Kiss, 2002, Cluster analysis of elemental constituents of individual atmospheric aerosol particles from the volcanic plume of Lonquimay eruption in 1989, *Journal of Radioanalytical and Nuclear Chemistry*, **251**(**1**), 25-36.

Kratzmann, D. J., S. Carey, R. Scasso, and J. A. Naranjo, 2009, Compositional variations and magma mixing in the 1991 eruptions of Hudson volcano, Chile, *Bulletin of Volcanology*, **71**(**4**), 419-439.

Kratzmann, D. J., S. Carey, R. A. Scasso, and J. A. Naranjo, 2010a, Role of cryptic amphibole crystallization in magma differentiation at Hudson volcano, Southern Volcanic Zone, Chile, *Contributions to Mineralogy and Petrology*, **159**(**2**), 237-264.

Kratzmann, D. J., S. N. Carey, J. Fero, R. A. Scasso, and J. A. Naranjo, 2010b, Simulations of tephra dispersal from the 1991 explosive eruptions of Hudson volcano, Chile, *Journal of Volcanology and Geothermal Research*, **190**(**3-4**), 337-352.

Krauskopf, K. B., 1948, Mechanism of eruption at paricutin volcano, mexico, *Geological Society of America Bulletin*, **59**(**8**), 711-&.

Krishnamurti, G. S. R., P. M. Huang, K. C. J. Vanrees, L. M. Kozak, and H. P. W. Rostad, 1995, Speciation of particulate-bound Cadmium of soils and its bioavalability, *Analyst*, **120**(**3**), 659-665.

Kyser, T. K., and J. R. Oneil, 1984, Hydrogen isotope systematics of submarine basalts, *Geochimica Et Cosmochimica Acta*, **48**(**10**), 2123-2133.

Lacasse, C., and P. van den Bogaard, 2002, Enhanced airborne dispersal of silicic tephras during the onset of Northern Hemisphere glaciations, from 6 to 0 Ma records of explosive volcanism and climate change in the subpolar North Atlantic, *Geology*, **30**(**7**), 623-626.

Lacroix, A., 1907, Les mineraux des fumerolles de l'eruption du Vesuve en avril 1906., *Bulletin de la Societe Francaise de Mineralogie*, **28**, 219-266.

Langmann, B., K. Zaksek, M. Hort, and S. Duggen, 2010, Volcanic ash as fertiliser for the surface ocean, *Atmospheric Chemistry and Physics*, **10**(**8**), 3891-3899.

Lantzy, R. J., and F. T. Mackenzie, 1979, Atmospheric trace-metals - global cycles and assessment of mans impact, *Geochimica Et Cosmochimica Acta*, **43**(**4**), 511-525.

Lara, L. E., 2009, The 2008 eruption of the Chaiten Volcano, Chile: a preliminary report, *Andean Geology*, **36**(**1**), 125-129.

Larsen, G., A. Dugmore, and A. Newton, 1999, Geochemistry of historical-age silicic tephras in Iceland, *Holocene*, **9**(**4**), 463-471.

Le Bas, M. J., R. W. Le Maitre, A. Streckeisen, and B. Zanettin, 1986, A chemical classification of volcanic rocks based on the total alkali-Silica diagram, *Journal of Petrology*, **27**, 745-750.

Le Maitre, R. W., 1989, A Classification of Igneous Rocks and Glossary of Terms. - Recommendations of the International Union of Geological Sciences, Subcommission on the Systematics of Igneous rocks, Blackwell Scientific Publications.

Le Sage, R. V., 1983, Chemistry of the volcanic aerosol., in *Forecasting Volcanic Events*, 445-474, Elsevier, Amsterdam.

Lebas, M. J., R. W. Lemaitre, A. Streckeisen, and B. Zanettin, 1986, A chemical classification of volcanic-rocks based on the total alkali silica diagram, *Journal of Petrology*, **27**(**3**), 745-750.

Lechler, P. J., and M. O. Desilets, 1987, A review of the use of loss on ignition as a measurement of total volatiles in whole-rock analysis, *Chemical Geology*, **63**(**3-4**), 341-344.

Lipman, P. W., Christia.RI, and Vanalsti.Re, 1969, Retention of alkalis by calc-alkalic rhyolites during crystallization and hydration, *American Mineralogist*, **54**(**1-2**), 286-&.

London, D., G. B. Morgan, H. A. Babb, and J. L. Loomis, 1993, Behavior and effects of phosphorus in the system Na2O-K2O-Al2O3-SiIO2-P2O5-H2O at 200 MPa(H2O), *Contributions to Mineralogy and Petrology*, **113**(**4**), 450-465.

Lopez-Escobar, L., R. Kilian, P. D. Kempton, and M. Tagiri, 1993, Petrography and geochemistry of Quaternary rocks from the Southern Volcanic Zone of the Andes between 41-degrees-30' and 46-degrees-00's, Chile, *Revista Geologica De Chile*, **20**(**1**), 33-55.

Luce, R. W., R. W. Bartlett, and G. A. Parks, 1972, Dissolution kinetics of magnesium silicates, *Geochimica Et Cosmochimica Acta*, **36**(**1**), 35-&.

Mader, H. M., J. C. Phillips, R. S. J. Sparks, and B. Sturtevant, 1996, Dynamics of explosive degassing of magma: Observations of fragmenting two-

phase flows, *Journal of Geophysical Research-Solid Earth*, **101**(**B3**), 5547-5560.

Mambo, V. S., and M. Yoshida, 1993, Behavior of arsenic in volcanic gases, *Geochemical Journal*, **27**(**4-5**), 351-359.

Mandeville, C. W., J. D. Webster, M. J. Rutherford, B. E. Taylor, A. Timbal, and K. Faure, 2002, Determination of molar absorptivities for infrared absorption bands of H2O in andesitic glasses, *American Mineralogist*, **87**(**7**), 813-821.

Manville, V., K. Nemeth, and K. Kano, 2009, Source to sink: A review of three decades of progress in the understanding of volcaniclastic processes, deposits, and hazards, *Sedimentary Geology*, **220**(**3-4**), 136-161.

Marshall, R. R., 1961, Devitrification of natural glass, *Geological Society of America Bulletin*, **72**(**10**), 1493-&.

Martin, R. S., S. F. L. Watt, D. M. Pyle, T. A. Mather, N. E. Matthews, R. B. Georg, J. A. Day, T. Fairhead, M. L. I. Witt, and B. M. Quayle, 2009, Environmental effects of ashfall in Argentina from the 2008 Chaiten volcanic eruption, *Journal of Volcanology and Geothermal Research*, **184**(**3-4**), 462-472.

Martin, U., and K. Nemeth, 2007, Blocky versus fluidal peperite textures developed in volcanic conduits, vents and crater lakes of phreatomagmatic volcanoes in Mio/Pliocene volcanic fields of Western Hungary, *Journal of Volcanology and Geothermal Research*, **159**(**1-3**), 164-178.

McDowell, H., T. M. Gregory, and W. E. Brown, 1977, Solubility of Ca5(PO4)3OH in system Ca(OH)2-H3PO4-H2O AT 5ºC, 15ºC, 25ºC and 37ºC, *Journal of Research of the National Bureau of Standards Section a-Physics and Chemistry*, **81**(**2-3**), 273-281.

Meijer, E. L., P. Buurman, A. Fraser, and E. Garcia-Rodeja, 2007, Extractability and FTIR characteristics of poorly ordered minerals in a collection of volcanic soils. , in *Soils of volcanic region of Europe*, 155-180, O. Arnalds, G. Stoops, P. Buurman, F. Bartoli, H. Oskarsson, and E. Garcia-Rodeja, eds., Spinger-Verlag, New York.

Meza, S. L., A. C. Garrabrants, H. van der Sloot, and D. S. Kosson, 2008, Comparison of the release of constituents from granular materials under batch and column testing, *Waste Management*, **28**(**10**), 1853-1867.

Meza, S. L., U. Kalbe, W. Berger, and F. G. Simon, 2010, Effect of contact time on the release of contaminants from granular waste materials during column leaching experiments, *Waste Management*, **30**(**4**), 565-571.

Middelburg, J. J., C. H. Vanderweijden, and J. R. W. Woittiez, 1988, Chemical processes affecting the mobility of major, minor and trace-elements during weathering of granitic-rocks, *Chemical Geology*, **68**(**3-4**), 253-273.

Middlemost, E. A. K., 1989, Iron oxidation ratios, norms and the classification of volcanic-rocks, *Chemical Geology*, **77**(**1**), 19-26.

Miravet, R., J. F. Lopez-Sanchez, R. Rubio, P. Smichowski, and G. Polla, 2007, Speciation analysis of antimony in extracts of size-classified volcanic ash by HPLC-ICP-MS, *Analytical and Bioanalytical Chemistry*, **387**(**5**), 1949-1954.

Moreno, H., and M. C. Gardeweg, 1989, La erupcion reciente en el complejo volcanico Lonquimay, *Revista Geologica De Chile*, **16**(**1**), 93-117.

Morrissey, M., B. Zimanowski, K. Wohletz, and R. Buettner, 2000, Phreatomagmatic fragmentation, in *Encyclopedia of volcanoes*, 431-447, H. Sigurdsson, B. F. Houghton, S. R. McNutt, H. Rymer, and J. Stix, eds., Academic Press, San Diego.

Naranjo, J. A., and H. Moreno, 1991, Actividad explosiva postglacial en el volcan Llaims, Andes del Sur (38º 45' S), *Revista Geologica De Chile*, **18**(**1**), 69-80.

Naranjo, J. A., and E. Polanco, 2004, The 2000 AD eruption of Copahue Volcano, Southern Andes, *Revista Geologica De Chile*, **31**(**2**), 279-292.

Naranjo, J. A., R. S. J. Sparks, M. V. Stasiuk, H. Moreno, and G. J. Ablay, 1992, Morphological, structural and textural variations in the 1988-1990 andesite lava of Lonquimay volcano, Chile, *Geological Magazine*, **129**(**6**), 657-678.

Naranjo, J. A., and C. R. Stern, 1998, Holocene explosive activity of Hudson Volcano, southern Andes, *Bulletin of Volcanology*, **59**(**4**), 291-306.

Naranjo, J. A., and C. R. Stern, 2004, Holocene tephrochronology of the southernmost part (42 degrees 30'-45 degrees S) of the Andean Southern Volcanic Zone, *Revista Geologica De Chile*, **31**(**2**), 225-240.

NCh, N. C. O., 2005, Agua Potable- Parte 1- Requisitos, I. N. d. Normalización, ed.

Nesbitt, H. W., and G. M. Young, 1984, Prediction of some weathering trends of plutonic and volcanic-rocks based on thermodynamic and kinetic considerations, *Geochimica Et Cosmochimica Acta*, **48**(**7**), 1523-1534.

Newhall, C. G., and S. Self, 1982, The Volcanic Explosivity Index (VEI) - an estimate of explosive magnitude for historical volcanism, *Journal of Geophysical Research-Oceans and Atmospheres*, **87**(**NC2**), 1231-1238.

Nho, E. Y., M. F. LeCloarec, B. Ardouin, and W. S. Tjetjep, 1996, Source strength assessment of volcanic trace elements emitted from the Indonesian arc, *Journal of Volcanology and Geothermal Research*, **74**(**1-2**), 121-129.

Nickel, E., 1973, Experimental dissolution of light and heavy minerals in comparison with weathering and intrastratal dissolution *Contributions to Sedimentology*, **1**, 1-68.

Nicolli, H. B., J. Bundschuh, J. W. Garcia, C. M. Falcon, and J. S. Jean, 2010, Sources and controls for the mobility of arsenic in oxidizing groundwaters from loess-type sediments in arid/semi-arid dry climates Evidence from the Chaco-Pampean plain (Argentina), *Water Research*, **44**(**19**), 5589-5604.

Nicolli, H. B., J. Bundschuh, J. W. Garcia, C. M. Falcon, and J. S. Jean, 2011, Sources and controls for the mobility of arsenic in oxidizing groundwaters from loess-type sediments in arid/semi-arid dry climates Evidence from the Chaco-Pampean plain (Argentina), *Water Research*, **44**(**19**), 5589-5604.

Nicolli, H. B., J. M. Suriano, M. A. G. Peral, L. H. Ferpozzi, and O. A. Baleani, 1989, Groundwater contamination with arsenic and other trace-elements in an area of the pampa, province of cordoba, argentina, *Environmental Geology and Water Sciences*, **14**(**1**), 3-16.

Nicolli, H. B., A. Tineo, J. W. Garcia, C. M. Falcon, and M. H. Merino, 2001, Trace-element quality problems in groundwater from Tucuman, Argentina, *Water-Rock Interaction, Vols 1 and 2*, 993-996.

Niello, J. O. F., D. E. Alvarez, A. M. J. Ferrero, O. A. Capurro, D. Abriola, G. V. Marti, A. J. Pacheco, J. E. Testoni, and R. G. Liberman, 1999, AMS measurements of South American rainwater samples, *Acta Physica Polonica B*, **30**(**5**), 1629-1638.

Niemeier, U., C. Timmreck, H. F. Graf, S. Kinne, S. Rast, and S. Self, 2009, Initial fate of fine ash and sulfur from large volcanic eruptions, *Atmospheric Chemistry and Physics*, **9**(**22**), 9043-9057.

Noble, D. C., 1967, Sodium potassium and ferrous iron contents of some secondarily hydrated natural silicic glasses, *American Mineralogist*, **52**(**1-2**), 280-&.

Noble, D. C., V. C. Smith, and L. C. Peck, 1967, Loss of halogens from crystallized and glassy silicic volcanic rocks, *Geochimica Et Cosmochimica Acta*, **31**(**2**), 215-&.

Nriagu, J. O., 1989, A global assessment of natural sources of atmospheric trace metals, *Nature*, **338** 47-49

Obenholzner, J. H., H. Schroettner, P. Golob, and H. Delgado, 2003, Particles from the plume of Popocatepetl volcano, Mexico - the FESEM/EDS approach, in *Volcanic Degassing*, 123-148, C. Oppenheimer, D. M. Pyle, and J. Barclay, eds., Geological Society Special Publication.

Oelkers, E. H., and S. R. Gislason, 2001, The mechanism, rates and consequences of basaltic glass dissolution: I. An experimental study of the dissolution rates of basaltic glass as a function of aqueous Al, Si and oxalic acid concentration at 25 degrees C and pH=3 and 11, *Geochimica Et Cosmochimica Acta*, **65**(**21**), 3671-3681.

Oelkers, E. H., S. V. Golubev, C. Chairat, O. S. Pokrovsky, and J. Schott, 2009, The surface chemistry of multi-oxide silicates, *Geochimica Et Cosmochimica Acta*, **73**(**16**), 4617-4634.

Oppenheimer, C., D. M. Pyle, J. Barclay, Publications, 123-148.0305 8719/03/$15.00, and T. G. S. o. L. 2003., 2003, Volcanic degassing, in *Treatise on geochemistry*, R. L. Rudnik, ed.

Oskarsson, N., 1980, The interaction between volcanic gases and tephra - fluorine adhering to tephra of the 1970 Hekla eruption, *Journal of Volcanology and Geothermal Research*, **8**(**2-4**), 251-266.

Papale, P., A. Neri, and G. Macedonio, 1998, The role of magma composition and water content in explosive eruptions - 1. Conduit ascent dynamics, *Journal of Volcanology and Geothermal Research*, **87**(**1-4**), 75-93.

Papastergios, G., J. L. Fernandez-Turiel, A. Georgakopoulos, and D. Gimeno, 2009, Natural and anthropogenic effects on the sediment geochemistry of Nestos river, Northern Greece, *Environmental Geology*, **58**(**6**), 1361-1370.

Papastergios, G., J. L. Fernandez-Turiel, A. Georgakopoulos, and D. Gimeno, 2010, Arsenic Background Concentrations in Surface Soils of Kavala Area, Northern Greece, *Water Air and Soil Pollution*, **209**(**1-4**), 323-331.

Papelis, C., W. Um, C. E. Russell, and J. B. Chapman, 2003, Measuring the specific surface area of natural and manmade glasses: effects of formation process, morphology, and particle size, *Colloids and Surfaces a-Physicochemical and Engineering Aspects*, **215**(**1-3**), 221-239.

Parks, G. A., 1967, Aqueous surface chemistry of oxides and complex oxide minerals. In Equilibrium Concepts in Natural Water Systems (ed. W. Stumm). *Am. Chem. Soc. Adv. Chem*, **67**, 121-160.

Parks, G. A., 1990a, Surface energy and adsorption at mineral-water interfaces: An introduction, in *Reviews in Mineralogy - Mineral-water interface geochemistry*, 133-175, M. F. Hochella, and A. F. White, eds., Mineralogical Society of America, Washington.

Patterson, C. C., and D. M. Settle, 1987, Magnitude of lead flux to the atmosphere from volcanoes, *Geochimica Et Cosmochimica Acta*, **51**(**3**), 675-681.

Perez-Lopez, R., A. M. Alvarez-Valero, J. M. Nieto, R. Saez, and J. X. Matos, 2008, Use of sequential extraction procedure for assessing the environmental impact at regional scale of the Sao Domingos Mine (Iberian Pyrite Belt), *Applied Geochemistry*, **23**(**12**), 3452-3463.

Petit, J. C., G. Dellamea, J. C. Dran, M. C. Magonthier, P. A. Mando, and A. Paccagnella, 1990, Hydrated-layer formation during dissolution of

complex silicate-glasses and minerals, *Geochimica Et Cosmochimica Acta*, **54**(**7**), 1941-1955.

Petrovic, R., R. A. Berner, and M. B. Goldhaber, 1976, Rate control in dissolution of alkali feldspars .1. study of residual feldspar grains by x-ray photoelectron-spectroscopy, *Geochimica Et Cosmochimica Acta*, **40**(**5**), 537-548.

Ping, C.-L., 2000, Volcanic soils, in *Encyclopedia of volcanoes*, 1259-1271, H. Sigurdsson, B. F. Houghton, S. R. McNutt, H. Rymer, and J. Stix, eds., Academic Press, San Diego.

Polanco, E. V., 2010, Volcanoestratigrafía, geoquímica y peligro volcánico del volcán Lonquimay (38°30'S), Andes del Sur (Chile) (in spanish), Universidad de Barcelona, 256 p.

Proussevitch, A. A., G. K. Mulukutla, and D. L. Sahagian, 2011, A new 3D method of measuring bubble size distributions from vesicle fragments preserved on surfaces of volcanic ash particles, *Geosphere*, **7**(**1**), 62-69.

Pyle, D. M., 1989, The thickness, volume and grainsize of tephra fall deposits, *Bulletin of Volcanology*, **51**(**1**), 1-15.

R, Development Core Team 2010, R: a language and environment for statistical computing, V. R Foundation for Statistical Computing, ed.

Rango, T., N. Colombani, M. Mastrocicco, G. Bianchini, and L. Beccaluva, 2010, Column Elution Experiments on Volcanic Ash: Geochemical Implications for the Main Ethiopian Rift Waters, *Water Air and Soil Pollution*, **208**(**1-4**), 221-233.

Rango, T., N. Colombani, M. Mastrocicco, G. Bianchini, and L. Beccaluva, 2011, Column Elution Experiments on Volcanic Ash: Geochemical Implications for the Main Ethiopian Rift Waters, *Water Air and Soil Pollution*, **208**(**1-4**), 221-233.

Rauret, G., 1998, Extraction procedures for the determination of heavy metals in contaminated soil and sediment, *Talanta*, **46**(**3**), 449-455.

Rauret, G., J. F. Lopez-Sanchez, A. Sahuquillo, E. Barahona, M. Lachica, A. M. Ure, C. M. Davidson, A. Gomez, D. Luck, J. Bacon, M. Yli-Halla, H. Muntau, and P. Quevauviller, 2000, Application of a modified BCR sequential extraction (three-step) procedure for the determination of extractable trace metal contents in a sewage sludge amended soil

reference material (CRM 483), complemented by a three-year stability study of acetic acid and EDTA extractable metal content, *Journal of Environmental Monitoring*, **2**(**3**), 228-233.

Reich, M., A. Zuniga, A. Amigo, G. Vargas, D. Morata, C. Palacios, M. A. Parada, and R. D. Garreaud, 2009a, Cristobalite nanofibers in volcanic ash from the ongoing explosive eruption at Chaiten Volcano, Chilean Patagonia, *Geochimica Et Cosmochimica Acta*, **73**(**13**), A1083-A1083.

Reich, M., A. Zuniga, A. Amigo, G. Vargas, D. Morata, C. Palacios, M. A. Parada, and R. D. Garreaud, 2009b, Formation of cristobalite nanofibers during explosive volcanic eruptions, *Geology*, **37**(**5**), 435-438.

Rice, C. M., 1973, Chemical weathering on carnmenellis granite, *Mineralogical Magazine*, **39**(**304**), 429-447.

Richards, J. A., 1986, Remote Sensing Digital Image Analysis: An Introduction: Berlin, Springer-Verlag.

Risacher, F., and H. Alonso, 2001, Geochemistry of ash leachates from the 1993 Lascar eruption, northern Chile. Implication for recycling of ancient evaporites, *Journal of Volcanology and Geothermal Research*, **109**(**4**), 319-337.

Risse, A., R. B. Trumbull, B. Coira, S. M. Kay, and P. van den Bogaard, 2008, Ar-40/Ar-39 geochronology of mafic volcanism in the back-arc region of the southern Puna plateau, Argentina, *Journal of South American Earth Sciences*, **26**(**1**), 1-15.

Rollinson, H., 1993, Using geochemical data: evaluation, presentation, interpretation, Pearson Education Limited editors, 352 p.

Rose, W. I., 1977a, Scavenging of volcanic aereosol by ash- Atmospheric and volcanologic implications, *Geology*, **5**(**10**), 621-624.

Ross, C. S., and R. L. Smith, 1961, Ash flow tuffs: their origin, geologic relations and identification, *U.S. Geol. Survey Prof Paper*, **336**, 1-77.

Rubin, C. H., E. K. Noji, P. J. Seligman, J. L. Holtz, J. Grande, and F. Vittani, 1994, Evaluating a fluorosis hazard after a volcanic-eruption, *Archives of Environmental Health*, **49**(**5**), 395-401.

Ruggieri, F., J. Fernandez-Turiel, J. Saavedra, D. Gimeno, E. Polanco, and J. A. Naranjo, 2011, Environmental geochemistry of recent volcanic ashes

from Southern Andes, *Environmental chemistry,* **8***,* 1–12*.*
doi:10.1071/EN10097

Ruggieri, F., J. L. Fernandez-Turiel, D. Gimeno, M. Garcia-Valles, and J. Saavedra, 2010b, Environmental geochemistry of ancient volcanic ashes, *Journal of hazardeous materials*, **183**(**1-3**), 353-365.

Sastre, J., A. Sahuquillo, M. Vidal, and G. Rauret, 2002, Determination of Cd, Cu, Pb and Zn in environmental samples: microwave-assisted total digestion versus aqua regia and nitric acid extraction, *Analytica Chimica Acta*, **462**(**1**), 59-72.

Scasso, R. A., and S. Carey, 2005, Morphology and formation of glassy volcanic ash from the August 12-15, 1991 eruption of Hudson Volcano, Chile, *Latin American journal of sedimentology and basin analysis*, **12**(**1**), 3-21.

Scasso, R. A., H. Corbella, and P. Tiberi, 1994, Sedimentological analysis of the tephra from the 12-15 august 1991 eruption of Hudson volcano., *Bulletin of Volcanology*, **56**(**2**), 121-132.

Schmid, R., 1981, Descriptive nomenclature and classification of pyroclastic deposits and fragments - recommendations of the iugs subcommission on the systematics of igneous rocks, *Geology*, **9**(**1**), 41-43.

Schnurr, W. B. W., R. B. Trumbull, J. Clavero, K. Hahne, W. Siebel, and M. Gardeweg, 2007, Twenty-five million years of silicic volcanism in the southern central volcanic zone of the Andes: Geochemistry and magma genesis of ignimbrites from 25 to 27 degrees S, 67 to 72 degrees W, *Journal of Volcanology and Geothermal Research*, **166**, 17-46.

Schott, J., and E. H. Oelkers, 1995, Dissolution and crystallization rates of silicate minerals as a function of chemical affinity, *Pure and Applied Chemistry*, **67**(**6**), 903-910.

Schwartz, J., G. Norris, T. Larson, L. Sheppard, C. Claiborn, and J. Koenig, 1999, Episodes of high coarse particle concentrations are not associated with increased mortality, *Environmental Health Perspectives*, **107**(**5**), 339-342.

Seaman, J., V. VM, S. AG, J. BP, A. SA, and B. P. M, 2005, Metal extractability from contaminated SRS sediments: Comparison of column and batch results, *Environmental Geosciences*, **12**(**4**), 235-242.

Self, S., 2006, The effects and consequences of very large explosive volcanic eruptions, *Philosophical Transactions of the Royal Society a-Mathematical Physical and Engineering Sciences*, **364**(**1845**), 2073-2097.

SERNAGEOMIN, 2009, Erupción del volcán Chaitén, Informes Tecnicós, 05-2008/03-2009.

Severin, K. P., 2004, Energy Dispersive Spectrometry of common rock forming minerals, Kluwer Academic Publishers.

Sheridan, M. F., and J. R. Marshall, 1983, Interpretation of pyroclast surface-features using SEM images, *Journal of Volcanology and Geothermal Research*, **16**(**1-2**), 153-159.

Sheridan, M. F., and K. H. Wohletz, 1981, Hydrovolcanic explosions - the systematics of water-pyroclast equilibration, *Science*, **212**(**4501**), 1387-1389.

Sheridan, M. F., and K. H. Wohletz, 1983, Hydrovolcanism - basic considerations and review, *Journal of Volcanology and Geothermal Research*, **17**(**1-4**), 1-29.

Shoji, S., and Y. Fujiwara, 1984, Active Al and Fe in the humus horizons of andosols from northeastern Japan- Their forms, properties, and significance in clay weathering, *Soil Science*, **137**(**4**), 216-226.

Shoji, S., M. Nanzyo, Y. Shirato, and T. Ito, 1993, Chemical-kinetics of weathering in young andisols from northeastern japan using soil age normalized to 10-degrees-c   *Soil Science*, **155**(**1**), 53-60.

Sigurdsson, H., 2000, Introduction, in *Encyclopedia of volcanoes*, 1-15, H. Sigurdsson, B. F. Houghton, S. R. McNutt, H. Rymer, and J. Stix, eds., Academic Press, San Diego.

Smith, D. B., R. A. Zielinski, and W. I. Rose, 1982, Leachability of uranium and other elements from freshly erupted volcanic ash, *Journal of Volcanology and Geothermal Research*, **13**(**1-2**), 1-30.

Smith, D. B., R. A. Zielinski, H. E. Taylor, and M. B. Sawyer, 1983, Leaching characteristics of ash from the May 18, 1980, eruption of Mount St. Helens volcano, Washington., *Bulletin Volcanologique*, **46**(**2**), 103– 124.

Soler, M. M., P. J. Caffe, B. L. Coira, A. T. Onoe, and S. M. Kay, 2007, Geology of the Vilama caldera: A new interpretation of a large-scale explosive

event in the Central Andean plateau during the Upper Miocene, *Journal of Volcanology and Geothermal Research*, **164**(**1-2**), 27-53.

Sondag, F., 1981, Selective extraction procedures applied to geochemical prospecting in an area contaminated by old mine workings, *Journal of Geochemical Exploration*, **15**(**1-3**), 645-652.

Souto, C. P., A. C. Premoli, and P. B. Reich, 2009, Complex bioclimatic and soil gradients shape leaf trait variation in Embothrium coccineum (Proteaceae) among austral forests in Patagonia, *Revista Chilena De Historia Natural*, **82**(**2**), 209-222.

Sparks, R. S. J., 1978, Dynamics of bubble formation and growth in magmas - review and analysis, *Journal of Volcanology and Geothermal Research*, **3**(**1-2**), 1-37.

Sparks, R. S. J., 2003, Forecasting volcanic eruptions, *Earth and Planetary Science Letters*, **210**(**1-2**), 1-15.

Sparks, R. S. J., M. I. Bursik, G. J. Ablay, R. M. E. Thomas, and S. N. Carey, 1992, Sedimentation of tephra by volcanic plumes .2. controls on thickness and grain-size variations of tephra fall deposits, *Bulletin of Volcanology*, **54**(**8**), 685-695.

Sparks, R. S. J., M. I. Bursik, S. N. Carey, J. S. Gilbert, L. S. Glaze, H. Sigurdsson, and A. W. Woods, 1997, Volcanic plumes: Chichester, England, John Wiley & sons.

Sparks, R. S. J., P. W. Francis, R. D. Hamer, R. J. Pankhurst, L. O. Ocallaghan, R. S. Thorpe, and R. Page, 1985, Ignimbrites of the cerro galan caldera, nw argentina, *Journal of Volcanology and Geothermal Research*, **24**(**3-4**), 205-248.

Sparks, R. S. J., and L. Wilson, 1982, Explosive volcanic-eruptions .5. Observations of plume dynamics during the 1979 Soufriere eruption, St Vincent, *Geophysical Journal of the Royal Astronomical Society*, **69**(**2**), 551-570.

Sparks, R. S. J., S. R. Young, J. Barclay, E. S. Calder, P. Cole, B. Darroux, M. A. Davies, T. H. Druitt, C. Harford, R. Herd, M. James, A. M. Lejeune, S. Loughlin, G. Norton, G. Skerrit, M. V. Stasiuk, N. S. Stevens, J. Toothill, G. Wadge, and R. Watts, 1998, Magma production and growth of the lava dome of the Soufriere Hills Volcano, Montserrat, West Indies:

November 1995 to December 1997, *Geophysical Research Letters*, **25**(**18**), 3421-3424.

Stefansson, A., S. R. Gislason, and S. Arnorsson, 2001, Dissolution of primary minerals in natural waters - II. Mineral saturation state, *Chemical Geology*, **172**(**3-4**), 251-276.

Stern, C. R., 1991, Role of subduction erosion in the generation of andean magmas, *Geology*, **19**(**1**), 78-81.

Stern, C. R., 2004, Active Andean volcanism: its geologic and tectonic setting, *Revista Geologica De Chile*, **31**(**2**), 161-206.

Stern, C. R., 2008, Holocene tephrochronology record of large explosive eruptions in the southernmost Patagonian Andes, *Bulletin of Volcanology*, **70**(**4**), 435-454.

Stern, C. R., H. Moreno, L. López-Escobar, J. Clavero, L. Lara, J. A. Naranjo, M. A. Parada, and M. A. Skewes, 2007, Chilean volcanoes, in *Geology of Chile*, 147-178, Moreno T., and G. W., eds., The Geological Society of London, London.

Stevenson, R. J., N. S. Bagdassarov, D. B. Dingwell, and C. Romano, 1998, The influence of trace amounts of water on the viscosity of rhyolites, *Bulletin of Volcanology*, **60**(**2**), 89-97.

Stewart, C., D. M. Johnston, G. S. Leonard, C. J. Horwell, T. Thordarson, and S. J. Cronin, 2006, Contamination of water supplies by volcanic ashfall: A literature review and simple impact modelling, *Journal of Volcanology and Geothermal Research*, **158**(**3-4**), 296-306.

Stoiber, R. E., and W. I. Rose, 1970, Geochemistry of central american volcanic gas condensates, *Geological Society of America Bulletin*, **81**(**10**), 2891-2910.

Stolper, E., 1982a, The speciation of water in silicates melts, *Geochimica Et Cosmochimica Acta*, **46**(**12**), 2609-2620.

Stolper, E., 1982b, Water in silicate glasses- an infrared spectroscopic study, *Contributions to Mineralogy and Petrology*, **81**(**1**), 1-17.

Stolper, E. M., 1989, Temperature dependence of the speciation of water in ryolitic melts and glasses, *American Mineralogist*, **74**, 1247-1257.

Strecker, M. R., R. N. Alonso, B. Bookhagen, B. Carrapa, G. E. Hilley, E. R. Sobel, and M. H. Trauth, 2007, Tectonics and climate of the southern

central Andes, *Annual Review of Earth and Planetary Sciences*, **35**, 747-787.

Stumm, W., and G. Furrer, 1987, The dissoltuion of oxides and aluminum silicates; Examples of surface coordination-controlled kinetics, in *Acquatic surface chemistry*, p. 197, W. J. W. a. S. Stumm, ed.

Symonds, R. B., M. H. Reed, and W. I. Rose, 1992, Origin, speciation, and fluxes of trace-element gases at augustine volcano, alaska - insights into magma degassing and fumarolic processes, *Geochimica Et Cosmochimica Acta*, **56**(**2**), 633-657.

Symonds, R. B., W. I. Rose, G. J. S. Bluth, and T. M. Gerlach, 1994a, Volcanic gas studies- Methods, results and application, in *Volatiles in Magmas*, 1-66, Reviews in Mineralogy, Mineralogical Soc America, Washington.

Symonds, R. B., W. I. Rose, M. H. Reed, F. E. Lichte, and D. L. Finnegan, 1987a, Volatilization, transport and sublimation of metallic and non.metallic elements in high temperature gases at Merapi-Volcano, Indonesia, *Geochimica Et Cosmochimica Acta*, **51**(**8**), 2083-2101.

Taddeucci, J., M. Pompilio, and P. Scarlato, 2004, Conduit processes during the July-August 2001 explosive activity of Mt. Etna (Italy): inferences from glass chemistry and crystal size distribution of ash particles, *Journal of Volcanology and Geothermal Research*, **137**(**1-3**), 33-54.

Taylor, P. S., and R. E. Stoiber, 1973, Soluble material on ash from active central-american volcanos, *Geological Society of America Bulletin*, **84**(**3**), 1031-1041.

Taylor, S. R., and S. M. McLennan, 1985, The Continental Crust: Its Composition and Evolution.: Oxford.

Terashima, S., S. Itoh, M. Ujiie, H. Kamioka, T. Tanaka, and H. Hattori, 1993a, 3 new GSJ rock reference samples- rhyolite JR-3, gabbro JGB-2 and hornoblendite JH-1, *Geostandards Newsletter*, **17**(**1**), 1-4.

Terashima, S., S. Itoh, M. Ujiie, H. Kamioka, T. Tanaka, and H. Hattori, 1993b, 3 new gsj rock reference samples - rhyolite JR-3, gabbro JGB-2 and hornblendite JH-1, *Geostandards Newsletter*, **17**(**1**), 1-4.

Tessier, A., P. G. C. Campbell, and M. Bisson, 1979, Sequentilal extraction procedure for the speciation of particulate trace-metals, *Analytical Chemistry*, **51**(**7**), 844-851.

Teutsch, N., Y. Erel, L. Halicz, and O. A. Chadwick, 1999, The influence of rainfall on metal concentration and behavior in the soil, *Geochimica Et Cosmochimica Acta*, **63**(**21**), 3499-3511.

Thorpe, R. S., and P. W. Francis, 1979, Variations in andean andesite compositions and their petrogenetic significance, *Tectonophysics*, **57**(**1**), 53-70.

Toscano, G., C. Caristi, and G. Cimino, 2008, Sorption of heavy metal from aqueous solution by volcanic ash, *Comptes Rendus Chimie*, **11**(**6-7**), 765-771.

Tosdal, R. M., E. Farrar, and A. H. Clark, 1981, K-Ar geochronology of the late cenozoic volcanic-rocks of the cordillera occidental, southernmost peru, *Journal of Volcanology and Geothermal Research*, **10**(**1-3**), 157-173.

Ubilla, M., D. Perea, C. G. Aguilar, and N. Lorenzo, 2004, Late Pleistocene vertebrates from northern Uruguay: tools for biostratigraphic, climatic and environmental reconstruction, *Quaternary International*, **114**, 129-142.

Ure, A. M., 1996, Single extraction schemes for soil analysis and related applications, *Science of the Total Environment*, **178**(**1-3**), 3-10.

Ure, A. M., P. Quevauviller, H. Muntau, and B. Griepink, 1993, Speciation of heavy metals in soils and sediments- An account of the improvement and harmonization of extraction techniques undertaken under the auspices of the BCR of the Commision of the European Communities, *International Journal of Environmental Analytical Chemistry*, **51**(**1-4**), 135-151.

USEPA, 1998, Method 3051a, microwave assisted acid digestion of sediments, sludges, soils and oils, 24.

Usero, J., M. Gamero, J. Morillo, and I. Gracia, 1998, Comparative study of three sequential extraction procedures for metals in marine sediments, *Environment International*, **24**(**4**), 487-496.

Valsami-Jones, E., K. V. Ragnarsdottir, A. Putnis, D. Bosbach, A. J. Kemp, and G. Cressey, 1998, The dissolution of apatite in the presence of aqueous metal cations at pH 2-7, *Chemical Geology*, **151**(**1-4**), 215-233.

Van der Sloot, H., L. Heasman, and P. Quevauviller, 1997a, Harmonization of leaching/extraction tests., in *Studies in environmental science*, Elsevier, Amsterdam.

van der Sloot, H. A., R. N. J. Comans, and O. Hjelmar, 1996, Similarities in the leaching behaviour of trace contaminants from waste, stabilized waste, construction materials and soils, *Science of the Total Environment*, **178**(**1-3**), 111-126.

Van der Sloot, H. A., L. Heasman, and P. Quevauller, 1997b, Harmonisation of leaching/extraction tests, in *Studies in environmental science*, 292, E. Science, ed., Amsterdam.

Varekamp, J. C., J. F. Luhr, and K. L. Prestegaard, 1984, The 1982 eruptions of el-chichon volcano (chiapas, mexico) - character of the eruptions, ash-fall deposits, and gas-phase, *Journal of Volcanology and Geothermal Research*, **23**(**1-2**), 39-68.

Varekamp, J. C., A. P. Ouimette, S. W. Herman, A. Bermùdez, and D. Delpino, 2001, Hydrothermal element fluxes from Copahue, Argentina: A "beehive" volcano in turmoil *Geology*, **29**(**11**), 1059-1062.

Varekamp, J. C., A. P. Ouimette, S. W. Herman, K. S. Flynn, A. Bermudez, and D. Delpino, 2009, Naturally acid waters from Copahue volcano, Argentina (vol 24, pg 208, 2009), *Applied Geochemistry*, **24**(**7**), 1354-1354.

Velbel, M. A., 1993, Constancy of silicate mineral weathering-rate ratios between natural and experimental weathering - implications for hydrologic control of differences in absolute rates, *Chemical Geology*, **105**(**1-3**), 89-99.

Venzke, E., S. K. Sennert, and R. Wunderman, 2009, Reports from the Smithsonian's Global Volcanism Network, June 2008, *Bulletin of Volcanology*, **71**, 229-231.

Verhoogen, J., 1951, Mechanism of ash formation, *American Journal of Science*, **249**(**10**), 729-739.

Wada, K., 1987, M minerals formed and mineral formation from volcanic ash by weathering, *Chemical Geology*, **60**(**1-4**), 17-28.

Walker, G. P. L., 1973, Explosive volcanic eruptions -- a new classification scheme, *Geologische Rundschau*, **62**, 431-446.

Walker, G. P. L., L. Wilson, and E. L. G. Bowell, 1971, Explosive volcanic eruptions .1. rate of fall of pyroclasts, *Geophysical Journal of the Royal Astronomical Society*, **22**(**4**), 377-&.

Watt, S. F. L., D. M. Pyle, T. A. Mather, R. S. Martin, and N. E. Matthews, 2009, Fallout and distribution of volcanic ash over Argentina following the May 2008 explosive eruption of Chaiten, Chile, *Journal of Geophysical Research-Solid Earth*, **114**.

Wentworth, C., and H. Williams, 1932, The classification and terminology of the pyroclastic rocks, *National Academy of Science Natural Research Council*, **89**, 19-53.

Wenzel, W. W., N. Kirchbaumer, T. Prohaska, G. Stingeder, E. Lombi, and D. C. Adriano, 2001, Arsenic fractionation in soils using an improved sequential extraction procedure, *Analytica Chimica Acta*, **436**(**2**), 309-323.

White, A. F., 1984, Weathering characteristics of natural glass and influences on associated water chemistry, *Journal of Non-Crystalline Solids*, **67**(**1-3**), 225-244.

White, A. F., and S. L. Brantley, 2003, The effect of time on the weathering of silicate minerals: why do weathering rates differ in the laboratory and field?, *Chemical Geology*, **202**(**3-4**), 479-506.

White, A. F., and H. C. Claassen, 1980a, Kinetic-model for the short-term dissolution of a rhyolitic glass, *Chemical Geology*, **28**(**1-2**), 91-109.

Whitney, D. L., and B. W. Evans, 2010, Abbreviations for names of rock-forming minerals, *American Mineralogist*, **95**(**1**), 185-187.

WHO, 2008, Guidelines for Drinking-water quality: incorporating 1st and 2nd addenda, Vol. 1, Reccomendations, pp. 515, World Health Orgaization, Geneva.

Wilson, L., 1999, Explosive volcanic eruptions. The influence of pyroclast size distributions and released magma gas contents on the eruption velocities of pyroclasts and gas in Hawaiian and Plinian eruptions, *Geophysical Journal International*, **136**(**3**), 609-619.

Wilson, L., and G. P. L. Walker, 1987, Explosive volcanic-eruptions .6. ejecta dispersal in plinian eruptions - the control of eruption conditions and

atmospheric properties, *Geophysical Journal of the Royal Astronomical Society*, **89**(**2**), 657-679.

Wilson, T., C. Stewart, J. Cole, D. Johnston, and S. Cronin, 2010, Vulnerability of farm water supply systems to volcanic ash fall, *Environmental Earth Sciences*, **61**(**4**), 675-688.

Witham, C. S., C. Oppenheimer, and C. J. Horwell, 2005, Volcanic ash-leachates: a review and recommendations for sampling methods, *Journal of Volcanology and Geothermal Research*, **141**(**3-4**), 299-326.

Witt-Eickschen, G., H. Palme, H. S. C. O'Neill, and C. M. Allen, 2009, The geochemistry of the volatile trace elements As, Cd, Ga, In and Sn in the Earth's mantle: New evidence from in situ analyses of mantle xenoliths, *Geochimica Et Cosmochimica Acta*, **73**(**6**), 1755-1778.

Wohletz, K., 2010, KWare geological software, http://internet.cybermesa.com/~wohletz/KWare/KWare.htm.

Wohletz, K. H., 1983a, Mechanism of hydrovolcanic pyroclast formation- Grain size, Scanning electron microscopy, and experimental study, *Journal of Volcanology and Geothermal Research*, **17**(**1-4**), 31-63.

Wohletz, K. H., 1986, Explosive magama-water interactions: thermodynamics, explosion mechanism, and field study., *Bulletin of Volcanology*, **48**, 245-264.

Wohletz, K. H., and D. Krinsley, 1982, Scanning electron microscopy of basaltic hydromagmatic ash, 43pp., L.-U.-. Los Alamos National Laboratory Report, ed.

Wohletz, K. H., M. F. Sheridan, and W. K. Brown, 1989, Particle-size distributions and the sequential fragmentation transport-theory applied to volcanic ash, *Journal of Geophysical Research-Solid Earth and Planets*, **94**(**B11**), 15703-15721.

Wolff-Boenisch, D., S. R. Gislason, and E. H. Oelkers, 2004a, The effect of fluoride on the dissolution rates of natural glasses at pH 4 and 25 degrees C, *Geochimica Et Cosmochimica Acta*, **68**(**22**), 4571-4582.

Wolff-Boenisch, D., S. R. Gislason, and E. H. Oelkers, 2006, The effect of crystallinity on dissolution rates and CO2 consumption capacity of silicates, *Geochimica Et Cosmochimica Acta*, **70**(**4**), 858-870.

Wolff-Boenisch, D., S. R. Gislason, E. H. Oelkers, and C. V. Putnis, 2004b, The dissolution rates of natural glasses as a function of their composition at pH 4 and 10.6, and temperatures from 25 to 74 degrees C, *Geochimica Et Cosmochimica Acta*, **68**(**23**), 4843-4858.

Wollast, R., and L. Chou, 1992, Surface-reactions during the early stages of weathering of Albite, *Geochimica Et Cosmochimica Acta*, **56**(**8**), 3113-3121.

Yokoyama, T., S. Okumura, and S. Nakashima, 2008, Hydration of rhyolitic glass during weathering as characterized by IR microspectroscopy, *Geochimica Et Cosmochimica Acta*, **72**(**1**), 117-125.

Zemberyova, M., I. Hagarova, J. Zimova, J. Bartekova, and H. M. Kuss, 2010, Determination of molybdenum in extracts of soil and sewage sludge CRMs after fractionation by means of BCR modified sequential extraction procedure, *Talanta*, **82**(**2**), 582-586.

Zhang, Y. X., E. M. Stolper, and G. J. Wasserburg, 1991, Diffusion in water rhyolitic glasses, *Geochimica Et Cosmochimica Acta*, **55**(**2**), 441-456.

Appendixes

Appendix 1

In this appendix are presented the protocols of the chemical analytical techniques used in this research.

Protocol for the determination of loss on ignition (LOI) in rocks by means of calcination

Introduction

The 'loss on ignition' (LOI) is the rapid valuation of the content on volatiles (H_2O and CO_2, mainly) obtained from the weight lost at high temperature (~950 ºC). There are different methods for their determination. The one now described is easy and rapid. There must be taken into account that an oxidizing atmosphere makes easier the acceptance of oxygen by ferrous iron during the ignition and the result of LOI might be smaller than expected or result in an increase of weight obtaining a GOI (gain on ignition) (Lechler & Desilets, 1987).

Methodology

The method used for the determination of LOI is the following:

1. Before starting calcination, samples and ceramic crucibles must be in the oven at 105 °C for at least 12 hours.
2. Remove crucibles and samples from the oven and put them into desiccator until they reach room temperature.
3. Weigh the crucibles. The values obtained will be written in a worksheet column called 'A'.
4. Weigh 0.5 - 1 g of sample, depending of its availability, in the crucibles and weigh the whole. This value will be written in the column 'B'.
5. Put the crucibles with the corresponding samples in the furnace. This is switched on and programmed at 1000 °C. Once this temperature is reached it is left at constant temperature for at least 2 hours.
6. Later, the furnace is switched off and left to cool up to 500 °C. It is opened in order to let it cool faster. Do not take the crucibles off the furnace until they have reached 100 °C approx.
7. Take out the samples, put them in the desiccator and let them reach room temperature. Once they are cool, the crucibles with the calcinated samples are weighed and the result is written in a column 'C'.

The following formula is used to calculate the LOI value:

$$LOI= [(B – C) / (B – A)] * 100$$

Reference: Lechler P.J., Desilets M.O. (1987) A review of the use of loss on ignition as a measurement of total volatiles in whole rock analysis. *Chemical Geology 63 (3-4): 341-344.*

Protocol for whole–rock acid digestion for major and trace element analysis by ICP-OES and ICP-MS

Introduction

This protocol describes a method for whole rocks acid digestion (with HNO_3, HF and $HClO_4$) for major and trace element (including REE and except Zr and Nb) analysis by ICP-OES and ICP-MS. As with any technique, there are some exceptions. With this method all the elements can be determined except Si. Strontium, Zn and Ba are better detected by means of ICP-OES, whereas the rest of trace elements. Finally, it is observed that better results are obtained with Zr and Nb if they are analysed with XRF.

Methodology

The developed method for the determination of major, trace and REE elements by means of total attack is based in the indications given by the Serveis Científico – Tècnics, Universitat de Barcelona, but with significant modifications. The process followed is described below:

1. Sample preparation: Dry the sample rock at room temperature or maximum 40 ºC in an oven. Crush the sample to minus 5 mm. Split the rock. Pulverize the rock in a widia mortar to <0.25 mm particle size. If W is an analyte of interest, the mortar to be used will be of agatha.

2. Device cleaning**:** PFA digestion vessels (60ml, Ref. Savillex 301-060-03058-04) must be cleaned the day before the total attack. For all necessary blanks, standards, and samples, take into account the necessary replicates. In order to carry out this cleaning, about 3-5 ml of concentrated HNO_3 must be poured in each beaker. The beakers must be tightly closed and left in the furnace at 90 °C for about 12 hours. Once they are cooled, they must be rinsed with both distilled and deionized water, milliQ Plus type (18.2 MΩ cm^{-1}).

3. Sample weighing**:** Dry the sample rock in an oven at 60 ºC for 12 hours (minimum). When the vessels are dry, approximately 0.1 g of powdered sample is weighed. The exact weight of each sample is noted on the notebook. It is recommended to use consecutive numbers (for example, S1, S2, S3, etc.).

4. Once all the samples have been weighed, 2.5ml HNO_3 + 5ml HF + 2.5ml $HClO_4$ (v/v) are added to the vessels. They are then closed and left in the oven at 90°C for at least 12 hours.

5. Evaporation**:** Open the vessel inside a perchloric acid hood; check and note if the sample is completely dissolved. Evaporate to incipient dryness in a sand bath inside a perchloric acid hood. Left the vessels in the sand bath until perchloric fumes are evolved (the incipient dryness is achieved after the white perchloric vapour disappears).

6. Add twice 1 ml HNO_3 and evaporate to incipient dryness. This step and the next decompose most insoluble fluorides and drive off excess fluoride as HF.

7. Add 1 ml HNO_3 to the final waste and transfer the solution to a volume flask (100 ml), rinse with deionized water several times the PFA vessel and transfer also this solution to the volume flask. The resultant solution has 1 % of HNO_3 and it is ready for ICP-OES and ICP-MS analyse.

When the process is finished, the beakers are washed with tap water. Ask the laboratory technician if the beakers can be washed in the dishwasher. Otherwise, after washing the beakers with tap water, rinse them with distilled water.

Additional information: Use of perchloric acid hood

Perchloric acid hood has wash-down capabilities to prevent the buildup of explosive perchlorate salts within the exhaust system. When using perchloric acid the hood must be specifically designed such that it will not cause an explosion when it is turned on. Deadly and catastrophic explosions can result from perchlorate compounds that precipitate out onto the motors as their vapors are evacuated.

Protocol for the determination of major and trace elements in rocks by XRF

Introduction

The determination of major and trace elements can be carried out by X-Ray Fluorescence (XRF) spectrometry. In the case of this research, just Zr and Nb are analyzed by XRF while the rest of elements are determined by ICP-OES and ICP-MS.

Methodology

The method developed for the determination of major and trace elements by XRF follows the indications given by the XRF Unit of the *Serveis Científico – Tècnics, Universitat de Barcelona*. This is the process followed:

Determination of major elements

Before starting the process, we must be sure that the samples to be used (0.9 g of powder sample) have been in the oven at 90 °C at least 12 hours. We must also control that the pyrex glasses to be used have been previously washed with deionized water and then dried.

1. Weigh 0.3 g of sample in one of the pyrex glasses. The sample is mixed with lithium tetraborate 1:2 (usually 0.3 g of sample are mixed with 5.7 g of lithium tetraborate). They are mixed with a glass rod until homogeneous powder is obtained. The process is repeated twice to prepare two fused pearls for each sample.

2. Before starting the fusion, we will check that the platinum dish of the Perlex instrument is clean. Then the mixture is poured and 5 ml of lithium iodur is added (it acts as tensoactive).

3. Then press 'start' to begin the fusion. The mixture melts at about 1150 °C in the induction oven por radiofrequence. Once melt, the mixture is poured in a platinum dish. Then coolness starts (automatically) and it lasts for about 3 minutes. Finally the result is a pearl of about 30 mm of diameter with a surface completely flat. This process is done three times for each sample: the first pearl is used for the crucible cleaning, the second one is the measure and the third one is the duplicate.

Determination of trace elements

Before starting the process, we must make sure that the samples to be used (about 5 g of powdered sample) have been in the oven at 90 °C for at least 12 hours.

1. Powdered sample is weighed (6 g) and mixed with 2 ml of Elvacite 2044 diluted in acetone (20% solution) in an agate mortar, until homogeneous powder is obtained.

2. The bottom of an aluminum dish is filled with boric acid (powder). Then the sample with Elvacite is added over the boric acid layer. The dish is pressed and compacted using an Herzog press at a maximum pressure of 200 kN for 1 minute.

Protocol for the determination of fluoride in water ash leachate by means of Ion Selective Electrode (ISE)

Introduction

This method can be used for measuring total solubilised fluoride (F$^-$) rather than total F$^-$ Total solubilised fluoride is determined potentiometrically using a fluoride ion-selective electrode (ISE) in conjunction with a standard single-junction reference electrode, or a fluoride combination ISE, and a pH meter with an expanded millivolt scale (mV) or an ISE meter capable of being calibrated directly in terms of fluoride concentration.

ISEs must be used carefully and results must be interpreted cautiously, since an ISE may be affected by numerous analytical interferences which may either increase or decrease the apparent analyte concentration, or which may damage the ISE. Effects of most interference can be minimized or eliminated by adding appropriate chemical reagents to the sample. In this method standards and samples are mixed 1:1 with a total ionic strength adjustment buffer (TISAB III). TISAB adjusts ionic strength, buffers pH to 5-5.5, and contains a chelating agent to break up metal-fluoride complexes. TISAB III solution is available commercially (Orion 940999). Calibration is performed by analyzing a series of standards and plotting mV vs. fluoride concentration. Obtaining the most accurate results, therefore, requires some knowledge of the sample composition.

Methodology

The methodology developed for the determination of fluorine is based on the indications given in Model 96-09 Fluoride combination Electrode Instruction manual. Orion research, Inc, Boston, MA, 1988. The process carried out is described below:

1. Sample preparation: Samples must be stored and handled in polyethylene containers. Samples should be stored at 4 ºC.
2. Devices cleaning: Use only polyethylene beaker previously cleaned with HNO_3 50%. The solutions are left in their containers for 12 hours. Then all the devices are rinsed with both distilled and deionized water, milliQ Plus type (18.2 MΩ cm^{-1}).
3. Ensure that the ISE is filled with the solution recommended by the manufacturer. Change the solution if the ISE not has been used for a week.

4. Calibration: Calibrate the fluoride ISE using standards that narrowly bracket the expected sample concentration. If the sample concentration is unknown, calibrate with 1.00 mg l^{-1} and 10.0 mg l^{-1} fluoride standards. Add 20 mL of standard and 20 mL of TISAB to a 50 mL polyethylene beaker. Add a PTFE-coated magnetic stir bar, place the beaker on a magnetic stir plate, and stir at slow speed (no visible vortex). Immerse the electrode tips to just above the rotating stir bar. If using an ISE meter, calibrate the meter in terms of fluoride concentration following the manufacturer's instructions. If using a pH/mV meter, record the meter reading (mV) as soon as the reading is stable, but in no case should the time exceed five minutes after immersing the electrode tips. Prepare a calibration curve by plotting measured potential (mV) as a function of the logarithm of fluoride concentration. The slope must be 54-60 mV per decade of fluoride concentration. If the slope is not acceptable, the ISE may not be working properly.

5. Allow samples and standards to equilibrate to room temperature.

6. Prior to and between analyses, rinse the electrode thoroughly with reagent water and gently shake off excess water. Low-level measurements are faster if the electrode tips are first immersed for five minutes in reagent water.

7. Add 20 ml of sample and 20 mL of TISAB to a 50 mL polyethylene beaker. Add a PTFE-coated magnetic stir bar. Place the beaker on a magnetic stir plate and stir at a slow speed (no visible vortex). Immerse the electrode tips to just above the rotating stir bar. Record the meter reading (mV) as soon as the reading is stable, but in no case should the time exceed five minutes after immersing the electrode tips. Reading mV, determine fluoride concentration from the calibration curve.

8. When analyses have been completed, rinse the electrode thoroughly and store it in a 10.0 mg l^{-1} fluoride standard solution. If the electrode will not be used more than one day, drain the internal filling solution, rinse with deionised water, and store it dry.

Appendix 2

Additional SEM images of the samples under study
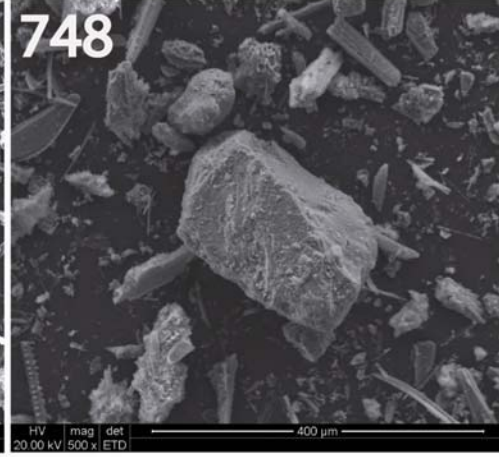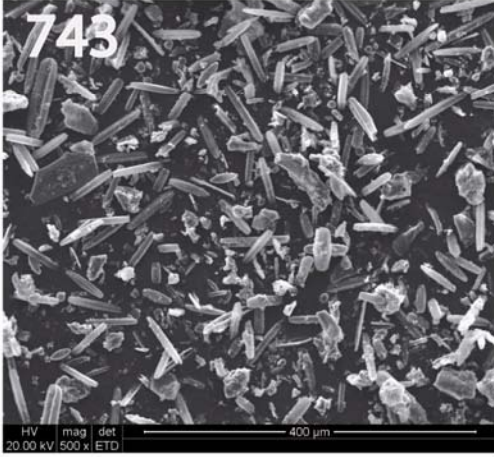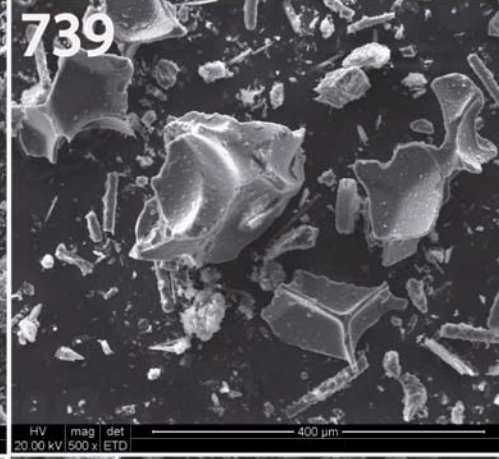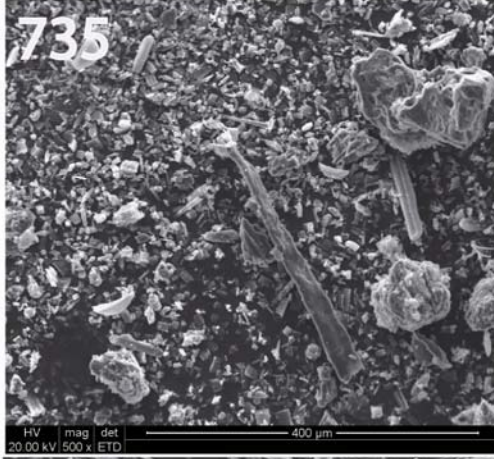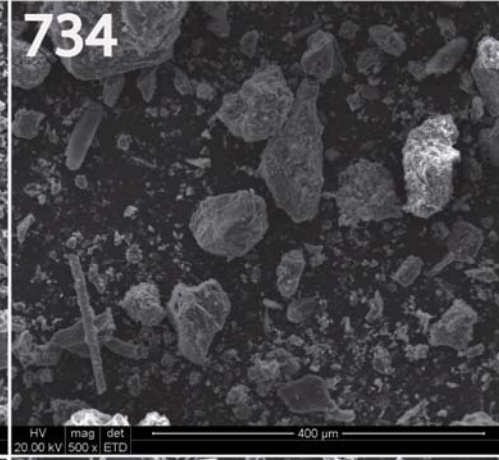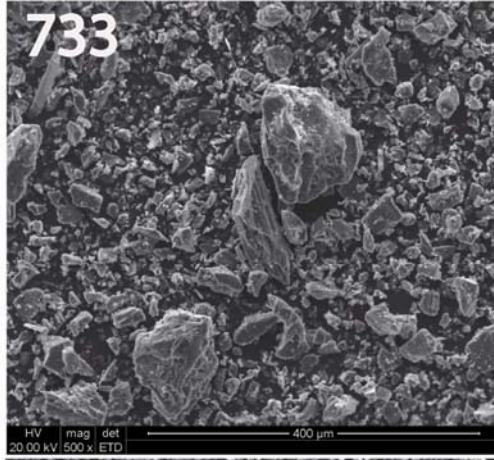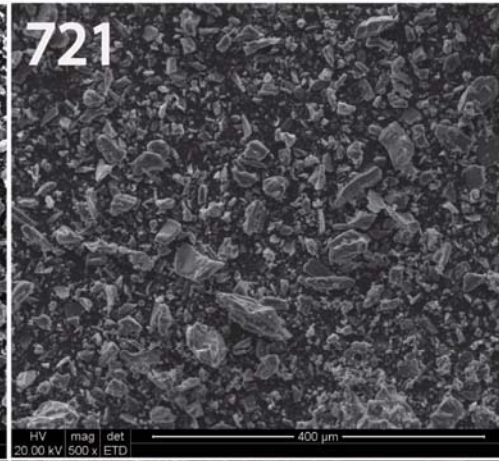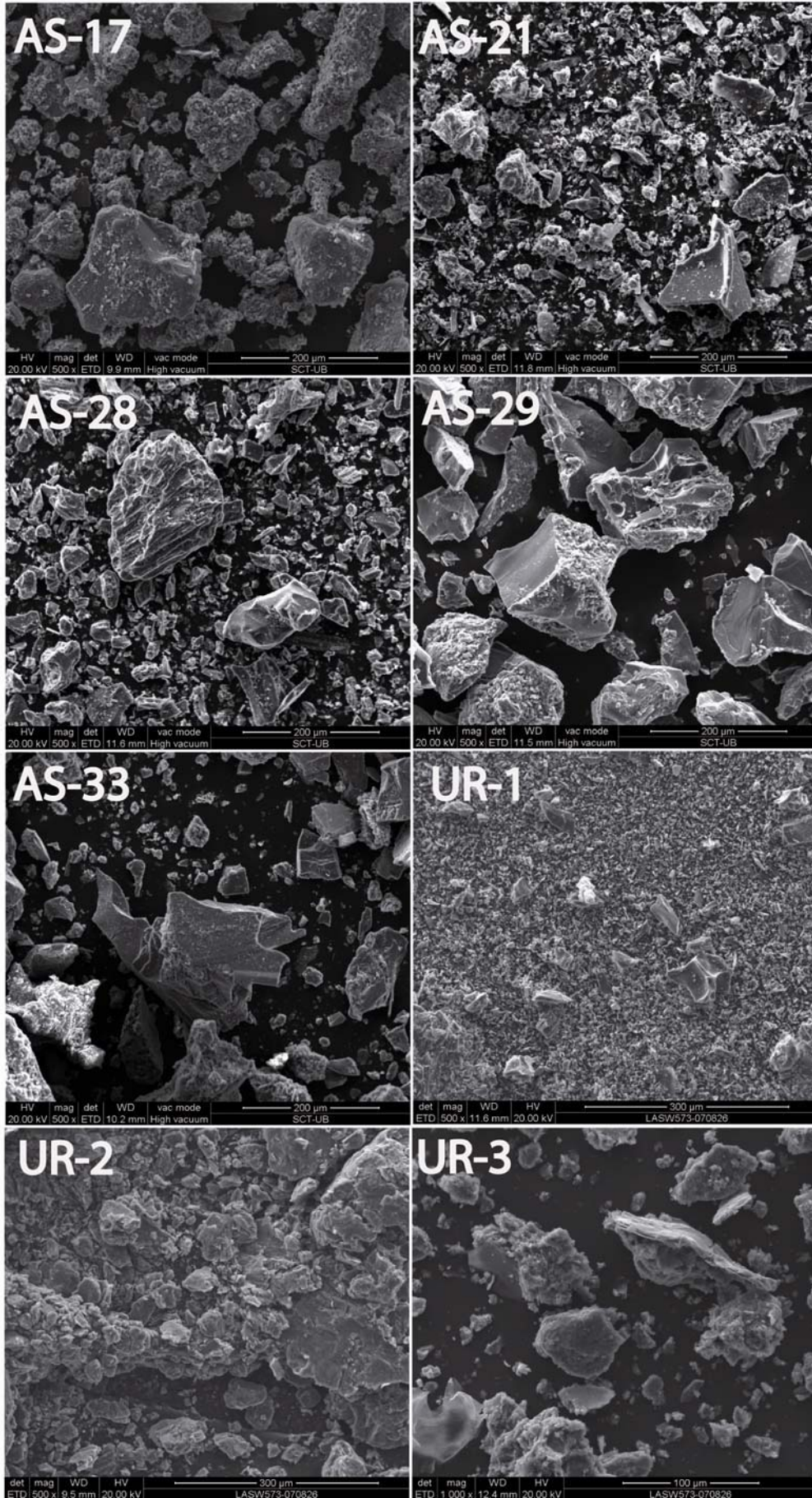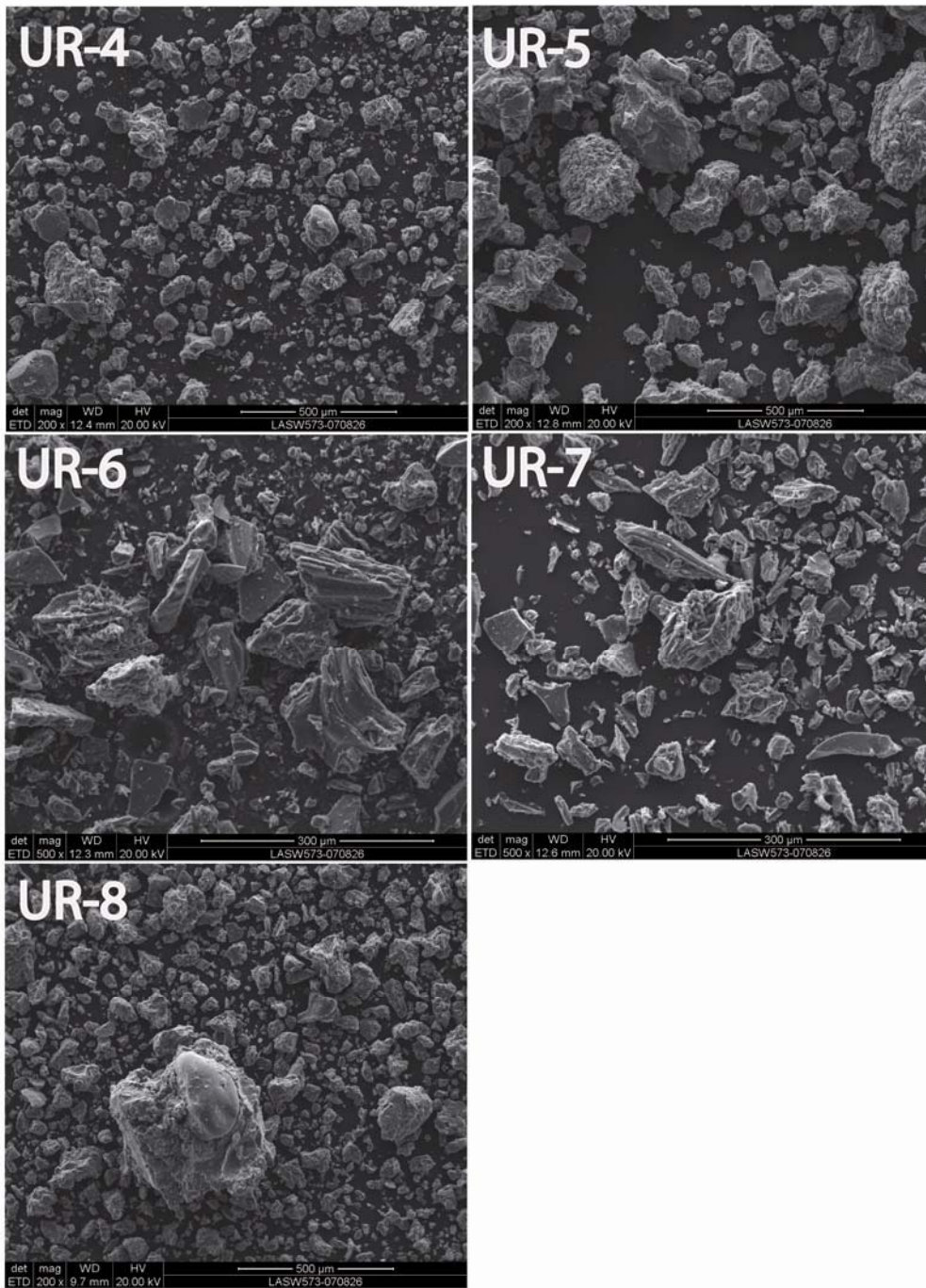
Figure 2.1 SEM images of the sample collected in the southern Puna and Uruguay.

Appendix 3

XRD patterns of the volcanic ashes under study
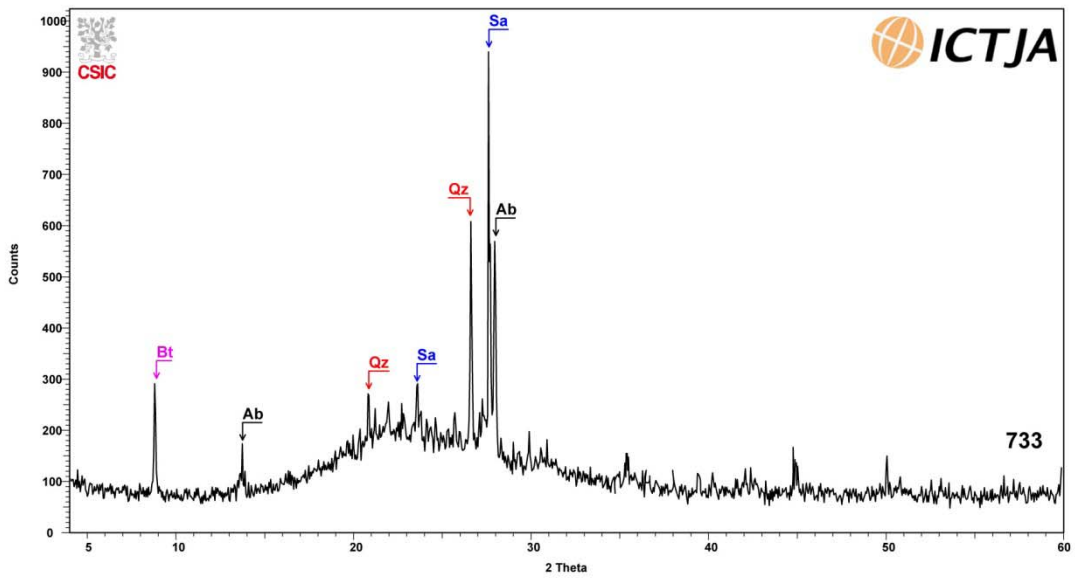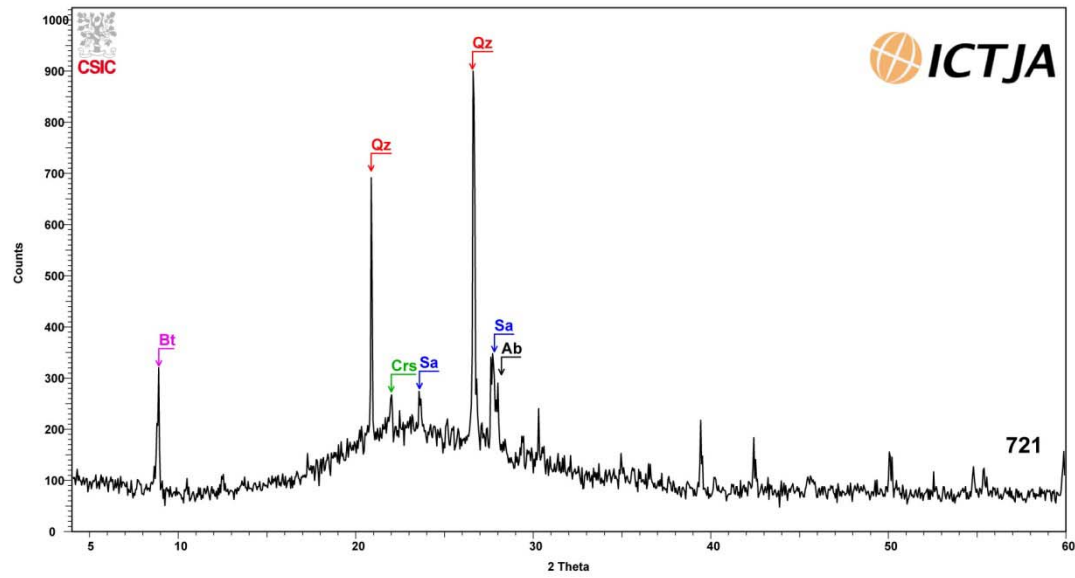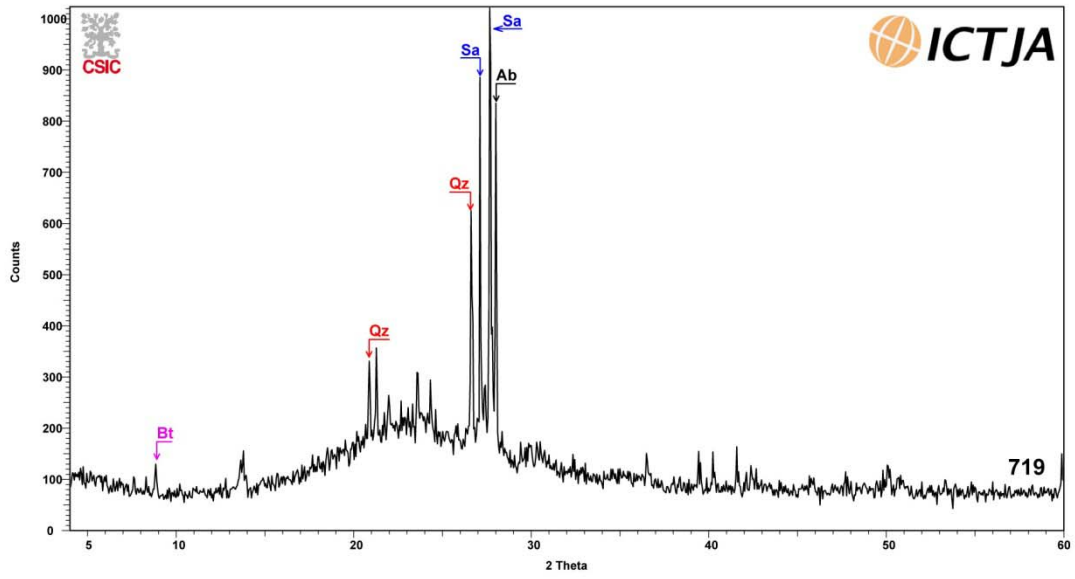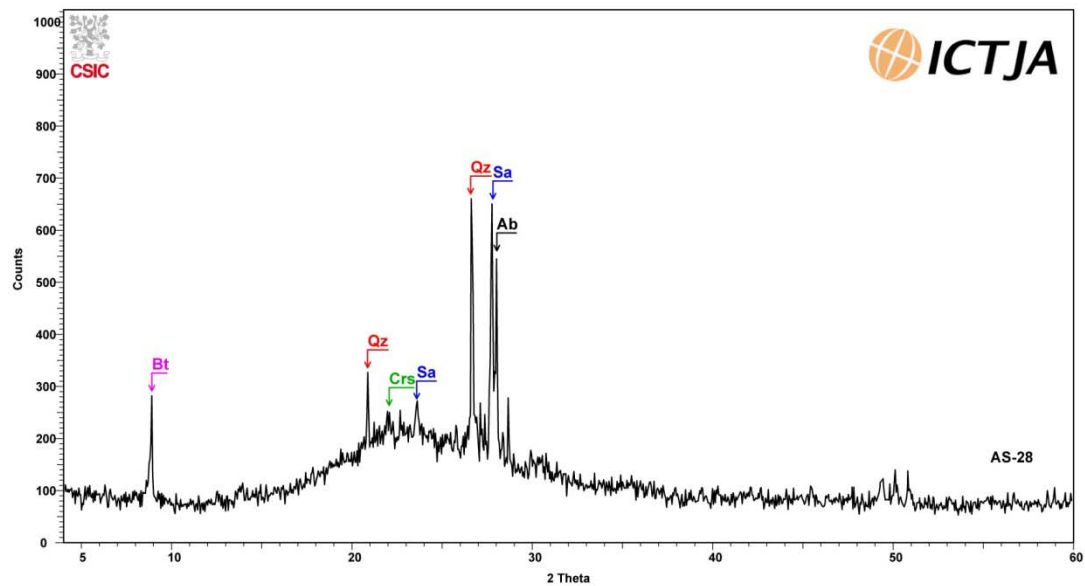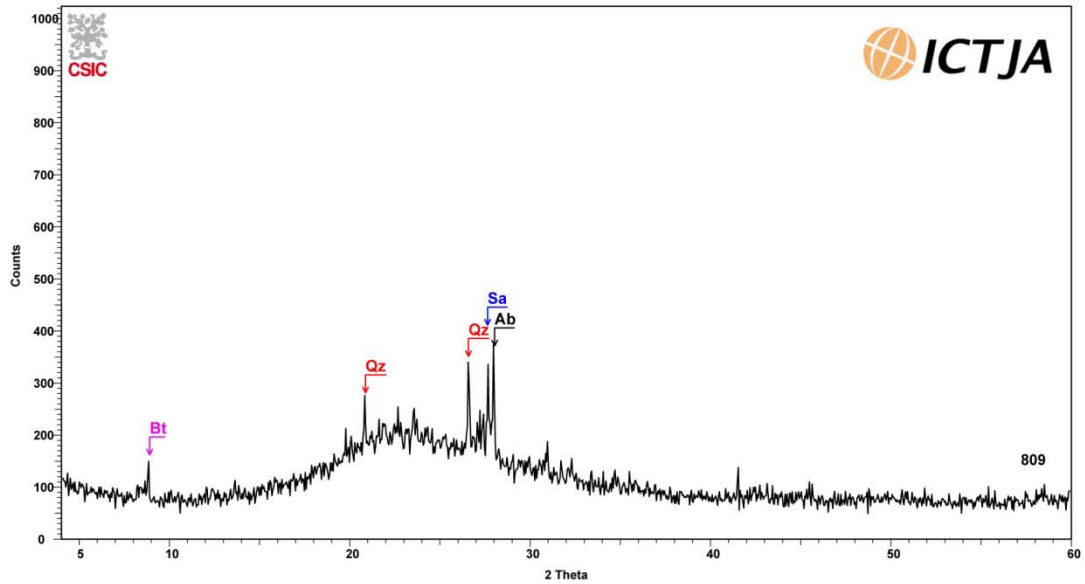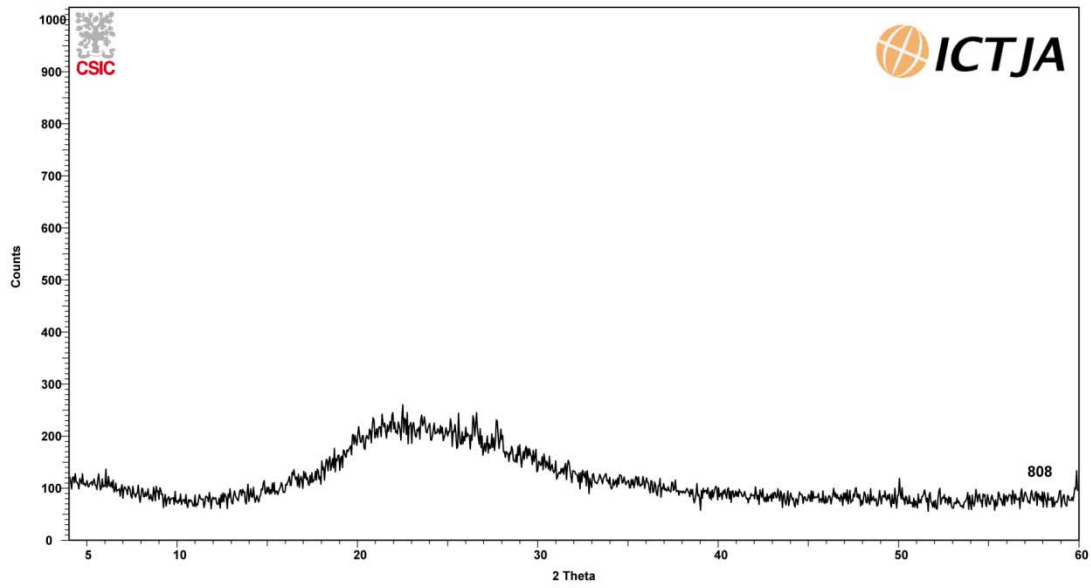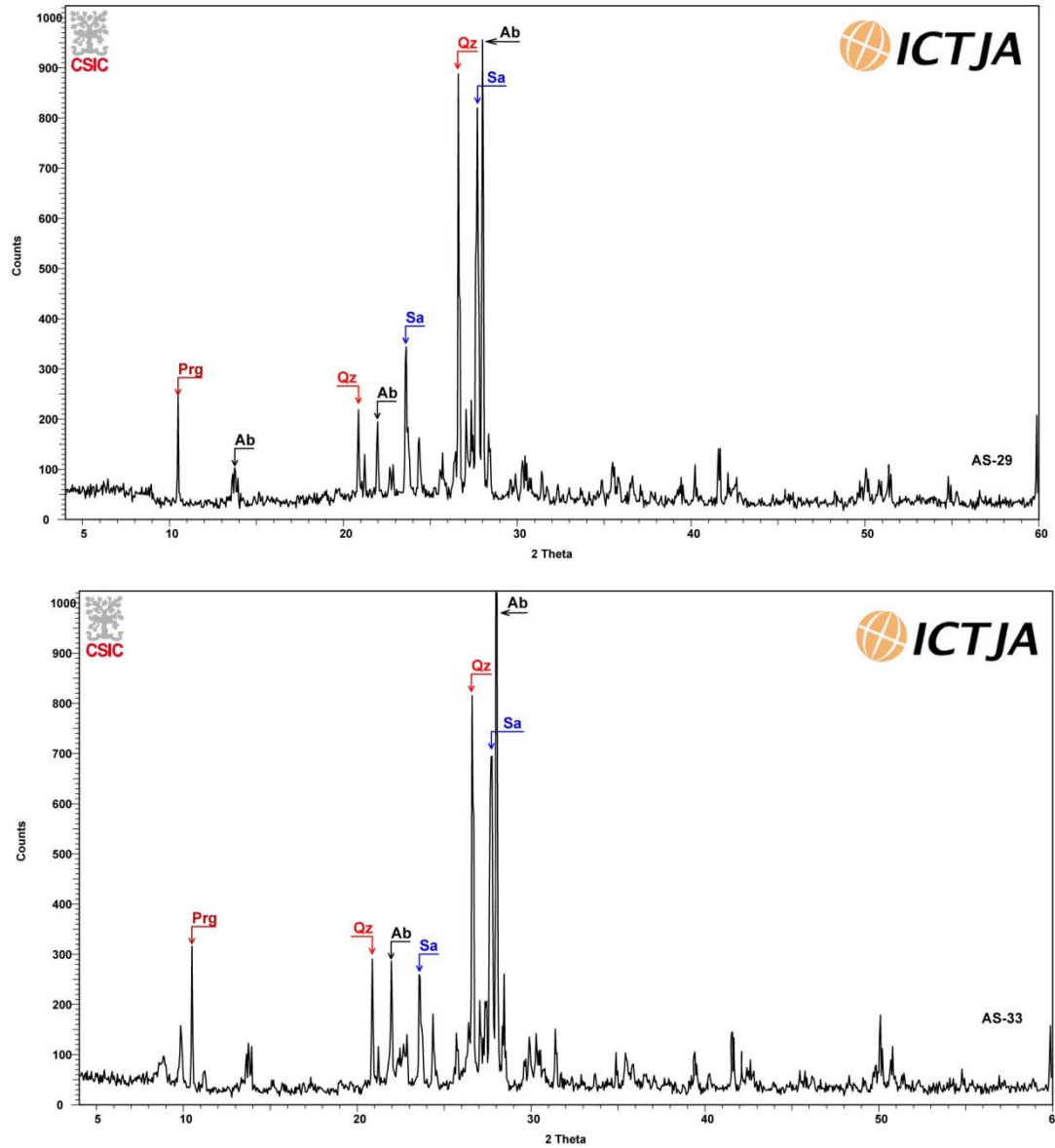
Figure 3.1 XRD patterns of the volcanic ashes from southern Puna and neighbouring areas. Qz, Quartz; Ab, Albite; Sa, Sanidine; Bt, Biotite; Crs, Cristobalite; Prg, Pargasite (mineral abbreviations from Whitney and Evans, 2010).
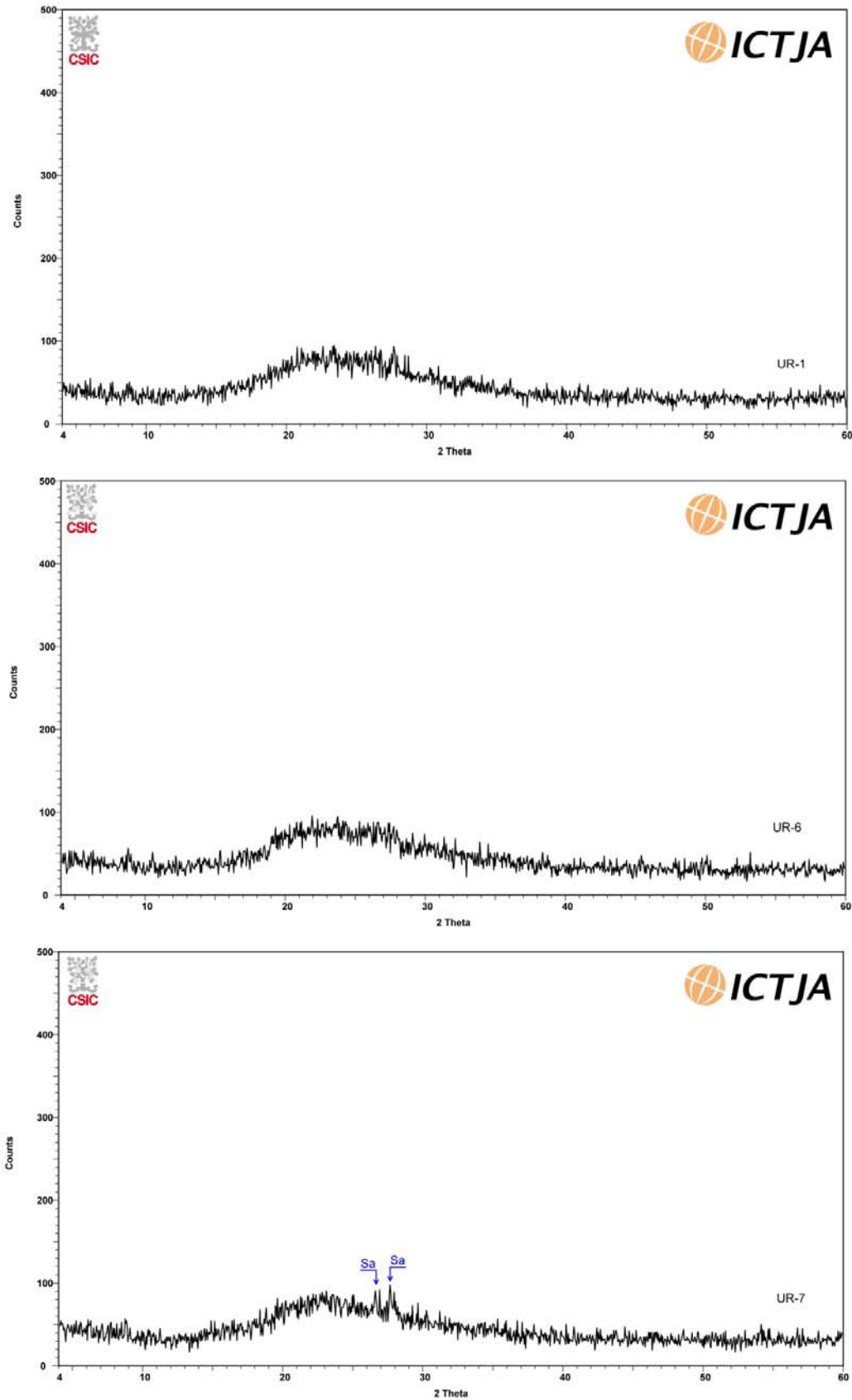
Figure 3.2 XRD patterns of the volcanic ash from Uruguay. Sa, Sanidine (mineral abbreviations from Whitney and Evans, 2010).
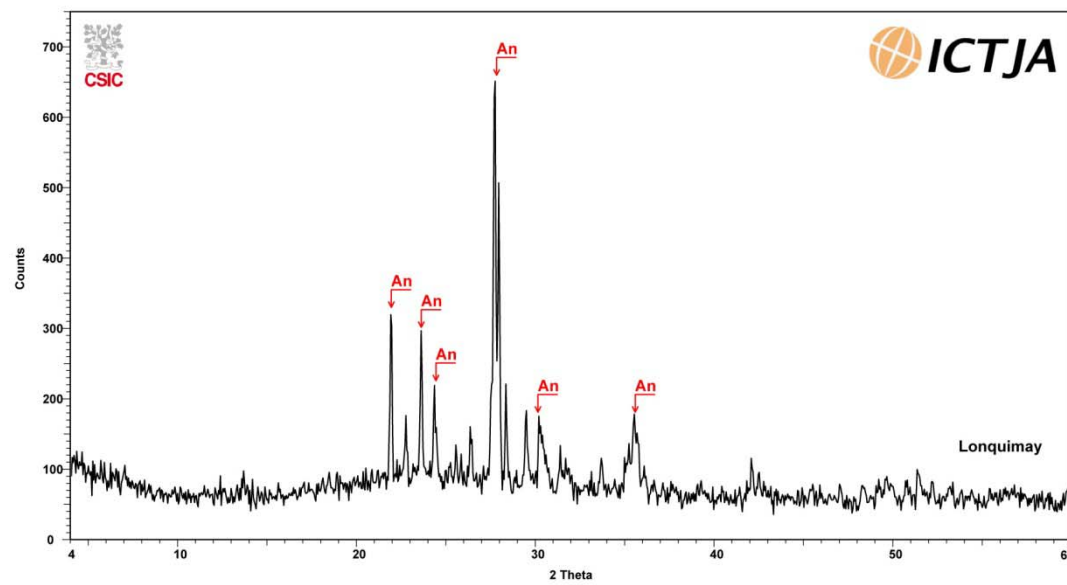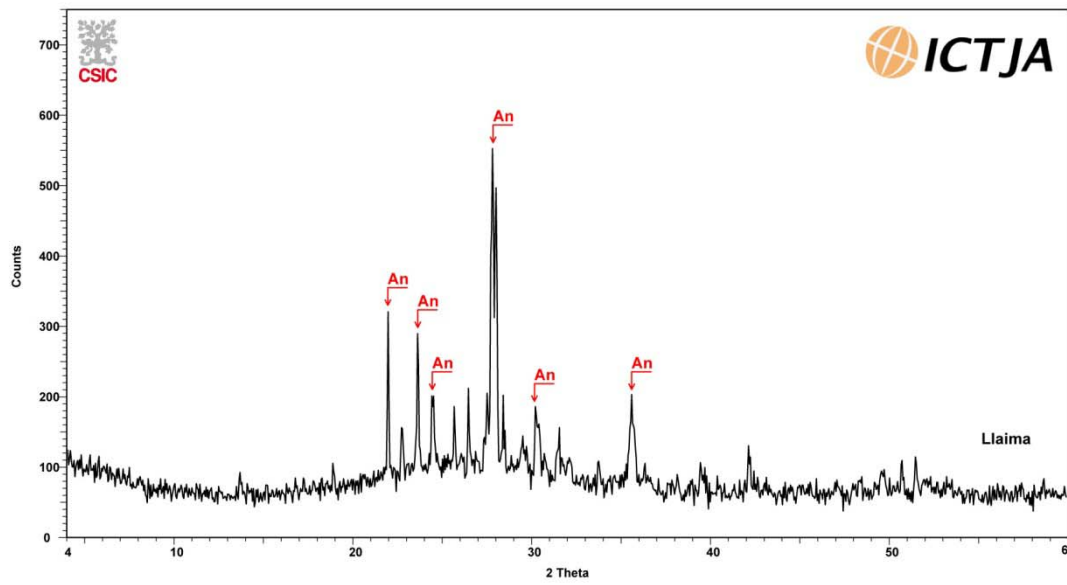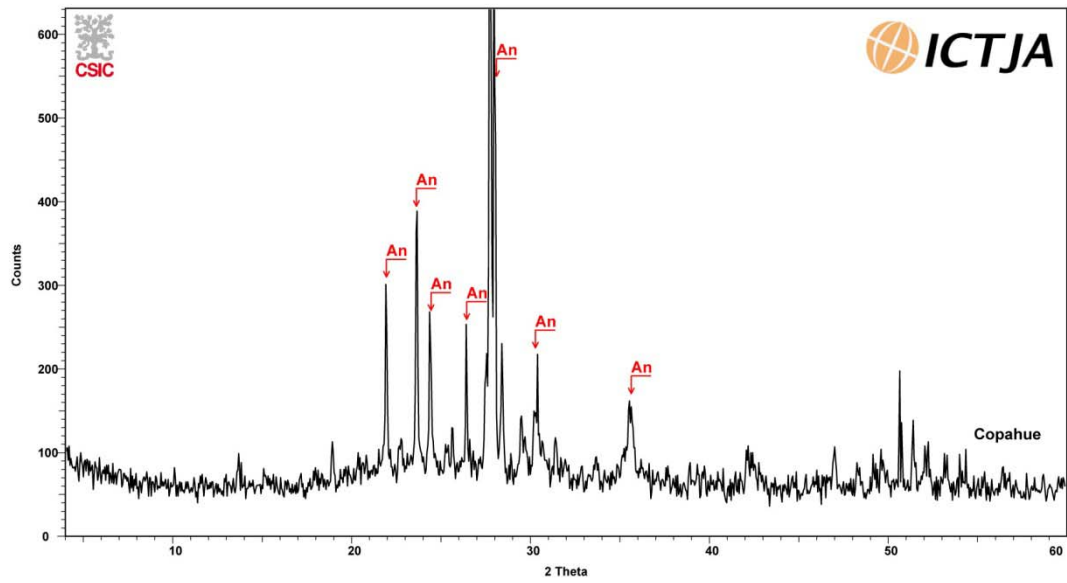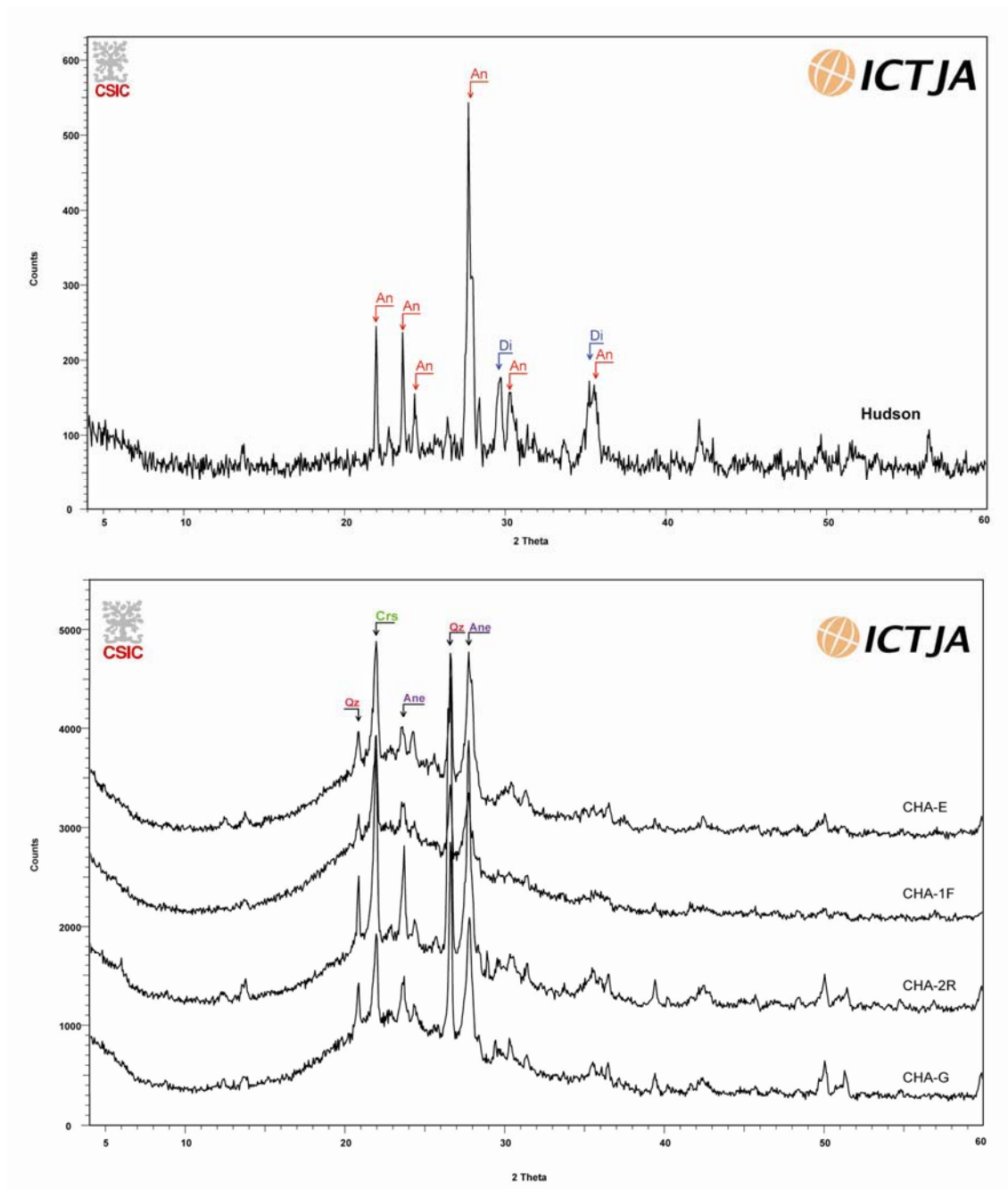
Figure 3.3 XRD patterns of the recent volcanic ashes from the SVZ. Qz, Quartz; Crs, Cristobalite; Di, Diopside; An, Anorthite; Ane, Andesite (mineral abbreviations from Whitney and Evans, 2010).

Appendix 4

Average element concentrations and relative standard deviation of the SBLT data set

Table 4.1 Statistical observation of CHA-1F data set (µg g^{-1}). LoD, limit of detection; nd, not determined.

	mean	RSD%	mean	RSD%	mean	RSD%	mean	RSD%	mean	RSD%
Weight (g)	0.1		0.1		0.1		0.1		0.1	
Time (h)	1.5		1.5		1.5		16		16	
Volume (ml)	1		2.5		5		1		2.5	
Ca	123	4.5	133	18.8	140	20.1	152	20.1	132	16.4
Mg	128	5.6	90.6	17.4	87	10.0	226	8.5	150	13.6
Na	102	37.0	106	17.5	87	10.0	415	8.0	383	8.8
K	199	36.1	108	35.2	135	23.9	56.8	89.4	59.8	39.7
Si	322	12.7	235	5.0	220	9.6	591	12.0	391	11.8
Cl	273	75.7	< LoD	nd	< LoD	nd	< LoD	nd	< LoD	nd
SO$_4^{2-}$	365	25.7	371	28.7	257	20.6	266	36.7	332	20.5
Li	196	14.4	211	9.0	161	14.4	458	11.4	347	11.4
Be	6.6	172	4.7	260.1	10.8	56.2	16.8	58.6	12.9	86.5
B	3222	50.6	6110	32.5	4695	75.9	3151	31.7	3332	67.8
Al	180549	15.0	118820	9.2	94256	8.8	332337	10.5	220633	14.1
P	10280	31.8	5653	27.3	2954	33.8	7454	17.6	5165	24.1
Ti	1764	11.8	1211	18.4	860	19.8	3816	13.4	2524	11.3
V	397	11.7	284	11.3	213	17.5	861	12.1	590	15.7
Cr	61.9	131.7	< LoD	nd	< LoD	nd	129	42.3	14.9	315.9
Fe	164599	12.7	116420	7.0	106777	10.9	370830	10.8	246465	13.5
Mn	5437	8.4	4212	6.3	3529	6.6	12146	10.0	8387	11.8
Co	63.3	9.8	49.5	25.1	39	9.2	148	9.5	104	14.1
Ni	371	122.4	91.6	15.7	151	15.2	239	11.4	174	22.4
Cu	370	41.9	2026	163.6	354	64.4	506	21.4	395	15.7
Zn	4044	13.9	4090	60.7	3594	31.2	4013	6.2	3842	18.5
Ga	66.8	14.1	48.4	17.4	35	11.5	122	11.0	85.0	9.7
Ge	4.3	9.6	3.6	33.9	4.5	65.7	10.0	43.8	6.8	66.1
As	3716	5.9	3672	3.8	3492	6.1	5581	6.8	4883	6.9
Br	3076	24.5	2799	19.7	2137	14.5	2138	26.3	1779	29.2
Rb	309	5.7	255	4.8	227	2.6	415	4.6	317	9.9
Sr	458	49.0	430	30.7	386	25.5	697	21.9	453	31.5
Zr	114	17.1	93.1	33.2	74	15.6	105	33.8	98.9	25.5
Nb	28.0	29.4	16.1	11.8	13	14.9	15.8	5.6	11.6	17.7
Mo	71.0	19.9	67.6	20.6	48	14.2	55	14.5	54.9	11.3
Cd	56.8	99.8	< LoD	nd	< LoD	nd	< LoD	nd	< LoD	nd
Sn	39	41.5	22.9	35.8	13.1	18.5	35.2	22.1	41.6	28.0
Sb	151	29.0	97.5	12.3	80.4	11.9	199.5	8.6	213	7.1
Te	65.7	56.9	27.6	66.2	12.4	205.7	10.3	122.5	24.0	23.4
Cs	39.8	7.8	29.9	5.9	27.0	9.7	71.0	6.8	53.2	13.7
Ba	1145	12.1	789	3.7	705	7.0	2084	9.5	1451	22.9
Tl	4.3	67.0	2.3	30.4	1	56.8	3	25.9	3	47.8
Pb	226	53.3	215	84.5	112	10.5	309	17.9	226	25.5
Bi	16.2	12.9	13	8.7	8	5.7	16	6.7	13.6	16.3
Th	31.2	12.2	20	12.2	15	13.3	30	9.5	22.9	9.9
U	4.7	24.9	6	26.6	4	79.9	6	8.6	3.4	20.2

Table 4.1 continuation

	mean	RSD%	mean	RSD%	mean	RSD%	mean	RSD%	mean	RSD%
Weight (g)	0.1		0.1		0.1		0.1		1	
Time (h)	16		4		4		4		1.5	
Volume (ml)	5		1		2.5		5		10	
Ca	292	25.1	49.0	13.1	40.4	27.5	39.0	11.2	142	13.3
Mg	63	48.1	27.0	20.8	32.0	27.5	24.3	19.6	30.8	11.3
Na	297	149.4	63.8	334.1	< LoD	nd	< LoD	nd	50.2	10.9
K	70.6	56.4	26.8	62.3	28.5	149.6	14.1	165.1	33.7	8.9
Si	145	55.7	134	10.3	120	5.6	102	8.7	111	7.5
Cl	85.5	85.5	251	148.1	495	12.1	400	20.8	37.1	28.8
SO$_4^{2-}$	208	43.7	625	16.6	741	14.1	695	23.7	258	21.1
Li	236	23.1	138	17.4	150	5.1	140	9.4	91.3	5.4
Be	< LoD	nd	< LoD	nd	< LoD	nd	< LoD	-97.3	0.1	917.7
B	53358	98.5	1892	45.2	2212	41.4	1566	37.6	1268	63.4
Al	81581	79.1	63086	7.6	46794	10.7	36214	17.3	52322	11.5
P	< LoD	nd	< LoD	nd	< LoD	nd	< LoD	nd	1653	19.2
Ti	1214	124.9	1068	28.8	511	16.0	430	50.7	440	17.8
V	244	50.7	186	27.1	258	16.2	200	37.9	158	9.6
Cr	< LoD	nd	< LoD	nd	< LoD	nd	< LoD	nd	63.2	31.5
Fe	73377	84.6	57877	19.0	46260	7.6	35647	4.5	49209	9.2
Mn	5083	42.3	2126	10.6	1947	7.9	1447	13.0	1775	11.7
Co	23.3	115.2	14.9	37.5	12.6	13.4	10.1	48.5	16.2	9.0
Ni	278	55.1	126	12.8	150	14.0	256	92.0	31.1	3.5
Cu	569	36.5	241	19.0	446	59.7	240	31.9	162	114.2
Zn	4114	18.8	7859	61.3	7519	29.6	11394	70.1	625	37.2
Ga	29.2	84.0	23.2	5.7	18.5	18.4	13.5	14.7	16.7	10.6
Ge	1.8	364.3	< LoD	nd	< LoD	nd	< LoD	nd	1.0	35.2
As	2426	20.0	1923	27.5	2627	10.4	2562	16.6	2293	0.8
Br	454	91.6	270	275.6	898	47.4	534	65.6	69	93.1
Rb	237	29.5	156	7.5	159	6.1	141	18.3	108	9.9
Sr	677	42.9	149	58.8	94.5	72.6	75.7	198.3	278	15.8
Zr	44.9	59.9	61.5	52.7	30.3	10.9	126	155.9	20.8	11.8
Nb	15.0	118.9	10.5	24.0	< LoD	nd	< LoD	nd	1.8	13.1
Mo	82.9	43.4	90.6	66.1	85.8	37.3	70.7	42.3	34.3	16.8
Cd	2.7	145.5	< LoD	nd	3.8	78.0	3.4	139.4	22.8	201.0
Sn	24.1	36.0	18.4	28.7	22.3	24.3	16.9	14.1	8.5	97.0
Sb	35.9	21.8	24.9	19.9	30.9	4.1	27.6	7.6	27.6	6.3
Te	10.5	168.2	9.6	107.9	36.4	53.2	16.7	30.3	5.8	21.7
Cs	28.3	57.9	23.6	5.8	23.1	12.4	17.0	16.4	11.4	11.6
Ba	944	36.6	716	30.2	425	18.4	348	13.7	310	11.9
Tl	< LoD	nd	< LoD	nd	< LoD	nd	< LoD	nd	0.5	49.4
Pb	147	26.6	93	30.2	86.3	19.6	76.7	13.9	38.7	32.1
Bi	3.3	57.1	2.1	37.9	2.0	29.2	1.3	50.2	1.9	14.8
Th	3.5	124.4	27.9	159.9	< LoD	nd	< LoD	nd	4.3	11.9
U	3.4	63.1	2.9	59.1	0.4	166.5	0.2	431.4	0.9	24.6

Table 4.1 continuation

	mean	RSD%	mean	RSD%	mean	RSD%	mean	RSD%
Weight (g)	1		1		1		1	
Time (h)	1.5		1.5		16		16	
Volume (ml)	25		50		10		25	
Ca	153	24.8	167	5.6	208	9.9	326	14.9
Mg	26.7	95.0	16.3	57.9	22.8	30.5	36.3	22.0
Na	42.7	16.3	39.6	10.3	150	50.3	95.3	16.8
K	28.8	31.8	30.6	14.6	32.5	25.6	36.8	10.2
Si	98.1	69.1	73.8	40.7	63.2	3.9	91.9	15.3
Cl	12.3	64.3	< LoD	nd	137	32.6	229	7.7
SO_4^{2-}	205	8.2	250	9.8	280	19.8	262	12.9
Li	103	25.6	102.2	11.4	106	10.7	83.7	15.0
Be	0.7	144.2	0.1	642	0.5	205	2.5	56.9
B	1223	47.1	1142	35.5	1179	77.9	606	19.8
Al	45025	98.3	25438	55.3	20876	14.4	61992	32.7
P	1944	140.3	479	56.6	2253	40.8	7663	35.5
Ti	513	129.9	208	71.7	219	15.4	817	41.5
V	147	75.9	102	41.8	95.5	8.0	165	23.0
Cr	48.4	107.8	19.5	124.3	33.0	21.2	62.7	25.4
Fe	46873	116.2	22446	75.9	18830	25.9	50583	39.7
Mn	2241	116.7	1111	40.6	1151	14.9	3549	41.3
Co	17.3	123.8	7.3	64.6	21.2	102.2	28.0	35.3
Ni	39.3	102.9	22.3	47.7	80.8	26.9	98.4	17.3
Cu	246	80.0	228	84.6	603	61.6	659	16.0
Zn	649	64.7	599	38.6	3898	61.7	4088	48.6
Ga	19.8	72.1	9.6	48.3	8.4	13.9	19.6	26.1
Ge	0.7	123.4	0.6	84.6	0.5	65.7	0.9	40.0
As	2307	21.8	2199	6.5	2509	9.7	3968	16.9
Br	18.4	418.9	114	27.2	183	61.8	271	19.6
Rb	101	42.9	89.6	13.8	101	17.6	173	25.6
Sr	295	39.9	262	10.4	394	24.6	566	15.0
Zr	23.1	72.9	14.2	44.7	24.3	81.7	23.0	21.3
Nb	1.4	27.9	0.9	44.3	0.8	18.2	2.5	14.4
Mo	29.2	7.9	34.7	6.5	39.0	12.4	41.1	11.8
Cd	0.9	171.7	< LoD	nd	0.6	72.5	2.1	37.3
Sn	5.1	43.7	4.7	54.0	6.8	35.4	9.3	25.3
Sb	24.7	28.5	22.8	7.3	36.2	17.0	51.9	11.3
Te	2.7	74.7	2.1	11.3	1.7	103.6	9.3	29.2
Cs	10.8	88.3	6.7	41.8	12.1	32.3	34.6	31.6
Ba	290	91.0	176	44.2	384	34.8	812	28.8
Tl	0.5	101.4	0.2	139.5	0.3	61.4	1.5	16.7
Pb	62.9	75.7	30.8	27.3	73.5	48.4	170	33.7
Bi	2.2	87.1	1.0	34.9	1.6	41.0	5.1	55.3
Th	4.5	96.3	2.2	41.3	1.4	13.8	5.7	19.2
U	1.1	81.5	0.5	27.1	2.2	58.1	3.3	26.1

Table 4.1 continuation

	mean	RSD%	mean	RSD%	mean	RSD%	mean	RSD%
Weight (g)	1		1		1		1	
Time (h)	16		4		4		4	
Volume (ml)	50		10		25		50	
Ca	294	8.0	61.5	9.5	65.7	11.5	94.5	9.7
Mg	24.1	18.6	6.6	18.6	5.4	12.4	6.9	12.6
Na	102	13.6	56.3	30.0	68.4	20.8	78.9	19.8
K	27.3	3.8	16.4	2.8	26.8	12.5	23.9	11.0
Si	95.0	5.0	29.4	15.1	30.8	7.2	36.5	6.4
Cl⁻	192	14.1	71.4	6.5	72.3	10.3	66.3	17.3
SO₄²⁻	235	7.7	312	7.1	304	8.6	349	10.4
Li	84.6	7.7	126	3.6	108	2.0	119	5.7
Be	1.4	45.1	0.9	434.5	< LoD	nd	< LoD	nd
B	676	30.4	2649	65.6	1277	10.9	1585	93.9
Al	32076	13.1	9232	42.4	7420	46.5	6942	5.7
P	3539	12.4	< LoD	nd	3539	150.0	956	506
Ti	303	18.1	111	53.0	139	33.5	114	61.6
V	122	9.8	65.0	14.4	55.0	16.3	62.3	5.5
Cr	50.2	9.8	13.9	64.3	1.6	194.6	0.7	650
Fe	18435	24.4	6830	44.9	5043	31.8	5085	10.1
Mn	1415	13.8	721	17.7	558	22.8	835	9.6
Co	11	13.6	3.1	41.3	2.5	33.8	2.6	3.3
Ni	102	26.1	29.2	20.0	33.3	20.1	30	23.7
Cu	700	13.4	73.6	41.4	85.0	41.9	78	48.3
Zn	2426	27.5	1215	56.6	640	13.8	658	17.9
Ga	10.7	11.3	4.0	37.0	3.0	40.3	3.1	8.6
Ge	0.6	42.1	0.2	129.8	0.1	321.7	0.5	90.4
As	3511	4.0	1672	10.9	1596	3.2	1848	5.4
Br	373	12.0	125	9.3	85.9	59.1	68.7	59.8
Rb	106	3.9	91.3	15.7	79.4	11.3	88.2	3.9
Sr	518	17.8	108	5.1	123	8.1	148	12.2
Zr	17.3	47.5	10.8	46.0	8.6	19.2	9.2	45.8
Nb	1.5	24.1	0.2	170	0.1	297.4	0.4	87.9
Mo	38.2	7.1	35.0	8.4	32.0	20.6	36.7	5.2
Cd	1.9	67.0	0.4	117	1.3	38.4	0.9	62.1
Sn	22.5	61.9	3.0	9.0	3.3	15.5	3.2	25.2
Sb	46.7	9.5	13.7	10.3	11.6	3.3	13.5	3.6
Te	5.1	31.2	2.1	81.6	3.2	84.8	2.7	33.9
Cs	12.5	19.3	6.5	26.4	5.0	18.1	6.0	4.7
Ba	477	4.1	90.5	18.2	85.1	31.6	100	7.1
Tl	0.4	21.8	< LoD	nd	< LoD	nd	0.1	78.8
Pb	126	32.1	17.1	19.2	26	46.2	17.2	40.3
Bi	2.3	25.5	0.4	50.5	0.4	34.0	0.4	20.8
Th	2.4	30.0	0.5	56.3	0.2	163.6	0.4	26.8
U	2.3	9.7	0.3	52.3	0.3	45.9	0.4	30.2

Table 4.2 Statistical observation of the 719 data set(μg g^{-1}). LoD, limit of detection; nd, not determined.

	mean	RSD%	mean	RSD%	mean	RSD%	mean	RSD%	mean	RSD%
Weight (g)	0.1		0.1		0.1		0.1		0.1	
Time (h)	1.5		1.5		1.5		16		16	
Volume (ml)	1		2.5		5		1		2.5	
Ca	103	23.6	80	19.1	105	20.7	748	4.5	731	3.4
Mg	< LoD	nd	< LoD	nd	< LoD	nd	32.2	9.2	15.6	47.2
Na	111	304	238	71.9	55.2	515	149	107	266	26.0
K	157	36.1	63.3	46.2	51.2	51.8	85.6	34.0	132.0	23.1
Si	90	2.2	73.5	8.1	66.4	19.1	160.3	23.5	97.3	8.2
Cl$^-$	679	13.6	569	15.2	489	8.2	614	3.1	564	15.5
SO$_4^{2-}$	619	36.0	393	40.2	375	17.7	< LoD	nd	356	29.2
Li	171	6.9	173	11.1	228	74.9	394	17.6	284	17.5
Be	31.9	40.4	50.4	19.3	55.3	19.1	78.8	11.7	65.2	15.2
B	2736	59.9	1748	31.4	1883	82.9	63406	57.6	16777	79.9
Al	13577	14.1	27159	109	7726	21.1	59244	20.6	32295	16.0
P	24940	36.9	23041	51.6	47885	42.1	28269	60.7	< LoD	nd
Ti	385	13.9	460	13.0	253	38.4	1454	26.5	789	23.4
V	18.8	236.4	8.4	434	< LoD	nd	30.3	95.6	13.2	62.4
Cr	-265	-12.8	< LoD	nd	< LoD	nd	< LoD	nd	< LoD	nd
Fe	1357	53.7	1817	103.2	< LoD	nd	20208	29.0	13186	13.6
Mn	370	18.4	529	23.0	317	24.5	2598	23.3	1411	9.0
Co	9.4	8.0	8.7	21.9	8.9	25.8	26.2	15.8	22.7	47.6
Ni	255	68.5	172	24.5	171	14.8	235	52.6	242	21.1
Cu	492	14.1	388	59.1	266	24.7	603	9.6	622	24.1
Zn	9377	32.2	8622	86.2	9784	27.7	4350	22.4	5961	43.1
Ga	8.3	18.6	11.0	37.4	6.8	2.9	28.1	28.7	18.2	21.2
Ge	< LoD	nd	< LoD	nd	< LoD	nd	7	31.7	3.5	58.6
As	< LoD	nd	< LoD	nd	< LoD	nd	< LoD	nd	< LoD	nd
Br	< LoD	nd	< LoD	nd	< LoD	nd	< LoD	nd	< LoD	nd
Rb	209	7.5	176	8.8	136	13.1	506	24.7	326	11.1
Sr	246	31.2	191	61.7	230	30.8	1751	4.1	1751	7.9
Zr	47.5	44.6	38.3	37.2	22.0	50.6	65.4	42.1	39.9	41.5
Nb	10.7	20.1	8.7	24.2	5.0	19.0	31.0	29.3	19.9	37.8
Mo	66.5	14.7	382	163	58.3	24.4	39.0	30.4	69.0	87.7
Cd	1.5	178.1	2.9	123.3	5.9	71.3	56.1	198	4.7	116.5
Sn	23.5	38.1	25.9	50.1	18.5	12.6	25.6	10.1	65.8	73.3
Sb	29.2	40.0	13.6	30.0	10.8	14.3	19.0	22.1	17.6	39.7
Te	17.2	76.6	5.2	494.4	5.9	194.6	6.2	393	< LoD	nd
Cs	7.6	15.4	9.3	9.7	5.6	29.0	36.3	28.2	22.5	23.0
Ba	341	49.6	398	20.7	237.0	16.5	943	15.5	701	20.1
Tl	< LoD	nd	< LoD	nd	< LoD	nd	< LoD	nd	< LoD	nd
Pb	80.7	31.1	110.7	95.6	67.4	57.8	197	24.5	151	24.2
Bi	1.4	44.5	1.4	59.0	0.4	43.6	199	194	3.5	39
Th	4.2	13.4	4.4	10.2	2.6	51.9	12.0	10.6	10.2	22.8
U	7.6	32.6	4.1	26.6	4.6	85.7	19.3	23.6	14.7	13.2

Table 4.2 continuation

	mean	RSD%	mean	RSD%	mean	RSD%	mean	RSD%	mean	RSD%
Weight (g)	0.1		0.1		0.1		0.1		1	
Time (h)	16		4		4		4		1.5	
Volume (ml)	5		1		2.5		5		10	
Ca	747	10.6	98.5	23.0	56.0	18.3	92.2	6.8	177	9.4
Mg	22.4	34.1	< LoD	nd	< LoD	nd	< LoD	nd	5.3	30.5
Na	328	29.5	334	74.0	255	102.3	159	99.4	43.4	68.1
K	104	37.6	62.0	46.9	47.5	49.6	54.2	63.2	13.4	24.2
Si	126	35.0	124	60.3	89.5	19.4	73.6	6.6	16.9	5.4
Cl	502	27.2	342	8.2	262	8.7	340	16.8	95.2	6.4
SO$_4^{2-}$	238	38.3	692	21.3	572	34.3	351	52.4	612	9.0
Li	315	36.0	118	18.4	100	10.3	122	13.7	84.9	8.2
Be	4.5	441	16.9	121	8.1	120.5	14.9	98.6	2.9	81.5
B	9990	68.1	3524	23.8	4856	2.6	3198	37.5	3956	68.8
Al	43331	57.4	16331	7.0	< LoD	nd	14664	15.2	1222	25.0
P	< LoD	nd	< LoD	nd	< LoD	nd	1359	3419.8	1969	235.2
Ti	1419	89.3	191	77.3	< LoD	nd	199	37.5	< LoD	nd
V	105.0	36.3	69.3	35.0	25.2	99.4	12.4	81.5	3.9	44.2
Cr	< LoD	nd	< LoD	nd	< LoD	nd	< LoD	nd	< LoD	nd
Fe	23277	59.8	7463	51.0	4812	16.1	5888	13.3	548	28.9
Mn	2431	59.9	652	13.7	509	1.5	587	12.9	87	10.2
Co	19.4	51.9	6.5	42.2	5.0	67.1	7.7	21.9	1.5	31.6
Ni	535	51.4	675	7.5	627	3.3	680	5.3	55	9.5
Cu	1065	67.7	405	32.3	358	72.6	405	70.3	72	10.3
Zn	7093	23.0	14389	73.9	4692	44.9	8177	38.9	919	16.4
Ga	25.9	61.3	7.4	26.1	7.0	34.2	7.0	26.9	0.5	49.7
Ge	< LoD	nd	< LoD	nd	4.2	80.5	2.2	171.2	0.5	103.5
As	50.9	232.9	< LoD	nd	< LoD	nd	< LoD	nd	22.2	25.3
Br	< LoD	nd	< LoD	nd	< LoD	nd	< LoD	nd	7	390.6
Rb	506	55.2	211	8.5	193	7.7	189	10.9	43	7.4
Sr	1685	13.5	338	21.7	176	60.1	395	22.4	464	7.2
Zr	42.3	27.4	31.9	9.1	24.1	42.3	34.8	24.4	4.9	37.4
Nb	31.5	66.9	8.6	27.9	9.1	32.5	9.7	34.8	0.5	65.0
Mo	235.4	155.1	201	19.4	164	6.7	154	7.3	16	44.4
Cd	0.2	1887	3.7	90.9	< LoD	nd	0.5	483.5	2.4	159.9
Sn	41.0	12.4	30.4	42.2	15.3	108.3	21.2	24.6	3.1	24.6
Sb	21.9	26.0	13.0	27.0	27.5	124.3	14.0	18.6	1.7	14.8
Te	< LoD	nd	3.65	351	< LoD	nd	0.34	2353.2	< LoD	nd
Cs	31.8	76.5	6.1	10.8	5.3	11.4	6.4	33.7	0.4	27.1
Ba	892	31.4	327	16.7	228	12.1	267	23.5	117	5.1
Tl	< LoD	nd	< LoD	nd	-9.0	-17.2	< LoD	nd	< LoD	nd
Pb	236	56.4	87	10.6	72	40.6	111	27.8	12	47.2
Bi	2.3	115	< LoD	nd	< LoD	nd	< LoD	nd	< LoD	nd
Th	8.1	36.5	3.4	21.1	3.3	22.0	2.4	28.0	0.2	34.3
U	20.1	50.2	3.6	16.1	4.0	26.6	4.1	27.3	0.5	17.1

Table 4.2 continuation

	mean	RSD%	mean	RSD%	mean	RSD%	mean	RSD%
Weight (g)	1		1		1		1	
Time (h)	1.5		1.5		16		16	
Volume (ml)	25		50		10		25	
Ca	196	9.7	194	4.8	314	48.6	458	3.4
Mg	2.5	25.3	3.1	23.0	7.8	44.7	11.4	14.8
Na	62.9	31.0	65.7	65.2	62.8	58.4	59.4	65.6
K	13.5	10.1	15.7	24.9	19.0	33.4	17.1	19.1
Si	18.3	10.9	22.5	6.6	39.3	20.7	36.1	10.7
Cl	39.6	25.0	30.7	11.2	62.6	41.2	32.9	16.2
SO_4^{2-}	576	7.9	549	6.6	574	10.6	585	5.1
Li	83.5	8.4	99.8	4.0	144	16.6	151.6	3.0
Be	< LoD	nd	< LoD	nd	< LoD	nd	2.9	61.8
B	1335	51.5	1018	19.9	2180	46.5	916	31.2
Al	2527	22.2	2360	20.2	3957	43.5	6693	9.3
P	4761	71.0	1769	309.6	3783	29.9	3190	122
Ti	47.7	27.3	33.0	26.9	53.1	80.4	152	13.7
V	2.4	104.0	2.6	207.6	4.1	149.4	11.8	21.4
Cr	< LoD	nd	< LoD	nd	< LoD	nd	< LoD	nd
Fe	533	24.4	670	17.4	1042	44.4	1811	5.4
Mn	102	14.5	88.5	12.9	168.5	29.6	277.6	9.0
Co	0.5	21.5	0.6	103.3	1.7	33.3	2.0	7.5
Ni	38.2	6.6	39.0	18.3	59.5	100.7	24.0	22.6
Cu	144	8.0	102	35.6	170	92.7	155	65.8
Zn	865	57.2	598	22.8	800	26.3	971	51.5
Ga	1.0	50.4	0.8	24.1	2.2	42.4	3.2	8.6
Ge	0.3	128.6	0.4	30.1	0.7	47.3	0.6	75.7
As	43.6	19.2	53.9	17.0	67.0	36.3	88.1	12.2
Br	84.3	32.2	147	27.6	190	24.3	112	8.7
Rb	66.4	3.7	69.7	8.0	80.8	12.3	90.8	4.9
Sr	476	8.0	450	3.3	881	51.4	1175	2.2
Zr	4.9	48.2	3.4	30.0	6.7	16.7	9.6	51.9
Nb	1.0	37.8	0.9	39.6	2.3	53.9	5.5	57.8
Mo	23	61.9	11.4	3.7	8.1	81.4	4.1	27.3
Cd	0.2	272.6	< LoD	nd	0.5	147	0.3	107
Sn	4.5	7.1	3.6	27.6	5.7	43.3	3.7	29.2
Sb	1.5	29.0	1.2	40.8	2.3	65.4	1.1	12.0
Te	1.36	81.2	0.41	517	< LoD	nd	1.80	54.8
Cs	1.5	10.5	1.4	18.6	2.7	33.3	3.8	13.1
Ba	104	9.1	93.5	6.5	128	3.9	141	5.5
Tl	< LoD	nd	< LoD	nd	< LoD	nd	< LoD	nd
Pb	17	116.8	9	34.7	21.6	51.0	18.2	19.8
Bi	< LoD	nd	< LoD	nd	< LoD	nd	< LoD	nd
Th	0.7	27.7	0.5	21.1	1.2	48.9	1.4	22.9
U	2.7	106	1.6	43.6	7.0	56.7	10.2	11.4

Table 4.2 continuation

	mean	RSD%	mean	RSD%	mean	RSD%	mean	RSD%
Weight (g)	1		1		1		1	
Time (h)	16		4		4		4	
Volume (ml)	50		10		25		50	
Ca	290	41.9	201	13.2	190	14.1	202	5.4
Mg	7.5	30.7	4.6	22.4	4.7	26.0	4.9	25.9
Na	108	16.9	68.2	18.0	66.9	35.7	88.8	21.1
K	13.7	35.5	13.8	11.7	7.8	31.1	10.2	22.5
Si	39.3	11.6	20.1	6.2	20.9	7.4	26.0	8.9
Cl	50.8	31.6	23.8	22.6	19.6	19.0	20.9	16.7
SO_4^{2-}	654	11.5	554	7.3	507	2.0	481	11.4
Li	130	8.5	140	28.5	140	9.4	230	31.1
Be	< LoD	nd	< LoD	nd	< LoD	nd	< LoD	nd
B	1452	35.9	1331	53.0	1171	49.3	988	15.4
Al	6348	93.6	5246	15.5	3077	28.1	4254	14.5
P	885	221.8	72.4	1910	< LoD	nd	< LoD	nd
Ti	121.2	62.7	72.1	20.3	45.8	47.4	53.8	43.5
V	7.4	115	8.2	38.7	5.1	50.4	6.2	30.7
Cr	< LoD	nd	< LoD	nd	< LoD	nd	< LoD	nd
Fe	1662	68.2	4721	103	468	23.7	661	25.4
Mn	232.0	47.6	168	8.3	102	23.4	123	15.1
Co	1.3	37.2	< LoD	nd	< LoD	nd	< LoD	nd
Ni	22.8	60.6	71.3	3.9	67.6	5.0	71.1	6.4
Cu	118	55.9	46.3	31.6	45.3	20.9	59.8	19.3
Zn	901	55.9	487	28.5	437	47.1	465	23.4
Ga	2.4	87.7	1.8	22.2	1.3	31.6	1.6	9.0
Ge	0.5	59.5	< LoD	nd	< LoD	nd	< LoD	nd
As	106	23.2	79.2	33.5	54.5	16.0	69.0	12.6
Br	131	23.8	106	24.1	78.9	18.9	97.9	55.4
Rb	94.4	29.7	82.6	8.8	61.9	7.6	71.9	3.7
Sr	730	40.4	474	13.2	445	10.4	441	5.8
Zr	5.3	38.6	5.6	30.7	1.8	57.1	2.4	24.2
Nb	3.3	92.0	2.0	32.4	1.2	46.4	1.6	27.6
Mo	12.0	96.5	26.6	40.4	19.5	11.4	19.5	5.9
Cd	0.5	295	< LoD	nd	< LoD	nd	< LoD	nd
Sn	4.5	45.3	2.0	23.4	1.9	18.7	2.3	13.9
Sb	1.5	26.6	2.0	62.7	0.9	13.9	1.3	32.7
Te	< LoD	nd	0.6	238.5	0.4	266	2.4	59.4
Cs	3.6	57.1	2.2	17.8	1.4	26.4	1.8	18.1
Ba	142	14.8	111	3.3	94.2	10.8	102	5.7
Tl	< LoD	nd	< LoD	nd	< LoD	nd	< LoD	nd
Pb	17.3	26.7	11.9	18.8	6.7	21.8	11.7	45.1
Bi	< LoD	nd	< LoD	nd	< LoD	nd	< LoD	nd
Th	1.7	88.4	1.1	28.2	0.6	32.0	0.6	52.2
U	3.8	121	2.3	36.2	1.4	42.9	1.9	10.2

Appendix 5

In this appendix are presented the protocols of the ash leaching tests carried out

Protocol of Single Batch Leaching Test (SBLT) with deionised water

Introduction

The aim of this protocol is the determination of the elements leached from rocks, soils and sediments which causing heavy loadings to soils and water bodies.

Methodology

No sieved and no ground ash has been used for leachate experiments. The process followed is described below:

1. Sample weighing: Approximately 1g of dry sample is weighed in polyethylene tubes (three replicates a, b, c in essay tubes). The exact weight of each sample is noted on the notebook. It is recommended to use consecutive numbers (for example, S1a, S1b, S1c, S2a, S2b, S2c, etc.). Once all samples have been weighed, 10 ml of deionised water (milliQ Plus type, 18.2 MΩ cm^{-1}) to the polyethylene tubes are added.

2. Determine leachate pH immediately after contact between the ash and deionised water with specific electrode for pH in a first replicate (for example S1a).

3. The vessels are then closed and the ash-leach mixture is stored in a sealed container by shaking for 4 hours at 20 rpm.

4. Is necessary to centrifuge the samples prior to filtration in order to prevent clogging of the membranes and to facilitate ash sample recovery.

5. Filter mixture using 0.45 µm surfactant-free cellulose acetate membrane filters (e.g., Whatman or Millipore).

6. Transfer the solution of the second replicate (for example S1b) to a volume flask (100 ml) and add 1 ml HNO$_3$ for the ICPs analyses. Two 14 ml tubes are arranged (one for the ICP-OES and another one for the ICP-MS).

7. The first replicate (S1a) has to be used to determine leachate pH at the end of the experiment, while the third (S1c) to determine F both with a specific electrodes.

Protocol of Single Batch Leaching Test (SBLT) with acid nitric

Introduction

The aim of this protocol is the determination of the maximum load of PTTEs environmentally available. Concentrated HNO_3 has been selected because it produces extreme conditions and maintains, at the same time, the compatibility of the leachate with the input solution for chemical analysis by ICP-OES and ICP-MS (direct determination after dilution). This protocol has been developed following the literature observations by Papastergios et al., 2009, 2010.

Methodology

No sieved and no ground ash has been used for leachate experiments. The process followed is described below:

1. Sample weighing**:** Approximately 0.1g of dry sample is weighed in polyethylene tubes. The exact weight of each sample is noted on the notebook. It is recommended to use consecutive numbers (for example, S1, S2, S3 etc.). Once all samples have been weighed, 1 ml of analytical grade HNO_3 (65%) to the polyethylene tubes is added.

2. The essay tubes are then closed and the ash-leach mixture is stored in a sealed container by shaking overnight (ca. 12h) at 20 rpm.

3. Deionised water was added to the resulting leached solution to facilitate the filtering. They are centrifugated prior to filtration in order to prevent clogging of the membranes and to facilitate ash sample recovery.

4. Filter mixture using 0.45 µm surfactant-free cellulose acetate membrane filters (e.g., Whatman or Millipore).

5. Transfer the solution to a volume flask (100 ml) and add deionised water up to reach a final volume of 100 ml with 1% (v/v) HNO_3. Two 14 ml tubes are arranged (one for the ICP-OES and another one for the ICP-MS).

References

Papastergios G., Fernandez-Turiel J. L., Georgakopoulos A., Gimeno D. Natural and anthropogenic effects on the sediment geochemistry of Nestos river, Northern Greece. Environ. Geol. 2009, 58(6), 1361.

Papastergios G., Fernandez-Turiel J. L., Georgakopoulos A., Gimeno D. Arsenic background concentrations in surface soils of Kavala Area, Northern Greece. Water Air Soil Poll. 2010, 209(1-4), 323.

Protocol for column leaching test with deionised water

Introduction

The aim of this protocol is the determination of potential toxic trace elements (PTTEs) in order to obtain information on their temporal mobility.

Methodology

No sieved and no ground ash has been used for leaching experiments. The process followed is described below:

1. Sample weighing**:** Approximately 10-15 g of sample is weighed in polyethylene vessels. The exact weight of the sample is noted on the notebook.

2. A vertical column (Teledyne ISCO Ref. 69-3873-140) of 8 cm height and - a cross-sectional area of 2.25 cm^2 - is filled with the volcanic ash sample. Loading of column was carried out gradually, under mild shaking in order to compact the ash. This filling process prevents the entrapment of air bubbles and a grain size fractionation.

3. A peristaltic pump (Minipuls 3, Gilson) at the head of the column assured the constant and stable deionised water (MilliQ Q Plus type, 18.2 MΩ cm^{-1}) flow from top to bottom (15 rpm).

4. A fraction collector at the column outlet took samples from the leaching solution (FC 204,Gilson) in 14x100 mm polypropylene test tubes. In this protocol we employ the drop mode collection, counting 400 drops per tube of aqueous solutions from the column outlet. One litre of percolate solution must to be collected resulting in a set of ~100 tube samples. We must weigh the empty tubes (before being filled with the leachate solution) and once they are filled with the aqueous solution in order to know exactly the volume of percolate solution in each tube (and then the .

5. A subset of 40 samples are analyzed for major and trace elements, preparing acidified (1% HNO$_3$) dilutions of 1:5 ml, v/v, for ICP-OES and 1:10 ml, v/v, ICP-MS with MilliQ Q Plus type deionised water. Another subset of 25 samples was removed for pH determination (X-Mate MX300, Mettler-Toledo). Samples were stored at 4ºC until analysis.

Appendix 6

In this appendix are presented the results obtained through the batch leaching tests

Relative Mass Leached (RMLs, %) in water ash leachates

Table 6.1 Relative Mass Leached factors or RMLs (%) in water ash leachates of samples from Puna and neighbouring area and Uruguay (nd, not determined).

	719	721	733	808	809	AS-28	AS-29	AS-33	UR-1	UR-6	UR-7
Ca	3.58	1.25	0.47	0.95	0.59	1.42	0.10	0.12	0.22	0.15	0.14
Mg	0.45	0.14	0.08	0.17	0.08	0.21	0.36	0.24	0.15	0.08	0.09
Na	0.12	0.22	0.61	4.15	2.56	0.46	0.66	1.39	0.19	0.09	0.27
K	0.05	0.07	0.13	0.14	0.05	0.05	0.07	0.08	0.03	0.04	0.04
Si	0.02	0.01	0.01	0.02	0.02	0.01	0.08	0.08	0.01	0.01	0.03
Li	0.09	0.20	0.07	0.32	1.75	0.28	0.67	0.69	0.19	0.13	0.16
Al	0.02	0.02	0.01	0.02	0.02	0.02	0.07	0.04	0.01	0.01	0.01
P	0.27	0.09	0.35	0.18	2.00	0.69	0.13	1.74	0.16	0.09	0.13
Ti	0.02	0.02	0.01	0.02	0.01	0.01	0.05	0.10	0.02	0.01	0.02
V	0.07	0.04	0.68	0.79	5.62	0.43	0.02	0.19	0.59	0.33	0.56
Cr	0.32	0.05	0.09	0.13	0.20	0.15	0.07	0.15	0.18	0.12	0.11
Fe	nd	nd	nd	0.01	nd	nd	0.16	0.24	nd	0.01	0.03
Mn	0.01	0.02	0.02	0.02	0.01	0.01	0.21	0.14	0.02	0.02	0.02
Co	0.21	0.03	0.12	0.02	0.02	0.08	0.04	0.03	nd	nd	nd
Ni	0.76	0.16	0.79	0.55	1.71	0.40	0.31	0.67	1.16	0.70	0.29
Cu	0.58	0.28	0.91	0.49	1.59	0.90	0.39	0.78	0.53	0.27	0.21
Zn	nd	nd	0.03	nd	nd	0.05	0.84	1.66	nd	nd	nd
As	0.27	0.32	0.65	1.17	2.92	1.10	0.45	3.39	0.59	0.20	0.74
Rb	0.01	0.01	0.01	0.03	0.01	0.01	0.02	0.11	0.01	0.01	0.01
Sr	3.00	0.87	0.33	0.49	0.51	0.72	0.02	0.03	0.06	0.05	0.05
Zr	0.07	0.05	0.02	0.03	0.02	0.15	0.31	0.07	nd	nd	nd
Nb	0.01	0.02	0.02	0.05	0.02	0.01	0.15	0.65	nd	nd	nd
Mo	0.09	0.13	0.13	0.28	2.04	0.22	0.08	1.21	0.14	0.04	0.13
Sb	nd	nd	0.17	nd	0.13	0.06	0.02	0.10	nd	nd	0.20
Cs	0.02	0.02	0.02	0.03	0.02	0.02	0.02	0.28	nd	nd	0.02
Ba	0.27	0.04	0.07	0.01	0.11	0.07	0.01	0.03	0.01	0.02	0.01
La	nd	nd	nd	nd	0.09	nd	0.02	0.09	0.01	0.01	0.03
Ce	0.07	0.05	0.02	0.03	0.03	0.06	0.02	0.10	0.02	0.01	0.02
Pb	0.15	0.17	0.08	0.32	0.06	0.22	0.74	1.31	0.06	0.06	0.06
Th	nd	nd	nd	nd	nd	0.01	0.08	0.40	nd	0.02	nd
U	nd	nd	nd	nd	nd	0.02	0.46	1.16	nd	nd	nd

Table 6.2 Relative Mass Leached factors or RMLs (%) in water ash leachates of samples from SVZ (nd, not determined).

	CHA-1F	CHA-2R	CHA-G	CHA-E	COP	LON	LLA	HUD
Ca	0.71	0.89	0.97	0.90	0.69	0.04	0.10	0.25
Mg	0.31	0.16	0.20	0.23	2.25	0.02	0.04	0.07
Na	0.21	0.10	0.28	0.09	1.04	0.02	0.24	0.71
K	0.06	0.08	0.09	0.06	0.13	0.12	0.24	0.22
Si	0.02	0.02	0.02	0.02	0.01	0.01	0.01	0.01
Li	0.20	0.19	0.45	0.17	1.64	0.08	1.00	0.35
Al	0.02	0.02	0.02	0.02	0.02	0.01	0.01	0.02
P	0.11	0.11	0.13	0.29	0.01	0.01	0.03	0.02
Ti	0.02	0.02	0.02	0.02	0.01	0.01	0.01	0.01
V	0.20	0.27	0.43	0.30	0.01	0.01	0.02	0.02
Cr	0.05	0.05	0.04	0.04	0.02	0.04	0.02	0.02
Fe	nd	0.02	0.01	0.01	nd	nd	nd	nd
Mn	0.09	0.04	0.03	0.02	1.15	0.02	0.03	0.11
Co	nd	nd	1.16	nd	2.34	0.04	0.03	nd
Ni	2.93	0.77	1.52	2.04	2.49	2.14	0.06	0.29
Cu	0.62	0.35	0.50	0.80	0.24	0.07	0.10	0.64
Zn	0.33	0.55	0.99	0.09	0.76	0.29	0.22	2.46
As	1.94	1.52	7.83	0.86	0.09	0.04	0.42	0.99
Rb	0.03	0.04	0.05	0.02	0.16	0.04	0.07	0.08
Sr	0.10	0.11	0.18	0.27	0.29	0.02	0.05	0.10
Zr	0.01	0.02	0.06	0.04	0.02	0.02	0.04	0.02
Nb	0.64	0.66	0.55	0.55	0.64	1.12	1.64	0.58
Mo	1.77	4.25	4.36	1.13	nd	1.91	1.02	10.69
Sb	0.41	0.47	0.62	0.24	nd	nd	0.41	3.54
Cs	0.03	0.04	0.05	0.02	0.04	nd	nd	nd
Ba	0.01	0.02	0.01	0.03	0.02	0.01	0.02	0.02
La	nd	nd	nd	nd	0.12	nd	nd	nd
Ce	0.02	0.01	0.02	0.01	0.17	nd	nd	nd
Pb	1.68	0.79	9.0	1.00	0.72	2.90	15.9	0.32
Th	nd	nd	nd	nd	nd	nd	nd	nd
U	nd	nd	nd	nd	nd	nd	nd	nd

Amount of element environmental available (EA, mg kg^{-1})

Table 6.3 Amount of element environmental available (EA) in mg kg^{-1} of ashes from Puna and neighbouring area and Uruguay (nd, not determined).

	719	721	733	808	809	AS-28	AS-29	AS-33	UR-1	UR-6	UR-7
Ca	22838	14728	3046	5510	2985	10443	2088	2474	1376	1099	978
Mg	421	648	147	435	110	409	1992	1344	208	172	235
Na	3506	5874	16772	129276	79564	14557	20851	41509	3723	2197	5758
K	1694	2506	5001	4978	1966	1682	1886	2104	1357	1815	1574
Si	5737	3958	4598	7810	6488	3630	24844	26277	4680	3448	8339
Li	7.82	18.70	6.23	18.0	196	25.9	8.38	11.93	3.08	3.21	4.60
Al	1266	1034	887	1281	1084	1150	5807	3083	865	1043	924
P	24.1	21.8	51.79	36.5	128	47.7	55.3	636	34.3	29.7	51.5
Ti	9.86	24.8	8.18	18.5	8.57	10.6	88.9	214	15.2	16.0	33.8
V	0.49	1.21	6.03	6.50	34.7	3.65	0.84	11.60	3.98	4.00	8.97
Cr	1.42	1.08	1.00	0.60	0.73	1.06	1.15	3.18	0.70	0.77	0.88
Fe	nd	nd	nd	83.5	nd	nd	3230	5210	nd	121	354
Mn	7.41	12.0	9.36	12.4	6.66	7.65	95.7	63.4	10.4	7.23	16.0
Co	0.18	0.15	0.22	0.37	0.22	2.08	0.87	1.07	nd	nd	nd
Ni	1.92	1.78	4.57	1.66	3.13	2.06	3.83	6.17	2.68	2.13	2.00
Cu	4.14	2.64	3.99	2.54	7.35	6.30	5.01	8.51	2.97	2.02	2.41
Zn	nd	nd	1.15	nd	nd	5.15	60.6	93.3	nd	nd	nd
As	1.58	2.34	3.53	7.43	19.54	7.97	0.65	4.59	0.85	0.62	1.52
Rb	5.13	4.47	3.97	4.74	5.74	7.32	2.23	9.24	2.55	2.01	1.87
Sr	73.8	81.8	13.6	44.0	13.2	26.8	7.43	13.91	8.04	6.20	6.98
Zr	4.61	4.70	1.44	2.69	0.89	10.0	6.87	5.33	nd	nd	nd
Nb	0.36	0.57	0.57	0.53	0.53	0.30	2.21	5.02	nd	nd	nd
Mo	0.24	0.38	0.37	0.72	5.90	0.62	0.14	0.26	0.36	0.11	0.32
Sb	nd	nd	0.20	nd	0.15	0.14	0.22	0.28	nd	nd	0.14
Cs	0.45	0.39	0.43	0.15	0.44	0.41	0.13	0.75	nd	nd	0.16
Ba	9.37	6.11	4.36	11.9	4.69	4.76	5.96	17.0	5.58	10.3	7.25
La	nd	nd	nd	nd	1.65	nd	1.54	4.74	0.48	0.61	1.38
Ce	2.19	2.09	0.79	1.16	1.00	2.06	1.80	8.44	1.58	1.05	1.86
Pb	5.63	5.97	2.93	8.12	2.17	8.53	16.1	23.8	1.83	1.88	1.85
Th	nd	nd	nd	nd	nd	0.44	2.56	7.69	nd	0.56	nd
U	nd	nd	nd	nd	nd	0.43	2.78	4.69	nd	nd	nd

Table 6.4 Amount of element environmental available (EA) in mg kg^{-1} of ashes from SVZ (nd, not determined).

	CHA-1F	CHA-2R	CHA-G	CHA-E	COP	LON	LLA	HUD
Ca	7993	12976	13795	10461	35132	1585	7062	14866
Mg	657	549	714	484	59518	258	1641	1880
Na	6421	2885	8797	2946	27719	888	5271	21413
K	1420	1817	2142	1404	2040	1003	1122	2333
Si	5280	5414	6168	5833	2875	3130	2747	2659
Li	9.55	8.84	18.5	7.58	19.2	0.99	6.94	2.63
Al	1260	1254	1301	1418	2031	1032	1202	1666
P	37.3	40.4	42.7	125	13.9	19.2	21.6	63.7
Ti	19.0	22.6	22.3	19.5	90.8	105	71.2	139
V	1.02	3.50	5.98	1.73	2.10	0.94	4.17	4.71
Cr	0.72	0.86	0.78	0.67	1.54	0.54	1.44	0.55
Fe	nd	246	136	111	nd	nd	nd	nd
Mn	47.3	20.9	14.5	11.0	1241	27.7	34.5	172
Co	nd	nd	3.2	nd	57.0	1.5	1.6	nd
Ni	4.90	2.82	6.57	3.18	72.6	2.78	3.42	2.40
Cu	3.95	3.72	4.19	4.75	12.6	3.08	10.4	34.5
Zn	16.8	29.5	50.9	4.94	77.9	45.0	23.7	348
As	35.2	72.6	301	13.0	0.65	0.30	1.96	0.92
Rb	2.67	4.16	4.89	2.46	8.52	0.77	0.74	2.28
Sr	14.6	18.2	29.6	40.9	147	7.4	25.1	54.3
Zr	1.41	1.43	5.83	3.78	3.16	1.76	3.08	3.30
Nb	4.69	4.74	3.98	4.03	4.49	2.88	3.22	4.73
Mo	1.6	3.2	4.5	0.90	nd	0.11	nd	0.30
Sb	0.4	0.8	0.9	0.24	nd	nd	0.10	0.20
Cs	0.2	0.2	0.3	0.16	0	nd	nd	nd
Ba	8.5	10.7	9.0	20.1	7.38	4.49	3.36	8.53
La	nd	nd	nd	nd	2.9	nd	nd	nd
Ce	0.88	0.53	0.87	0.61	8.97	nd	nd	nd
Pb	34.8	15.5	201	25.7	10.2	39.2	107	2.41
Th	nd	nd	nd	nd	nd	nd	nd	nd
U	nd	nd	nd	nd	nd	nd	nd	nd

Table 6.5 Relative Mass leached factors or RMLs (%) in nitric batch leachates of ash from Puna and neighbouring area and Uruguay (nd, not determined).

	719	721	733	808	809	AS-28	AS-29	AS-33	UR-1	UR-6	UR-7
Ca	38.4	42.9	33.5	33.3	33.8	28.5	14.3	11.1	25.8	16.0	26.8
Mg	17.6	19.2	16.8	15.0	26.6	30.8	3.53	10.5	22.2	18.6	31.3
Na	0.68	1.14	1.76	8.62	5.10	1.17	2.51	9.68	3.79	0.77	1.28
K	0.68	1.19	1.05	1.42	1.05	1.28	1.64	8.78	1.12	0.95	1.03
Si	0.03	0.05	0.04	0.05	0.09	0.06	0.05	0.11	0.01	0.02	0.02
Li	1.67	2.81	1.72	9.14	8.83	3.02	7.62	19.2	1.91	2.16	3.69
Be	0.79	1.13	0.83	10.3	0.77	1.39	6.47	3.56	0.83	4.40	8.95
Al	0.55	0.81	0.41	2.19	0.80	1.00	0.61	2.67	0.71	1.21	2.24
P	95.5	63.7	88.5	52.6	96.1	92.2	79.4	97.0	27.6	32.7	29.5
Ti	2.01	0.97	1.36	0.54	5.59	6.38	1.12	3.99	1.62	1.77	1.04
V	5.29	4.51	7.95	12.67	27.3	20.4	2.06	4.33	10.5	8.88	12.9
Cr	5.86	4.01	3.61	19.56	25.3	17.2	2.26	4.08	12.3	2.74	7.20
Fe	4.38	5.72	5.11	4.16	9.66	14.5	1.60	4.99	2.99	4.63	6.34
Mn	3.97	7.66	3.03	13.17	6.29	7.99	4.43	8.39	4.17	4.22	4.40
Co	23.7	17.8	46.1	88.8	2.57	2.05	61.2	78.0	0.35	1.17	2.56
Ni	90.1	48.7	58.3	75.5	84.2	53.0	17.7	30.5	36.1	16.1	18.2
Cu	17.8	24.5	25.2	21.0	42.9	26.7	5.98	19.2	75.8	25.8	23.6
Zn	97	76.5	94.3	62.4	95.1	38.7	33.5	61.9	26.1	16.1	14.0
Ga	0.69	1.08	0.59	1.49	1.18	1.69	0.94	4.10	0.82	1.85	3.04
Ge	0.00	0.04	0.00	0.45	0.34	0.13	0.19	1.44	0.51	1.10	1.24
As	17.1	23.7	16.7	18.6	7.83	28.5	57.4	77.7	18.5	6.91	3.02
Rb	0.74	1.16	0.63	1.85	0.80	1.06	4.83	18.7	0.95	2.68	3.13
Sr	19.8	12.8	12.0	18.1	17.3	9.86	1.07	4.43	6.30	5.53	11.6
Y	2.21	6.91	3.12	8.74	3.63	4.63	8.58	11.7	0.74	2.19	4.04
Zr	0.56	0.77	0.43	1.06	1.11	0.81	3.39	1.47	0.30	0.82	2.30
Nb	0.15	0.12	0.09	0.73	0.39	0.47	0.57	0.62	0.01	0.02	0.02
Mo	16.5	14.1	12.5	11.4	15.3	14.0	16.7	19.3	4.82	1.73	1.74
Cd	nd	nd	nd	nd	nd	16.5	9.75	3.81	24.4	4.08	3.01
Sn	nd	nd	nd	2.48	1.64	0.49	nd	0.10	3.28	1.84	1.52
Sb	11.2	6.76	6.90	41.8	13.7	4.51	1.17	3.71	nd	nd	nd
Cs	0.93	1.40	1.59	7.41	0.60	1.37	6.60	50.2	1.22	2.83	6.54
Ba	18.8	12.0	15.9	5.62	12.4	4.91	1.09	4.08	4.30	3.99	5.95
La	3.76	9.91	6.41	8.31	6.24	7.87	7.16	18.8	2.88	8.58	14.7
Ce	3.39	9.69	6.21	9.58	5.62	7.61	7.12	17.9	2.85	9.50	10.8
Pr	1.35	10.9	6.86	9.14	5.94	8.21	7.60	16.4	3.28	10.7	17.7
Nd	4.42	12.0	7.44	9.79	6.61	9.25	7.33	15.6	3.78	12.6	20.1
Sm	2.15	11.3	6.59	9.99	5.79	8.61	6.18	13.2	3.84	13.6	22.2
Eu	1.93	13.9	10.4	9.41	11.1	13.0	3.20	7.55	5.08	15.7	24.7
Gd	4.23	11.4	6.50	9.90	6.06	8.11	5.96	13.3	3.86	14.0	21.8
Tb	1.55	9.82	5.12	10.0	5.32	6.67	5.40	11.5	4.00	14.3	23.3
Dy	3.29	8.72	4.27	9.06	4.46	6.06	5.41	9.98	3.78	13.8	23.6
Ho	1.28	7.32	3.26	8.58	3.70	4.81	5.45	8.74	2.86	12.7	22.7
Er	2.41	6.34	2.77	8.34	3.23	4.42	5.06	8.47	3.44	11.7	21.7

Table 6.5 continuation.

	719	721	733	808	809	AS-28	AS-29	AS-33	UR-1	UR-6	UR-7
Tm	0.88	4.94	2.02	7.75	2.62	2.78	5.32	7.44	2.18	10.0	19.2
Yb	1.84	3.87	1.70	8.11	2.23	2.53	5.43	7.71	2.43	9.46	18.8
Lu	0.63	3.64	1.52	7.51	1.91	2.09	5.52	8.47	1.98	8.40	17.4
Hf	0.91	1.17	0.65	5.92	7.88	1.67	2.44	6.50	5.94	2.17	5.05
Ta	0.18	0.16	0.17	3.38	0.95	0.20	0.56	1.73	nd	nd	nd
Tl	0.70	1.98	1.03	2.52	1.45	3.23	2.34	23.1	1.11	3.04	3.76
Pb	2.42	3.61	2.14	11.5	2.78	3.25	1.85	15.8	4.84	4.23	5.40
Bi	2.48	2.20	1.88	6.54	2.00	2.92	6.82	23.8	1.69	<LoD	<LoD
Th	1.06	1.94	0.68	4.08	1.19	1.09	6.38	7.26	0.03	1.46	5.38
U	0.46	1.02	0.28	2.26	0.65	0.33	7.11	5.86	0.84	1.32	4.13

Table 6.6 Relative Mass leached factors or RMLs (%) in nitric batch leachate of ash from SVZ (nd, not determined).

	CHA-2R	CHA-1F	CHA-E	CHA-G	COP	LON	LLA	HUD
Ca	12.7	7.72	6.64	15.1	1.59	0.81	1.43	1.94
Mg	29.1	13.6	9.0	30.1	10.2	4.72	4.57	7.53
Na	0.37	0.73	0.51	0.99	1.35	0.13	0.68	1.14
K	0.56	0.41	0.24	0.81	1.47	0.07	0.45	0.66
Si	0.01	0.01	0.01	0.01	0.03	0.03	0.07	0.03
Li	2.7	1.24	0.98	4.22	3.93	2.26	3.14	7.48
Be	3.7	1.6	1.27	4.27	1.30	1.14	2.25	0.48
Al	1.42	0.58	0.45	1.56	0.75	0.28	0.88	0.26
P	21.7	10.0	6.83	29.3	3.90	1.82	0.54	4.88
Ti	3.27	0.79	0.93	1.18	0.16	0.51	0.33	0.65
V	30.9	19.5	13.2	31.1	1.12	0.37	0.61	1.12
Cr	10.6	3.32	1.58	11.97	0.77	<LoD	1.11	1.42
Fe	20.6	6.44	4.47	19.78	7.36	2.48	2.46	4.49
Mn	15.8	4.81	3.1	15.89	0.52	0.26	0.23	0.46
Co	41.8	17.9	16.4	42	12.8	4.87	4.54	7.63
Ni	59.3	64.4	60.9	55.5	19.01	59.67	9.23	21.6
Cu	29.7	35.7	28.1	37.3	27.7	11.49	4.64	30.2
Zn	25.3	19.1	26.3	44.8	12.0	7.64	6.34	22.9
Ga	3.62	1.39	0.96	4.44	1.02	0.34	0.86	0.53
Ge	0.74	0.38	0.36	0.35	0.97	0.12	0.30	0.82
As	54.1	39.4	21.3	62.3	36.0	4.24	13.0	21.7
Rb	1.28	0.73	0.6	1.53	0.66	0.22	0.15	0.67
Sr	2.05	1.15	1.33	2.11	1.55	0.26	1.08	0.56
Y	9.13	2.6	3.39	8.03	1.98	1.21	0.62	3.14
Zr	0.39	0.17	0.2	0.19	0.14	0.36	0.20	1.02
Nb	0.01	0.01	0.01	0.01	<LoD	<LoD	<LoD	0.31
Mo	30.5	23.1	20.4	30.5	17.2	nd	<LoD	nd
Cd	10.6	1.52	1.33	36	10.2	4.98	2.73	18.1
Sn	2.99	2.42	2.34	3.04	3.45	1.23	0.99	5.64
Sb	0.01	0.01	0.01	0.01	<LoD	<LoD	<LoD	<LoD
Cs	5.36	2.16	1.64	5.73	0.39	0.46	0.45	1.44
Ba	0.95	0.6	0.89	0.87	2.39	0.97	0.75	0.74
La	2.37	1.05	0.9	2.49	2.81	1.14	0.77	3.19
Ce	2.82	1.13	1.07	2.99	2.85	1.16	0.71	3.18
Pr	3.4	1.33	1.24	3.63	2.86	1.07	0.62	3.13
Nd	4.43	1.65	1.67	4.7	2.98	1.07	0.65	3.01
Sm	6.12	1.96	2.25	6.18	2.79	1.16	0.51	2.96
Eu	5.27	1.41	1.66	4.93	1.61	0.87	0.49	2.01
Gd	5.64	1.88	2.06	6.07	2.62	1.03	0.50	2.93
Tb	6.26	1.69	2.00	6.17	2.03	0.88	0.17	2.53
Dy	7.08	2.18	2.5	6.58	2.04	0.98	0.48	2.63
Ho	6.53	1.61	1.85	6.12	1.43	0.84	0.10	2.36
Er	6.72	1.88	1.97	5.79	1.70	1.05	0.43	2.50

Table 6.6 continuation.

	CHA-2R	CHA-1F	CHA-E	CHA-G	COP	LON	LLA	HUD
Tm	4.87	1.00	0.95	4.45	0.83	0.58	<0.01	2.14
Yb	5.41	1.73	1.71	4.81	1.42	0.91	0.39	2.60
Lu	4.57	1.09	1.25	3.7	1.11	0.68	<0.01	1.92
Hf	2.68	1.98	1.92	1.48	1.90	0.95	1.72	7.01
Ta	0.73	0.37	1.28	0.01	<LoD	0.22	<0.01	0.44
Tl	1.07	0.01	0.01	0.86	4.77	0.63	8.23	34.2
Pb	7.54	2.83	7.82	6.27	8.48	2.47	2.37	25.5
Bi	19.3	0.01	0.01	46.7	25.4	2.43	<LoD	<LoD
Th	2.58	0.31	0.01	0.34	0.61	<LoD	<LoD	1.90
U	1.39	0.7	0.71	1.27	1.06	1.45	1.93	3.00

Appendix 7

In this appendix are reported the dissemination of the results from this study until 2011

7.1 Publications

1. RUGGIERI F., FERNANDEZ-TURIEL J.L., GIMENO D., GARCIA-VALLES M., SAAVEDRA J. Environmental geochemistry of volcanic ashes from the Southern Puna, NW Argentina. Geochimica et Cosmochimica Acta [Special Supplement Awards and Abstracts of the 19th Annual V, M. Goldschmidt Conference, Davos, Switzerland, June, 2009, 73(13S), A1130.

2. RUGGIERI F., FERNANDEZ-TURIEL J.L., GIMENO D., GARCIA-VALLES M., SAAVEDRA J. Environmental geochemistry of ancient volcanic ashes. SCI – Journal of Hazardous Meaterials (2010) 183(1-3):353–365.

3. RUGGIERI F., FERNANDEZ-TURIEL J.L., GIMENO D., GARCIA-VALLES M., SAAVEDRA J Environmental geochemistry of recent volcanic ashes from Southern Andes. SCI – Environmental chemistry- *(*2011), 8, 1–12. doi:10.1071/EN10097.

7.2 Books, monographs and collective volumes

1. RUGGIERI F., FERNANDEZ-TURIEL J.L., GIMENO D., GARCIA-VALLES M.T., SAAVEDRA J., CORDOBA G. DEL V. 2008 Caracterización de cenizas volcánicas de la región de Antofagasta de la Sierra, Argentina. In: Tripaldi A., Veiga G., XII Reunión Argentina de Sedimentología: Resúmenes. Asociación Argentina de Sedimentología, La Plata, Buenos Aires, Argentina. p. 157. ISBN 978-987-96296-3-5.

2. RUGGIERI F., FERNÁNDEZ-TURIEL J.L., GIMENO D., GARCIA-VALLES M.T., SAAVEDRA J., CÓRDOBA G. DEL V., 2009. Contenido y distribución de arsénico y otros elementos trazas en aguas de Antofagasta de la Sierra, Catamarca, Argentina. En: Galindo G., Fernández-Turiel J.L., Storniolo A. (eds.), Presencia de flúor y arsénico en aguas subterráneas. Grupo Argentino de la Asociación Internacional de Hidrogeólogos y Ediciones Ameriondia. Santa Rosa, pp. 71-80. ISBN 978-987-1082-35-3.

3. GALINDO G., MARQUEZ J.J.,SAINATO C.M.,, FERNÁNDEZ TURIEL J.L., RUGGIERI F., 2010. Contenido y Distribución de Elementos Mayoritarios y Trazas En Aguas Subterráneas Someras de La Pampa Arenosa, Buenos Aires, Argentina. En: Hacia la Gestión Integral de los Recursos Hídricos en Zonas de Llanura. Azul, Buenos Aires, pp

4. FERNANDEZ-TURIEL J.L., RUGGIERI F., SAAVEDRA J., GIMENO D., MARTINEZ L.D., GALINDO G., GARCIA-VALLES M.T., POLANCO E., PEREZ-TORRADO F.J., RODRIGUEZ-GONZALEZ A., RODRIGUEZ- FERNANDEZ D. Design of a single batch leaching test to assess the environmental impact of volcanic ash. AGU Fall Meeting, San Francisco, USA. December 13-17, 2010. Poster V13E-2403.

5. FERNANDEZ-TURIEL J.L., RUGGIERI F., SAAVEDRA J., GIMENO D., MARTINEZ L.D.,

PEREZ-TORRADO F.J., RODRIGUEZ-GONZALEZ A., GIL R.A., REJAS M., RODRIGUEZ-FERNANDEZ D. Environmental impact assessment of volcanic ashes using ICP-OES and ICP-MS. European Winter Conference on Plasma Spectrochemistry, Zaragoza, January 30-February 4, 2011. Poster PC105. Book of Abstracts, 245

7.3.1 Spanish Symposiums

1. RUGGIERI F., FERNANDEZ-TURIEL J.L., GIMENO D., GARCÍA-VALLES M.T., SAAVEDRA J., CÓRDOBA G. DEL V. Caracterización de cenizas volcánicas y su influencia en la calidad de las aguas superficiales de la región de Antofagasta de la Sierra, Catamarca, Argentina.
VII Congreso Geológico de España, Las Palmas de Gran Canaria, 14-18 julio 2008.

7.3.2 International Symposium

1. RUGGIERI F., FERNANDEZ-TURIEL J.L., GIMENO D., GARCIA-VALLES M.T., SAAVEDRA J., CORDOBA G. DEL V. Caracterización de cenizas volcánicas de la región de Antofagasta de la Sierra, Argentina.
XII Reunión Argentina de Sedimentología., Buenos Aires, 3-6 junio 2008, Argentina. Resúmenes, p. 157.

2. RUGGIERI F., FERNANDEZ-TURIEL J.L., GIMENO D., GARCIA-VALLES M., SAAVEDRA J. Environmental geochemistry of volcanic ashes from the Southern Puna, NW Argentina.
Geochimica et Cosmochimica Acta [Special Supplement Awards and Abstracts of the 19th Annual V, M. Goldschmidt Conference, Davos, Switzerland, June, 2009, 73(13S), A1130.

3. RUGGIERI F., FERNÁNDEZ-TURIEL J.L., GIMENO D., GARCIA-VALLES M.T., SAAVEDRA J., CÓRDOBA G. DEL V. Contenido y distribución de arsénico y otros elementos trazas en aguas de Antofagasta de la Sierra, Catamarca, Argentina.
III Taller sobre arsénico en aguas: Presencia de Flúor y Arsénico en aguas subterráneas - VI Congreso Argentino de Hidrogeología - IV Seminario Hispano-Latinoamericano de Temas Actuales de la Hidrología subterránea, Santa Rosa (La Pampa, Argentina), 24-28 agosto 2009.

4. FERNANDEZ-TURIEL J.L., RUGGIERI F., SAAVEDRA J., GIMENO D., MARTINEZ L.D., GALINDO G., GARCIA-VALLES M.T., POLANCO E., PEREZ-TORRADO F.J., RODRIGUEZ-GONZALEZ A., RODRIGUEZ- FERNANDEZ D. Design of a single batch leaching test to assess the environmental impact of volcanic ash. AGU Fall Meeting, San Francisco, USA. December 13-17, 2010. Poster V13E-2403.

5. FERNANDEZ-TURIEL J.L., RUGGIERI F., SAAVEDRA J., GIMENO D., MARTINEZ L.D., PEREZ-TORRADO F.J., RODRIGUEZ-GONZALEZ A., GIL R.A., REJAS M., RODRIGUEZ-FERNANDEZ D.
Environmental impact assessment of volcanic ashes using ICP-OES and ICP-MS. European Winter Conference on Plasma Spectrochemistry, Zaragoza, January 30-February 4, 2011. Poster PC105. Book of Abstracts, 245